3 mic

CR 137496

16

FINAL REPORT
SYSTEM DESIGN OF THE PIONEER VENUS SPACECRAFT

VOLUME 9
ATTITUDE CONTROL/MECHANISMS SUBSYSTEMS STUDIES

■

By
A. L. NEIL
ET AL.

■

July 1973

Prepared Under
Contract No. [redacted] NAS2-7250

By
HUGHES AIRCRAFT COMPANY
EL SEGUNDO, CALIFORNIA

For
AMES RESEARCH CENTER
NATIONAL AERONAUTICS AND SPACE ADMINISTRATION

PREFACE

The Hughes Aircraft Company Pioneer Venus final report is based on study task reports prepared during performance of the "System Design Study of the Pioneer Spacecraft." These task reports were forwarded to Ames Research Center as they were completed during the nine months study phase. The significant results from these task reports, along with study results developed after task report publication dates, are reviewed in this final report to provide complete study documentation. Wherever appropriate, the task reports are cited by referencing a task number and Hughes report reference number. The task reports can be made available to the reader specifically interested in the details omitted in the final report for the sake of brevity.

This Pioneer Venus Study final report describes the following baseline configurations:

- "Thor/Delta Spacecraft Baseline" is the baseline presented at the midterm review on 26 February 1973.
- "Atlas/Centaur Spacecraft Baseline" is the baseline resulting from studies conducted since the midterm, but prior to receipt of the NASA execution phase RFP, and subsequent to decisions to launch both the multiprobe and orbiter missions in 1978 and use the Atlas/Centaur launch vehicle.
- "Atlas/Centaur Spacecraft Midterm Baseline" is the baseline presented at the 26 February 1973 review and is only used in the launch vehicle utilization trade study.

The use of the International System of Units (SI) followed by other units in parentheses implies that the principal measurements or calculations were made in units other than SI. The use of SI units alone implies that the principal measurements or calculations were made in SI units. All conversion factors were obtained or derived from NASA SP-7012 (1969).

The Hughes Aircraft Company final report consists of the following documents:

Volume 1 - Executive Summary - provides a summary of the major issues and decisions reached during the course of the study. A brief description of the Pioneer Venus Atlas/Centaur baseline spacecraft and probes is also presented.

Volume 2 - Science - reviews science requirements, documents the science-peculiar trade studies and describes the Hughes approach for science implementation.

Volume 3 - Systems Analysis - documents the mission, systems, operations, ground systems, and reliability analysis conducted on the Thor/Delta baseline design.

Volume 4 - Probe Bus and Orbiter Spacecraft Vehicle Studies - presents the configuration, structure, thermal control and cabling studies for the probe bus and orbiter. Thor/Delta and Atlas/Centaur baseline descriptions are also presented.

Volume 5 - Probe Vehicle Studies - presents configuration, aerodynamic and structure studies for the large and small probes pressure vessel modules and deceleration modules. Pressure vessel module thermal control and science integration are discussed. Deceleration module heat shield, parachute and separation/despin are presented. Thor/Delta and Atlas/Centaur baseline descriptions are provided.

Volume 6 - Power Subsystem Studies

Volume 7 - Communication Subsystem Studies

Volume 8 - Command/Data Handling Subsystems Studies

Volume 9 - Altitude Control/Mechanisms Subsystem Studies

Volume 10 - Propulsion/Orbit Insertion Subsystem Studies

Volumes 6 through 10 - discuss the respective subsystems for the probe bus, probes, and orbiter. Each volume presents the subsystem requirements, trade and design studies, Thor/Delta baseline descriptions, and Atlas/Centaur baseline descriptions.

Volume 11 - Launch Vehicle Utilization - provides the comparison between the Pioneer Venus spacecraft system for the two launch vehicles, Thor/Delta and Atlas/Centaur. Cost analysis data is presented also.

Volume 12 - International Cooperation - documents Hughes suggested alternatives to implement a cooperative effort with ESRO for the orbiter mission. Recommendations were formulated prior to the deletion of international cooperation.

Volume 13 - Preliminary Development Plans - provides the development and program management plans.

Volume 14 - Test Planning Trades - documents studies conducted to determine the desirable testing approach for the Thor/Delta spacecraft system. Final Atlas/Centaur test plans are presented in Volume 13.

Volume 15 - Hughes IR&D Documentation - provides Hughes internal documents generated on independent research and development money which relates to some aspects of the Pioneer Venus program. These documents are referenced within the final report and are provided for ready access by the reader.

Data Book - presents the latest Atlas/Centaur Baseline design in an informal tabular and sketch format. The informal approach is used to provide the customer with the most current design with the final report.

CONTENTS

1. SUMMARY

The Pioneer Venus mission study was conducted for a probe spacecraft and an orbiter spacecraft to be launched by either a Thor/Delta or an Atlas/Centaur launch vehicle. Both spacecraft are spin stabilized. The spin speed is controlled by ground commands to as low as 5 rpm for science instrument scanning on the orbiter and as high as 71 rpm for small probes released from the probe bus. A major objective in the design of the attitude control and mechanism subsystem (ACMS) was to provide, in the interest of costs, maximum commonality of the elements between the probe bus and orbiter spacecraft configurations. This design study was made considering the use of either launch vehicle.

The basic functional requirements of the ACMS are derived from spin axis pointing and spin speed control requirements implicit in the acquisition, cruise, encounter and orbital phases of the Pioneer Venus missions. A summary of the derived ACMS functional requirements are shown in Table 1-1. The ACMS will provide the means of controlling the spacecraft attitude, angular momentum, translational velocity and mechanically articulated elements during all phases of the mission after separation from the launch vehicle. The following primary functions will be performed by the ACMS:

1) Attitude sensing. Provide attitude sensors, sensor data processing and telemetry data conditioning required for ground determination of the spin axis attitude in celestial coordinates.

2) Attitude/velocity control. Provide controls for the firing of propulsion subsystem reaction jets to precess the spin axis attitude and change the spacecraft velocity in response to ground commands.

3) Spin speed control. Provide control of the firing of propulsion subsystem reaction jets to change the rotor spin speed in response to ground commands.

4) Nutation damping. Provide positive damping of the spin axis nutation motions.

5) Spin angle reference. Provide a spin angle reference relative to celestial references for science experiments.

TABLE 1-1. ACMS FUNCTIONAL REQUIREMENTS SUMMARY

Function	Thor/Delta Mission Requirement	Atlas/Centaur Mission Requirement
Spin axis attitude sensing	Error ≤ 0.9 deg when spin axis within 5 deg of ecliptic normal	Error ≤ 0.9 deg when spin axis within 5 deg of ecliptic normal
Attitude/ΔV control	Control attitude within ±2.5 deg of ecliptic normal during cruise	Control attitude within ±2.5 deg of ecliptic normal during cruise
	Control thrust vector to ±4 percent magnitude and ±4 deg direction	Control thrust vector to ±4 percent magnitude and ±4 deg direction
Spin speed control	Vary spin speed over range of 5 to 100 rpm to ±0.6 rpm	Provide automatic spinup following separation to 5 rpm
		Vary spin speed over range of 5 to 60 rpm to ±0.6 rpm
Despun antenna control	Control pointing of beam to ±2 deg of earthline in spin plane (orbiter only)	Control pointing of beam to ±1 deg of earthline in spin plane (orbiter only)
Spin angle science reference	Provide spin angle reference signal to ±0.4 deg	Provide spin angle reference signal to ±0.4 deg
Magnetometer sensor deployment	Extend sensor radially 1.07 m (42 in.)	Extend sensor radially 4.4 m (14.5 ft) (orbiter only)
Bicone antenna deployment	Extend axially 21.5 in. (probe bus only)	Not required

6) Despun antenna control (orbiter only). Provide automatic azimuth rate stabilization and pointing control of the despun antenna in response to ground commands.

7) Bicone deployment (Thor/Delta probe bus only). Provide mechanism for extension of bicone antenna following separation from Thor/Delta launch vehicle

8) Magnetometer deployment. Provide mechanism for extension of magnetometer head following separation from launch vehicle.

1.1 SUBSYSTEM DESIGN ISSUES

The baseline ACMS design and its elements were selected as the result of extensive performance and design tradeoffs conducted during the study contract. The use of existing hardware elements and technology, as well as the incorporation of substantial operational flexibility were emphasized during these tradeoffs. During the course of the system design study contract the Atlas/Centaur was selected as the baseline launch vehicle. As a result of this selection the original Thor/Delta baseline ACMS subsystem design was modified accordingly. The key issues resolved in the subsystem design were:

1) The attitude determination concept

2) The attitude/velocity/spin speed control concept

In addition, many hardware design tradeoffs were required to select the baseline design. The results of these tradeoffs are summarized in Table 1-2. The primary criteria considered in the tradeoffs were weight, cost and complexity (reliability) to achieve the required performance.

1.2 BASELINE SUBSYSTEM DESIGN SUMMARY

The spacecraft spin stabilization concept employs basic gyroscope stability of the spinning rotor to minimize the frequency of attitude corrections, and exploits the attitude control simplicity and long life advantages associated with spinning spacecraft. The main elements of the spacecraft are the spinning rotor, and in the case of the orbiter, the despun earth-oriented assembly containing the communication antenna on the orbiter, a rotating interface, which consists of conventional ball bearings, dc torque motor, and sliprings, permits rf and electrical signal transfer to take place. Primary control of the rotor spin speed and orientation is accomplished by the ACMS. Figure 1-1 illustrates the functional block diagram of the baseline ACMS. The operational sequence of the subsystem functions is summarized for the probe bus mission in Table 1-3 and for the orbiter mission in Table 1-4.

The proposed attitude determination design utilizes dual slit sun and star sensors to measure the sun and star positions relative to spacecraft

TABLE 1-2. ACMS KEY TRADEOFF AND ISSUES SUMMARY FOR ATLAS CENTAUR BASELINE

Tradeoff/Issue	Baseline Selection	Other Alternatives Considered	Rationale For Selection
Attitude determination concept	Use sun and stars for inertial target	Use earth and Venus as inertial targets	Provide best operational flexibility Sun and stars provide better point source targets throughout mission Existing sensor design technology can be used
Star visibility versus spin axis orientation during cruise	Point spin axis parallel to south ecliptic normal	Point spin axis parallel to north ecliptic normal	More detectable stars in southern hemisphere
Thruster configuration	2 axial jets (3 on orbiter) 4 radial jets	Various configurations which would provide acceptable performance	Minimum number of jets for complete operational redundancy and minimum system weight
Sun sensor type	Dual slit type	Digital sun aspect type and analog type sensor	Simplest design Lowest cost Can use common data processor electronics with star sensor Existing design and space proven
Star sensor type	Solid state dual slit detector type	Photomultiplier tube (PMT) detector type	Lowest weight Lowest program cost Most reliable
BAPTA design			
Motor	Brushless motor	Brush motor	Existing design and space proven
Shaft and housing material	Beryllium	Titanium	Lowest weight
Shaft angle encoder	Optical	Magnetic and Mechanical	Lowest weight Low spin speed operation capability
Magnetometer deployment boom design	3 segment (non-retractable) type	5 segment (non-retractable) type; SPAR bi-stem (retractable) type and coilable lattice (retractable) type	Failure of retractable boom to "retract" during retro firing will cause spacecraft mission failure Lowest weight

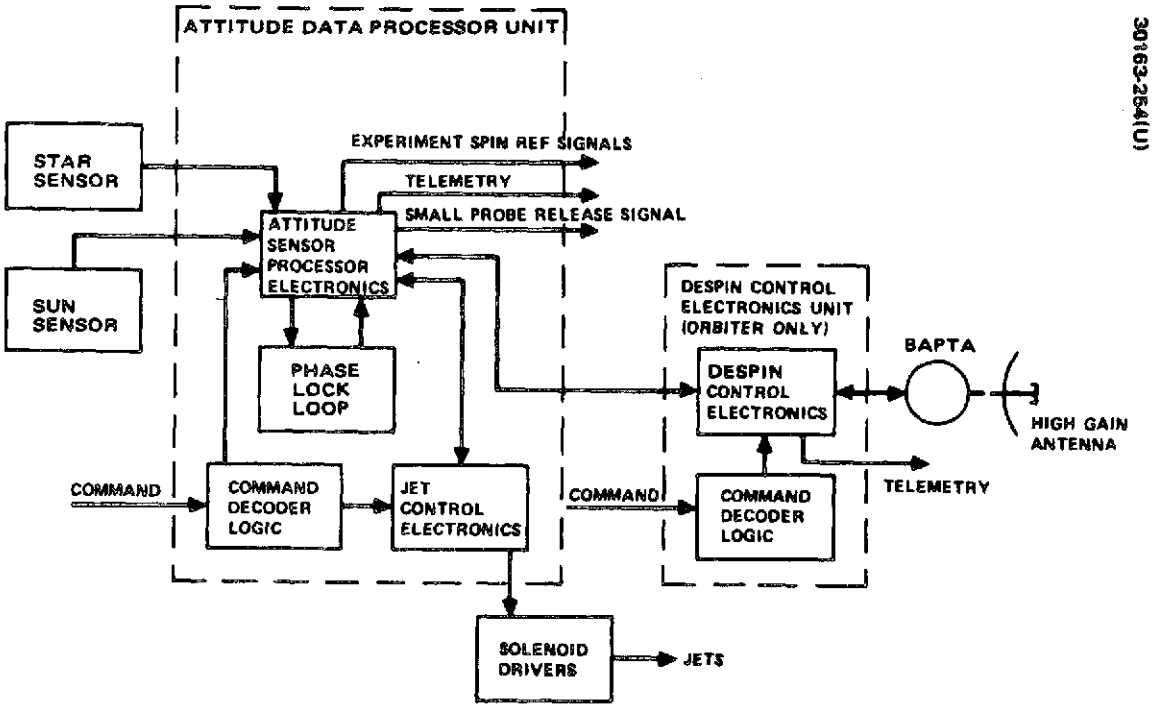

FIGURE 1-1. ACMS FUNCTIONAL BLOCK DIAGRAM

TABLE 1-3. MISSIONS SEQUENCE PROBE BUS ACMS FUNCTIONS

Mission Time	Event	ACMS Functions	Notes
Separation = S	Booster/spacecraft separation	ACMS activated by commands from command subsystem	
		Spin down rotor from 90 to 60 rpm	Thor/Delta (T/D)
		Spin up rotor from 0 to 5 rpm	Atlas/Centaur (A/C)
		Deploy bicone antenna	T/D
S + 0.3 h	Reorient spin axis to south elliptic normal	Attitude maneuver with axial jets	T/D
		Nutation damping	
S + 1.0 h	Cruise operations (after acquisition)	Spin speed trim	
		Attitude determination using sun and star data	
		Deploy magnetometer boom	T/D
		Attitude trims to maintain spin axis normal to ecliptic ±2.50 deg	
		Nutation damping	
S + 5, 20 and 50 days; and encounter (E) -30 days	Trajectory corrections	Attitude maneuvers with axial jets	
		ΔV maneuvers using axial jets and/or radial jets	
		Attitude determinations as required	
		Nutation damping	
E - 23 days	Large probe release	Attitude maneuvers with axial jets	
		Spin speed trim to 15 rpm	
		Attitude determination	
		Nutation damping	
E - 20 days	Small probe targeting and release	Spin speed trim to 71 rpm	T/D
		Spin speed trim to 47 rpm	A/C
		Attitude maneuvers with axial jets	
		ΔV maneuver with radial jets	
		Nutation damping	
		Attitude determination	
		Spin angle release signal for small probes	
E-20 to E-18 days	Probe bus coast	Spin speed trim to 60 rpm	
		Attitude maneuver with axial jets	
E-18 days	Probe bus trajectory correction	Attitude maneuver with axial jets	
		Attitude determination	
		ΔV maneuver with axial jet	
		Attitude determination	
E-18 day to entry	Probe bus coast	Attitude determination	
		Attitude trims as required	

TABLE 1-4. MISSION SEQUENCE OF ORBITER ACMS FUNCTIONS

Mission Time	Event	ACMS Functions	Notes
Separation = S	Booster/spacecraft	ACMS activated by commands from command subsystem Spin down rotor from 90 to 60 rpm Spin up rotor from 0 to 5 rpm	 Thor/Delta (T/D) Atlas/Centaur (A/C)
S + 0.3 h	Reorient spin axis to south ecliptic normal	Attitude maneuver with axial jets Nutation damping	T/D
S + 1.0 h to encounter	Cruise operations (after acquisition)	Spin speed trims Attitude determinations as required Deploy magnetometer boom Spin up to 30 rpm Attitude trims to maintain spin axis normal to ecliptic ±2.5 deg	 A/C
S + 5, 20 and 50 days; and insertion (I) -20 days	Trajectory corrections	Attitude maneuvers with axial jets ΔV maneuvers using axial and/or radial jets Attitude determinations as required Nutation damping	
S + 5 days (after first midcourse)	Initial despin of hi-gain antenna	Spin down rotor to 30 rpm Activate antenna despin control and point toward earth line of sight	T/D
I - 1 day	Inversion maneuver	Reorient spin axis to north ecliptic normal Attitude determination Nutation damping	T/D T/D
I - 2.5 h	Orbit insertion maneuver	Attitude maneuver Attitude determination Nutation damping "Preburn" ΔV with axial jets in the blind	
I + 0.5 h	Sun reorientation	Attitude maneuver normal to sunline Nutation damping Attitude determination after reacquisition	
I + 1.0 h to + 2 days	Initial orbit operation	Attitude maneuver to south ecliptic normal Attitude maneuver to north ecliptic normal Attitude determination ΔV maneuvers with axial jets Nutation damping Despin hi-gain antenna	T/D A/C
I + 2 days to +225 days	Science operations	Periodic attitude determinations Weekly attitude maneuvers to maintain spin axis normal to elliptic ±2.5 deg Weekly ΔV maneuvers to maintain 24 hour orbit period and periapsis altitude Despin hi-gain antenna	

coordinates. The sensors detect a field of view (FOV) crossing of the selected inertial target each spin period due to vehicle spin rotation. Both sensors use silicon detectors to develop an electrical pulse when the target crosses the FOV. Three sun sensors used to cover an elevation FOV of 90 ± 75 deg relative to the spin axis. The star sensor is capable of detecting +1.0 silicon magnitude stars with a FOV of 25 deg centered nominally 58 deg from the + spin axis. During the cruise phase of the mission, the spin axis is pointing toward the south ecliptic pole to provide the best star visibility. A significant feature of the proposed design is that both start sensor slits are utilized independently for attitude determination. This is possible since each slit contains its own silicon detector and signal conditioning electronics. By taking advantage of sun-star-spacecraft geometry and the capability of selecting several different stars as stellar targets throughout the mission, the two star slit measurements are redundant to one another. Therefore, one star sensor with independent dual slit detectors provides equipment redundancy.

The electrical signals from the sensors are processed by a common attitude data processor (ADP) electronics unit. The time intervals between pulses are measured and transmitted to the ground station for computation of the spacecraft attitude. In addition, on board azimuth spin pulses are processed for spin period synchronization of star gates, reaction jet firings, probe release timing and science instruments references. A commandable spin angle star gate is utilized in conjunction with a commandable star detection threshold setting to provide star reference selection capability. Both star phase angle and brightness discrimination is used to minimize the false alarm rate (FAR) and maximize the probability of detection. This provides the operating flexibility to select the best stars to be used with the sun for attitude determination throughout all mission phases.

The performance of the proposed attitude maneuver control design is largely dependent on the reaction jet configuration (part of the propulsion subsystem). The baseline arrangement has been selected to provide the most reliability and flexibility for accurate execution of ΔV, precession, spinup, and spindown maneuvers with six jets. Two axial jets pulsed together or separately at spin frequency generate spin axis precession; fired continuously and separately, they generate translational ΔV along the spin axis direction. Two pairs of radial jets thrust perpendicular to the spin axis at different c.g. locations. Any pair pulsed at spin frequency will generate translational ΔV as well as some precession. A single radial jet of either pair fired continuously generates spinup or spindown. Addition of a seventh jet on the orbiter spacecraft provides redundancy for orbital operations as well as several other desirable features, e.g., another attitude control mode; redundancy for the retro-preburn maneuver; and two additional ΔV modes, one of which allows a balanced thrust to execute orbital corrections at 5 rpm with minimal attitude perturbations. The latter feature is significant since a single axial jet must be pulsed in a 180 deg bang-bang mode when used for orbital corrections at 5 rpm. This mode consists of pulsing the jet at twice spin frequency to accumulate ΔV and limit attitude movement when angular momentum is low. A mercury tube damper provides for passive damping of induced nutational disturbances, thereby guaranteeing asymptotic nutational stability for the spacecraft.

The orbiter high gain directional antenna necessitates continuous antenna boresight pointing towards the earth line-of-sight. A despin control electronics (DCE) unit provides the control of the orientation of the despun assembly section to satisfy this objective. Sun or star sensor information is utilized to establish the inertial attitude of the rotor. A shaft angle encoder (SAE) located in the bearing and power transfer assembly (rotating interface) establishes the relative phase relationship between the rotor and the platform. A brushless dc torque motor provides the torque to control the antenna boresight pointing at a ground commandable phase relationship relative to the selected inertial reference. This control torque continuously compensates for disturbance torques produced by the bearing and sliprings. The resultant steady state pointing error shall be less than ±1.0 deg.

The hardware elements which comprise the baseline ACMS are listed in Table 1-5, along with their prior program usage. The location of these elements on the spacecraft is indicated on Figure 1-2. The cross strapping of the ACMS elements is illustrated in Figure 1-3. The only elements not redundant are the star sensor sun shade and optics, BAPTA bearings and motor core iron, and the nutation damper. However, these items have such high reliability that the weight required for redundancy is not warranted.

The sun sensor design is essentially identical to those flow on the ATS, Intelsat IV, and Telesat satellites, differeing only in the sensor mounting bracket design.

The star sensor is a new design utilizing existing solid state detector technology. A survey of existing star sensor manufacturers concluded that no existing sensor is available with the capability of operating over the wide range of spin speeds required for the Pioneer Venus mission. Relaxing the weight constraints makes a photomultiplier tube (PMT) detector star sensor feasible. However, two star sensors would be required per spacecraft for detector redundancy. In addition, existing PMT sensors (such as the OSO-I sensor) would require modifications to accommodate the wide range of spin speeds. Two PMT sensors per spacecraft were estimated to be much less cost effective than one solid state star sensor per spacecraft. As a result, a solid state star sensor was also selected for the Atlas/Centaur launch vehicle baseline design. Stray light from sources outside the star sensor FOV is considered the major problem in star sensor design. Rejection of stray light interference is accomplished by using a sunshield or baffle to prevent the "out of the FOV" scattered light from striking the sensor optics. In addition, the star gate prevents the sensor from responding when unwanted light sources are in the FOV; i.e., Sun, Venus, Earth, or other stars.

The controls electronics design is similar to units built for other Hughes spin stabilized satellites (Intelsat IV, Telesat, and military satellites). The primary difference will be scale factor changes required for the wide spin speed range (5 to 60 rpm) of operation required for the Pioneer Venus mission.

The BAPTA design is similar to the units Hughes built for the Telesat program, except for a modification to the shaft angle encoder for the low

TABLE 1-5. ACMS BASELINE EQUIPMENT LIST

Component	Number Per Spacecraft	Mass, kg (lb)	Power, W	Deviation
Sun sensors	3	0.1(0.2)/unit	--	Telesat
Star sensors	1	2.5 (5.5)	1.0	New
Attitude data processor	2	1.6(3.6)/unit	4.0	Milsat
Solenoid drivers (jet and latch valves)	1	1.04 (2.3)	2.0 (1 percent duty cycle)	Intelsat IV
Nutation damper	1	1.36(3.0)	--	Telesat
BAPTA (orbiter only)	1	6.62 (14.6)	1.0	Telesat
Despin control electronics (orbiter only)	2	1.95(4.3)/ unit	5.0	Telesat
Thermal Louvers (probe bus) (orbiter)	10 12	0.29(0.65)/ unit	--	Milsat
Pin pullers (orbiter only)	1	0.06(0.14)/ unit	--	OSO
Magnetometer deployment mechanism (orbiter only)	1	(7.2)	--	New

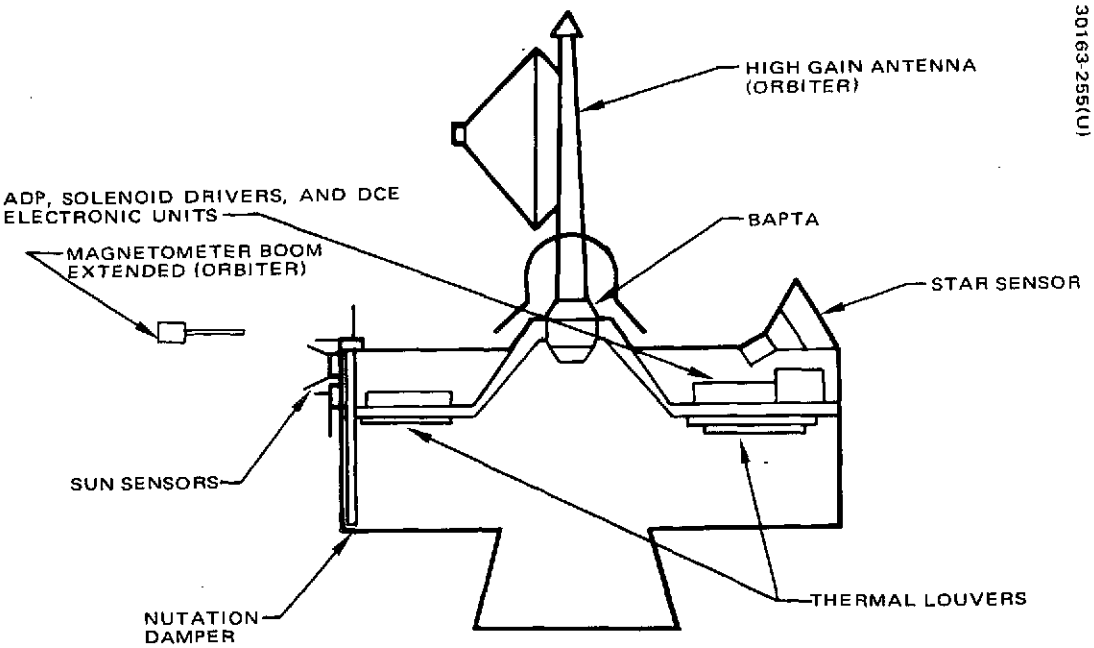

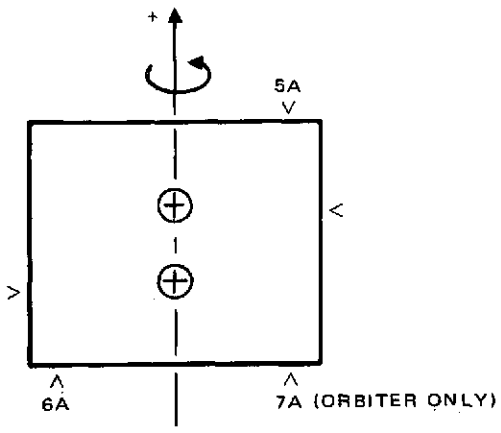

AXIAL JETS ARRANGEMENT

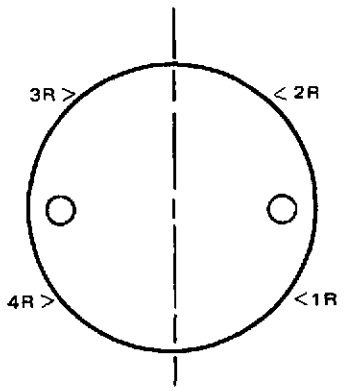

RADIAL JETS ARRANGEMENT

FIGURE 1-2. ACMS ELEMENTS ARRANGEMENTS

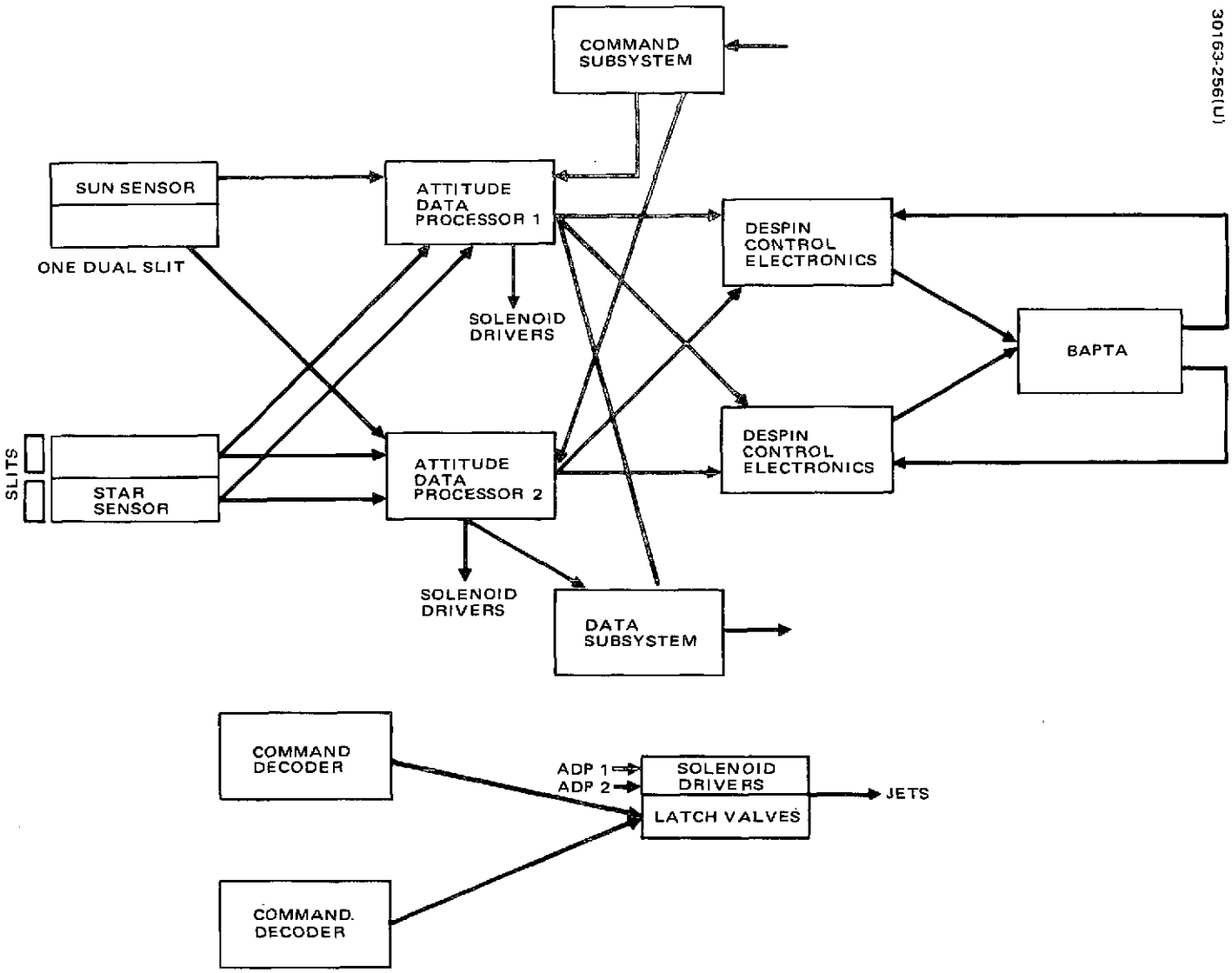

FIGURE 1-3. ACMS ELECTRICAL CROSS STRAPPING CONFIGURATION

spin speed requirements, addition of sliprings, and a material change (beryllium) to reduce weight.

The nutation damper is a scaled Telesat satellite design.

The deployment mechanisms are a new design since the requirements are unique to the Pioneer Venus spacecraft design and mission. The principal designs concerns are the deployment dynamics of the magnetometer boom. To insure success, the design must be analyzable and testable prior to launch. To this end, a detailed mathematical model of the proposed design will be formulated in order to predict and analyze the load dynamics and stresses on the mechanism during deployment.

In conclusion, no major technical problems are anticipated in the design and development of the attitude control and mechanisms subsystem for the Pioneer Venus mission utilizing existing hardware and technology. The design of the star sensor sunshield and the preamplifier to achieve a low noise level (i.e., good signal-to-noise ratio), and the design of the magnetometer deployment mechanism are areas which design emphasis will be applied during the spacecraft development.

2. INTRODUCTION

The purpose of this report is to present the baseline attitude control and mechanisms subsystem (ACMS) design approach and to show how the design concept satisfies detail mission requirements using a Thor/Delta launch vehicle. The baseline design approach stems from a series of trade studies (bibliography) guided by mission objectives, simplicity of design, and maximum utilization of space proven hardware. The specific objectives accomplished in the task studies were:

1) Define the mission attitude determination requirements

2) Identify candidate celestial references sources for attitude determination

3) Analysis and tradeoff candidate sensing schemes

4) Develop preliminary inertial attitude determination mechanization scheme for the selected sensor configuration

5) Identify candidate jet thruster configurations

6) Identify attitude and ΔV errors associated with jet thruster configuration and required maneuvers

7) Develop alternate jet thruster modes for selected baseline configuration

8) Identify and develop candidate despin control mechanizations for orbiter hi-gain antenna pointing

9) Survey current hardware designs being used on existing space programs to determine applicability for the Pioneer Venus mission

10) Analyze the proposed baseline design to assess the performance and feasibility of implementation

11) Define hardware performance and design characteristics of the baseline design

12) Identify potential problem areas associated with proposed design

Section 3 of the report contains the mission requirements relative to attitude determination for probe spacecraft launch in January 1977 and an orbiter spacecraft launch in May 1978.

Section 4 contains the conceptual design tradeoffs and considerations made in selecting a baseline attitude sensor and thruster configuration.

Section 5 functionally describes the baseline design for the spacecraft to be launched by Thor/Delta launch vehicle.

Appendices A and B describe the analysis and models used to verify the performance aspects of the baseline design.

Appendix C describes the detail hardware components that comprise the baseline design.

An additional study task was added which required the investigation of the use of an Atlas/Centaur as the spacecraft launch vehicle. As a result, mission requirements, science requirements, and weight allocations were modified in an attempt to reduce spacecraft cost. Section 6 of this report summarizes the changes in requirements and the subsystem design tradeoffs made in selecting a baseline design for the Atlas/Centaur launched spacecraft.

Sections 3 through 5 of this report are based on the mission and spacecraft baseline design existing at the midterm study review presented to NASA-Ames Research Center on 26 February 1973 using the Thor/Delta launch vehicle. Section 6 of this report is based on the science payload definition and mission requirements existing on 30 April 1973 and represents a preliminary analysis of the design impact of these requirements on the subsystem design.

3. FUNCTIONS AND REQUIREMENTS

The Pioneer Venus mission employs two spacecraft, a probe bus and an orbiter, as transport vehicles for the science instruments. The attitude control and mechanisms subsystem (AMCS) shall provide the means for controlling the spacecraft attitude, angular momentum, translational velocity, and mechanically articulated elements during all phases of the mission after separation from the launch vehicle.

The primary functions to be performed by the ACMS are tabulated in Table 3-1. Conventions and definitions used in this section are presented in Table 3-2. Spacecraft mass properties assumed are shown in Table 3-3.

The purpose of this section is to summarize the preliminary design and performance requirements of the ACMS. Requirements are obtained from contractual requirements, mission operational requirements, and system design requirements. Performance requirements and error sources are identified so that they may be controlled in subsequent design specifications.

3.1 OPERATIONAL REQUIREMENTS

The attitude and velocity control maneuver requirements are derived from the planned mission scenarios. To maximize commonality of the designs between the probe bus and the orbiter spacecraft, the mission scenarios have been made as similar as is possible. To accomplish this, the transit phase sequence of events for both spacecraft are planned to be nearly identical. The maneuvers requirements for the probe bus encounter phase must differ from the orbiter Venus orbit insertion maneuvers because of different mission requirements. The in-orbit science phase maneuvers for the orbiter will be similar to the transit phase of the missions, thus resulting in similar performance requirements.

Transit Phase

The transit phase of both missions will require initial spin speed corrections and spin axis precession maneuvers following acquisition of the spacecraft by the ground tracking stations. The spin speed will be adjusted to approximately 60 rpm, and the plus spin axis will be positioned to point normally toward the south ecliptic pole for the cruise phase of the mission.

TABLE 3-1. BASIC ACMS FUNCTIONS

Function	Provision
Attitude sensing	Provide attitude sensors, sensor data processing, and telemetry data conditioning required for ground determination of the spin axis attitude in celestial coordinates.
Attitude/velocity control	Provide controls for the firing of propulsion subsystem reaction jets to precess the spin axis attitude and change the spacecraft velocity in response to ground commands.
Spin speed control	Provide control of the firing of propulsion subsystem reaction jets to change the rotor spin speed in response to ground commands.
Nutation damping	Provide positive damping of the spin axis nutation motions.
Spin angle reference	Provide a spin angle reference relative to celestial references for science experiments.
Despun antenna control (orbiter only)	Provide automatic azimuth rate stabilization and pointing control of the despun antenna in response to ground commands.
Bicone deployment (probe only)	Provide mechanism for extension of bicone antenna following separation from Thor/Delta launch vehicle.
Magnetometer deployment	Provide mechanism for extension of magnetometer head following separation from launch vehicle.

TABLE 3-2. CONVENTIONS AND DEFINITIONS

Term	Definition
Primary reference plane	The separation plane between the launch vehicle adapter and the spacecraft
Spacecraft coordinate system	Consists of three mutually perpendicular axes: x, y, and z. The x and y axes lie parallel with the primary reference plane. The z axis is perpendicular to the primary reference plane. The spacecraft shall spin about the z axis. The origin of coordinate system is at the spacecraft center of mass.
Spacecraft angular reference	The roll axis is coincident with the spacecraft z axis. The pitch (x) axis passes through the center of gravity and lies in the plane containing the z axis and the sun sensor. The yaw (y) axis forms a right-hand coordinate system.
Spacecraft station numbers	The Hughes Station 0.00 shall be the planar surface at the primary reference plane. Positive station numbers shall be assigned along the z axis in the +z direction (forward). Negative numbers shall be below the separation plane (aft), i.e., into the additional volume provided outside or within the adapter.
Field of view	The solar angle through which the optical sensors are sensitive to external stimulation
Alignment reference axis	Defined by a physical reference fixture which has a known relationship to the center lines of the field of view
Line of sight	A line passing through the spacecraft center of the mass and a point in inertial space
Sun or star angle	The angle between the sun or star line of sight and the spacecraft z-axis
Spin axis	The inertial spin axis of the spinning section
Angular momentum vector	The vector which defines the total angular momentum of the spacecraft, including the motions of all elements relative to the spacecraft center of mass. The direction of the angular momentum vector is normally in the direction of the +z axis.
Rotor bearing axis	The axis about which the spinning section nominally rotates relative to the despun section (orbiter only)
Bearing runout	The instantaneous deviation of a rotational axis from the nominal axis of rotation (orbiter only)
Nutation	The coning motion of the spin axis relative to the angular momentum vector
Wobble	The coning motion of the spacecraft z-axis at rotor spin frequency relative to the spin axis due to dynamic unbalance of the rotor

TABLE 3-3. PIONEER VENUS SPACECRAFT MASS PROPERTIES ANALYSIS — THOR/DELTA BASELINE MISSION PROFILE

Condition	Mass		Center of Gravity		Moment of Inertia						I_R/I_T
					I_x		I_y		I_z		
	kg	lb	M	In.	kg-M^2	Slug-ft^2	kg-M^2	Slug-ft^2	kg-M^2	Slug-ft^2	
Multiprobe spacecraft											
At launch, boom retracted	384.10	846.8	1.07	42.3	139.8	103.1	132.5	97.7	163.8	120.8	1.20
At launch, boom extended	384.10	846.8	1.07	42.3	141.0	104.0	134.6	99.3	167.2	123.3	1.21
After large probe separation	248.75	548.4	0.94	32.1	94.8	69.9	96.1	70.9	147.6	108.9	1.55
After small probe separation	146.83	323.7	0.73	28.8	48.8	36.0	50.3	37.1	88.4	65.2	1.79
Orbiter spacecraft											
At launch, boom retracted	292.84	645.6	0.71	28.0	72.1	53.2	64.8	47.8	111.0	81.9	1.62
At launch, boom extended	292.84	645.6	0.71	28.0	73.5	54.2	67.0	49.4	114.4	84.4	1.63
Before Venus orbit insertion	279.82	616.9	0.72	28.4	68.3	50.4	65.9	48.6	110.1	81.2	1.64
In Venus orbit	191.10	421.3	0.74	29.1	66.3	48.9	63.9	47.1	108.2	79.8	1.66
Spent spacecraft	179.75	396.3	0.75	29.7	61.0	45.0	62.5	46.1	103.9	76.6	1.68

Following the initial reorientation maneuver, the bicone antenna will be mechanically deployed on the probe bus and the magnetometer will be mechanically extended by a boom on each spacecraft. Midcourse trajectory correction maneuvers are planned to occur at 5, 20, and 50 days after launch. A final trajectory correction is planned at 30 days from encounter for the probe bus, and at 20 days from orbit insertion for the orbiter. The probe bus transit phase is approximately 108 days duration. A mechanically despun antenna satisfies the orbiter rf requirements during both the transit and orbital phases of the mission. The attitude determination and maneuver requirements for the transit phase of the mission are summarized in Table 3-4 for the probe bus, and Table 3-5 for the orbiter.

Probe Bus Encounter Phase

The encounter phase (starting at E-20 days) of the probe bus mission requires reorientation of the spin axis along the spacecraft velocity vector and spin down to approximately 15 rpm for large probe separation. Following large probe release, a small probes targeting (ΔV) maneuver and rotor spin up to approximately 71 rpm prior to small probes separation will be required. After small probes separation, the spin axis will be reoriented to the north ecliptic pole and the spin speed adjusted to approximately 60 rpm to allow battery charging, thermal control and use of the bicone antenna for approximately 2 days. At E-18 days, a bus targeting (ΔV) maneuver will be required to adjust the entry trajectory. Following the bus targeting maneuver, the spin axis attitude will be oriented to obtain a sun angle of 45 deg for the power subsystem and thermal control. At E-10 days, the spin axis attitude will be adjusted to the final position for entry into the Venus atmosphere.

Orbiter Encounter Phase

The Venus orbit insertion phase of the orbiter mission starts at I-1 day with a reorientation of the spin axis to the north ecliptic pole. At approximately 1.5 h prior to firing of the retro motor for orbit insertion, the spin axis will be precessed (in the orbit plane) 27 deg from the north ecliptic pole for thrust-vector alignment. Immediately prior to retro firing, a preburn firing of the propulsion subsystem reaction jets will be required to dump excess propellant not used during the transit phase of the mission. The preburn and retro motor firing maneuvers must be executed automatically from stored (on board) ground commands because of earth occultation by Venus. If the spacecraft has not been reacquired by the ground station, 30 min following retro firing, the spin axis attitude will be precessed automatically to the north ecliptic pole for thermal control. After reacquisition of communication by the ground station, the spin axis will be precessed to the south ecliptic pole to start the in-orbit cruise science operations. Initial orbit trim (ΔV) maneuvers will be required to correct the orbit period and periapsis altitude. Subsequent orbit trims and attitude corrections will be required on a weekly basis for a period of 225 days.

TABLE 3-4. PROBE BUS ATTITUDE DETERMINATION AND MANEUVER REQUIREMENTS

Mission Phase	Time,* days L. = Launch E = Encounter	Spin Axis Orientation (Ecliptic Coordinate)		Attitude Measurement Uncertainty		Spin Rate, rpm	Nominal Sun Angle, deg	Nominal Maneuvers			Operation Time, Hours
		Right Ascension, deg	Declination, deg	Spin Axis, deg	Spin Angle, deg			Δ MPS	Δdeg	Δrpm	
Acquisition	L + 0	39	-25	±5.0	±0.4	60±10	38	--	66.4	-30	0.7
Cruise	L + 0 to 108	Random	-90 ±3	±0.9	±0.4	60	90	—	—	—	—
Midcourse maneuvers	L + 5, 20, 50, 98	Random	$-90 < \delta < 0$	±3.0+	±0.4	60	15 to 165	<72	<190.4	—	1.0
Large probe separation	E - 20	13	+28	±2.5	±0.4	15	45	—	126.9	-45	3.0
Small probe separation	E - 20	39	+36	±2.5	±0.4	71	37	< 5.4	24.1	+56	1.5
Bus coast	E - 20 to -18	Random	+90 ±3	±1.0	±0.4	60	90	—	52.9	—	0.3
Bus targeting	E - 18	16	+ 7	±3.0	±0.4	60	38	<16.7	83.1	-11	3.0
Bus coast	E - 18 to -10	8	0	±2.5	±0.4	60	45 to 58	—	11.6	—	0.3
Bus entry	E - 10 to E	14	+ 3	±2.5	±0.4	60	50 to 68	—	7.5	—	0.3

*Assumes launch date January 1977

+Assumes thrust parallel to the spin axis

TABLE 3-5. ORBITER ATTITUDE DETERMINATION AND MANEUVER REQUIREMENTS

Mission Phase	Time,* days L = Launch E = Encounter	Spin Axis Orientation (Ecliptic Coordinate)		Attitude Measurement Uncertainty		Spin Rate, rpm	Nominal Sun Angle, deg	Nominal Maneuvers			Operation Time, Hours
		Right Ascension, deg	Declination, deg	Spin Axis, deg	Spin Angle, deg			ΔMPS	Δdeg	Δrpm	
Acquisition	L + 0	199	-11	±5.0	±0.4	60±10	92	–	80	-30	0.7
Cruise	L + 0 to +5	Random	-90 ±3	±0.9	±0.4	60	90	–	–	–	–
Midcourse maneuvers	L + 5, 20, 50, 167	Random	-90<δ<0	±3.0†	±0.4	60 to 30	15 to 165	<72	<190.4	–	1.0
Cruise	L + 5 to 186	Random	-90 ±3	±0.9	±0.4	30	90	–	–	-30	0.3
Insertion reorientation	I - 1	Random	+90 ±3	±0.9	±0.4	30	90	–	180	–	0.5
Orbit insertion (retro)	I - 0	27	+63	±2.5	±0.4	30	108	–	27	–	2.0
Post insertion reorientation	I - 0	Random	+90 ±3	±0.9	±0.4	30	90	–	<207	–	2.0
In orbit cruise, (science)	I + 1 to +225	Random	-90 ±3	±0.9	±0.4	5	90	–	–	-25	0.3
In orbit periapsis ΔV	I + every 7	Random	-90 ±3	±0.9	±0.4	5	90	<5.0	–	–	<3.0
In orbit apoapsis ΔV	I + every 7	Random	-90 ±3	±0.9	±0.4	5	90	<0.5	< 5.0	–	<3.0

*Assumes launch date May 1978 and 27 deg North periapsis latitude Venus orbit

†Assumes thrust parallel to the spin axis

3.2 SUBSYSTEM REQUIREMENTS

The ACMS must provide an attitude reference and science instruments, thrust vector control, and communication antenna pointing capability. It will therefore be necessary to determine and control both the inertial attitude of the spacecraft spin axis and the phase of the inertial spin angle throughout all mission phases. Time and operational conditions permitting, the attitude control function can be accomplished most reliably by minimizing the complexity of spacecraft performed functions and performing all attitude and maneuver computations at the ground station. An analysis of both the probe and orbiter spacecraft mission scenarios indicates this philosophy is practical and can be implemented. Therefore, the spacecraft will be required to make only attitude data measurements. The data will be telemetered to the ground station for processing to obtain near-real-time attitude determination. Following the attitude determination by the ground station, commands will be generated and transmitted back to the spacecraft as required for velocity and attitude control maneuvers, antenna pointing and spin angle pointing references for the science instruments. The subsystem functional requirements are discussed in the following paragraphs.

Attitude Determination Requirements

The system (including both the spacecraft and the ground station) shall be capable of measuring the spacecraft spin axis orientation relative to selected inertial references throughout the operational phases of both the probe mission and the orbiter mission. The measurements shall be made by spacecraft sensors and the data transmitted via telemetry to the ground station for processing and attitude determination computations. Attitude determinations will be made prior to and following all orbital and attitude orientation maneuvers to ascertain the spacecraft attitude.

The spin axis orientations necessary to fulfill the mission objectives will have a significant impact on the attitude determination scheme. Both the probe and orbiter spacecraft spin axis shall be oriented normal to the ecliptic plane throughout the cruise mode of operation to provide maximum science coverage and to minimize the weight of the power and thermal control subsystems. The spin axis attitude shall be determined to an accuracy of ± 0.9 deg to provide a known inertial reference for the science instrument pointing, antenna pointing, and thrust vector pointing. The spin axis attitude needs only periodic measurement; the spin angle must be measured continuously.

Since most of the available celestial references lie within ± 60 deg declination of the ecliptic plane, simple stellar detectors can be placed on the spinning spacecraft for viewing selected celestial references each spin period. In general, all key spacecraft maneuvers will start from the cruise mode attitude, i.e., normal to the ecliptic. Assuming that the required attitude precession and ΔV maneuvers can be accurately and predictably performed, only the initial cruise mode attitude determination is essential to mission success. However, it is highly desirable to have positive confirmation of the new spacecraft attitudes following any maneuvers. As a primary objective, therefore, the attitude determination scheme should be capable of

determining the spacecraft attitude at all required attitudes. In addition, the attitude determination scheme should permit recovery of attitude control from all random spacecraft attitudes.

The attitude determination scheme must be capable of proper operation in the presence of full sun light and maximum Earth and Venus albedo on both the probe and orbiter buses. In addition, an inertial reference will be required on the orbiter bus for the antenna despin control system and science instruments for up to 3 h during sun eclipse and earth occultation periods. The eclipse and occultation periods may occur simultaneously during some periods of the mission.

The time from the initiation of an attitude determination operation to the availability of valid attitude data should not exceed 3 h. Quick look attitude determination checks should be capable of being performed using raw telemetry data. The attitude determination scheme must be compatible with the science data gathering requirements.

The system shall be capable of determining the actual spacecraft attitudes for orientations shown in Tables 3-4 and 3-5 to the accuracies indicated.

Maneuver Control Requirements

The ACMS must provide the control required for a combination of jets that satisfies all attitude, ΔV, and spin speed requirements during the various mission phases. The spacecraft is also required to be spin stabilized for attitude stability. In addition, the ACMS must provide damping of any nutational transients induced by maneuvers.

The firing of reaction jets to control the spacecraft spin speed, spin axis attitude and velocity shall be executed from stored commands received from the ground. The spacecraft will be in view of the ground station during all required maneuvers, except during the retro firing for orbit insertion of the orbiter spacecraft. However, direct real time maneuver control will not be possible due to long communication time delays (see Figure 3-1). Therefore, the magnitude and direction of each required maneuver will be computed on the ground and executed automatically by the spacecraft at the proper time upon receipt of ground control commands.

A preliminary spin axis attitude error budget has been originated and is summarized in Table 3-6. The average spin axis attitude must be maintained to ± 2.5 deg of ecliptic normal for communication antennae coverage in cruise and orbit as well as science instruments pointing in orbit. During cruise and orbital operations, the average spin axis attitude will be measured to an accuracy of ± 0.9 deg. The attitude correction frequency will depend on the disturbance torques (solar, aerodynamic, maneuver). The average spin axis attitude must be controlled to ± 3 deg of desired attitudes required for probe separation, probe bus entry, and orbit insertion. In these instances, the average spin axis attitude is nominally measured to an accuracy of 2.5 deg. However, if initial attitude uncertainty and open loop precession errors are

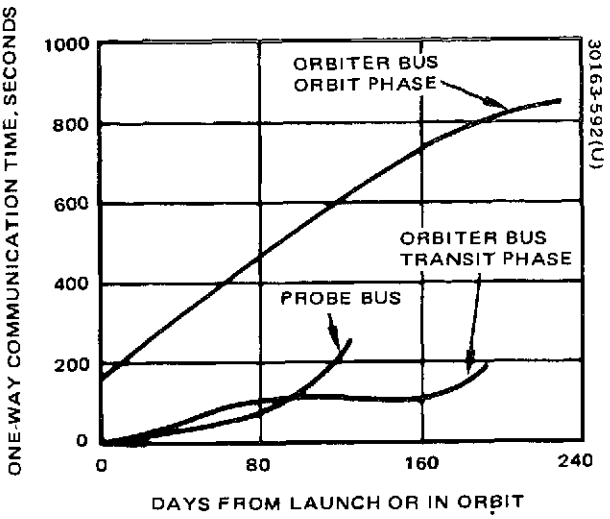

FIGURE 3-1. ONE-WAY COMMUNICATION TIME DELAYS

TABLE 3-6. SPIN AXIS ATTITUDE ERROR BUDGET (3σ)

Mission Phase	Total Attitude Error Allowed (e_a), deg	Allowable Measurement Error (e_m), deg	Allowable Control Error (e_c), deg
Cruise and orbit	2.5	0.9	2.3
ΔV maneuvers			
Axial	4.0	3.0 {0.9 open loop}	2.5 {3.0 open loop}
Radial	2.0	1.0	1.7
Probe separation Bus entry Orbit insertion	3.0	2.5 {0.9 open loop}	1.7 {2.7 open loop}

Where

$$e_a^2 = e_m^2 + e_c^2$$

sufficiently small, this requirement may be satisfied without an attitude determination and touchup. The average spin axis attitude will not be allowed to be within 15 deg of the sunline so that the sun sensor can always be used as the primary roll reference.

During ΔV maneuvers, the cumulative jet impulse shall be controlled to ±4 percent magnitude and ±4 deg in direction. For a spinning vehicle, the impulse is nominally delivered at a fixed angle with respect to the inertial spin axis. Therefore, the average spin axis attitude must be controlled during ΔV maneuvers. The amount of control depends upon which type of jet is used. For thrust parallel to the spin axis (axial jets), the attitude error is the dominant one, and consumes almost the entire directional error allowed. For thrust perpendicular to the spin axis (radial jet), the attitude error is one of several significant error sources and is allocated only part (typically 2 deg) of the total directional error.

The ΔV required for midcourse maneuvers can be in an arbitrary direction. If the attitude is measured, the ΔV directional error due to attitude error is defined to be the root sum square of the measurement error and the execution error. Since the attitude determination scheme may not always allow measurement of the average spin axis attitude, the precession to the required ΔV attitude must be able to be accurately performed open loop to limit the attitude error to that allocated for the maneuver. Since the required ΔV direction may be within 15 deg of the sunline, a jet combination which permits an impulse component orthogonal to the average spin axis is required. The ACS shall appropriately constrain itself and the propulsion subsystem to satisfy these constraints.

The ΔV required for small probe targeting shall be in a direction perpendicular to the small probe separation attitude. The ΔV required to retard the probe bus shall be nearly parallel to the probe bus entry attitude. Prior to orbital insertion, a preburn parallel to the spin axis (insertion motor ΔV) direction is probably required to best fit transit and orbit trajectories. The ΔV required to correct orbital perturbations due to solar and drag effects are always parallel to the nominal spin axis direction (ecliptic normal) in the polar orbit.

The Thor/Delta spacecraft spin rate shall be controlled to 60 ±10 rpm throughout the probe bus mission, except for the large probe separation when the spin rate shall be reduced to 15 ±1 rpm and small probes separation when the spin rate shall be increased to 7$\overline{1}$ ±0.6 rpm. The orbiter bus shall operate at 60 ±10 rpm until after the first midcourse maneuvers, then the spin rate will be reduced to 30 ±5 rpm for despun antenna operation. Following firing of the retro motor for Venus orbit insertion, the spin rate shall be reduced to 5 ±1 rpm for in-orbit science operation.

Stability Requirements

The spacecraft shall be statically and dynamically balanced to reduce the wobble of the spin axis. The wobble angle shall not exceed 0.2 deg during the science phases of the mission.

The spin axis nutation due to maneuver disturbance torques shall not exceed 1.6 deg on the probe bus and 3.9 deg on the orbiter. Nutation damping shall be provided to reduce the residual nutation to 0.1 deg within 3 h following any maneuver. The attitude control system shall be capable of proper operation in the presence of these spacecraft motions.

High Gain Antenna Despin Control (Orbiter Only)

The attitude control system shall provide the means of despinning the high gain antenna and controlling the centerline of the beam to ±2 deg of the earthline in the spin plane. The inertial pointing of the antenna shall be commanded from the ground. The system shall be capable of automatic despin control and pointing to the commanded inertial angle over the rotor spin speed range of 4 to 35 rpm. The pointing command resolution shall be 0.4 deg.

Spin Angle Reference

The attitude control system shall provide an inertial spin angle reference for controlling the spin phase angle release of the small probes, and as a spin phase angle reference for science instruments. The phase error of the reference signal shall be ≤0.4 deg.

Mechanism Requirements

The detail requirements for each of the mechanisms are presented below. The overriding requirements implied in each design are simplicity of design, minimum weight and maximum reliability.

1) Thermal Louvers Requirements

Actuation	Unit actuated by direct sensing of the mounting surface temperature
Closing temperature set point	13 ±1°C (55 ±2°F)
Opening temperature set point	27 ±1°C (80 ±2°F)

2) Bicone Antenna Deployment Requirements (Thor/Delta baseline)

Deployment stroke	44.6 cm (21.5 in) minimum
Deployment time	10 sec
Deployment accuracy	±0.254 cm (±0.1 in)
Deployment loads	2.0 kg (4.4 lb) antenna mass Two 1 cm (3/8 in) flex coax cables

Deployed position
natural frequency

Bending	20 Hz
Torsional	20 Hz

Summary

Attitude control subsystem functional requirements are summarized in Table 3-7. These requirements form the basis for the trade studies described in the subsequent section.

TABLE 3-7. ATTITUDE CONTROL SUBSYSTEM FUNCTIONAL REQUIREMENTS SUMMARY

Function	Requirement	Derivation
Spin axis attitude determination	Error $\leq 2.5^{\circ}$ at all spin axis attitudes $>15^{\circ}$ from sunline, except error $\leq 0.9^{\circ}$ for spin axis within 5° of ecliptic normal	Initial spacecraft acquisition Midcourse maneuvers Antenna pointing Orbit insertion Probe targeting and separation Science pointing
Attitude/ΔV control	Maintain average spin axis attitude to $\pm 2.5^{\circ}$ of normal to ecliptic	Same as above
	Orient spin axis ± 3.0 of other required attitudes	Orbit period trim
	Control jet thrust vector to $\pm 4^{\circ}$ magnitude, $\pm 4\%$ direction in inertial space	Periapsis altitude adjust
Spin speed control	Vary spin speed over range of 5 to 100 rpm to $<\pm 0.6$ rpm	Third stage attitude stability, (<100 rpm) Cruise attitude stability (30 to 60 rpm) Large probe separation (15 rpm) Small probe separation (71 rpm) Experiments (5 rpm)
Nutation damping	<20 min time constant at 60 rpm <45 min time constant at 5 rpm	Transients induced by maneuvers
	Residual nutation 0.1 deg in 3 h after any maneuver	Science pointing stability
Despun antenna control	Control G_L of beam to ± 2 percent of earthline in spin plane	Mechanically despun antenna on orbiter
Spin angle reference	Measure and control inertial spin angle reference marks for experiments to ± 0.4 deg	Probe separation Strobe signal for experiments

4. DESIGN TRADEOFFS

Several design tradeoffs were required in the functional areas of attitude determination and attitude/ΔV/spin speed control. These tradeoffs are summarized in the following sections. The trades associated with fixed versus despun antenna and mechanically versus electronically despun antenna are discussed in the communications subsystem final report, Volume 7. The detailed design tradeoffs associated with the high gain antenna despin control are discussed in Appendix B of this report. The fundamental trades associated with the configuration of the mechanisms are covered in the probe bus and orbiter spacecraft trades final report, Volume 4. The detail design tradeoffs of the mechanisms is covered in Appendix C of this report.

4.1 ATTITUDE DETERMINATION

The fundamental trades associated with attitude determination were:

1) Choice of inertial attitude references: Angles between the spacecraft spin axis and two appropriately separated inertial target are required to define attitude. The optimum selection of inertial attitude references is constrained by specific mission profile.

2) Selection of attitude determination scheme: A reliable method for obtaining these two angular measurements must be selected.

Candidate Inertial Attitude References

Many celestial targets are available as candidates for taking attitude measurements throughout the Pioneer Venus spacecraft mission phases. However, in order to periodically determine the spacecraft attitude, at least two inertial references are required with a preferred angular separation of 25 to 155 deg. In addition, one inertial reference is required continuously to provide the spacecraft a spin angle reference throughout all mission phases. The primary candidates considered for this mission were the sun, Earth, Venus and stars.

The mission geometry of the spacecraft relative to the sun and planets was a primary consideration in selecting the inertial references. Figures 4-1 through 4-4 illustrate the position of the spacecraft relative to the sun, Venus, and the Earth for the multiprobe mission and the orbiter mission. The spacecraft nominal spin axis attitude is perpendicular to the plane of the ecliptic.

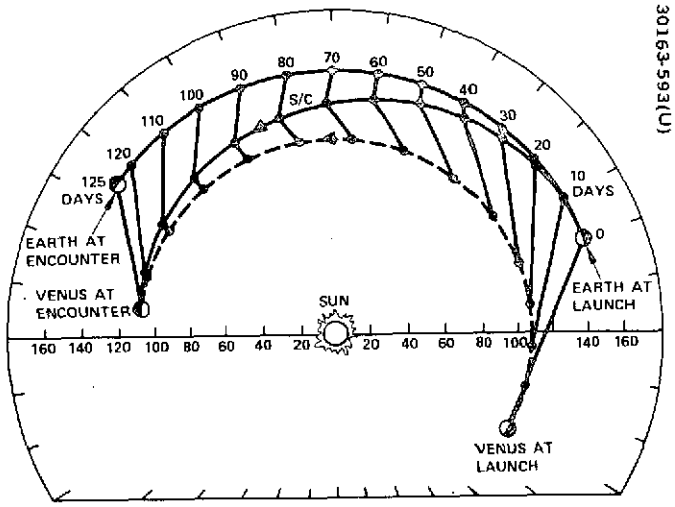

FIGURE 4-1. MULTIPROBE MISSION TRANSIT GEOMETRY

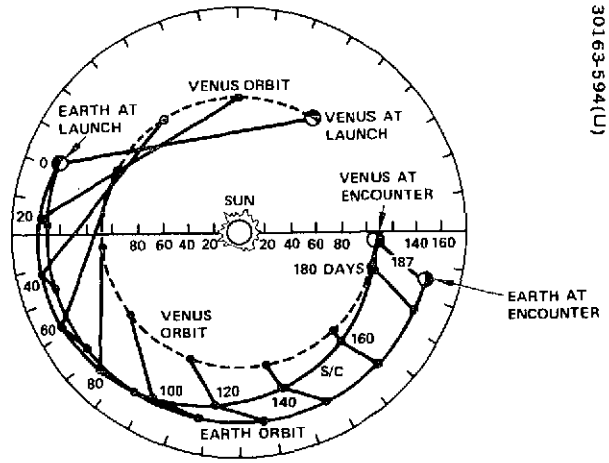

FIGURE 4-2. ORBITER TRANSIT GEOMETRY

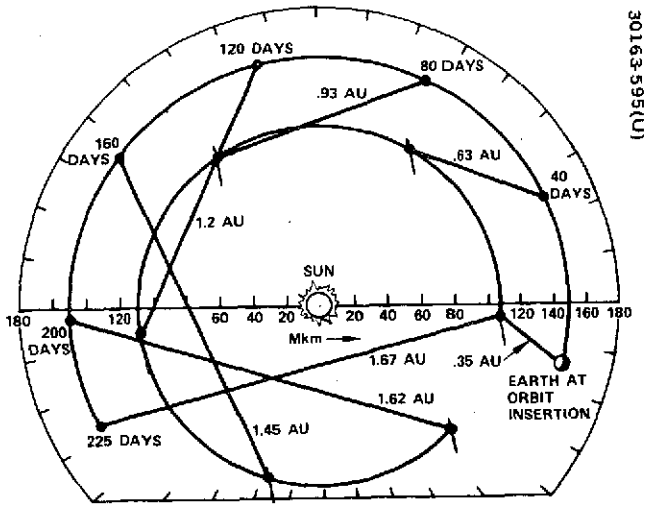

FIGURE 4-3. ORBIT PHASE GEOMETRY

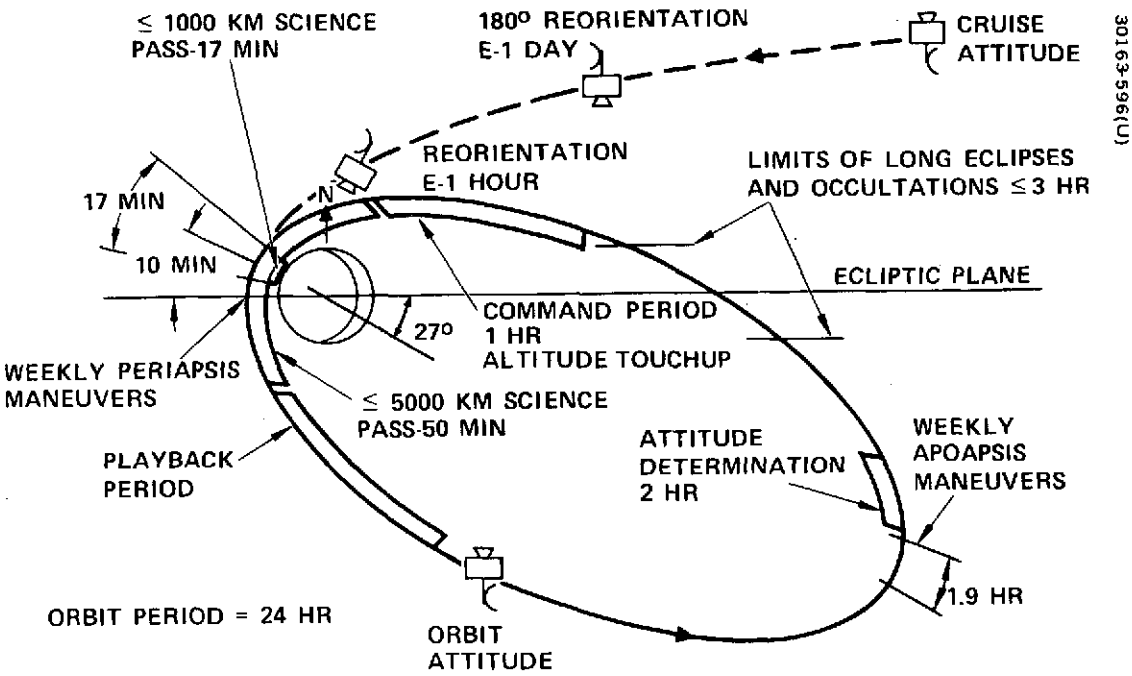

FIGURE 4-4. ORBITAL OPERATIONS

During the transit phase, the Earth and Venus as seen from the spacecraft vary considerably in distance, target size, and irradiance. If optical or passive detection systems were used to obtain line of sight measurements of the spacecraft attitude relative to these targets, the design parameter variations would require relative complex system designs. In addition, during many phases of the mission the Earth and Venus are nearly colinear and the line of sight geometry is unfavorable for accurate attitude measurements. For these reasons, the Earth and Venus were not considered to be good optical targets for the Venus mission.

The sun, on the other hand, is an easy target to detect because of its high irradiance. In addition, it is a relatively small target and will provide a relatively precise reference when scanned by a photovoltaic detector. The sun is available throughout all phases of the mission except when being eclipsed by Venus. The eclipse periods occur only for relatively short durations of the orbiter mission. Throughout the cruise and Venus orbit phase of the mission, the sun will be normal to the spacecraft spin axis. Therefore, the sun has been chosen as a primary inertial reference for attitude determination.

Another inertial reference possibility considered was use of the spacecraft communication system to provide an amplitude or frequency modulated rf signal proportional to the pointing error. One such technique, Conscan, has been used successfully on Pioneer Jupiter spacecraft. However, the Conscan approach requires the spacecraft spin axis be pointing fairly near the earth line ($\approx$ 30 deg) to get adequate angular resolution. A doppler shift detection scheme using the wide beam antenna was also considered. This scheme requires that the antennae be offset from the spacecraft spin axis to provide a carrier frequency modulation at spin frequency, the peak deviation being proportional to the sine of the angle between the spin axis and the Earth line. This scheme, then, requires the spin axis to be pointing to within 60 to 70 deg of the earth line to be effective. In addition, during combined earth occultation and sun eclipse periods, no spin angle reference would be available onboard the spacecraft for the science instruments. For these reasons, the rf schemes were not chosen; however, the doppler shift approach can be used during some phases of the mission; i.e., probe release attitudes and some midcourse maneuver attitudes, if the ground station is capable of detecting the frequency modulation.

The most numerous inertial references available are the stars. Selected stars are available as steller targets at all spacecraft attitudes throughout all phases of the missions. Selected stars can also be used during sun eclipse and earth occultation periods as an onboard spin angle reference. Due to a common characteristic of similar irradiance (low) from hundreds of detectable stars, a major problem is target discrimination. However by using only a few of the brightest stars as targets, the star identification problem can be resolved with ground operational procedures. A component tradeoff on use of star sensors indicated that the solid state design using a silicon detector is easily capable of detecting +1 silicon magnitude stars. There are approximately 25 stars brighter than +1.0 magnitude (si). A list of the 25 brightest stars obtained from the Kollsman's Silicon Star Catalog is shown in Table 4-1. The

TABLE 4-1. 25 BRIGHTEST SILICON STARS

	BS	Name		R.A.	DEC	V	SIL	VAR	Common Name
1)	2491	ALF	CMA	103.72	-39.65	-1.41	-1.41		Sirius
2)	2061 V	ALF	ORI	88.38	-16.11	0.39	-1.39	1.1	Betelgeus
3)	2326 K	ALPHA	CAR	104.67	-75.72	-0.75	-0.98		Canopus
4)	5340	ALF	BOO	203.77	30.76	-0.07	-0.93		Arcturus
5)	6134 V	ALF	SCO	249.30	- 4.48	0.91	-0.88	0.9	Antares
6)	5459 K	ALPHA	CEN	239.15	-42.46	-0.28	-0.75		Rigil Kentaurus
7)	1708	ALF	AUR	81.48	22.75	0.04	-0.45		Capella
8)	4763 K	GAMMA	CRU	216.41	-47.72	1.63	-0.37		Gacrux
9)	1457	ALF	TAU	69.39	- 5.55	0.92	-0.35		Aldebaran
10)	7001	ALF	LYR	284.96	61.74	0.03	0.03		Vega
11)	2943	ALF	CMI	115.43	-16.09	0.35	0.08		Procyon
12)	1713	BET	ORI	76.43	-31.19	0.16	0.1		Rigil
13)	8636 W	BET	GRU	321.90	-35.33	2.10	0.12		Beta Grus
14)	681 V	CMI	CET	31.10	-15.97	3.21	0.22	8.0	Mira
15)	6406 V	ALF	MER	255.73	37.34	3.13	0.22	1.0	Alpha Hercules
16)	472 K	ALPHA	ERI	344.78	-59.27	0.47	0.46		Achernar
17)	2990	BET	GEM	110.84	6.59	1.14	0.51		Pollux
18)	7557	ALF	AGL	301.42	29.36	0.73	0.61		Altair
19)	5267 K	BETA	CEN	233.44	-44.01	0.62	0.66		Hadar
20)	8775 V	BET	PEG	359.03	31.12	2.49	0.69	0.9	Scheat
21)	4730 K	ALPHA1	CRU	221.56	-52.75	0.76	0.70		Acrux
22)	337	BET	AND	30.05	25.87	2.09	0.73		Mirach
23)	5080 V	R	MYA	209.03	-12.84	4.98	0.85	7.0	(no name)
24)	3634	LAM	VEL	160.95	-55.84	2.21	0.88		Al Suhail
25)	6217 K	ALPHA	TR A	260.53	-46.00	1.92	0.98		Atria

CODE: BS – Identification number, Yale University Observatory Catalog of Bright Stars (an asterisk denotes a star not contained in the Johnson List)

R.A. – Right Ascension (degrees, ecliptic coordinates)

DEC – Declination (degrees, ecliptic coordinates)

V – Visual magnitude

SIL – Silicon Magnitude

VAR – Magnitude Variability

TABLE 4-2. CANDIDATE INERTIAL ATTITUDE REFERENCES FOR VARIOUS MISSION PHASES

Requirement

1) Attitude determination requires at least two inertial references
2) Spin angle determination requires one inertial reference

Mission Phase	Available for Reference			
	Optical		RF-Earth	
	Sun	Stars	Conscan	Doppler
Initial acquisition	Yes	Yes	Maybe	Yes
Midcourse	Yes	Yes	No	Probably
Cruise	Yes	Yes	Yes*	Yes*
Probes separation	Yes	Yes	Maybe	Yes
Probe bus entry	Yes	Yes	Yes	Yes
Polar orbit insertion	Yes	Yes	No	No
In orbit	Yes	Yes	Yes*	Yes*
Periapsis				
Occultation	Yes	Yes	No	No
Eclipse	No	Yes	Yes	Yes
Both	No	Yes	No	No

*Precession required.

Conclusion

1) Sun sensor provides primary reference source and easy identification
2) Star sensor provides attitude determination and spin angle reference for all mission phases
3) Conscan and doppler schemes require more propellant and provide limited visibility for attitude determination

star positions are given in terms of a right ascension angle measured eastward from the vernal equinox (γ) in the ecliptic plane and a declination angle measured north (+) or south (-) from the ecliptic plane. The sun can also be used to aid in the star identification procedures by appropriate spin angle gating.

The combination of the sun and star as inertial targets provides the most mission flexibility for attitude determination under all attitude conditions. Table 4-2 illustrates this mission flexibility of the selected inertial references by a comparative tradeoff summary of all the candidate inertial attitude references studies for the various mission phases.

Candidate Attitude Determinations Schemes and Sensors

Two angles are required to define the location of the spin axis in an inertial set of coordinates. This is equivalent to the statement that the angle between the spin axis and the spacecraft line of sight (LOS) to two appropriately separated inertial targets be known. For example, knowledge of the sun aspect angle (angle between spin axis and the sun LOS) and one star aspect angle (angle between spin axis and a star LOS) is sufficient to define spin axis attitude provided that the minimum sun-spacecraft-star angle is greater than 25 deg. Equivalently, only two stars are necessary providing they are within the field of view of the spinning sensor.

A standard method of measuring the aspect angle of an inertial target uses the so-called spin scan dual slit sensor which consists of two fan beam fields of view. For example, one sensing plane is placed parallel to the spin axis while the other is inclined with respect to the first. The spin angle between the pulse generated by each of the sensing planes is a function of the relative inclination of the planes and the aspect angle of the inertial target. Therefore, pulse interval measurements made by dual slit sun and star sensors are sufficient to define spin axis attitude in inertial space.

The spin axis attitude can also be determined by schemes other than that requiring measurement of aspect angles of two inertial targets. Figure 4-5 serves to illustrate these additional methods. The spin axis is depicted as the reference pole of a unit sphere centered at the spacecraft center of mass. The sun LOS and two star lines of sight are shown emerging from the sphere, with sun aspect angle = γ and a star aspect angles = λ_1, λ_2, respectively. The angle between sun and star 1 is defined as E_1; sun and star 2 is defined as E_2; and star 1 and star 2 is defined as E_3. These angles are known from ephemeris data. Note first, the measurements of γ and λ_1, or γ and λ_2 along with E_1 or E_2 define an inertial spherical triangle that uniquely locates the spin axis attitude. This approach represents the dual slit scheme discussed above. Note further, however, that measurement of sun aspect angle, γ, together with the spin angle between a sun pulse and a star pulse, A_1 or A_2, also defines along with E_1 or E_2 an inertial spherical triangle that uniquely determines spin axis attitude. This approach has been called the single slit scheme in this report. With reference to the figure, equivalent sets of measurements for this scheme are λ_1 and A_1 or λ_2 or A_2. All of these measurements can be made by the same dual slit sensors previously identified with the first approach.

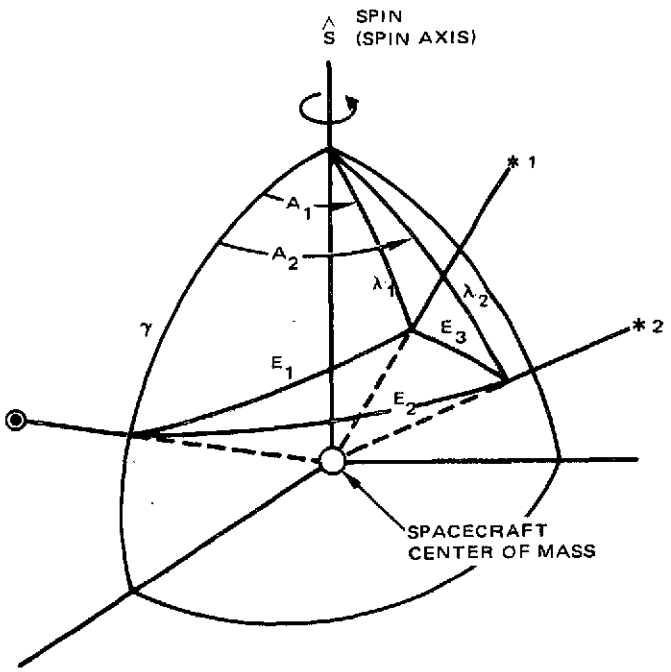

DEFINITIONS

γ= SUN ASPECT ANGLE

$\lambda_1; \lambda_2$ = STAR 1, 2 ASPECT ANGLES

A_1, A_2 = SUN-STAR 1, SUN-STAR 2 SPIN ANGLES

E_1, E_2 = SUN STAR 1, SUN-STAR 2 INERTIAL ANGLES

E_3 = STAR 1-STAR 2 INERTIAL ANGLE

NOTE: E_1, E_2 AND E_3 ARE DEFINED BY EPHEMERIS DATA

ATTITUDE DETERMINATION SCHEME	MEASUREMENTS REQUIRED	MEASUREMENT EXAMPLES
1) DUAL SLIT	ASPECT ANGLES OF TWO INERTIAL TARGETS	$(\gamma, \lambda_1), (\gamma, \lambda_2), (\lambda_1, \lambda_2)$
2) SINGLE SLIT	ASPECT ANGLE OF ONE INERTIAL TARGET PLUS SPIN ANGLE BETWEEN TWO INERTIAL TARGETS	$(\gamma, A_1), (\gamma, A_2), (\lambda_1, A_1), (\lambda_2, A_2)$
3) MAPPING	TWO SPIN ANGLES BETWEEN THREE INERTIAL TARGETS	(A_1, A_2)

FIGURE 4-5. ATTITUDE MEASUREMENT SCHEMES

Another scheme to define spin axis attitude consists of measuring the two spin angles between a sun pulse and the two star pulses; i.e., A_1 and A_2. While the data pairs (A_1, E_1) and (A_2, E_2) are insufficient to define the two spherical triangles defined by sun-spin axis-star 1 and sun-spin axis-star 2, introduction of the constraint triangle, defined by sun-star 1-star 2, will uniquely define spin axis attitude. This approach is called the mapping scheme Once again, all required measurements can be made by the same dual slit star sensors used for the other two approaches.

The choice of dual slit sun and star sensors provides a triple option for spin axis attitude determination. This capability is significant for the Pioneer Venus mission when one considers the various spin axis attitudes that will be experienced and the restricted flexibility available with a limited number of stars. For example, since each scheme has an error sensitivity problem for different sun-star-spin axis geometries, one scheme (dual slit) might encounter a geometry problem at a given attitude (spin axis, sun and star LOS coplanar), while another scheme (single slit) would offer superior performance and still only require a single measurement on the same star. Another significant advantage of the triple option is its redundancy features. The dual slit sun sensor can be made redundant for a relatively insigificant increase in cost and weight. With a sun aspect angle always available and each slit of a dual slit star sensor redundant to the other, only a single star measurement is required for the single slit scheme. Therefore, a single slit scheme has been emphasized in the analysis since it provides the basis of the redundancy argument for a single star sensor (minimum cost design) and requires only one star measurement.

The attitude sensor configuration selected for Pioneer Venus consists of a redundant dual slit sun sensor and a single dual slit star sensor. Spin axis attitude is nominally determined by anyone of three schemes: dual slit (sun and star aspect angle measurements), single slit (sun aspect and sun-star spin angle measurements), and mapping (multiple sun-star angle measurements). Complete redundancy is obtained by only requiring the availability of one of the two star sensor slits. Table 4-3 summarizes the rationale for this selection.

4.2 ATTITUDE/ΔV/SPIN SPEED CONTROL

The fundamental trades associated with attitude/ΔV/spin speed control were:

1) Thruster arrangement: A combination of thrusters that can execute all required maneuvers in a redundant manner must be defined.

2) Spin rate and thruster parameters: Spin rate thrust level and moments arms must be consistent with allowable attitude disturbances and maneuver time constraints.

3) Nutation damping: The nutation damper must provide asymptotic stability over a broad spin speed range.

TABLE 4-3. ATTITUDE DETERMINATION RATIONALE SUMMARY

Attitude sensor configuration.	Redundant dual slit sun sensor, single dual slit star sensor, each slit independent
Features	
Mission flexibility:	Triple attitude determination option
1)	Dual slit scheme – measure aspect angles of two inertial targets
2)	Single slit scheme – measure aspect angle of one inertial target and spin angle between two inertial targets
3)	Mapping scheme – measure two spin angles between three inertial targets
Mission redundancy.	Complete mission attitude determination in the event of a sun sensor failure and/or a single star sensor slit failure.

Thruster Arrangement

Any combination of jets schemes that satisfies all attitude/ΔV/spin speed control requirements can be analyzed by superposition of fundamental jets, each performing specific task(s), on a spinning vehicle. The most generally known schemes use axial jets, radial jets, and spin jets.

The axial jet is a thruster radially offset from the spin axis that delivers its linear impulse parallel to the spin axis. Continuous firing of an axial jet continuously generates a ΔV nearly parallel to the initial inertial spin axis direction. Since the jet is offset from the spin axis, an angular torque also results. This effect can be minimized in two ways: spinning the vehicle faster to render it more resistent to angular motion; locating another axial jet radially opposite the first one so that when both are fired together, a pure linear impulse is nominally imparted. Pulsing an axial jet at spin frequency generates a torque fixed in an inertial plane and thus a precession of the angular momentum vector in that same plane. Since the jet also imparts a linear impulse parallel to this plane, an inertial ΔV component will also be introduced. This latter effect can be minimized by locating another axial jet that thrusts in the opposite direction radially opposite the first one so that when both are pulsed together, a pure angular impulse is nominally imparted. Note that a trio of axial jets is required to generate a pure force parallel to the spin axis and a pure couple perpendicular to the spin axis. If a pure force antiparallel to the spin axis is also required, a quartet is necessary. Without any spin axis attitude constraints, only one axial jet is required to deliver a ΔV in an arbitrary direction; coupling between precession and ΔV could be calibrated into the maneuver. Without any spin axis constraints, only two axial jets (radially opposite, thrust antiparallel) are required to redundantly deliver a ΔV in an aribtrary direction. This scheme also has the advantages of providing a pure couple mode for precession and requiring a maximum precession of 90 deg from the initial to the required (but arbitrary) ΔV attitude.

The radial jet is offset from the spin axis so that delivers its thrust through the center of mass and perpendicular to the spin axis. Pulsing a radial jet at spin frequency generates a pure linear impulse perpendicular to the spin axis. The radial jet has no capability to precess the spin axis or to change spin speed. However, a combination of one axial jet and one jet has the capability of delivering a ΔV in an arbitrary direction in an inertial hemisphere whose axis of revolution is some arbitrary spin axis attitude. If one adds another axial jet thrusting antiparallel to the first, the capability is extended to the entire inertial sphere. The power of radial pulse thrusting is that it permits ΔV maneuvers without reorientation of the spacecraft.

The spin jet is a thruster radially offset from the spin axis that delivers its linear impulse in the plane perpendicular to the spin axis containing the center of mass and in the direction perpendicular to the radius. Firing a spin jet continuously for an integral number of spacecraft revolutions generates a pure couple about the spin axis and thus spin speed change. The spin jet has no capability to precess the spin axis. A ΔV component perpendicular to the spin axis is obtained at the expense of spin speed change. One spin jet each is required for spinup and spindown. Note that if the two spin jets are radially opposite and thrust parallel to one another, pulsing the two together

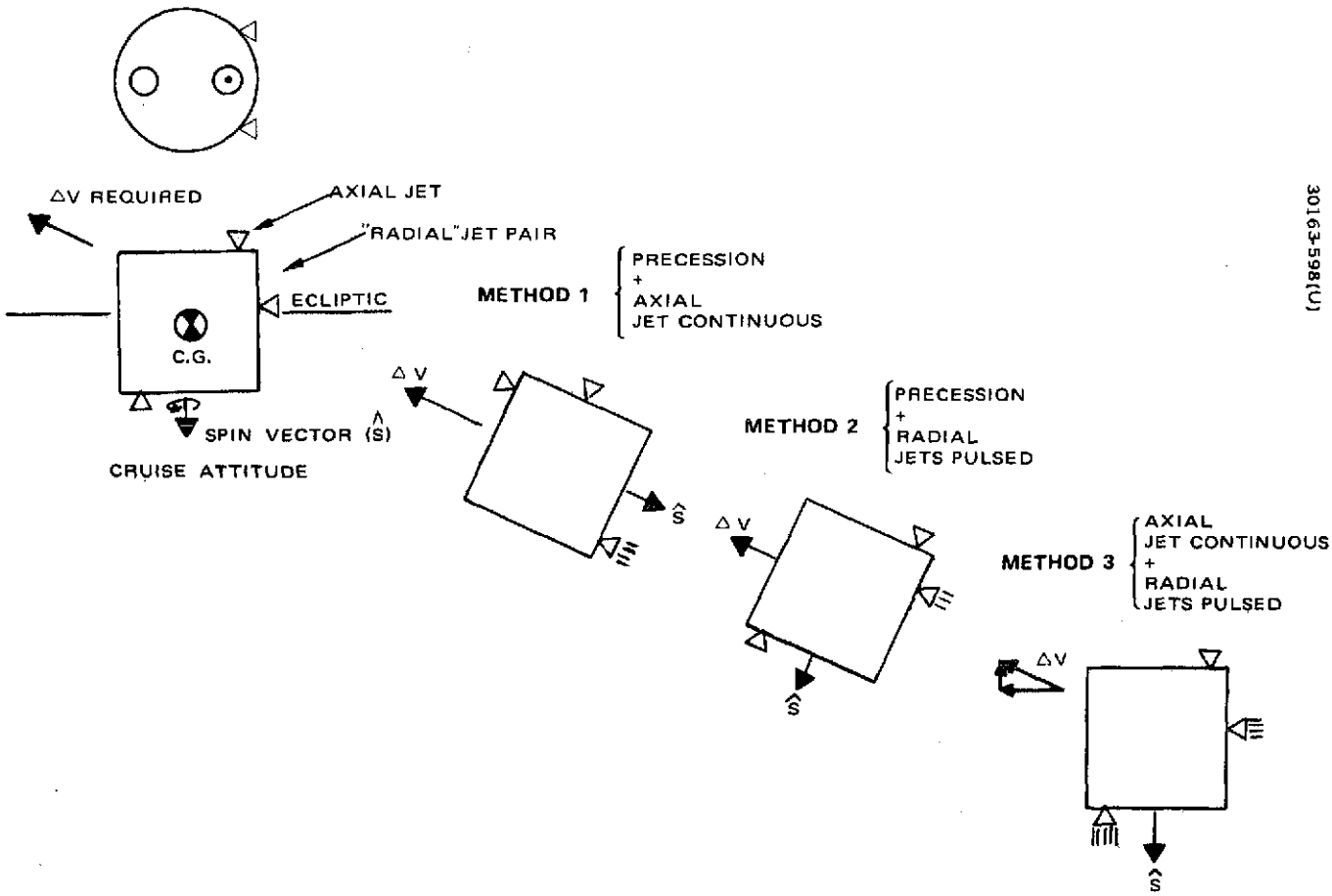

FIGURE 4-6. METHODS OF MIDCOURSE MANEUVER EXECUTION

at spin frequency will generate a pure linear impulse perpendicular to the spin axis as do radial jets. A combination of such a "radial" jet pair with an axial jet pair (radially opposite, thrust antiparallel) has the capability of: 1) delivering a ΔV in an arbitrary direction for any spin axis attitude, and 2) spin speed increase or decrease. This combination is called the "Pioneer Quartet". Since attitude/ΔV/spin speed control are inherently a part of the Pioneer Venus mission, this quartet represents a point of departure for a thruster arrangement that can satisfy mission requirements with suitable redundancy and commonality for both missions.

The quartet offers three standard methods of midcourse maneuver execution illustrated in Figure 4-6: the axial jet mode, the radial jet mode, and the vector mode. The axial jet mode (Method 1) can be used when the required ΔV direction is never closer than 15 deg to the sunline. This mode requires a maximum 95 deg open loop rhumb line precession to the required attitude, an axial jet continuous burn and a precession back to the cruise attitude. The precession is nominally executed with the axial jet couple. For large maneuvers such as the first midcourse, this mode requires minimum propellant (continuous I_{sp}) and least maneuver time. The radial jet mode (Method 2) can be used when the required ΔV direction is within 15 deg of the sunline and the spin axis is within 15 deg of normal to the ecliptic. This mode requires a maximum 15 deg precession to an attitude perpendicular to the required ΔV direction, a radial jet pair pulsed, and return to the cruise attitude. This mode can also be used to deliver a ΔV in an arbitrary direction by precessing (with the axial jet(s)) a maximum of 90 deg around the sunline and pulsing at the appropriate phase of the spin cycle. However, for large maneuvers, the radial jet pair can induce significant secular precession and spin speed changes and thus the maneuver would have to be monitored and probably partitioned. For attitudes within 15 deg of ecliptic normal, the attitude is readily assessed. This mode requires more propellant (pulsed I_{sp}) and more maneuver time (pulsed). The vector mode (Method 3) requires no change in attitude to deliver a ΔV in an arbitrary direction (fundamental property of the quartet). Axial jet continuous thrust is vectored with radial jet pulsed thrust. The vector mode is the choice for small ΔV corrections while the axial jet mode is the choice for large ΔV corrections.

In the event one axial jet fails, the axial jet mode is degraded but not lost. The operative axial jet executes a maximum precession of 180 deg as well as the required ΔV. Failure of one axial jet limits the vector mode to an inertial hemisphere. In the event one radial jet fails, either spinup or spindown capability is lost and the radial jet mode has severe spin-radial ΔV coupling. These effects could sacrifice the first midcourse maneuver, required probe spin rates, orbit insertion and orbital operations at 5 rpm. For redundancy considerations, an additional radial jet pair should be added to the quartet. Then, two radial jet pairs displaced 180 deg with respect to one another about the spin axis provide redundant spin speed control and radial ΔV capability. The two axial jets provide redundant attitude control and axial ΔV capability. This sextet represents the first iteration on the "Pioneer Quartet" considering the impact of single jet failure on mission success.

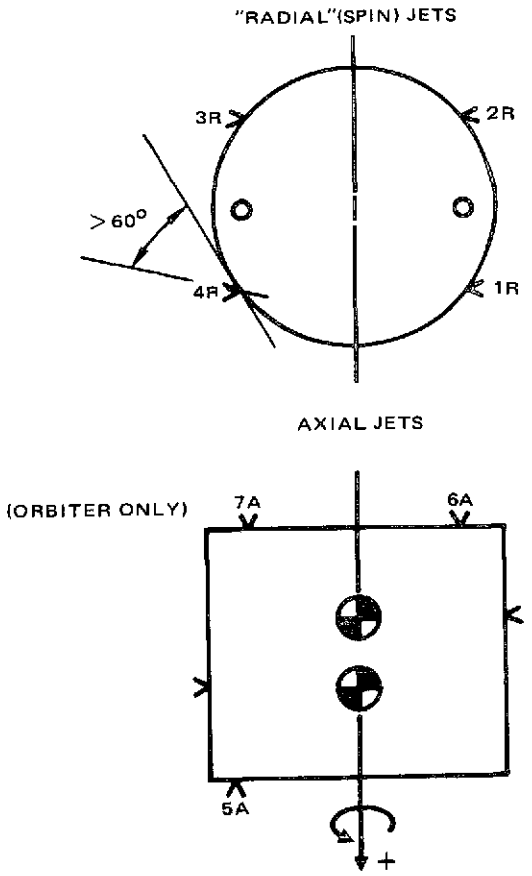

RADIAL THRUSTERS (4 ON PROBE BUS OR ORBITER)

- REDUNDANT SPINUP AND SPINDOWN (ONE THRUSTER FIRED CONTINUOUSLY)
- REDUNDANT $\Delta V\perp$ TO SPIN AXIS (ONE PAIR OF THRUSTERS PULSED)
- BACKUP ATTITUDE TRIM (ONE PAIR OF THRUSTERS PULSED)

AXIAL THRUSTERS (2 ON PROBE BUS, 3 ON ORBITER)

- REDUNDANT ATTITUDE PRECESSION (SINGLE OR DIAGONAL PAIR OF THRUSTERS PULSED)
- REDUNDANT ΔV PARALLEL TO SPIN AXIS (SINGLE THRUSTER FIRED CONTINUOUSLY)
- FOR ORBITER ONLY, REDUNDANT ΔV ALONG + SPIN AXIS (SINGLE THRUSTER PULSED AT TWICE SPIN FREQUENCY OR PAIR FIRED CONTINUOUSLY)

FIGURE 4-7. THRUSTER ARRANGEMENT

After large probe separation, the spacecraft center of mass shifts significantly (≈15 cm). Since small probe targeting requires ΔV perpendicular to the spin axis, one of the probe bus radial jet pairs (cruise backup) should thrust through this center of mass. This strategy also allows the "radial" jet pairs to exhibit additional precession modes during the mission.

One of the axial jets easily delivers the ΔV required for probe bus retardation. In the event that this jet fails, the spin axis can be precessed and a radial jet pair pulsed appropriately.

The axial jet that thrusts parallel to the orbit insertion motor thrust easily executes any preburn maneuver required. If this jet failed, thermal constraints limit the duration of the preburn to be executed with a backup jet(s). This is one of several considerations that lead to the addition of a third axial jet on the orbiter. Compensation for solar and drag orbital perturbations only require axial thrust parallel to the orbit insertion motor thrust. The solar effect increases periapsis so that an impulse opposite the orbital velocity vector near apoapsis is required. The drag effect decreases apoapsis so that impulse in the same direction as the orbital velocity vector near periapsis is required. Since the orbital velocity vectors at apoapsis and periapsis are antiparallel, this implies thrust in the same inertial direction is required. For the baseline spacecraft this is always along the orbit insertion motor thrust direction. Thus, a single axial thruster comprises nearly the total work force for orbital operations. Corrections will be required at least weekly. In the event this thruster fails, the spacecraft must be precessed at least 360 deg per week, introducing operational difficulty as well as a weight penalty. Addition of a seventh jet provides redundancy for orbital operations as well as several other desirable features; i.e., another attitude control mode; redundancy for the preburn maneuver; and two additional axial ΔV modes, one of which allows a balanced thrust to execute orbital corrections at 5 rpm with minimal attitude perturbations. The latter feature is significant since a single axial jet must be pulsed in a 180 deg bang-bang mode when used for orbital corrections at 5 rpm. This mode consists of pulsing the jet at twice spin frequency to accumulate ΔV and limit the attitude movement (precession and nutation) when angular momentum is low. The jet effectively bangs the angular momentum vector each one half spin period back to its initial attitude.

As a result of these tradeoffs, a "Pioneer Sextet" was chosen for the probe mission and an additional axial jet was added for the orbiter mission to form the "Pioneer Septet." The latter is illustrated in Figure 4-7, with jet 7A removed for the probe mission. The fundamental differences between these arrangements and the basic quartet are based on redundancy arguments.

Spin Rate Profile and Thruster Parameters

The spin rate profile for certain key mission events is fairly well dictated. However, spin rates during cruise and maneuvers are open to some tradeoffs involving thruster parameters. For the thruster arrangement arrived at above, the thrust level and jet moment arms are parameters to be selected. The vehicle configuration constraints all thrusters to be located

radially at the periphery of the 214 cm diameter cylinder. Thus, the axial jet moment arm is approximately 100 cm (40 in.). The radial jet moment arm can be no greater than 50 cm (20 in.) because the radial jet thrust must be > 60 deg from the tangent to the cylinder to avoid a plume impingement problem. The moment arm is chosen to be this maximum value in order to minimize the propellant required for spin speed control. With thruster geometry defined, the only parameter remaining for the tradeoff is thrust level.

The choice of the axial jet mode as nominal for a large initial midcourse as in the Thor/Delta is based on the observations that it minimizes required propellant and maneuver time and can be executed open loop if necessary. For spin frequency pulsing, the precession rate is proportional to the thrust and inversely proportional to the spin speed. The rate of ΔV delivery is also proportional to the thrust. The resistance to attitude motion during continuous burn is proportional to the thrust and inversely proportional to the spin speed squared. Therefore, for equal spin stiffness, a 22 N (5 lb) thruster requires 2.2 times the spin speed as a 4.5 N (1 lb) thruster. The precession rate for the 22 N thruster is 2.3 times as fast at the higher spin speed. The rate of ΔV delivery is 5 times as fast for the first midcourse maneuver. At 60 rpm, the 22 N thruster would require $\approx$8 min to precess to the required ΔV attitude, 20 min to deliver the maximum ΔV (72 m/sec) and $\approx$8 min to return to cruise attitude. This implies a minimum maneuver time of 36 min. The corresponding minimum maneuver time for the 4.5 N thruster at 27 rpm is 137 min. An attitude determination is desirable prior to the actual ΔV delivery, so that some additional maneuver time is desirable. The 22 N thruster can reasonably satisfy the 1 h maneuver time allowed, while the 4.5 N thruster does not come close. If the first midcourse were performed with the radial jet mode at these spin rates, the larger thruster would require a minimum of 80 min, while the smaller would require a minimum of 185 min. If a large preburn for the orbiter were required, the smaller thruster could use a significant portion of the 2 h allowed at that attitude. The smaller thruster does have a comparative advantage for orbital operations at 5 rpm. The attitude perturbation due to a mismatched pair or single axial jet during a ΔV correction is reduced by a factor of five. However, the mismatch between a pair of larger axial thrusters can be limited to an acceptable level by a selection process. In addition, the disturbance due to a single larger axial thruster can be limited by the on-time in the 180 deg bang-bang mode. An advantage accruing to the larger thruster based on Hughes experience is that thrust misalignment is smaller ($\approx$0.05 deg compared to 0.2 deg). Since both thrusters are developed and use the same solenoid valve, the cost and weight differences are minimal. The overall selection of the Thor/Delta of the 22 N thruster has been made based on its minimal maneuver time and adequate pulse performance at 5 rpm.

The spin speed during attitude and ΔV maneuvers must generate sufficient spin "stiffness" to limit cross-coupling effects on maneuver errors. In general, nutation induced during spin axis precession is inversely proportional to spin speed; thrust pointing error and nutation induced by a continuous axis jet ΔV maneuver is inversely proportional to spin spin speed squared; precession induced by a pulsed radial jet ΔV maneuver is inversley proportional

to spin speed; and propellant weight required for precession maneuvers is proportional to spin speed. Therefore, the spin speed should be set as low as possible to save propellant weight consistent with gyroscopic stiffness requirements.

The spin speed selected for probe midcourse maneuvers using either axial or radial jets is 60 rpm. The probe bus is despun to 30 rpm for large probe separation reorientation to reduce propellant consumption. The spin speed selected for the first orbiter midcourse maneuver is dependent on which jet mode is used. Since the orbiter bus has a balanced pair of axial thrusters on the retro motor end of the spacecraft, thrust pointing error and nutation induced by a continuous burn of this axial jet pair is small. With nutation induced during the spin axis precession tolerable and required precession propellant halved at 30 rpm, the orbiter can satisfactorily execute the first midcourse at 30 rpm with this axial jet pair. If the orbiter requires a large midcourse with the axial jet on the other end of the spacecraft or with the radial jets, the maneuver will be executed in the same manner as the probe bus; i.e., at the intial cruise spin speed of 60 rpm. Since subsequent maneuvers are much smaller, their execution with the axial and/or radial jet mode (discussed below) at 30 rpm for the orbiter bus is acceptable. However, the axial jet mode requiring the single thruster on the top end of the spacecraft would be a 180 deg bang-bang mode. In summary, then, the orbiter will continue to cruise at 30 rpm if it is despun to this speed for the first midcourse. If it is not despun prior to the initial maneuver, it will be despun to 30 rpm after the maneuver and continue to cruise at this value. Since orbit insertion will take place at 30 rpm and orbital operations at 5 rpm, the mechanically despun antenna need only operate over a spin speed range of 5 to 30 rpm. The antenna will be despun during the remainder of cruise using the sun as a despin reference.

Nutation Damping

Since both the probe bus and orbiter are passively stable, nutation damping is most easily achieved with a passive device. The damper is required to operate over a broad spin speed range. Such a damper is provided by a passive mercury tube nutation damper of the design type utilized on Syncom, ATS, and Telesat. Extensive performance analyses and testing of mercury tube nutation dampers have been performed at Hughes during these programs and techniques have been developed to accurately predict nutation damping time constants for the various mission requirements and vehicle characteristics. A common damper can be utilized for both the probe and orbiter missions.

5. SUBSYSTEM DESCRIPTION (THOR/DELTA BASELINE)

5.1 FUNCTIONAL DESCRIPTION

The attitude control and mechanisms subsystem (ACMS) uses conventional spin stabilized spacecraft hardware and functional mechanizations to provide a simple and reliable design. The elements of the attitude control functions are shown in Figure 5-1. Subsystem analyses are given in Appendices A and B and detailed hardware description is given in Appendix C.

All elements of the ACS are mounted on the spinning rotor (see Figure 5-2) including the mercury nutation damper which provides the primary source of energy dissipation for nutational stability. The damper is a simple, space-proven passive mercury tube device partially filled for maximum damping effectiveness over the required mission profiles.

The attitude data processor (ADP) contains all the logic and signal processing to determine time intervals between sun and star sensor output pulses for transmission to the ground station for computation of spacecraft attitude. For on-board automatic operations, azimuth spin pulses are generated for spin period synchronization of star gates, reaction jet firing start signal, probe release timing and science instrument references. The jet control electronics contains all the logic and timing circuits to automatically operate the solenoid drivers for control of the propulsion system jet valves upon receipt of ground commands.

The bearing and power transfer assembly (BAPTA) provides the electrical and mechanical interface between the two sections of the orbiter spacecraft and contains despin motor and shaft angle encoder. The BAPTA uses a brush dc torque motor to generate the required torque to control the platform dynamics in azimuth for maintaining the high gain antenna pointing at the Earth LOS.

The motor torque commands to overcome friction and orient the orbiter high gain antenna toward the Earth line of sight (LOS) are derived in the despin control electronic (DCE) portion of the ACMS. The commands are based on pulse data from the shaft angle encoder (SAE), spin synchronous clock pulses derived from either sun or star sensor outputs and ground commandable delays. The DCE provides the required logic for both automatic antenna pointing acquisition and tracking.

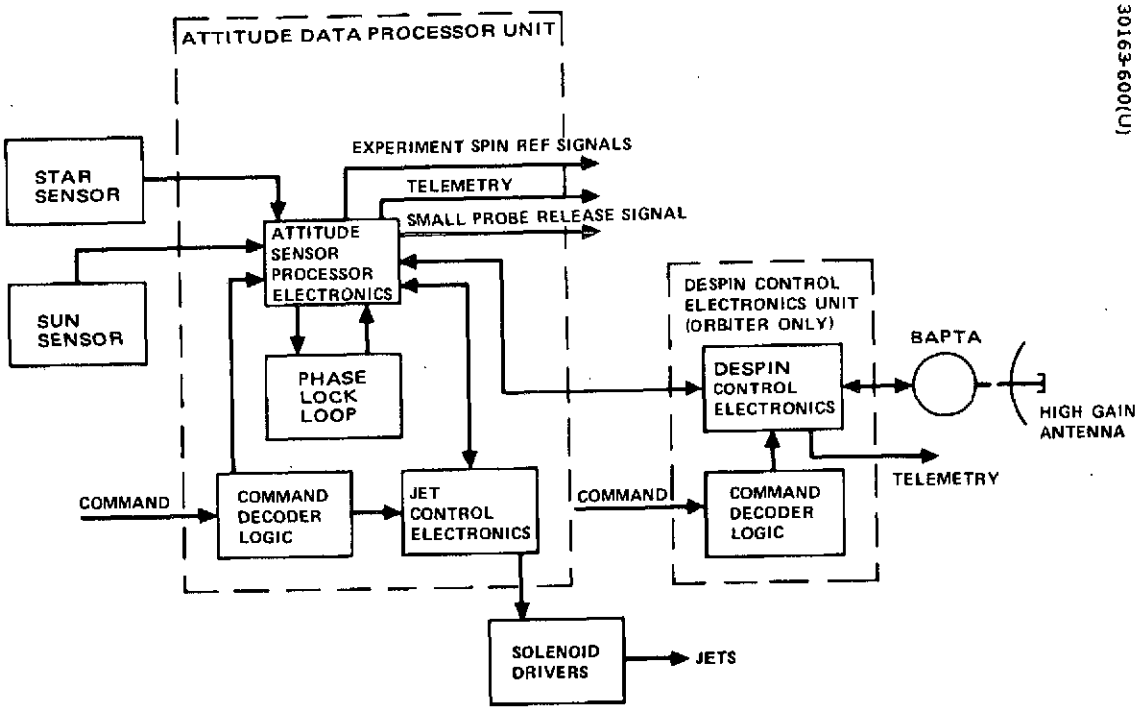

30163-600(U)

FIGURE 5-1. ATTITUDE CONTROL AND MECHANISM SUBSYSTEM BLOCK DIAGRAM

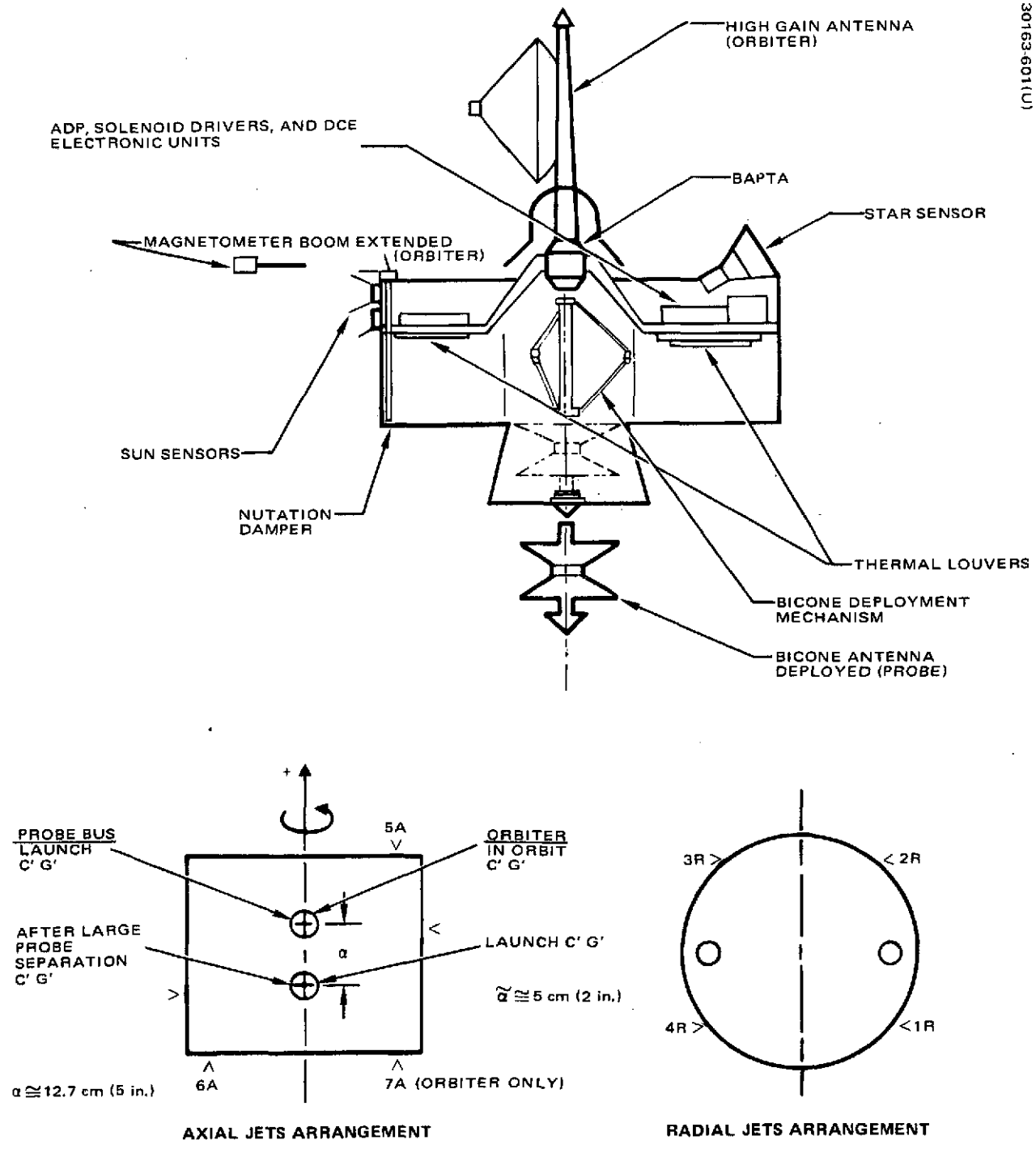

FIGURE 5-2. ACMS EQUIPMENT ARRANGEMENT

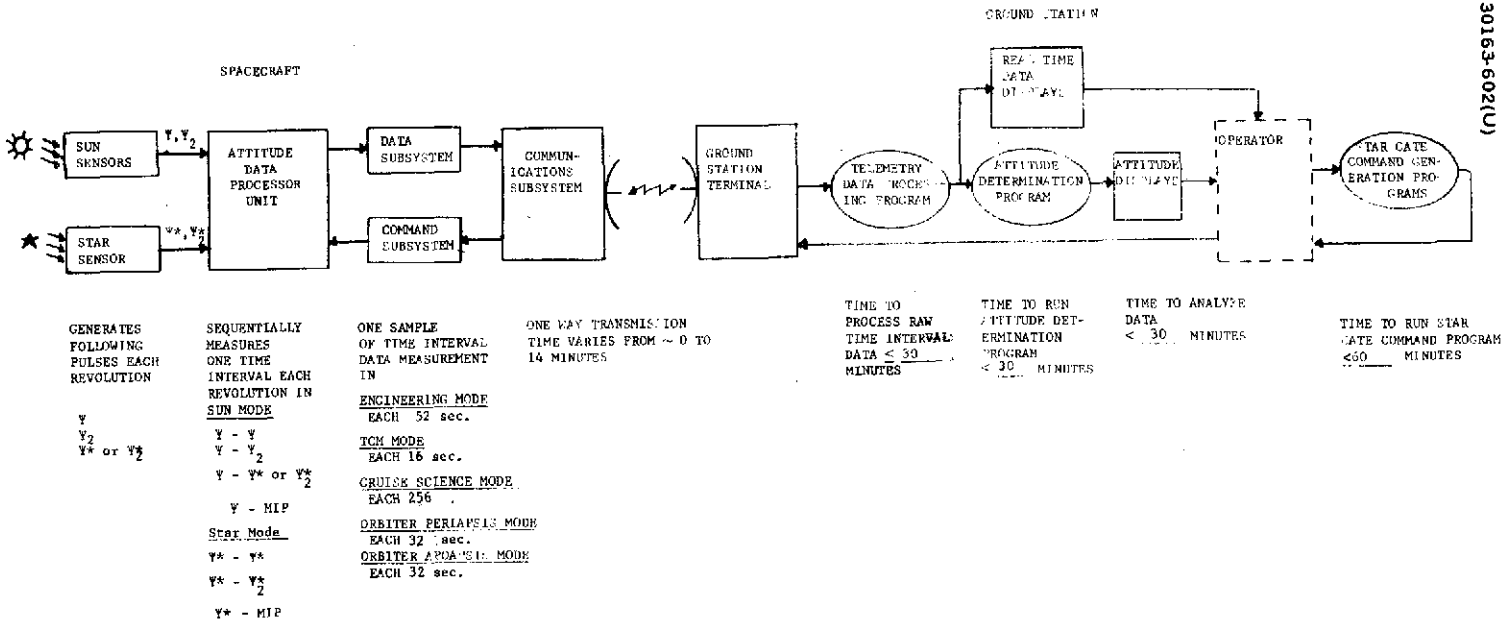

FIGURE 5-3. ATTITUDE DETERMINATION SYSTEM BLOCK DIAGRAM

The principle mechanisms are a bicone antenna deployment mechanism; a magnetometer sensor deployment mechanism; thermal control louvers and mechanical pin pullers. The bicone antenna deployment mechanism is a telescopic mast for extending the bicone antenna along the spin axis following separation of the spacecraft from the Thor/Delta launch vehicle. The magnetometer sensor deployment mechanism is a 107 cm (42 in.) boom which is extended radially following separation from the launch vehicle. The thermal control louvers are bimetallic actuated devices used to control the temperature of the spacecraft electronic equipment. The mechanical pin pulles are squib actuated devices used for the release of spacecraft mechanisms.

5.2 ATTITUDE DETERMINATION SYSTEM DESIGN

The recommended attitude determination scheme for the Pioneer Venus mission measures the sun and selected stars aspect angles and spin azimuth angles relative to spacecraft coordinates. The measured data is then transmitted to the earth for processing and attitude calculations using Euler angle relationships by the ground control center. A functional block diagram of the proposed system is shown on Figure 5-3. As can be ssen the spacecraft functions have been minimized to enhance total system reliability, reduce spacecraft weight and minimize systems development costs.

Sensors

The proposed sensor configuration uses three spin scan sun sensors and one spin scan star sensor as the inertial reference sensors. Since the sun can be detected unambiguously, the sun is used as the primary celestial reference. In addition, the sun is used as an aid in selecting the desired stars for attitude determination. To provide attitude measurements at random spacecraft attitudes the sun sensors will be aligned relative to the spacecraft spin axis such that one sensor scans the upper hemisphere, one sensor scans the lower hemisphere, and one sensor scans the midrange of sun aspect angles. The star sensor will be aligned to scan an area in the upper spacecraft hemisphere to provide the best star coverage when the spacecraft plus spin axis is pointing toward the south elliptic pole.

Each sun sensor is a dual slit fan shaped field of view (FOV) sensor. Each sensor has a ψ slit which is aligned parallel to the spin axis and a ψ_2 slit which is canted relative to the ψ slit, as illustrated below.

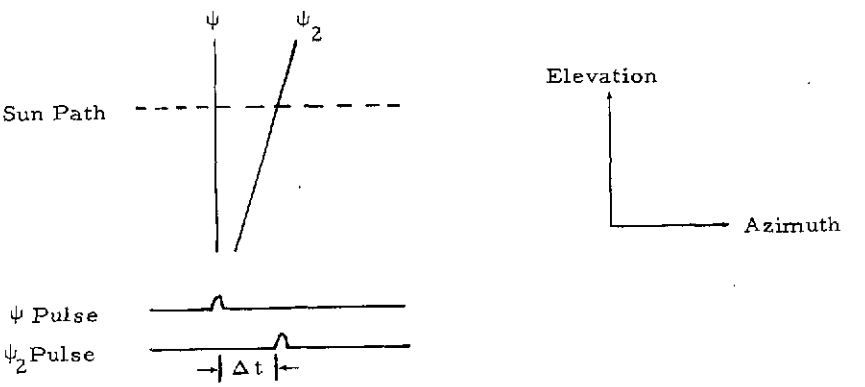

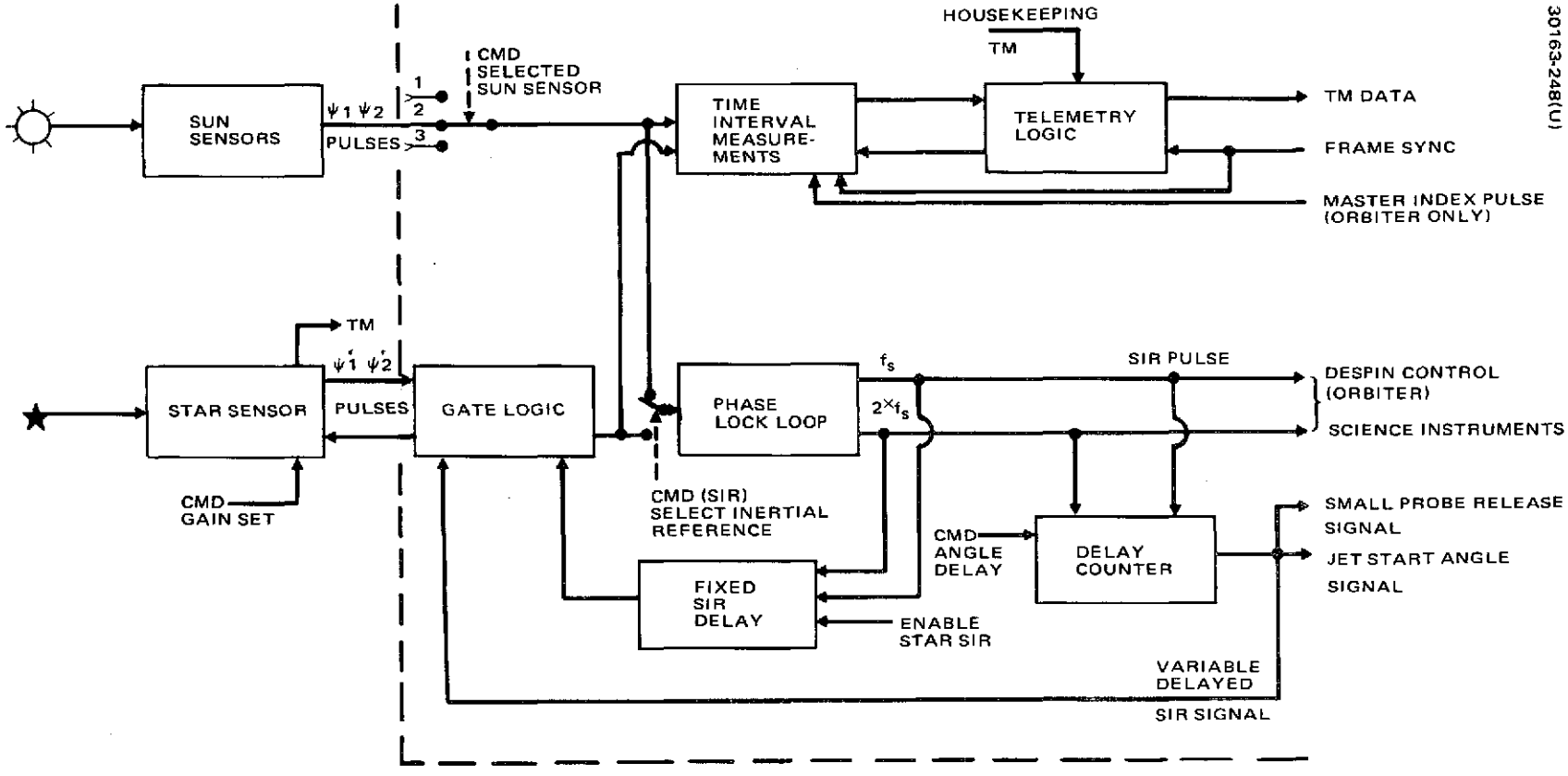

FIGURE 5-4. ATTITUDE DETERMINATION ELECTRONICS BLOCK DIAGRAM

A pulse from each slit will be generated each revolution when the sun passes through the slit FOV. The sun apsect angle relative to the spin axis is determined by measuring the time interval between pulses.

The star sensor is a dual slit solid state detector with a fan shaped FOV. The sensor has a ψ^* slit aligned parallel to the spin axis and a ψ_2^* slit which is canted relative to the ψ^* slit (see below). Since normally more than

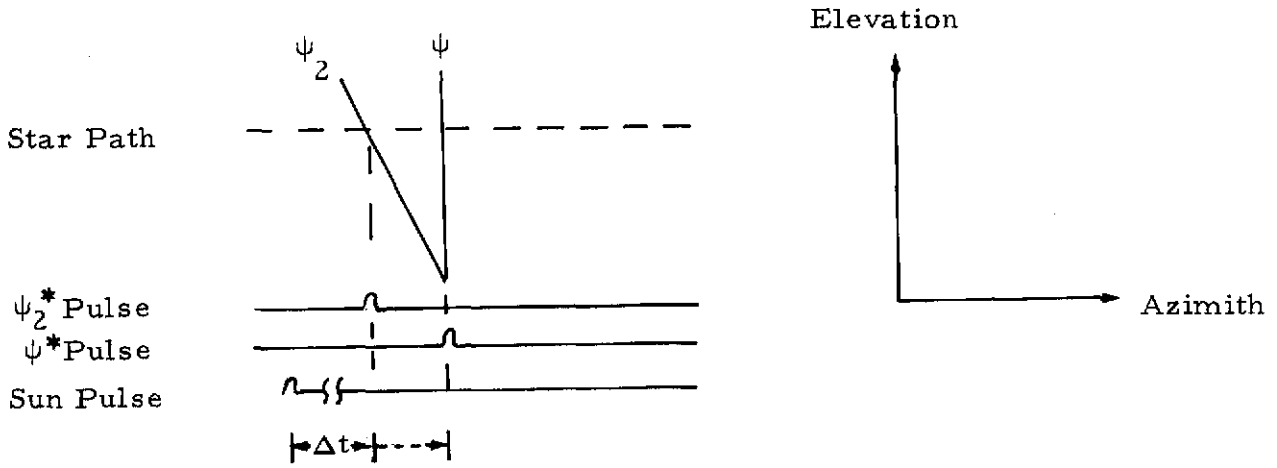

one star will appear in the FOV each revolution, angle and intensity discrimination will be required in order to obtain valid data from a known star. A commandable detection threshold setting will be used to provide amplitude discrimination against background noise and dim stars. A star gate commandable in spin angle from the sun ψ pulse will be used to angle discriminate against other bright stars. The star intensity will be measured and telemetered to the ground. Time interval measurements from the sun ψ pulse to star ψ^* pulse and the star ψ_2^* pulse will also be made. The star aspect angle relative to the spin axis is determined by the time difference between the two measurements. The time interval measurement is made from the sun sensor ψ pulse to permit the use of only one star slit (ψ^* or ψ_2^*) for attitude determination when favorable sun-star geometry exists. The cant angle of the ψ_2^* slit is negative to provide better single slit attitude determination accuracy during some periods of the mission.

Attitude Data Processor

The sun and star sensor pulses are processed by the attitude data processor (ADP) electronics unit. A block diagram of the unit is shown in Figure 5-4. The unit will have two data modes. When the sun is selected as the primary inertial reference, the unit will be operating in the sun mode. When the sun is not available (sun within 15 deg of spin axis or eclipsed by Venus) a star will be selected as the primary inertial reference and the unit will be operating in the star mode.

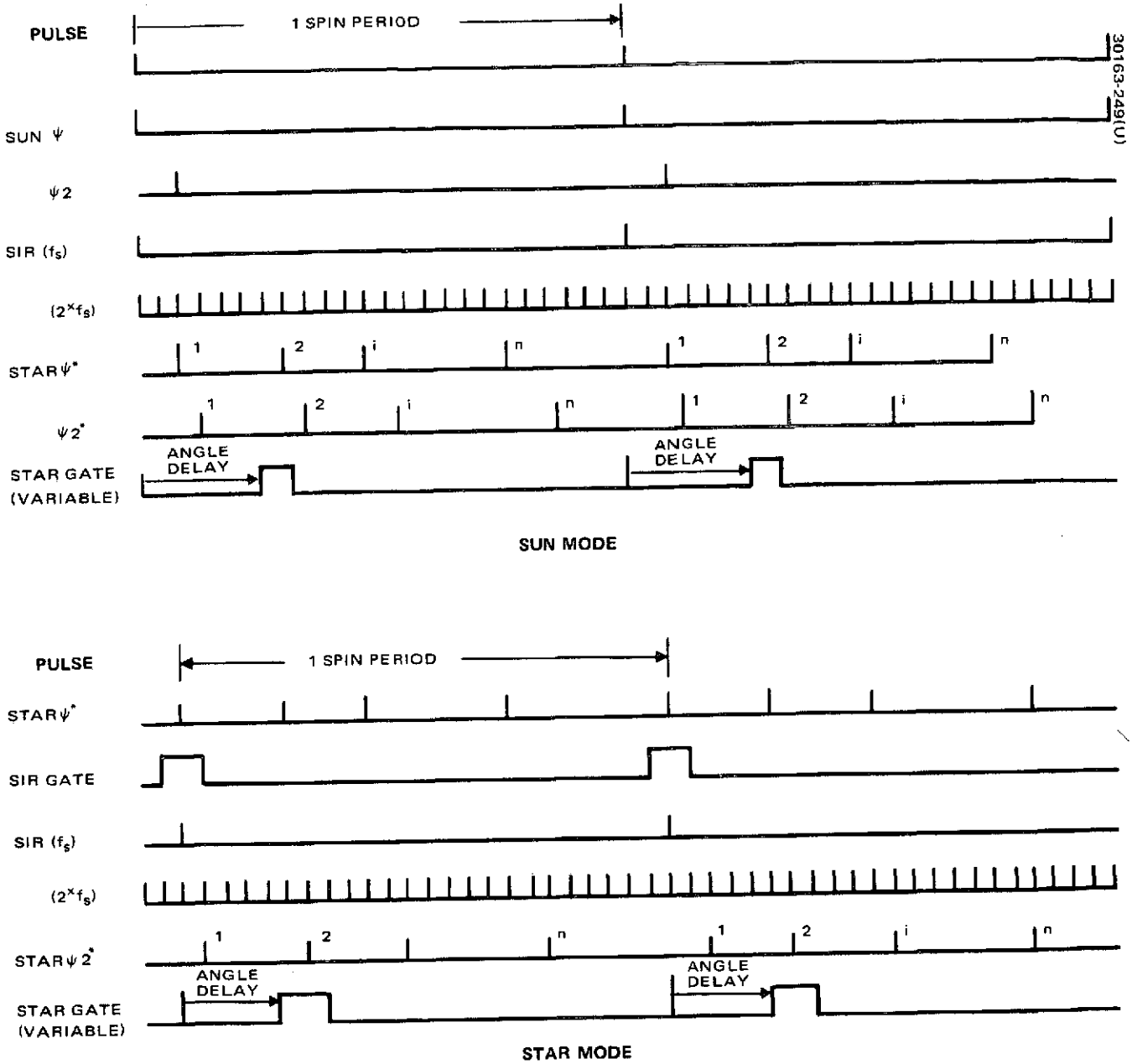

FIGURE 5-5. SUN AND STAR PULSE TIMING DIAGRAM

For the sun mode of operation one of the three sun sensors will be selected by ground command depending upon the approximate sun aspect angle. The time interval between ψ and ψ_2 pulses will be measured to obtain spin period and sun aspect data. The ψ pulses will also be used as a spin-angle reference input to a phase lock loop (PLL). The PLL will quantize a spin period into 2X sectors to provide on-board spin angle reference singals with respect to the selected inertial reference. A ground commanded angle delay will be used to gate the selected star pulses from the ψ^* or ψ_2^* slits for time interval measurements (see Figure 5-5). A star map of intensity versus angle can be made by moving the gate slowly through 360 deg. Following generation of the star map, the best star (based on the signal-to-noise and geometry) will be selected for making attitude determination measurements. One time interval measurement can be made during a spin period and the data stored until readout by the data subsystem. In the sun mode the following measurements can be made:

1) $\psi - \psi$ spin period

2) $\psi - \psi_2$; sun elevation angle

3) $\psi - \psi^*$ or ψ_2^*; sun-star or star elevation angle

4) ψ - MIP; despun antenna azimuth angle (orbiter only)

Because the slow data rate of the communications system the time interval measurements will be selected by ground command in pairs. This will provide the operational flexibility to obtain the most number of samples of desired data in the least amount of time; i.e., one can select, for example, $\psi - \psi_2$ and $\psi - \psi^*$ and obtain a measurement of each time interval every other spin period. Therefore, a minimum of two spin periods will be required to obtain one pair of attitude measurements. The time for a single attitude measurement as a function of spin speed is as shown in Figure 5-6 assuming no telemetry data rate limitations.

To obtain a complete set of attitude measurements a minimum of 25 data points will be taken of each required parameter. A typical data collection sequence would be as follows:

Step	Measurement	Samples	Required Time at 5 rpm
1	$\psi - \psi$; $\psi - \psi^*$	25	10 min
2	$\psi - \psi_2$; $\psi - \psi_2^*$	25	10 min

During the star mode of operation, a star will be used as a selected inertial reference (SIR) for the PLL by enabling a SIR star gate ~355 deg following the SIR pulse from the PLL. The PLL will lock on and track the star pulse occurring in the SIR star gate. The ground commanded star gate angle delay will be used to select star pulses from either the ψ^* or ψ_2^* slit for the time interval measurements relative to the SIR star being tracked by the PLL (see Figure 5-5). To change lock of the SIR star being tracked

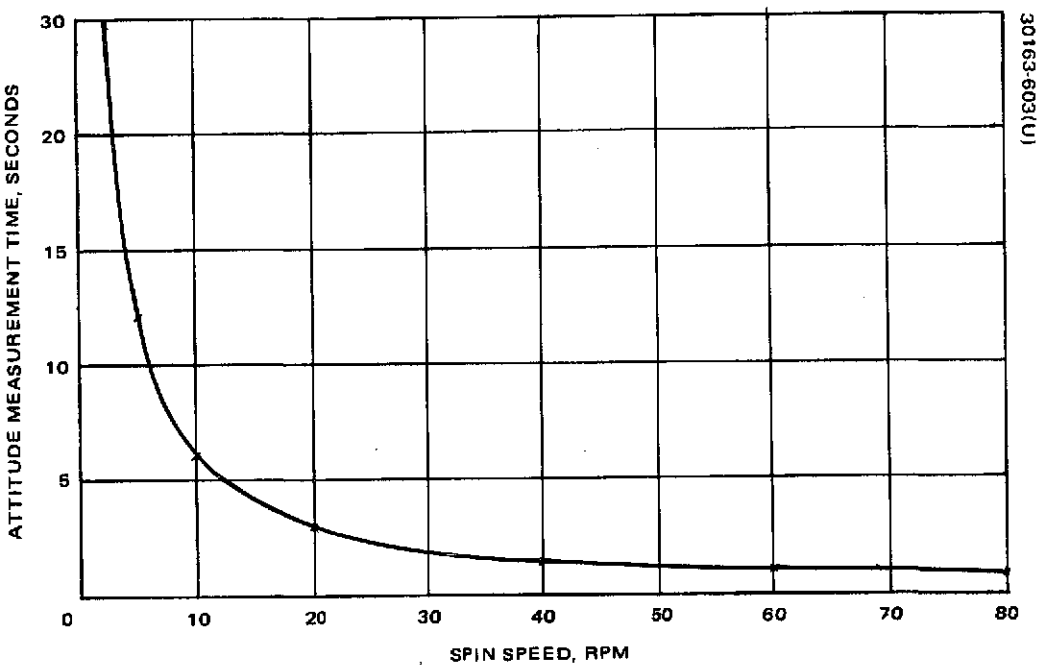

FIGURE 5-6. ATTITUDE MEASUREMENT RATE VERSUS SPIN SPEED

by the PLL the commanded star gate angle delay will be positioned on the desired ψ^* pulse; then a star advance ground command will be intiated to reset the PLL phase error to zero when the next ψ^* pulse occurs in the delayed star gate, thus resetting the SIR star gate and the PLL to track the new selected star. One time interval measurement can be made during a spin period, and the data stored until readout by the data subsystem. In the star mode the following measurements can be made:

1) $\psi^*1 - \psi^*1$: spin period (same star)

2) $\psi^*1 - \psi^*2$: spin azimuth (two stars)

3) $\psi^*1 - \psi_2^*1$ or ψ_2^*2: star elevation angle

4) ψ^*1 - MIP: despin antenna azimuth angle (orbiter only)

To determine attitude in star mode, two stars separated in azimuth 90 ± 65 deg should be used. One star would be selected as the SIR for locking the PLL as described previously. The star sensor threshold must be set using ground commands to allow at least two stars to be detected each revolution. The commanded star gate delay will be positioned by ground commands to obtain the desired star aspect data. A typical data collection sequence for this operation would be as follows:

Step	Measurements	Samples	Required Time at 5 rpm
1	$\psi^*1 - \psi^*1$; $\psi^*1 - \psi^*2$	25	10 min
2	$\psi^*1 - \psi_2^*1$; $\psi^*1 - \psi_2^*1$	25	5 min
3	$\psi^*1 - \psi_2^*2$; $\psi^*1 - \psi_2^*2$	25	5 min

Data Subsystem

The data subsystem will interrogate the ADP periodically to obtain the measured attitude data for transmission to the ground. The frequency of sampling will depend upon the available bit rate through the communication subsystem and the selected data mode. The attitude data words will be transmitted when either of the two attitude control system (ACS) telemetry data frames have been selected by ground command. One frame of ACS data will contain housekeeping data and will include at least one attitude data measurement sample per frame. The other frame of ACS data will contain trajectory correction maneuver (TCM) data and will include at least four attitude data measurement samples per frame. Based upon preliminary spacecraft telemetry data format assignments the minimum attitude data rates will be as shown in Table 5-1 for the indicated telemetry modes. Each data format is comprised of 16 frames of data. Each frame of data is 256 bits. Each frame contains 32 eight-bit words. A minimum of three words is required for each attitude measurement; i.e., 24 bits.

TABLE 5-1. MINIMUM EXPECTED ATTITUDE DATA RATE

TM Data Mode	Number of ACS Frames per Format	Bit Rate, bps	ACS Frame Rate, sec/frame	Attitude Samples per ACS Frame	Attitude Data Rate sec/sample
Engineering	5/16	16	51.2	1	51.2
TCM	8/16	8	64.0	4	16.0
Cruise science	1/16	16	256.0	1	256.0
Probe encounter science	1/16	1024	4.0	1	4.0
Orbiter periapsis science	1/16	128	32.0	1	32.0
Orbiter apoapsis science	2/16	64	32.0	1	32.0

The data system has the operational flexibility of serially formatting 16 frames of data. The serial bit stream telemetry format can be altered by ground command to optimize the desired sample rate. The number of ACS data frames per 16 frames of spacecraft data is shown in Table 5-1, along with the lowest expected telemetry bit rate, the nominal ACS frame rate, the attitude samples per ACS data frame, and the resulting average attitude data rate. During most phases of the mission, the bit rate will be twice that indicated, which means the time between data samples will be one/half (1/2) that indicated in the table.

Communication System

The one-way communication time between the spacecraft and earth has a significant effect on the operational time required to perform the attitude determination. The time to command the star gate angle from the ground station will induce a two-way communications time delay in order to obtain the star aspect angle data for attitude determination. Figure 3-1 shows these communications delays as a function of days from launch and in orbit. Because of the long communication time, making an attitude determination verification in real time while performing attitude and ΔV spacecraft maneuvers, will only be possible through the first midcourse correction.

Ground Station Data Processing

The raw telemetry data will be decoded at the mission operations center. The attitude measurement data will be converted to engineering units for real time display and quick look analysis by the operators. Using the

real time data the operator will command the star sensor threshold setting and star gate angle delays to obtain the desired attitude data measurement necessary to perform a valid attitude determination.

The attitude determination process involves several consecutive events: configuration of sensors and data handling subsystem for data transmission; propagation delay; accumulation of required data; quick look at the data; computation of spin rate, attitude and biases; evaluation of solution; and transmission of attitude to maneuver programs. As an example of the time required for these events, consider an attitude determination at probe encounter prior to large probe separation. The telemetry subsystem is in the TCM mode with 8 bps provided by wide beam omni during and after the attitude maneuver. Attitude data at the final attitude is intially received some 5 min after the maneuver. One datum point is transmitted every 16 sec. Allowing 25 samples of each of the four data types ($\psi\psi$, $\psi\psi_2$, $\psi\psi^*$,$\psi\psi^*_2$), approximately 30 min is required for accumulation of data. An additional 30 min is allocated to verify quality of the data and process the data through the attitude determination software. An evaluation of the solution obtained consumes 30 min more, thus, a minimum of 1.6 h is required. In the event data quality is bad, this sequence is delayed by the time required to recognize bad data, analyze why, initiate a solution (star gate or magnitude change), transmit commands to the spacecraft and receive good telemetry data. This delay has been estimated to be 1 h. Therefore, a realistic time allocation for an attitude determination operation is $\approx$2.5 h.

Attitude Determination Software Design

A functional block diagram of the Pioneer Venus attitude determination software is illustrated in Figure 5-7. Time interval measurement data generated on board by the dual slit sun and star sensors are transmitted to the ground via the attitude data processor and data handling subsystem. The ground software processes spin speed (sun sensor $\psi\psi$ or star sensor ψ^* ψ^*) and several types of attitude data: sun angle (sun sensor $\psi\psi_2$), star angle(s) (star sensor ψ^* ψ^*_2), spin angle(s) between sun and star(s) line of sight (sun-star sensors $\psi\psi^*$, $\psi\psi^*_2$). Star identification is assisted by magnitude and gating information provided by telemetry.

The data is initially processed through an editing routine where excessively noisy data of each type are sequentially culled on the basis of excessive deviation from the running mean of that data type. The output of the edit routine is in blocks of smoothed data corresponding to the n data types. Each block of data (containing an arbitrary number of points) represents a set of repeated measurements of an observable over a short interval of time. These sets of measurements on n observables are used with an optimal linear estimator to obtain the state vector of interest; i.e., the vector composed of the two Euler angles defining spin axis attitude and n biases corresponding to the n data types. The technique can be summarized as follows.

An initial estimate of the state vector is made and a set of values (corresponding in number to the measurements made) is computed for each observable. Dual slit sensor equations are used for the sun and star angle

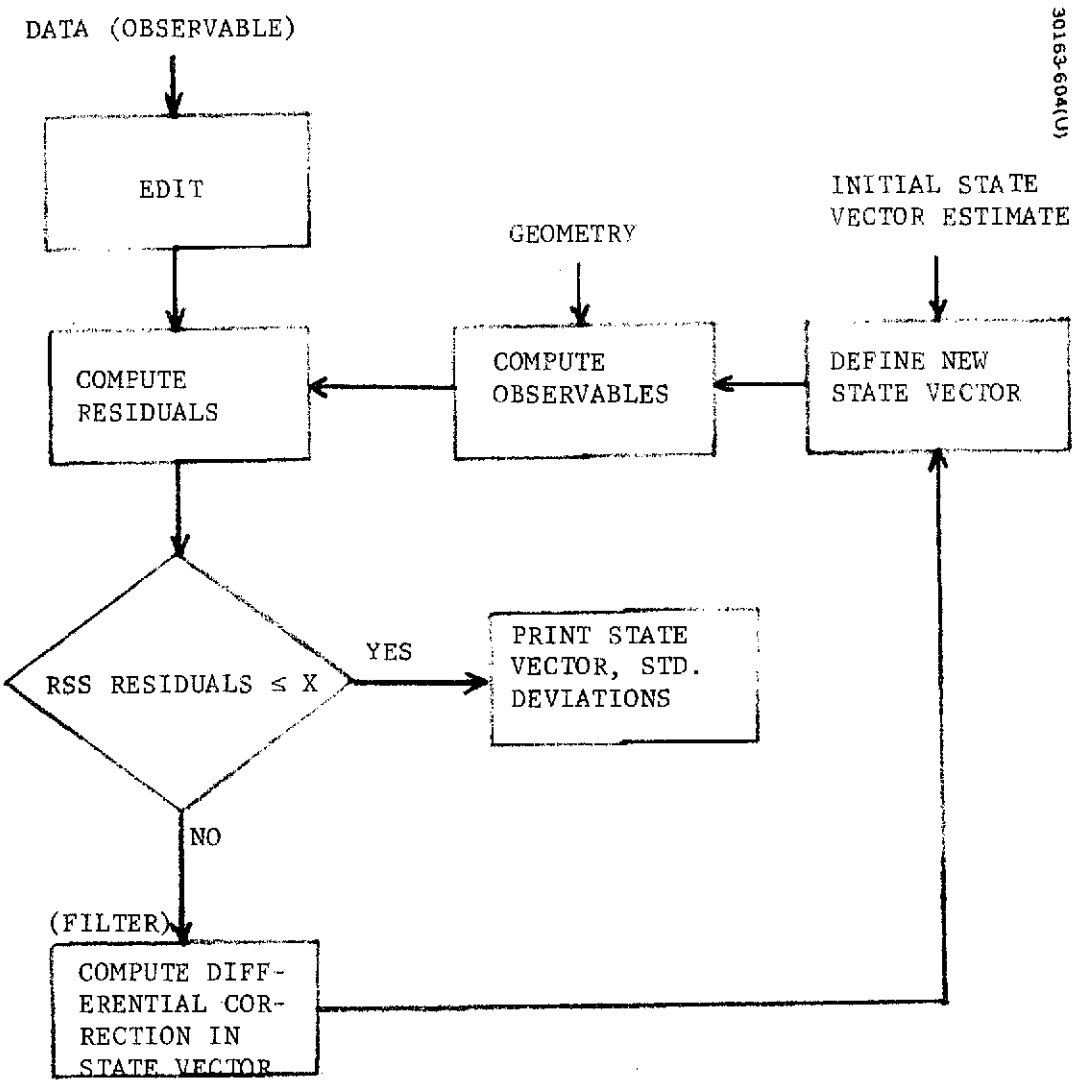

FIGURE 5-7. ATTITUDE DETERMINATION SOFTWARE

data types while single slit sensor equations are used for the sun-star spin angle data type. A vector of residuals is formed by taking the difference between the observed and computed values for each datum point in the n blocks. The linear estimator is then used (together with numerical differentiation) to define a differential correction in the state vector. The relative weights of the various data types can be chosen on the basis of block variances and inertial geometry. The new state vector is then used to recompute a set of values for each observable. The vector of residuals is reformed by taking the difference between the first and second computed values for each datum point. The root-sum-square (rss) of the residuals is compared to a selected value to ascertain convergence (acceptable minimization of the rss of residuals).

If convergence has not taken place, the vector of residuals is used in the filter to define a second differential correction. The process is repeated until convergence takes place. The output of the software, then, is an optimal estimate of spin axis attitude and biases together with their standard deviation.

In addition to this standard attitude determination software, several additional tools will be available for real time operations. For example, graphs of $\psi\psi_2$ versus $\psi\psi^*$ with the two Euler angles as parameters enable one to quickly define attitude from telemetry data. Similarly, consecutive pairs of $\psi\psi_2$ and $\psi\psi^*$ data can be transmitted in real time to a small computer to yield a running point solution of attitude; this is useful, for example, in defining instantaneous attitude during a large precession maneuver. These graphical and point solutions provide a quick-look capability which complements the sophisticated software capability.

5.3 ATTITUDE/ΔV/SPIN SPEED CONTROL SYSTEM DESIGN

The recommended attitude/ΔV/spin speed control scheme for the Pioneer Venus mission uses an optimized combination of axial and radial thrusters to accomplish all required maneuvers in a redundant manner. Maneuver commands are computed on earth, transmitted, stored onboard, and initiated by the command memory. The command distribution logic in the attitude data processing unit receives the commands from the command subsystem and generates the proper signals to enable their distribution to the jet control electronics. The latter then generates low level logic signals to the solenoid driver unit, which then provides drive power for the reaction control jets.

A mercury tube damper will provide damping of nutational transients induced by maneuvers. The damper shall be broadly tuned to operate over a spin speed range of 5 to 100 rpm.

Thruster Configuration

The recommended thruster arrangement is illustrated in Figure 5-8 and the redundant control modes are listed in Table 5-2. Four radial thrusters are placed on both the probe bus and orbiter as shown to provide

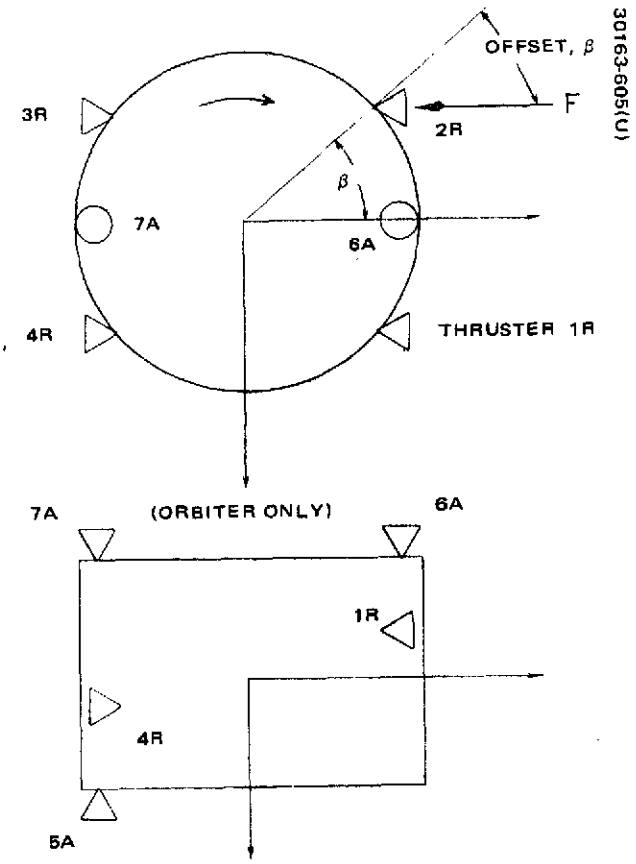

FIGURE 5-8. ARRANGEMENT OF THRUSTERS

TABLE 5-2. JET CONTROL MODES

Nominal Maneuver	Redundant Jet Control Modes Orbiter (Jets 1 to 7), Probe (Jets 1 to 6)
Spin control	
Spinup	Jet 1R continuous
	Jet 3R continuous
Spindown	Jet 2R continuous
	Jet 4R continuous
Radial ΔV	Jets 1R and 2R pulsed simultaneously at spin frequency
	Jets 3R and 4R pulsed simultaneously at spin frequency
Axial ΔV	Jet 5A continuous
	Jet 6A continuous
	Jet 5A pulsed at twice spin frequency
	Jet 6A pulsed at twice spin frequency
	Jet 7A continuous
	Jets 6A and 7A continuous
	Jet 7A pulsed simultaneously at twice spin frequency
Attitude	Jets 1R and 2R pulsed simultaneously at spin frequency
	Jets 3R and 4R pulsed simultaneously at spin frequency
	Jets 5A and 6A pulsed simultaneously at spin frequency
	Jet 5A pulsed at spin frequency
	Jet 6A pulsed at spin frequency
	Jet 7A pulsed at spin frequency

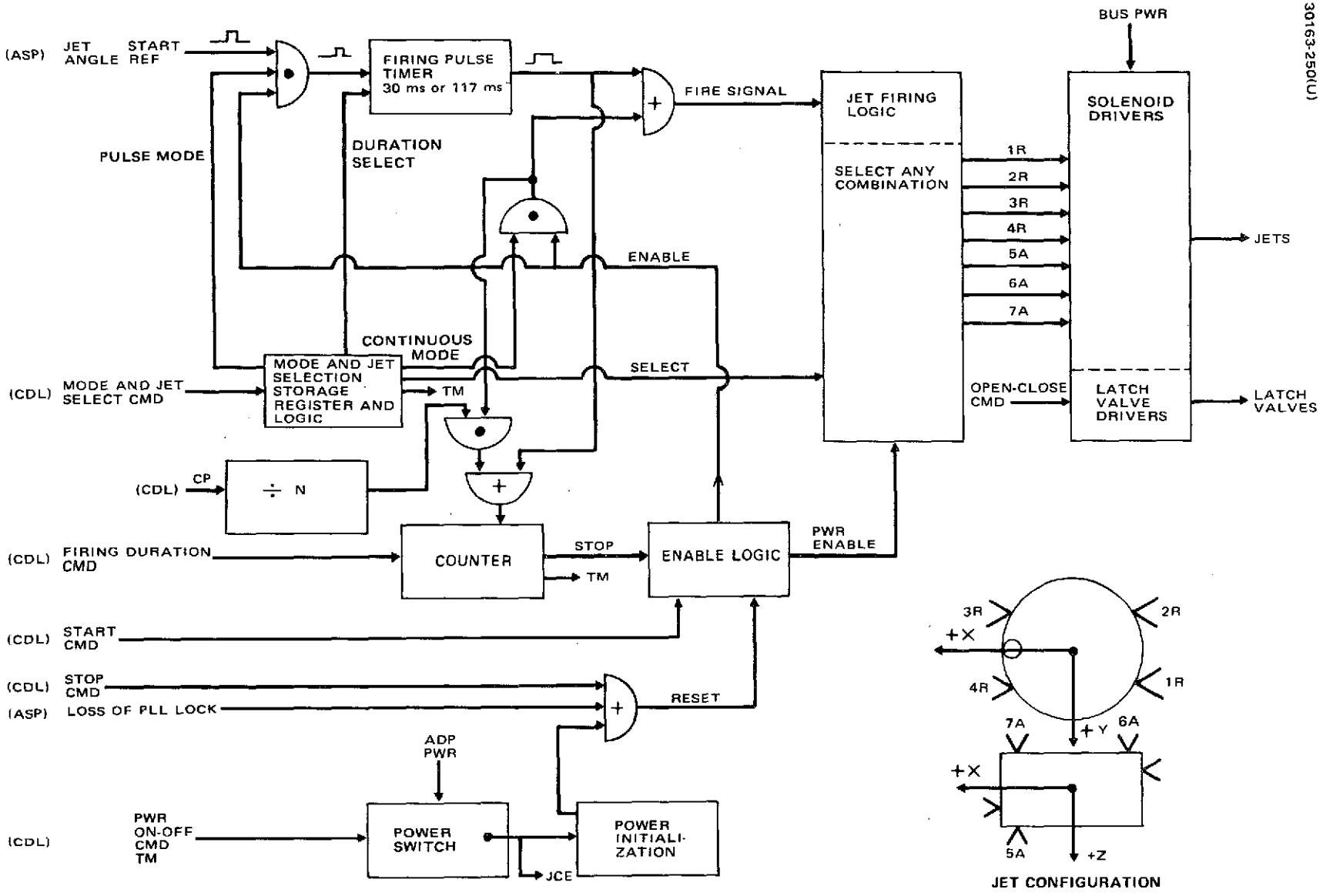

FIGURE 5-9. JET CONTROL ELECTRONICS BLOCK DIAGRAM

redundant spinup or spindown (one thruster fired continuously); redundant ΔV perpendicular to the spin axis (one pair of thrusters pulsed simultaneously): and backup attitude trim (one pair of thrusters pulsed). Axial thrusters are placed on both the probe bus and orbiter as shown (two on the probe bus, three on the orbiter) to provide redundant attitude precession (single or diagonal pair of thrusters pulsed); redundant ΔV parallel to the spin axis (single thruster fired continuously; and for the orbiter only, redundant ΔV along the plus spin axis (single thruster pulsed at twice the spin frequency or pair fired continuously). The salient thruster characteristics are: thrust range of 29 (6.5 lb) to 11 (2.5 lb) N specific impulse range of 230 to 200 sec; and pulse widths of 30 and 117 ms. The detailed thruster characteristics are contained in the propulsion subsystem final report (Volume 10).

Jet Control Electronics

A block diagram of the jet control electronics (JCE) is illustrated in Figure 5-9. The jet control electronics has the following functions: jet select and firing control, start angle and pulse width selection; enable and countdown control. All jet control modes are listed in Table 5-2.

The jet selection logic will enable by ground command any selected combination of the three axial (two axial on the probe) and four radial jets for a maneuver. The ground command selects whether the jets are pulse fired from the angle logic or continuously fired for a commanded time. The jets can be fired at the commanded delay angle θ or at θ and $\theta + 180$ deg when twice spin frequency pulsing is required.

The angle logic produces firing pulses 30 or 117 ms wide at the fire angle generated by the delay generator. The pulse width is selected by ground command.

The enable logic starts the firing duration counter and enables the appropriate jet firing logic. The enable logic also switches power to the power stage once the JCE unit has been energized. Power is turned on only by a JCE ON pulse command. Power is turned off by a JCE OFF pulse command, a PLL loss of lock signal or completion of the firing sequence. The enable logic is set to the disabled state at power turn on and can only be enabled by a JCE start pulse command.

The countdown is a 12-bit counter which counts either 0.5 sec clock time pulses or the number of θ pulses fired. The counter is preset with a number representing the desired number of pulses fired or the desired length of time. The counter is started by a star pulse command and ends when the full count has been reached. A loss of PLL lock will also stop the execution of a maneuver in progress.

5.4 HIGH GAIN ANTENNA DESPIN CONTROL SYSTEM DESIGN

The despin control system functions as a closed-loop autonomously operating control system which orients the antenna towards the earth line of sight while the rotor spins about an axis normal to the ecliptic plane. With reference to Figure 5-10 the motor torque commands to orient the platform

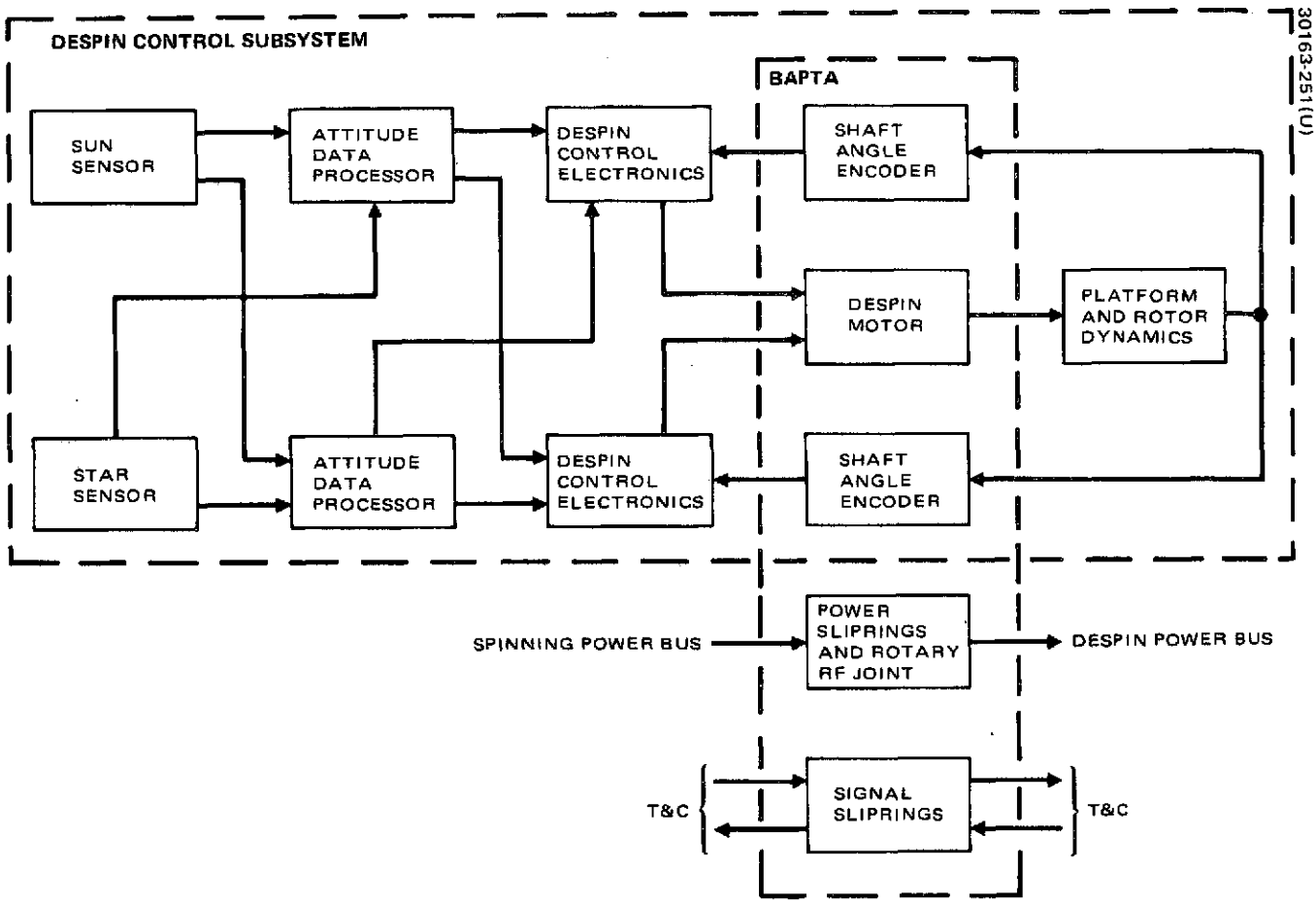

FIGURE 5-10. DESPIN CONTROL SYSTEM

are generated by the despin control electronics based on the selected inertial reference sensor (sun or star) and the bearing and power transfer assembly (BAPTA) master index pulses, and on command inputs. Ground commands provide control of the DCE modes and inertial antenna pointing. All active elements of the despin control are on the spinning rotor. Operation of the despin control is illustrated in Figure 5-11. Four control loops are used: 1) position, 2) rate, 3) friction compensation, and 4) command control. The friction torque compensation includes an integrator stage to null offsets biases caused by bearing friction torque and motor back-EMF. Command control of motor torque is provided for maximum flexibility; e.g., integrator failure (no output or saturation).

The derivation of a true position signal is the most complex function performed by the despin control. This process is illustrated in Figure 5-12 for one complete revolution of the spacecraft spinning section. The series of configuration drawings assumes a null condition with the payload antenna pointing towards the earth line of sight. The error signal is formed through a measurement of time between the occurrence of a phase-shifted sun or star sensor pulse and the master index pulse. The master index pulse generator which is aligned to the antenna boreseight will generate a pulse when the rotor mounted detector sweeps past the reference position. The phase-shifted sensor pulse is obtained by delaying the phase lock loop (PLL) selected inertial reference pulse (f_s), generated by the attitude data processor unit, by an angle commandable from ground. This measurement is obtained once per spin period and is referred to as the coarse position error signal. At very low spin speeds, the spin period becomes excessively long and position update information too infrequent for accurate antenna pointing. Therefore, the spin period is divided into $2^4 f_s$ or 16 sectors. Similarly, the platform circumference is divided into $2^4 f_z$ or 16 sectors by means of the shaft angle encoder. The time interval between the phase shifted $2^4 f_s$ simulated sensor pulse and the $2^4 f_z$ shift angle encoder pulse represents the fine error position signal. Rate information is also derived by taking the first back difference of position errors; i.e., the change in position error between the present value and the last previous value is a measurement of relative rate. The coarse and fine position errors and rate errors are used to derive a motor torque command and force a stable null condition.

Since the rotor rate is not constant during the mission, the measuring of the intervals between pulse occurrences in terms of fractional spin periods is a primary problem. A special "clock" is required and is provided by the phase lock loop. In addition to generating the selected inertial reference (f_s), the phase locked loop also generates a high frequency clocking signal having 2^{12} pulses per spacecraft revolution. This high frequency pulse sequence is phased locked to the actual sun or star sensor pulse and, therefore, each clock pulse represents $1/2^{12}$ of the spin period or 0.088 deg.

Despin Control Electronics

The despin control electronics block diagram is presented in Figure 5-13. Although the phase lock loop which generates the clock signals for time measurements and the simulated sensor pulses at 16 times the spin frequency is a part of the attitude data processor electronics unit, (see

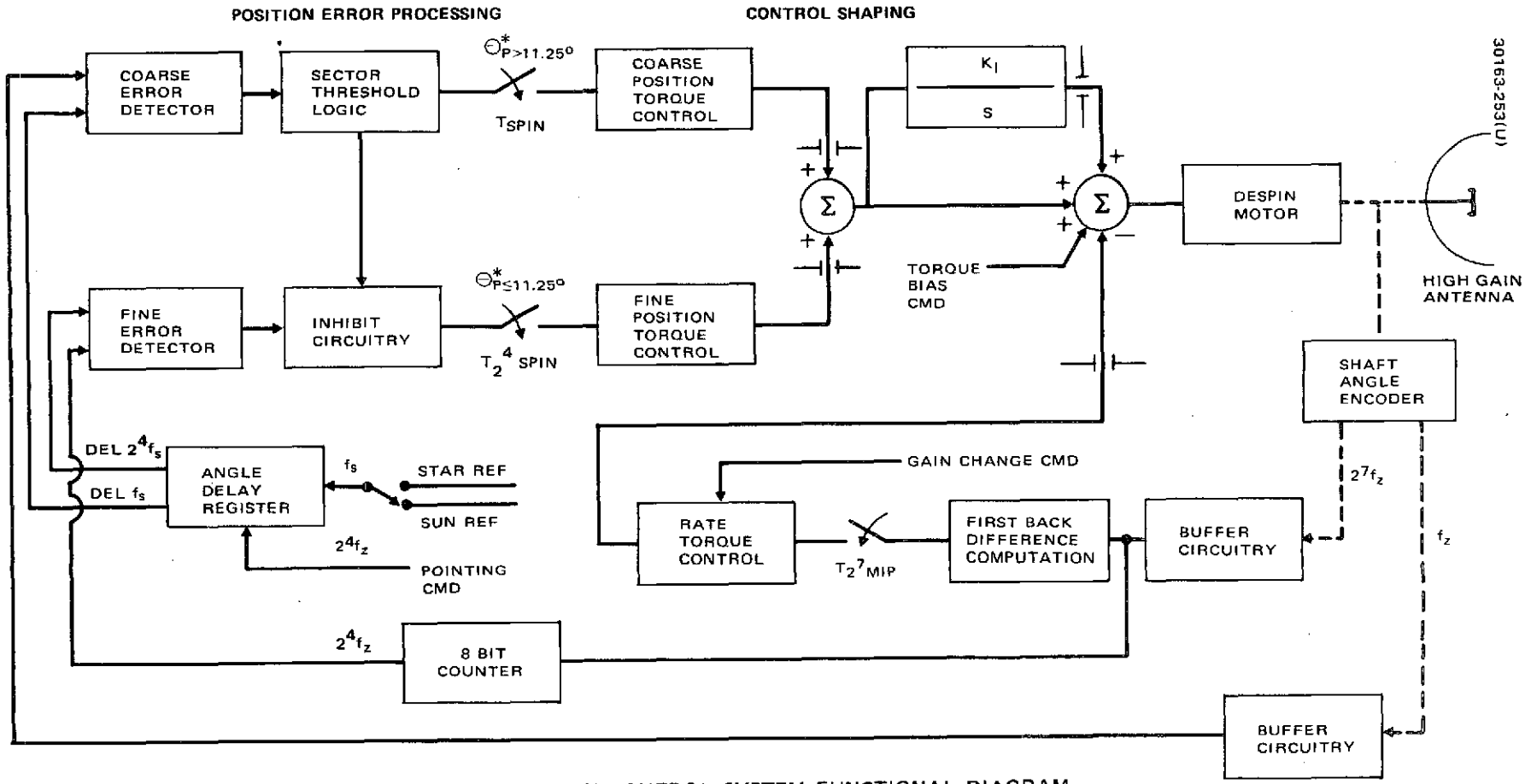

FIGURE 5-11. DESPIN CONTROL SYSTEM FUNCTIONAL DIAGRAM

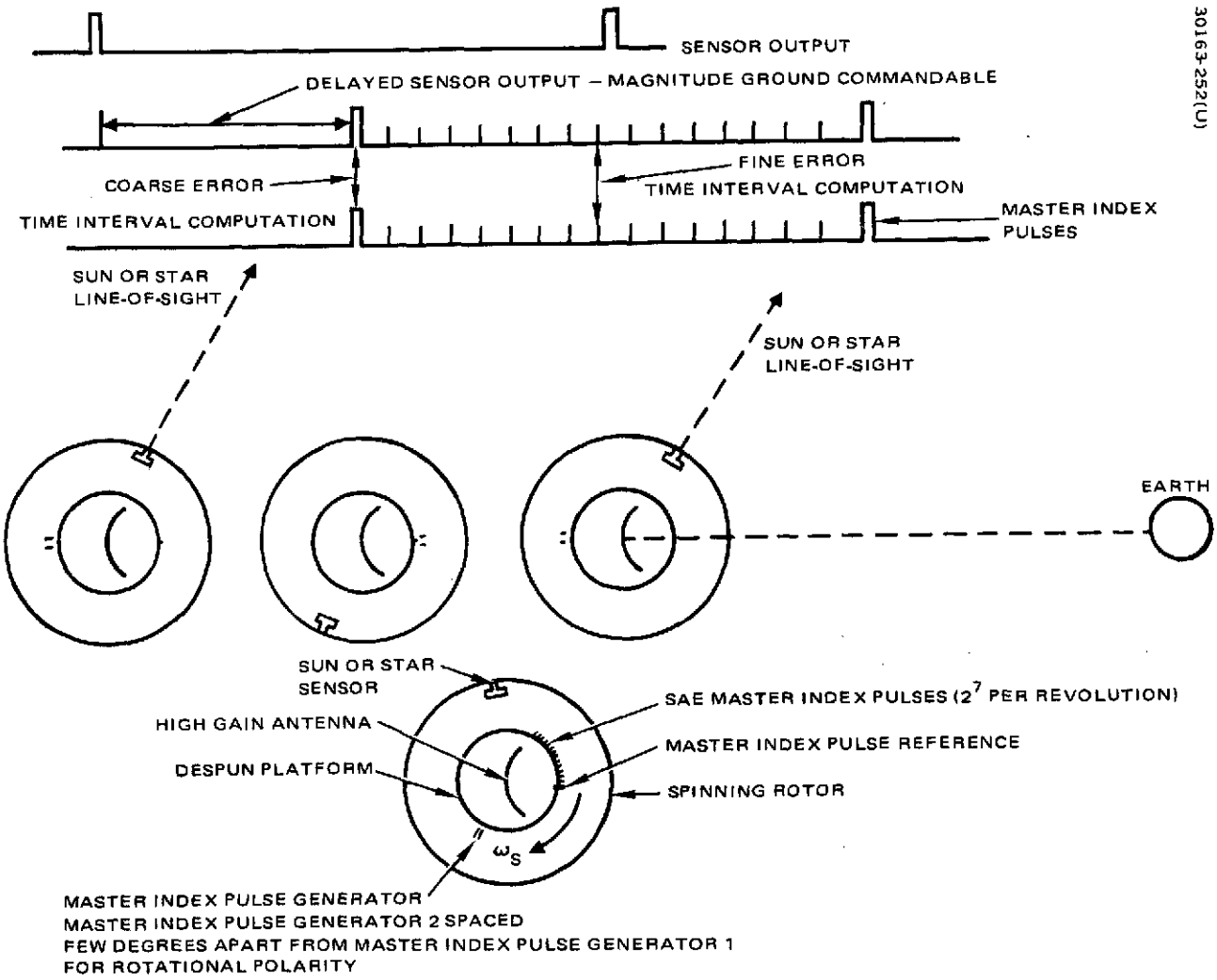

FIGURE 5-12. FORMATION OF DESPIN ERROR SIGNAL

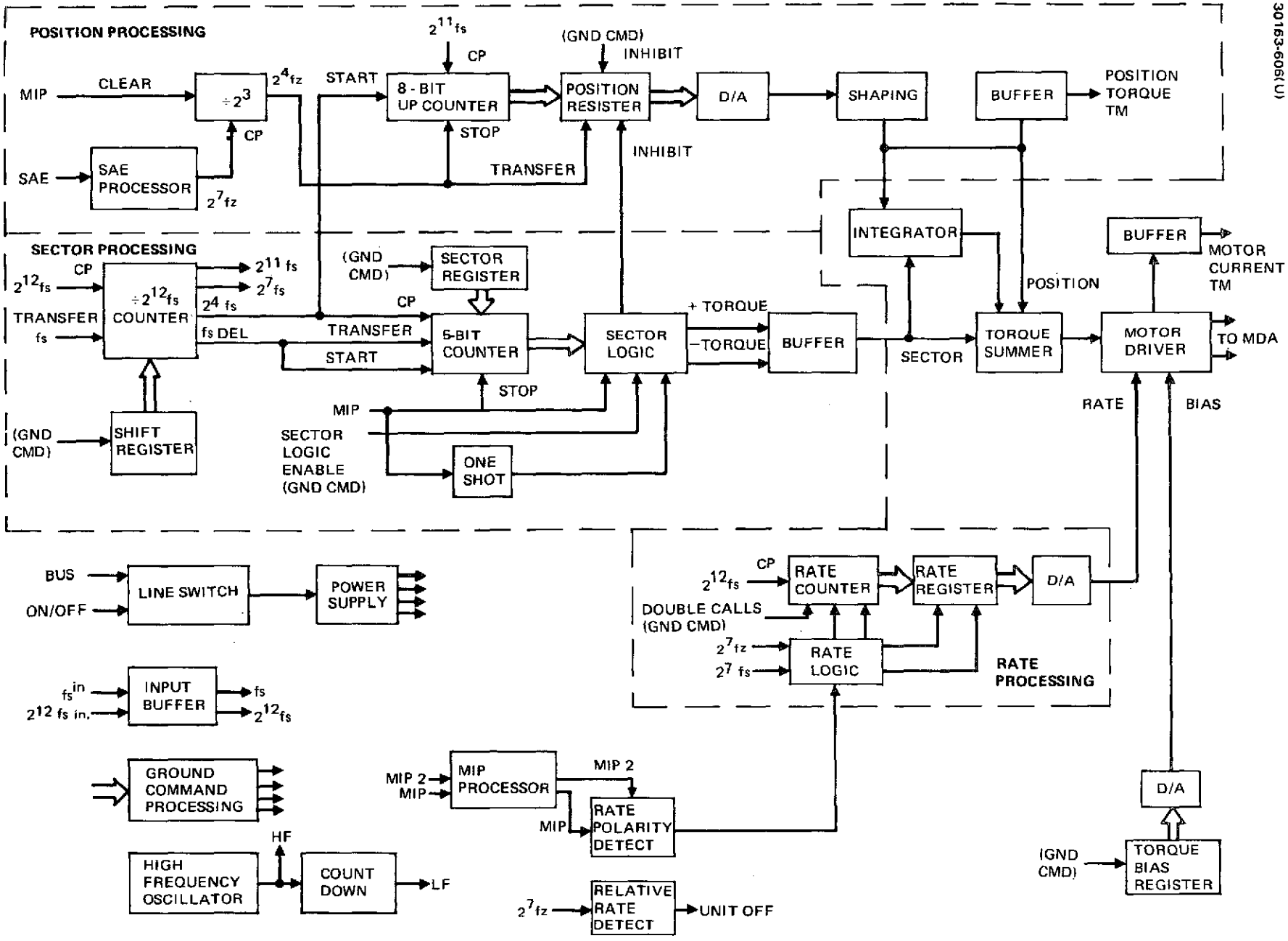

FIGURE 5-13. DESPIN CONTROL ELECTRONICS

Section 5.2), it warrants further discussion here along with the individual functions of the despin electronics unit.

Phase Lock Loop

As previously noted, position errors are derived based on time measurements having units of fractions of the spin period and, in addition, use simulated sun or star pulses interspaced between the real sun or star sensor pulses. The spin period synchronization is generated by the phase lock loop.

The phase locked loop is a variable frequency pulse generator which maintains both frequency and phase lock with the input sun or star signal. The prime element is a voltage controlled oscillator (VCO) whose frequency is controlled by a number stored in a digital register. Since the VCO is an analog circuit, a digital-to-analog converter is also required. Under zero error conditions for the phase locked loop (i.e., phase and frequency lock with the input signals), the VCO will generate 2^{12} pulses for each spacecraft revolution; i.e., during the time interval between the occurrence of two consecutive sun or star sensor pulses. A simple countdown register provides additional output frequencies f_s, where f_s is the spin frequency as stored in the VCO. The f_s pulses are then used by the despin control torque command generator to determine position error using the 2^{12} f_s pulses as clock signals. Each $2^{12}f_s$ pulse represents 0.088 deg of position error. The f_s output of the phase locked loop countdown register is fed back to a phase detector which measures the time difference between the real sensor pulse and the simulated (f_s) pulse, again using the $2^{12}f_s$ as a counting clock. The register controlling the VCO frequency is then altered until a zero error condition is achieved.

Position Loop and Sector Signal Processing

The 16 times spin speed (2^4f_s) sample rate of the position loop divides the 360 deg per spin period into 16 sectors of 22.5 deg each. The sectors are referenced to the f_s input from the phase lock loop. The desired sector of operation is chosen by ground command and stored in a sector register. A divide by 2^{12} counter using the f_s and $2^{12}f_s$ inputs from the attitude data processor provides the necessary spin synchronous frequencies. These outputs are delayed by the number in the delay register. The delay is sent by ground command and allows position control in 0.35 deg increments. The number of 2^4f_s pulses between the delayed f_s reference (f_s^{DEL}) and the master index pulse input are counted and the difference between the number counted and the number stored in the sector register is decoded and the polarity stored. The difference will be zero when operating in the desired sector. When the sector is not the desired one, a pulse of torque at the f_s reference time will be applied in the direction of the commanded sector and the position loop output will be inhibited. When the desired sector has been acquired, the sector logic can be disabled by ground command if desired.

The position loop processing controls the pointing in a 22.5 deg sector. The shaft angle encoder input is buffered to get a 2^7f_z signal, which is synched to the master index pulse input and counted down to get 2^4f_z for position processing. The number of $2^{11}f_s$ pulses between a 2^4f_s pulse and a 2^4f_z pulse is counted and stored in the position register. The null position is a phase difference of 11.25 deg, or a count of 64 $2^{11}f_s$ pulses. The number in the position register is digital-to-analog converted and shaped and summed with other

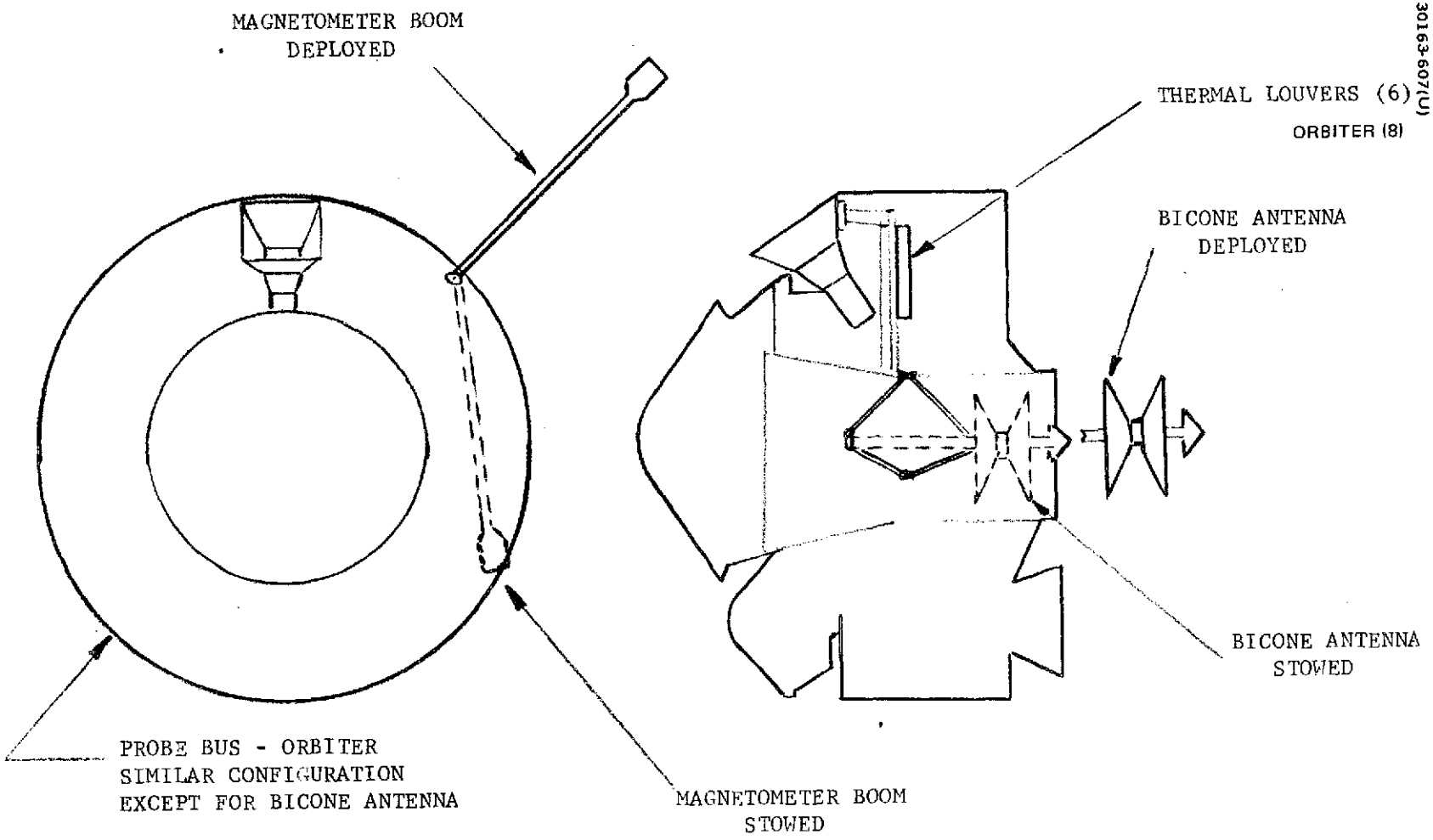

FIGURE 5-14. MECHANISMS/SPACECRAFT CONFIGURATION

torque inputs to provide position control. The position output can be inhibited by ground command.

Both the position and sector outputs are integrated and the integrator output also goes to the torque summer.

Rate Loop Signal Processing

The rate loop processing is performed by counting the number of $2^{12}f_s$ pulses between consecutive 2^7f_z pulses from the shift angle encoder processor. The number of $2^{12}f_s$ pulses counted is stored in the rate register, digital-to-analog converted, and summed with other torque inputs. The normal gain is selected for optimum performance at 5 rpm, but this can be doubled by ground command to improve performance at higher spin speeds.

Ground Command and Torque Bias

Ground commanded numbers are stored in the torque bias register, digital-to-analog converted and summed with the other torque inputs to provide a command bias capability.

5.5 MECHANISMS

The Pioneer Venus baseline mechanism configuration is designed to achieve the following functions: thermal control, pyrotechnic release of the bicone antenna and magnetometer boom, and bicone antenna and magnetometer boom deployment. Figure 5-14 shows the mechanisms location on the basic spacecraft bus. A brief functional description of mechanism technique used to achieve the desired functions is given below. Detailed performance characteristics are presented in Appendix C.

Thermal Control

Active thermal control for equipment mounted to the spacecraft equipment shelf will be accomplished by utilzing the bimetallic actuated thermal control louvers that have been previously qualified for military program. The effective emittance of the controller is automatically regulated as a function of average surface temperature under the thermal controller.

Pyrotechnic Devices

Dual pressure cartridge pin pullers will be utilized for the release of the mechanisms. These pin pullers will be operated by redundant single bridgewire pressure cartridges. Either the single bridgewire Apollo standard initiator or the single bridgewire Viking standard initiator will be utilized. The use of one of the initiators will provide the pyrotechnics with demonstrated reliability and performance characteristics.

TABLE 5-3. ESTIMATED MEASUREMENT ERRORS

Error Sources at 60 rpm	Bias Errors, deg	Pulse to Pulse (3σ) Random Errors, deg
Electronics (0.5 ms/bit)	0.18	0.02
Middle range sun sensor		
$(\psi_2 - \psi)$	0.25	0.07
(ψ)	0.3	0.05
Upper, lower range sun sensor		
$(\psi_2 - \psi)$	0.5	0.14
(ψ)	0.7	0.1
Star sensor		
$(\psi_2^* - \psi^*)$	0.1	0.5
$(\psi^* \text{ or } \psi_2^*)$	0.14	0.36
Spacecraft alignment (sensor)	0.1	-
Spacecraft dynamics	≤ 0.1 (wobble)	≤ 0.2 (nutation)

TABLE 5-4. UNPROCESSED LUMPED ERRORS (3σ)

Measurement	Using Upper or Lower Sun Sensor		Using Middle Sun Sensor	
	Bias, deg	Random, deg	Bias, deg	Random, deg
$\psi_2 - \psi$	0.55	0.25	0.34	0.10
$\psi - \psi^* \text{ or } \psi_2^*$	0.77	0.43	0.40	0.42
$\psi^* - \psi_2^*$	0.24	0.54	0.24	0.54

Bicone Antenna Mechanism

This antenna extension mechanism consists of a telescopic tube, a pyrotechnic pin puller and two negator extension springs. Two coaxial cable canisters are mounted to the outside tube containing the antenna cables in a large loop configuration. This provides a positive cable guide during deployment. This mechanism will be required on the probe bus when launched by the Thor/Delta.

Magnetometer Boom

The light-weight 42 in. magnetometer boom design utilizes a one-piece, rigid, pivoting tube. The boom is maintained in a stowed position and supported by a pyrotechnic pin puller during launch. Rotation of the boom, after pin puller actuation, is accomplished utilizing the centrifugal forces associated with the spinning spacecraft.

5.6 SUBSYSTEM PERFORMANCE (THOR/DELTA)

This section summarizes the principal performance aspects of the attitude controls and mechanisms subsystems. The models and analytic results are given in Appendices A and B.

Attitude Determination Performance

Two values of lumped sensor errors can be represented by unprocessed data measurements and processed data measurements. The processed measurements are assumed to be smoothed and the bias errors removed by obtaining measurements from more than one star at a given spin axis attitude. Table 5-3 lists the basic error sources and the estimated magnitude of the errors. The bias estimates are based on easily achievable tolerances with similar sensors at reasonably low cost and represent an expected worst case. The random errors represent an estimate of the pulse to pulse (or sample to sample) jitter. The bias errors are assumed to be independent as are the random errors.

Lumped errors can be calculated for specific measurements and various sun and star sensor combinations. The lumped bias errors shown in Table 5-4 are the rss of the appropriate bias errors and the lumped random errors are the rss of the appropriate random errors from Table 5-3 without smoothing. It is assumed that at least 25 samples of data will be used to estimate the mean value of the measurements; therefore, the standard deviation of the processed random errors will be reduced by at least a factor of 5 from that shown in the table. As can be seen from examining the lumped random errors, if 30 samples of data are used to estimate the mean value, all of the measurement errors should be ≤ 0.1 deg. Bias estimation is performed by the attitude determination software. In practice, however, a residual bias error will always remain due to a finite electronic quantization error of the time interval measurement between the sensor pulses. This bias error will vary between 0.18 deg (maximum) at 60 rpm to 0.015 deg

(maximum) at 5 rpm. In addition, only a finite number of iterations will be performed to estimate the bias corrections required to give the same spin axis attitude from multiple star measurements.

To demonstrate the effects of measurement errors on attitude determination, the attitude errors for various sun-star-azimuth angles and star declination were computed and graphed for the nominal Pioneer Venus attitude; i.e., with the spin axis approximately normal to the ecliptic plane. The 3σ deviation of the processed random errors for measurements of $(\psi_2-\psi)$, $(\psi-\psi^*$ or $\psi_2^*)$ were all estimated to be ≤ 0.1 deg after filtering by ground software. To illustrate the effects of large residual bias errors, plots were made assuming only slight improvement by the software in estimating the bias errors. Specifically, the bias errors shown in Table 5-5 for the middle sun sensor were used. Plots were also made assuming no bias estimation errors to show what is possible with multiple star measurements.

These attitude errors versus sun-star azimuth separation angle are graphed in Figures 5-15 through 5-18. Figures 5-15 and 5-16 show the effect of the lumped errors for the middle range sun sensor in Table 5-5 using the dual slit, single slit (canted and vertical) schemes. Figures 5-17 and 5-18 show the effect if the bias errors are removed. Figures 5-15 and 5-17 assume that the star appears at the upper edge of the sensor field of view (closest to the spin axis) and Figures 5-16 and 5-18 assume that the star appears at the lower edge of the sensor field of view. When the sun-to-star angle, measured in the ecliptic plane is ± 90 deg, the dual slit star sensor configuration is unusable. The canted slit star sensor becomes unusable at about +125 and -55 deg from the sun. Good coverage at 0 and 180 deg is provided by the straight slit star sensor configurations when dual slit operation is unsatisfactory. By comparing the Figures 5-15 and 5-16 or 5-17 and 5-18, greater accuracy (least error) is obtained for the star highest in the field of view. Figures 5-15 and 5-16 show that the 0.9 deg attitude determination requirement can be met over a large range of sun-star angles even with large residual bias errors, especially for star angles high in the field of view. Figures 5-17 and 5-18 show that if the biases are removed, the sun-star azimuth angle range over which any particular slit configuration cannot determine attitude to the required accuracy is rather small; i.e., only 50 deg of the total azimuth range of 360 deg, or 14 percent, is denied any one of the three slit configurations. These figures can be used to estimate the attitude determination accuracy associated with any sensor configuration at any point of cruise or orbital history. Therefore, they assist in selection of optimum stars and sensor configuration.

Quantitative studies were also made for non-nominal attitudes, corresponding to sun aspect angles of 15 and 55 deg (the upper and lower edges of the upper sun sensor field of view). The bias and random measurement errors in Table 5-5 associated with the upper sun sensor were summed. The star was positioned at both the upper and lower limits of the star sensor field of view. At a sun angle of 15 deg, attitude errors for each sensor configuration were within the ± 3 deg allowed for most sun-star azimuth angles; the single slit configuration provided superior accuracy over all sun-star geometries. At a sun angle of 55 deg the attitude errors for all sensor

TABLE 5-5. ASSUMED PROCESSED (RESIDUAL) LUMPED ERRORS (3σ) FOR ANALYSIS PURPOSES

Measurement	Using Upper or Lower Sun Sensor		Using Middle Sun Sensor	
	Bias, deg	Random, deg	Bias, deg	Random, deg
$\psi_2-\psi$	0.6	0.1	0.2	0.1
$\psi-\psi^*$ or ψ_2^*	0.5	0.1	0.3	0.1
$\psi^*-\psi_2^*$	0.2	0.1	0.2	0.1

configurations were within the ±3 deg allowed for a smaller sun-star azimuth angle range; however, the errors within the permissible range were larger than those corresponding to a sun angle of 15 deg. The poorer accuracy at the 55 deg angle is due to the smaller sensitivity of the upper sun sensor to sun angle changes. This sensitivity was traded for the ability of upper sensor to detect the sun at small sun angles. Multiple star measurements at this sun angle would reduce the residual bias error of the upper sensor and substantially improve its performance. In summary, multiple star measurements should be made to obtain estimates of the bias errors which will exist in the attitude measurements. Ground software should be used to filter the pulse-to-pulse random error dispersions and to compute an estimate of system bias errors. At least two independent attitude measurements should be made; i.e., two stars and the sun to obtain the bias estimator. In addition, at least 25 samples of each data set should be taken to compute the mean value of a data measurement in order to reduce the effects of random noise errors.

Star-sun geometry has a major effect on the accuracy of attitude determination. Once a particular launch date is set, the right ascension of the sun relative to the stars can be determined and an analysis can be made to determine the particular stars which will provide acceptable accuracy for attitude determination.

If smoothed random errors do not exceed 0.1 deg and the residual bias errors do not exceed 0.1 deg for the $\psi-\psi_2$, $\psi^*-\psi_2^*$, and $\psi-\psi_2^*$ measurements, the 0.9 deg attitude determination accuracy requirement for the nominal attitude is easily satisfied. The electronic quantization step size should not exceed 0.2 deg so that the average bias error will not exceed 0.1 deg for a large number of data samples. The system bias errors should be required to remain relatively constant (<0.1 deg per week drift) following inflight calibration to minimize the frequency of calibration. The pulse-to-pulse random errors should not exceed 0.5 deg (3σ) to minimize the number of data samples required to obtain a good estimate of the mean value of the measurement. Using these error tolerances, the range of sun-star azimuth angles must be $+90 \pm 65$ deg for the dual slit mode; 0 ± 65 deg, and 180 ± 65 deg for the single vertical slit mode; and 40 ± 65 deg and -140 ± 65 deg for the single canted slit ($\beta^* = -20$ deg) mode during the cruise phase of the mission.

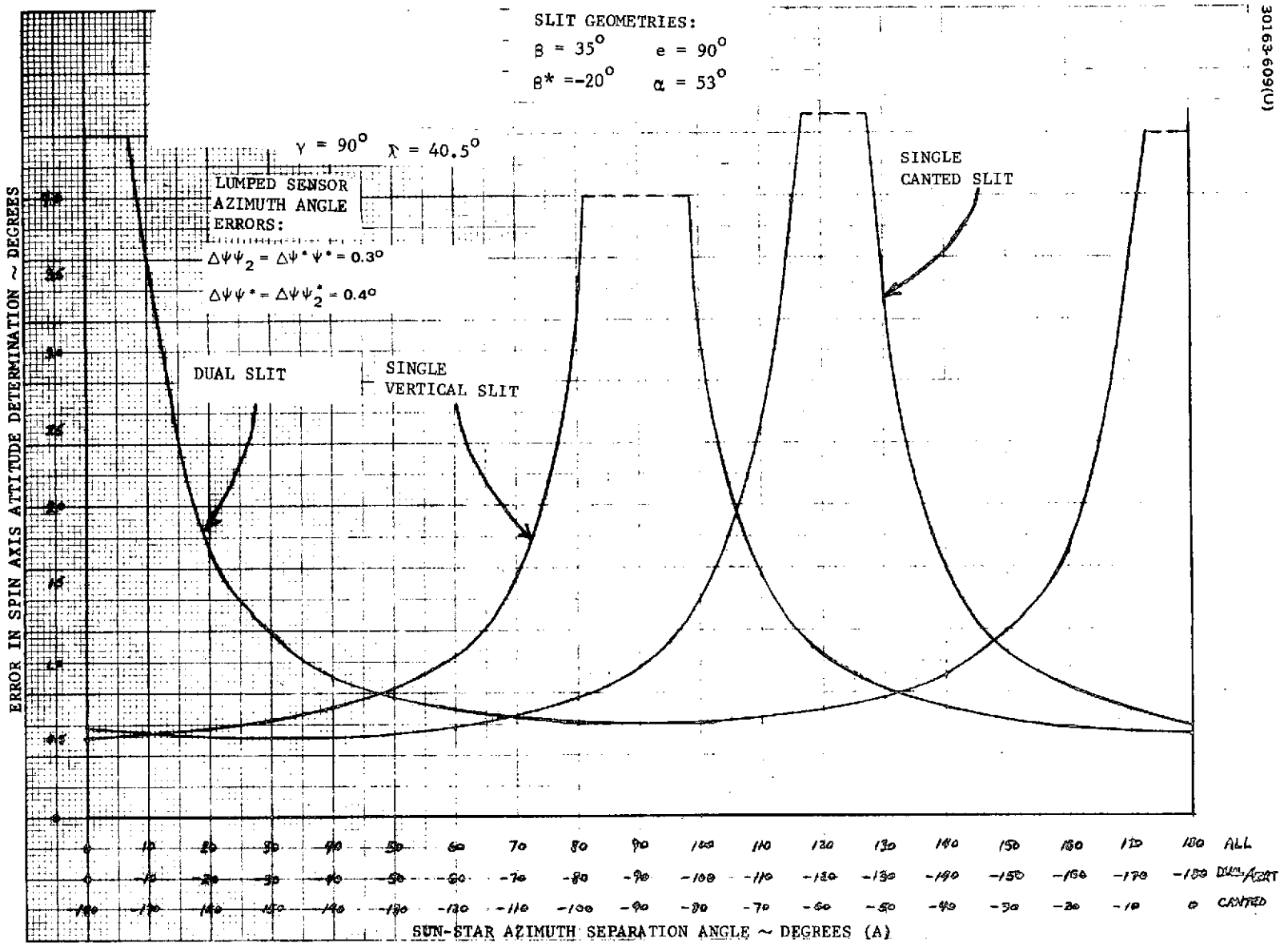

FIGURE 5-15. ATTITUDE ERRORS VERSUS SUN-STAR AZIMUTH SEPARATION ANGLE - LUMPED ERRORS STAR AT LOWER EDGE OF FOV

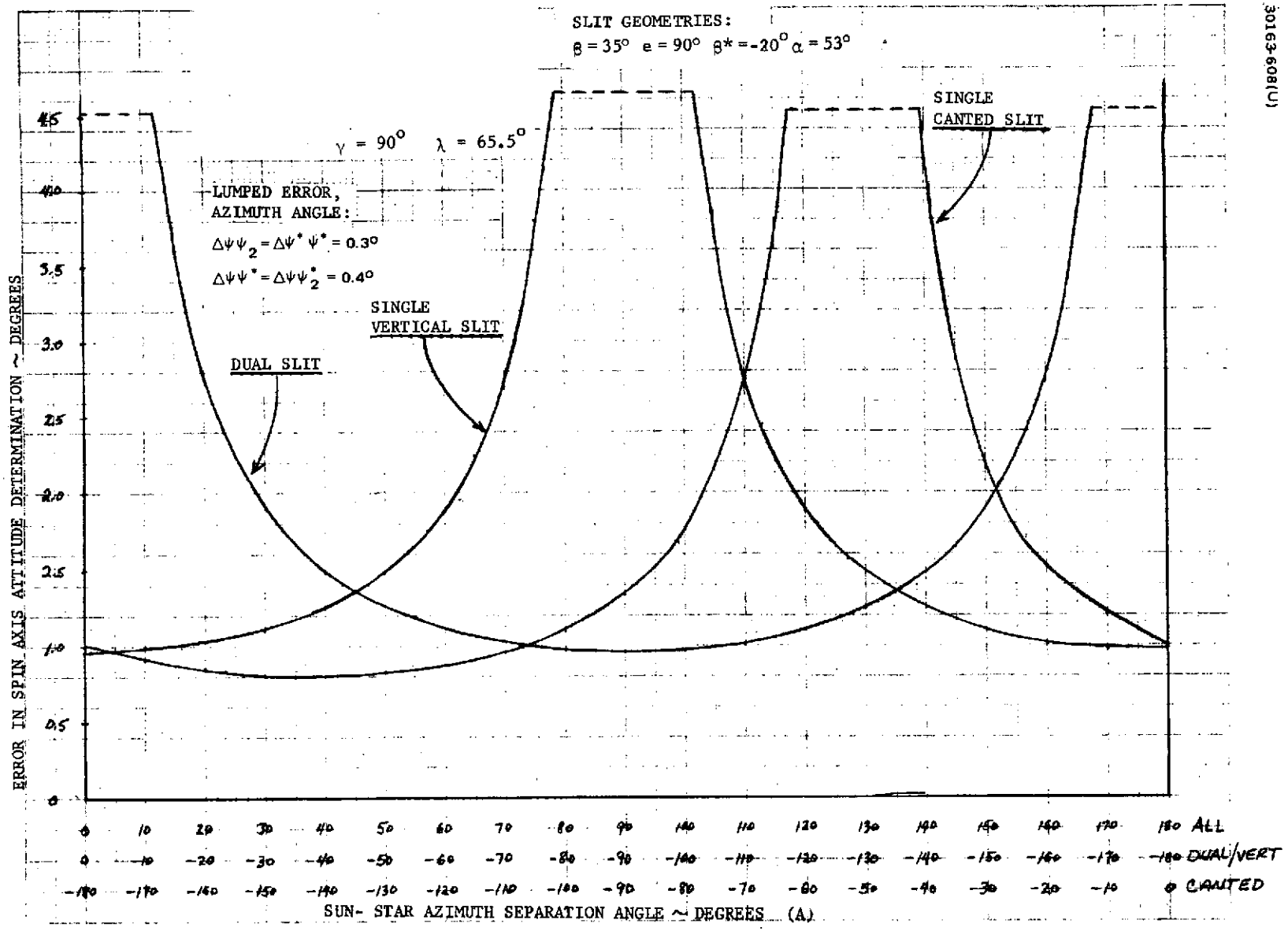

FIGURE 5-16. ATTITUDE ERRORS VERSUS SUN-STAR AZIMUTH SEPARATION ANGLE - LUMPED ERRORS-STAR AT LOWER EDGE OF FOV

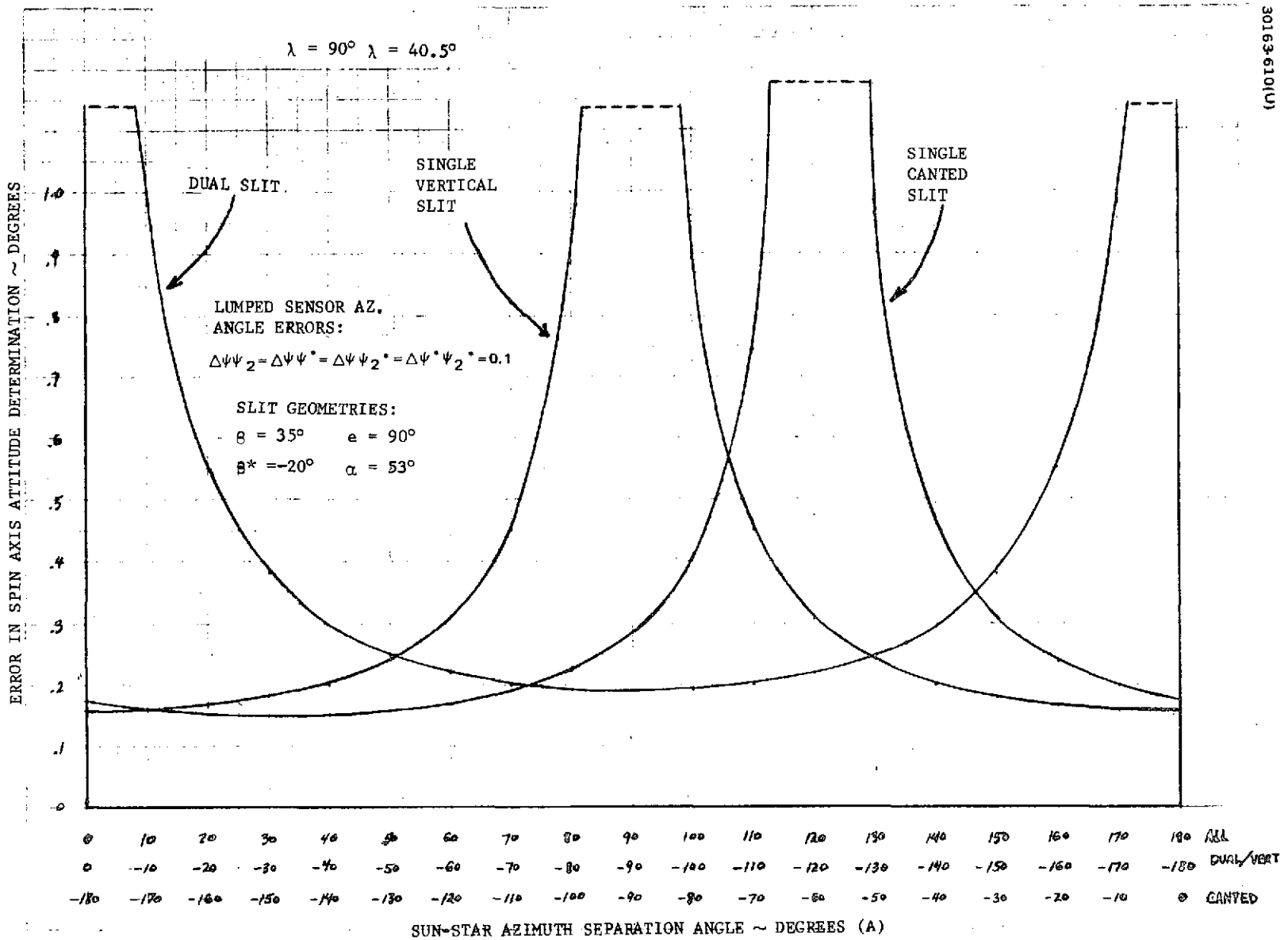

FIGURE 5-17. ATTITUDE ERRORS VERSUS SUN-STAR AZIMUTH SEPARATION ANGLE - BIAS ERRORS REMOVED - STAR AT UPPER EDGE OF FOV

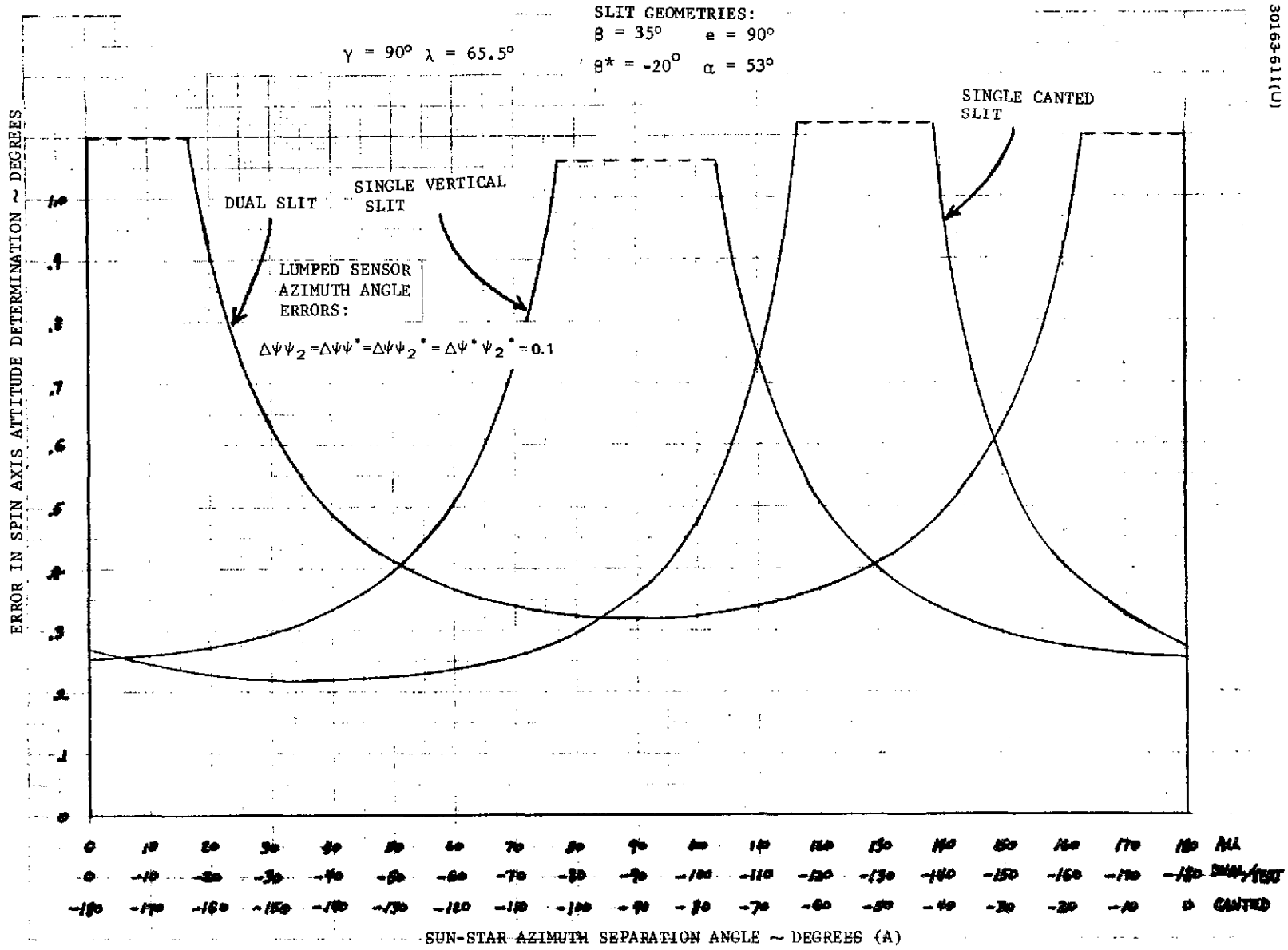

FIGURE 5-18. ATTITUDE ERRORS VERSUS SUN-STAR AZIMUTH SEPARATION ANGLE - BIAS ERRORS REMOVED - STAR AT LOWER EDGE OF FOV

TABLE 5-6. JET CONTROL PERFORMANCE

Maneuver	Jet Select	Mode	Probe at 60 rpm	Orbiter	
				At 60 rpm	At 5 rpm
Attitude Precession	1) 5A·64	P	0.4°/P	0.6°/P	1.0°/P
	2) 5A + 6A + 7A	P	0.2°/P	0.3°/P	0.5°/P
	3) 1R·2R + 3R·4R	P	0.05°/P	0.03°/P	0.07°/P
Spin speed	1) 1R + 2R + 3R + 4R	C	0.06 RPS/S	0.12 RPS/S	0.07 RPS/S
	2) 1R·3R + 2R·4R	C	0.12 RPS/S	0.24 RPS/S	0.14 RPS/S
ΔV	1) 6A·7A	C		0.17 MPS/S	0.15 MPS/S
	2) 5A + 6A + 7A	C	0.064 MPS/S	0.085 MPS/S	0.076 MPS/S
		P**	0.0085 MPS/P	0.0100 MPS/S	0.0025 MPS/P*
	3) 1R·2R + 3R·4R	P	0.015 MPS/P	0.019 MPS/P	0.018 MPS/P

Notes: P = pulse (117 ms)
C = continuous
* = 30 ms pulses
** = twice per spin period pulsing

Attitude/ΔV/Spin Speed Control

Maneuver Control

The Pioneer Venus spacecraft jet configuration can perform all attitude/spin speed/ΔV maneuvers redundantly; i.e., each maneuver can be performed with more than one jet or combination of jets. Table 5-6 summarizes the fundamental performance characteristics of the possible jet control modes applicable to maneuvers for the probe bus at 60 rpm (cruise spin rate) and for the orbiter at 60 rpm (initial cruise spin rate) and at 5 rpm (orbital spin rate).

Because of uncertainties in the mass and geometric properties of the spacecraft, in timing, and in the impulse and alignment of the thrusters, the executed maneuver will deviate from the nominal maneuver; in addition, these uncertainties will, in general, induce cross-talk or coupled maneuvers. As an example of cross-talk, the execution of an axial ΔV maneuver will cause incremental changes in attitude, spin speed, and radial ΔV. Furthermore, spacecraft nutation is generally induced. One can fully appreciate the uncertainty and cross-talk associated with a specific maneuver (spin speed, radial ΔV, axial ΔV, attitude precession) on a spinning body by examining an error block diagram for that maneuver. Error block diagrams for the Pioneer Venus selected Thruster arrangement and required maneuvers are given in Appendix A. Algorithms were developed (see Appendix A) for estimating performance parameters for every kind of maneuver, and their associated uncertainties and cross-coupling effects. These were then used in conjunction with typical values for the first order error sources (shown in Table 5-7 and 5-8) to assess the errors for all basic maneuvers required by both the probe and orbiter missions.

The various maneuvers and associated errors are summarized in Tables 5-9 through 5-12. Note that the axial jet mode can execute the first midcourse maneuver to the required accuracy even with an open loop precession to the required ΔV attitude. Open loop rhumb line precession was examined in some detail during the studyperiod. Figure 5-19 summarizes the key results. For an initial attitude uncertainty of 1 deg at cruise attitude, jet torque phase angle error of 1 deg and 4 percent impulse uncertainty, the uncertainty in the final attitude for ≈90 deg procession toward or around the sunline is ≈4 deg. Since impulse uncertainty contributes ≈3.6 deg to the final attitude error. The impulse uncertainty is the dominant error sources; limiting impulse uncertainty to 4 percent is equivalent to controlling open loop precession errors to 4 deg for the largest precession anticipated. Note that upon return to the cruise attitude following the midcourse maneuvers, an attitude touch-up and spin speed trim would probably be required. Using the radial jet mode for a large first midcourse maneuver would require an attitude and spin speed touch-up during and after the maneuver in order to deliver the ΔV to sufficient accuracy and reestablish cruise conditions. For the various attitude precessions required for the probe separation sequence, attitude errors are significant and indicate that attitude determination during this sequence is probably necessary. Typical in-orbit ΔV corrections at 5 rpm generate significant attitude errors and residual nutation; these disturbances

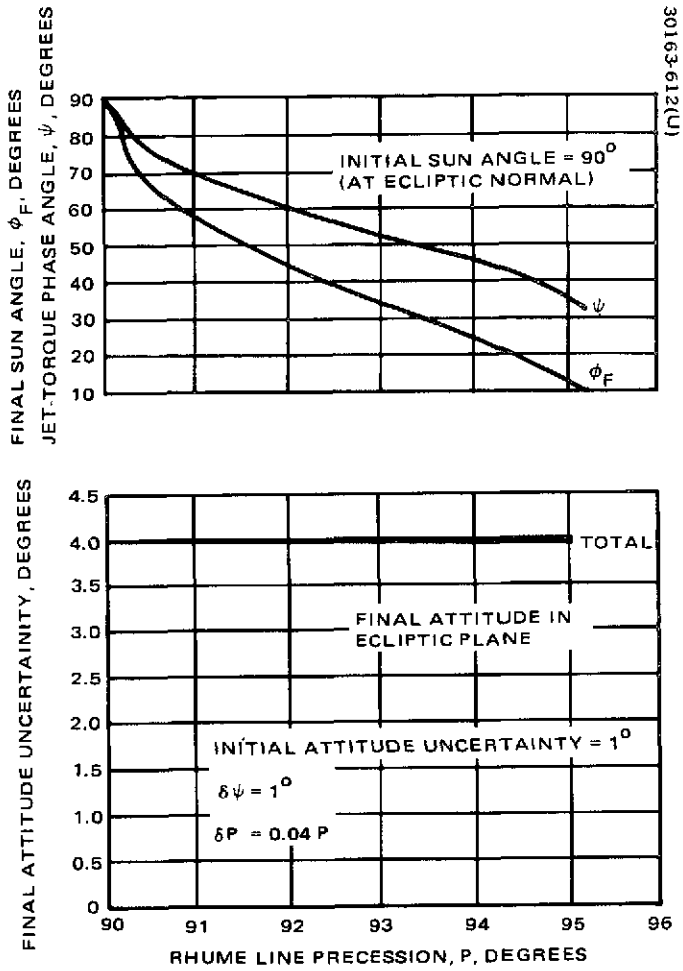

FIGURE 5-19. ATTITUDE UNCERTAINTY RESULTING FROM LARGE OPEN-LOOP PRECESSION

TABLE 5-7. ASSUMED UNCERTAINTIES (3σ)

Item	Units	Symbol	Numerical Value
Weight	kg	δW	0.23
Thrust (or nozzle) misalignment	deg	ϵ	0.1
Thruster (or setting) misalignment	deg	$\delta\beta$	0.1
Principal-axis tilt	deg	γ	0.15
Quantization	deg	$\delta\theta$	0.35
Radius	cm	δR	0.25
Axial offset	cm	ΔZ	0.25
Sun-pulse	deg	$\delta\alpha$	0.5
Thrust centroid	sec	δt_c	0.004
Duration	sec	$\delta\tau$	0.25
Spin speed	rad/s	$\delta\omega$	0
Initial X-attitude	deg	δA_x	0.7
Initial Y-attitude	deg	δA_y	0.7
Initial in-plane uncertainty	deg	$\delta\phi_I$	0.7
Initial out-of-place uncertainty	deg	ϵ_I	0.7

TABLE 5-8. ASSUMED PER-UNIT UNCERTAINTIES (3σ)

Item	Symbol	Numerical Value
Thrust	$\delta F/F$	For one jet, continuous mode: 0.03 For pulsed modes, radial or axial (calibrated): 0.03 For pair of axial jets (axial ΔV) continuous mode: 0.04
Spin moment of inertia	$\delta I_Z/I_Z$	0.01

deteriorate antenna pointing and imply that attitude corrections may be required after such maneuvers.

Attitude Stability

The Pioneer Venus spacecraft spin axis attitude will be perturbed during the missions by solar torque, aerodynamic torque and maneuver torques. Also, because the spacecraft is not perfectly balanced, the nominal spin axis will cone around the true principal axis at spin speed or, equivalently, the spacecraft will wobble. Table 5-13 summarizes the worst case attitude disturbances for both the probe and orbiter missions. Solar torque estimate indicates that the spin axis could be allowed to drift through ±2 deg deadband between orbital corrections with no attitude touch-up required. Aerodynamic torque could introduce daily attitude correction requirement if periapsis is sufficiently low. However, since precession is ≈ normal to the orbit plane and the earthline is close to orbit plane during first part of the mission, the initial effect is to precess the spin axis around the earthline. Attitude perturbations due to orbital corrections can be significantly reduced (< 0.5 deg) by use of the 180 deg bang-band ΔV mode. Also, if thrust mismatch were limited to 1 percent, a pair of axial jets would perturb the attitude < 1 deg; mismatch calibration and timing jet start could then be used to move the angular momentum vector in a preferred direction in inertial space; i.e., compensate for another disturbance. Therefore, with suitable calibration and sufficiently high periapsis, the attitude correction cycle can be made coincidental with the orbital correction cycle. The attitude distrubance due to aerodynamic precession torque at probe bus entry is small enough to maintain the earth within the endfire antenna 22 deg beamwidth.

Nutation Damper Performance

The nutation damper performance is illustrated in Figure 5-20 for both the probe and orbiter missions. All design requirements are satisfied.

TABLE 5-9. PROBE BUS NOMINAL MANEUVERS AND PROPELLANT CONSUMPTION

Mission Phase	Operation Time, h	Nominal Maneuvers			Propellant Consumption lb
		ΔV, m/sec	ΔP, deg	Δ, rpm	
Initial despin	0.7	—	—	-30	1.0
Initial reorientation		—	66.4	—	1.2
First midcourse	1.0	71.9	190.4	—	30.5
Second midcourse	0.6	4.2	90.0	—	3.1
Third midcourse	0.5	0.4	—	—	0.2
Large probe reorientation	3.0	—	126.9	-30	2.0
Large probe despin		—	—	-15	0.5
Small probe reorientation	4.5	—	24.1	+56	1.9
Small probe targeting		5.4	—	—	1.3
Probe bus E-20 reorientation	0.3	—	52.9	—	0.6
Probe bus targeting reorientation	3.0	—	83.1	-11	1.0
Probe bus retardation		16.7	—	—	22.0
Probe bus E-18 reorientation		—	11.6	—	0.1
Final reorientation	0.3	—	7.5	—	0.1

TABLE 5-10. PROBE BUS MANEUVER ERRORS

Mission Phase	Errors (3 σ)			
	ΔV	Final Attitude deg	Residual Nutation, deg	Spin Change rpm (rad/s)
Initial despin	0.025 m/sec	0.036	0.098	1.32 (0.13)
Initial reorientation	0.10 m/sec	3.2	0.50	0.2 (0.02)
First midcourse { Axial mode	3%, 3.4 deg	14.2	0.35	5.9 (0.59)
First midcourse { Radial mode	3%, 5.2 deg	12.0	0.003	25.1 (2.51)
Second midcourse { Axial mode	3%, 2.1 deg	2.8	0.35	0.33 (0.033)
Second midcourse { Radial mode	3%, 3.5 deg	2.8	0.003	1.4 (0.14)
Third midcourse	5%, 0.5 deg	0.15	1.28	0.1 (0.01)
Large probe reorientation	0.09 m/sec	4.5	0.70	1.3 (0.13)
Large probe despin	0.011 m/sec	0.014	0.11	0.64 (0.064)
Small probe reorientation	0.075 m/sec	1.22	0.28	2.3 (0.23)
Small probe targeting	3%, 2.7 deg	0.51	0.002	1.3 (0.13)
Probe bus E-20 reorientation	0.13	2.89	0.73	0.16 (0.016)
Probe bus targeting reorientation	0.17	3.23	0.84	0.58 (0.058)
Probe bus retardation	3%, 0.78 deg	0.66	0.47	0.96 (0.096)
Probe bus E-18 reorientation	0.023	1.07	0.80	0.03 (0.003)
Final reorientation	0.014	0.93	0.80	0.018 (0.0018)

TABLE 5-11. ORBITER NOMINAL MANEUVERS AND PROPELLANT CONSUMPTION

Mission Phase	Operation Time	Nominal Maneuvers			Propellant Consumption lb
		ΔV, m/sec	ΔP, deg	Δω, rpm	
Initial despin	0.7	—	—	-30	0.7
Initial reorientation		—	80	—	1.0
First midcourse	1.0	71.7	190.4	—	23.0
Despin	0.3	—	—	-30	0.7
Second midcourse	0.6	6.3	90	—	2.3
Third midcourse	0.5	0.3	—	—	0.12
Reorientation for orbit insertion	2.0	—	207	—	1.3
Reorientation for orbit insertions	2.0	—	207	—	1.3
Typical initial-orbit correction	0.5	5.0	—	—	1.0
Spindown for orbit operations	0.3	—	—	-25	0.6
Typical in-orbit ΔV	3.0	0.5	—	—	0.1
Typical in-orbit attitude change	0.3	—	5	—	0.005

TABLE 5-12. ORBITER MANEUVER ERRORS

Mission Phase	Errors (3σ)			
	ΔV	Final Attitude deg	Residual Nutation deg	Spin Change rpm (rad/s)
Initial despin	0.036 m/sec	0.039	0.054	1.4 (0.14)
Initial reorientation	0.10 m/sec	3.4	0.58	0.2 (0.02)
First midcourse Axial mode	3%, 3.4 deg	14.4	0.48	6.7 (0.67)
Radial mode	3%, 5.1 deg	13.3	0.004	27.8 (2.78)
Despin	0.018 m/sec	0.005	0.02	1.3 (0.13)
Second midcourse Axial mode	3%, 2.3 deg	2.8	0.76	0.6 (0.06)
Radial mode	3%, 2.8 deg	3.0	0.005	2.4 (0.24)
Third midcourse	4.0%, 1.8 deg	0.08	0.13	0.08 (0.008)
Reorientation for orbit insertion	0.10 m/sec	5.6	0.68	0.2 (0.02)
Reorientation for orbit operations	0.14 m/sec	5.6	0.70	0.2 (0.02)
Typical initial-orbit correction	2.2%, 0.70 deg	0.01	0.08	0.2 (0.02)
Spindown for orbit operations	0.02 m/sec	0.23	0.37	1.05 (0.105)
Typical in-orbit ΔV (0.5 m/sec)	2.2%, 1.10 deg	1.7	1.9	0.04 (0.004)
Typical in-orbit attitude change	0.010 m/sec	0.17	0.51	0.0016 (0.0002)

TABLE 5-13. ATTITUDE DISTURBANCES

Disturbance	Probe Bus	Orbiter Bus
Solar torque precession	≤0.03 deg/day at 60 rpm	≤0.09 deg/day at 30 rpm ≤0.48 deg/day at 5 rpm
Aerodynamic torque precession	≤3.5 deg for 7 m/sec ΔV loss and 5 deg angle of attack during entry	≤0.7 deg for 0.2 m/sec ΔV loss and 27 deg ϕ of attack
Nutation		
ΔV maneuver	≤1.6 deg at 60 rpm (1 jet)	≤3.9 deg at 5 rpm
Attitude maneuver	≤0.8 deg at 60 rpm (targeting)	≤0.7 deg at 30 rpm
Spin speed change	≤0.1 deg at 15 rpm	≤0.4 deg at 5 rpm
Booster separation	≤0.7 deg at 90 rpm	≤0.6 deg at 90 rpm
Attitude		
ΔV maneuver	≤0.7 deg (targeting) at 60 rpm	≤2.4 deg at 5 rpm
Spin speed change	≤0.04 deg (initial despin)	≤0.25 deg at 5 rpm
Booster separation	≤1.4 deg at 90 rpm	≤1.8 deg at 90 rpm
Wobble	≤0.2 deg with boom deployed	≤0.1 deg with boom deployed

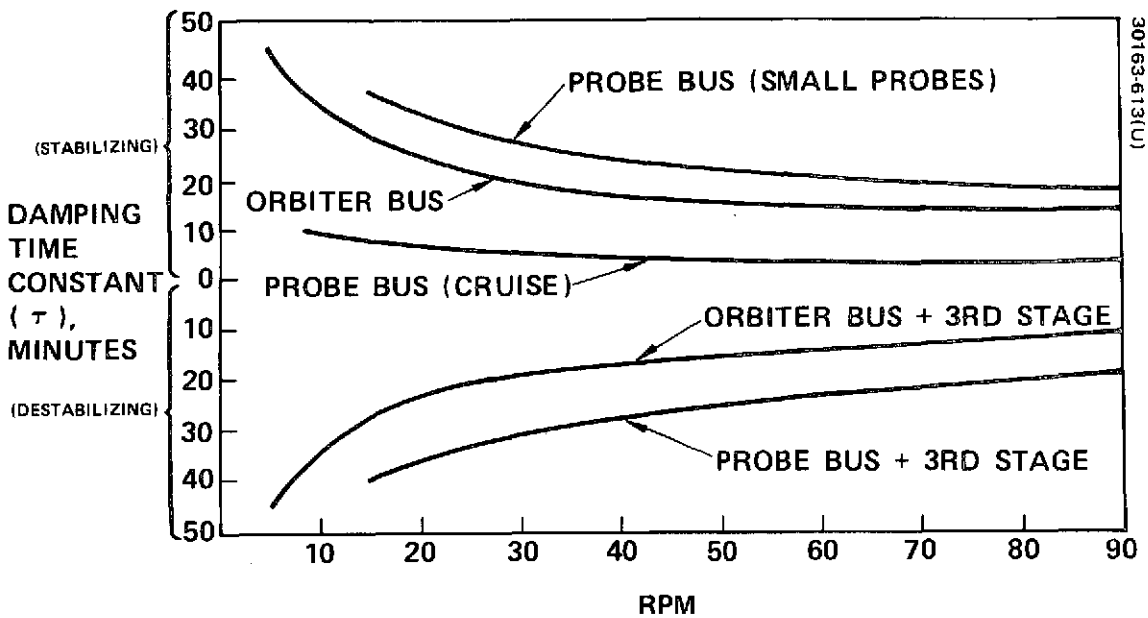

FIGURE 5-20. NUTATION DAMPER PERFORMANCE

Boom Deployment

The spacecraft will be statically and dynamically balanced with the boom deployed in order to avoid a significant thrust offset during orbit insertion, and to eliminate steady state wobble during cruise and orbit. The former effect degrades antenna pointing and sensor biases.

Prior to magnetometer boom deployment, the 0.46 kg magnetometer and 0.77 kg, 1.07 m boom are stowed at a radius of 1.07 m and at station 38 on the spacecraft. The static and dynamic imbalance contributions to the spacecraft in this state are given by 0.9 kg-m (probe and orbiter) and 0.046 kg-m^2 (probe, 0.27 kg-m^2 (orbiter), respectively. Thus, the laterial c.g. offset introduced by the stowed boom is 0.23 cm and 0.3 cm on the probe bus and orbiter bus, respectively. On the Delta launch vehicle prior to third stage burn, these offsets are reduced to 0.058 cm and 0.064 cm, respectively, and generate a thrust pointing error contribution about 50 percent of that due to third stage thrust misalignment (0.1 deg). Both of these contributions are small compared to the combined pointing error due to second stage guidance and third stage separation tipoff so that no significant degradation in third stage injection is generated by a statically unbalanced spacecraft with booms stowed.

The wobble introduced by the stowed boom is 0.077 and 0.41 deg on the probe bus and orbiter bus, respectively. On the Delta prior to third stage burn, these wobble angles are reduced to 0.0025 and 0.026 deg, respectively. Both wobble angles represent an insignificant cosine loss for the third stage burn.

At boom deployment, the wobble angle will transform into nutation as the vehicle now spins about a balanced axis. This nutation will be damped out by the mercury nutation damper. The fundamental dynamics of boom deployment resemble a conventional pendulum with the gravity field being replaced by a centrifugal acceleration field and a torsional restraint added at the pivot to absorb most of the kinetic energy generated by the pendulous swing outboard. The kinetic energy that must be absorbed or dissipated is very sensitive to spin speed, and requires that the latter be carefully controlled ($\pm$1 rpm) at deployment to minimize design complexity. At 60 rpm, a restraint torque $\approx$ 22 N m is required to absorb most of the 68 Joules of kinetic energy with the deployment completed in 0.1 sec.

Large Probe Separation

Prior to large probe separation, the spin axis is aligned for a nominal zero entry angle of attack, and the spin speed is reduced to 15 rpm. The residual nutation induced by the latter maneuver ($\approx$ 0.11 deg) will be damped out by the mercury damper with $\approx$8 min time constant; the induced attitude error is small ($\approx$0.02 deg) compared to the attitude uncertainty of 2.5 deg. At separation, three explosive nuts are fired to enable three compression springs to impart a relative velocity increment between the large probe and the bus. Each spring is compressed 0.87 in. to generate an initial force of 150 lb; for a 548 lb bus and 253 lb large probe, the three springs generate

a separation velocity of 2.5 ft/sec in 0.045 sec. The probe aft cover translates through the probe separation plane ≈0.25 sec later.

The tipoff rate induced at separation by axial force variation, lateral forces, spring circule uncertainty and bolt impulse variation is conservatively estimated to be ≤2 deg/sec for the large probe. This results in a large probe attitude error (bias) and nutation (coning) of 1 deg at the 15 rpm separation rate. Since the large probe principal axis can be misaligned with respect to the spacecraft spin axis prior to separation due to installation tolerances and probe dynamic imbalance, an additional attitude error and nutation will be induced at separation: these errors are conservatively estimated to be 1 deg. Therefore, the rss attitude uncertainty (angle of attack bus error) of the large probe after separation is $\sqrt{2.5^2 + 1^2 + 1^2} = 2.9$ deg; the rss nutation (angle of attack coning error) of the large probe after separation is $\sqrt{1^2 + 1^2} = 1.4$ deg. In the absence of nutation damping, the large probe will cone about its angular momentum vector (average attitude) up until entry.

The tipoff impulse at separation induces a 0.15 deg/sec tipoff rate on the probe bus. This results in a bus attitude error and nutation of 0.065 deg. In other words, the bus is a fairly stable launch platform. In general, the angular motions of the two separating bodies tend to reduce static clearance margins while the extremities of the two bodies overlap. A separation clearance analysis indicates that the conical shaped aft cover will easily clear the separation plane even with worst case attitude errors and nutation induced at separation.

Small Probe Separation

Prior to small probe separation, the attitude will be determined to an accuracy of 2.5 deg and the spin speed will be measured to an accuracy of 0.08 percent. Separation of the small probes takes place in a plane perpendicular to the actual spin axis. Therefore attitude uncertainty results in a small probe ΔV component parallel to the measured spin axis. The small probes are nominally separated with an "in plane" ΔV component of 5.7 m/sec; the maximum "out of plane" ΔV error induced is 0.25 m/sec. This ΔV error would result in a variation of ±1.7 min from computed small probe entry times. Spin speed uncertainty contributes to a magnitude error of the "in plane" ΔV component. A general analysis was made to determine the errors in the small probes "in plane" velocity vectors (magnitude and direction) resulting from various design tolerances. The method used and results obtained are now summarized.

The system was treated as though the probes were released sequentially. Since only the velocity components normal to the initial trajectory are of interest, each body may be treated as having only three degrees of freedom -- two linear and one rotational. Prior to its release, each probe is constrained to have a fixed position and angular orientation relative to the bus. The motion of each probe subsequent to its release is calculated by using the positions and velocities at the instant of its release to determine the initial conditions

for the three-degree of freedom equations of the motion of the probe. The bus with any of the remaining probes attached is still regarded as a single rigid body. Its subsequent motion may be determined from the velocity of its center of mass, together with its angular position and rate at the instant of release of the previous probe. Any impulse acting between the probe and the remaining body are taken into account at this point. It is readily apparent that the motion after the release of a subsequent probe may be calculated similarly, without considering further the motion of the previous probe. After the effects of the release of the final probe, the motion of all three probes and the remaining bus will be known.

A study of the effects of varying the parameters which could affect the probe velocity was performed. The parameter variations of importance were: radial offset of probe c.g. due to installation and spacecraft dynamic imbalance; angular offset of probe c.g. due to installation; common release time uncertainty due to quantization, sensor jitter and squib driver; non-simultaneity of release due to squibs; probe impulse due to preloaded clamp; bus c.g. offset; and initial spin speed uncertainty.

The errors which result from these various tolerances are shown in Table 5-14, assuming a sequential release of Probe 1, Probe 2, and Probe 3 a millisecond apart. There were no errors due to changes in weights or moments of inertia. The 3σ error in the magnitude of the "in plane" ΔV for any probe due to all error sources is ≤ 0.02 m/sec; the 3σ error in the direction of the "in plane" ΔV is ≤ 1 deg. These errors represent a small statistical contribution to the overall target impact dispersions.

At separation, the impulse due to the clamping mechanism could induce a tipoff rate of ≤ 4 deg/sec for the small probe. This results in a small probe attitude error and nutation of 0.5 deg; allowing an additional 0.5 deg error due to principal axis tilt, the rss attitude uncertainty and nutation after separation are 2.6 deg and 0.7 deg, respectively. Subsequent despin to 15 rpm with the spin jets will increase this nutation angle to 3.3 deg and introduce an additional 0.5 deg attitude error. In the absence of nutation damping, the small probe will cone about its angular momentum vector (average attitude) up until entry.

A detailed separation clearance analysis indicates that points of minimum separation clearance between the bus and small probes will comfortably clear one another (≥ 1 in.) ≈ 0.1 sec after squib firing.

Venus Orbit Insertion (Orbiter Spacecraft)

In the event all the propellant allocated for midcourse maneuvers has not been used, a preburn of the axial jet pair at the retro end of the orbiter spacecraft will be executed just prior to orbit insertion; this will match the motor impulse to initial orbited mass so that a near 24-h orbit period is achieved. The orbit insertion will take place at 30 rpm. The average thrust pointing error during the burn is proportional to the misalignment torque and inversely proportional to the spin kinetic energy. With thrust = 3850 lb, a thrust misalignment of 0.1 deg and c.g. to nozzle throat distance of 1.4 ft, one obtains a pointing error of 0.7 deg. This error together with the

TABLE 5-14. EFFECTS OF VARIOUS TOLERANCES ON PIONEER VENUS SMALL PROBE VELOCITY ACCURACY

	Effect of Tolerances											
	Probe 1						Probe 2				Probe 3	
	Probe 1		Probe 2		Probe 3		Probe 2		Probe 3		Probe 3	
	Velocity m/sec	Angle deg	Velocity m/sec	Angle deg	Velocity m/sec	Angle deg	Velocity m/sec	Angle deg	Velocity m/sec	Angle deg	Velocity m/sec	Angle deg
Design Value	5.7	90°	5.7	210°	5.7	330°	5.7	210°	5.7	330°	5.7	330°
Distance to probe c.g., ΔL = 0.25 cm	0.019	0	0	0	0	0	0.019	0	0	0	0.019	0
Angle tolerance, $\Delta\theta$ = 0.30 deg	0	0.3000	0	0	0	0	0	0.3000	0	0	0	0.300
Release time lag, Δt = 0.001 sec	0	0.3466	0	0.3466	0	0.3466	–	–	–	–	–	–
Sequential release, 00, 0.001, 0.002 sec	0	0	0.0058	0.3929	0.0058	0.7402	–	–	–	–	–	–
Probe impulse effects lb-sec (radial)	0.0005	0.3035	0.0041	0.023	0.0042	0.025	0.0005	0.3035	0.0085	0.0014	0.0005	0.3035
RSS error	0.019	0.550	0.0071	0.524	0.0072	0.818	0.019	0.427	0.0085	0.0014	0.019	0.427
Bus c.g. offset, 0.025 cm	–	–	–	–	–	–	–	–	–	–	–	–
Initial spin speed, 0.08 percent	0.0043	0	0.0043	0	0.0043	0	–	–	–	–	–	–
Total rss error	0.0195	0.550	–	–	–	–	0.0206	0.676	–	–	0.021	0.923

attitude measurement uncertainty of 3 deg combine to yield a worst case pointing error of 3.7 deg for orbiter insertion. The maximum nutation after burn is 2.2 deg; this will damp out with a time constant of 20 min.

Despin Control System

The Pioneer Venus mission objectives dictate pointing accuracy capability in the units of degrees regime. The mechanically despun hi-gain antenna provides a 3 dB beam width of 11 deg, thus allowing both the long term and short term pointing errors to be constrained within several degrees. Long term errors are associated with both internal and external disturbances while short term errors; i.e., time periods of 60 sec or less, are wholly associated with spacecraft induced disturbances.

Error contributors to azimuth pointing motion are summarized in Table 5-15. The error budget consists of two classes of errors: those that are oscillatory with time and those that are secular; i.e., monotonically increasing with time. Only the short term secular errors are considered because the despin design provides a full 360 deg azimuth pointing capability. The random or oscillatory errors consist of two components: a bounded antenna bias error, and sinusoidal terms occurring at spin rate. The systematic contribution to the azimuth pointing error is due to kinematic coupling of spacecraft nutation.

The despin control system has been modeled using both analog and digital simulation and it has been verified that the pointing stability performance requirement is met in the presence of expected worst case disturbances and sensor noise. The performance capabilities of the proposed design are summarized in Table 5-16.

The detailed rationale supporting the despin design (control loop analysis and simulated performance) is presented in Appendix B.

TABLE 5-16. DESPIN CONTROL SYSTEM PERFORMANCE SUMMARY

System Characteristics	5 rpm	30 rpm
Acquisition time, min	≤4.0	≤1.0
Gain margin, dB	≥9.0	≥12.0
Phase margin, deg	57.0	35.0
Torque margin	≥4.0	≥4.0
Effective loop bandwidth, Hz	0.7	0.7

TABLE 5-15. SUMMARY OF AZIMUTH POINTING ERRORS

Source	5 rpm		30 rpm	
	Sun Sensor Ref	Star Sensor Ref	Sun Sensor Ref	Star Sensor Ref
Random contributions				
Random noise and uncertainty	±0.25	±0.3	±0.25	±0.3
PLL limit cycle	±0.1	±0.1	±0.1	±0.1
Friction noise variations	±0.9	±0.9	±0.62	±0.62
Antenna misalignment	±0.1	±0.1	±0.1	±0.1
Sensor misalignment	±0.05	±0.05	±0.05	±0.05
SAE misalignment	±0.05	±0.05	±0.05	±0.05
Thermal distortions	±0.1	±0.1	±0.1	±0.1
Total rss	±0.95	±0.95	±0.7	±0.71
Systematic contributions				
Kinematic coupling (nutation ≤0.20 deg and star at 51.5 deg from ecliptic)	—	±0.26	—	±0.26
Total azimuth error	±0.95	±1.23	±0.7	±0.97

6. ATLAS/CENTAUR BASELINE

6.1 GENERAL

The Atlas/Centaur launch vehicle will be used for both missions in 1978, and this has resulted in the following major mission related changes affecting the ACMS performance requirements:

- Attitude orientation normal to ecliptic prior to separation from launch vehicle.
- Spacecraft spinup after booster separation, ≈5 rpm
- 4.42 m (14.5 ft) magnetometer, boom deployment on orbiter
- Spacecraft spinup to 25 rpm for cruise operations
- Reorientation of orbiter spin axis to north ecliptic normal for orbital operations (new Type II trajectory baseline)
- Retargeting probe impact points

A summary of the mission profile for the probe mission is depicted in Table 1-3, Section 1. A summary of the mission profile for the orbiter acquisition, cruise and encounter modes is depicted in Table 1-4, Section 1. The need for incorporating an X-band radio occultation experiment on the orbiter spacecraft is an additional requirement for the baseline Atlas/Centaur configuration only.

The primary control concept proposed for the Atlas/Centaur remains identical to that of the Thor/Delta, including all basic performance characteristics. The component changes proposed for the Atlas/Centaur different than those proposed for the Thor/Delta stem from a reassessment of the tradeoff studies allowing maximum use of cost effective hardware and the incorporation of the radio occultation experiment. These component changes and the mission related changes are described in detail in this section. A summary of the component changes is given below:

1) The star sensor boresight angle shall be centered at +32 deg from the ecliptic plane.

2) A three element segmented boom shall be used to deploy the magnetometer sensor head 4.42 m (14.5 ft) radially outboard of the solar cell array.

3) The bearing and power transfer assembly (BAPTA) will employ a brushless motor design.

6.2 MISSION CHANGES RELATED TO ACMS

Probe Mission

Orientation perpendicular to the ecliptic will be executed by the Atlas/Centaur attitude control system. Such a procedure is standard practice and imposes no undue stress on the Centaur capability as evidenced by four Intelsat IV launches to date. Spacecraft spinup is easily executed by the on-board spinup thrusters in response to commands from the on-board memory, and enabled via command subsystem memory after separation by redundant separation switches. This technique has been successfully demonstrated on four Intelsat IV spacecraft and several other classified spacecraft.

The spacecraft will be spunup to ≈5 rpm and remain at this rate until changed by ground command. Propellant in plenums between the latch valves and the two spinup thrusters ensure only hydrazine feed during the initial stages of a 0 g spinup. The time interval between termination of the initial spinup and ground station acquisition will allow the hydrazine in the tanks to settle out-board and be available for any commanded maneuvers. Residual nutation at 5 rpm is damped out by the passive mercury damper.

After ground station acquisition, the probe bus spin axis attitude and spin rate will be determined, and then adjusted for cruise, i.e., spin axis perpendicular to ecliptic, forward end pointing south, and spin speed at 25 rpm. The use of the Atlas/Centaur significantly reduces midcourse maneuver requirements; the 99 percentile midcourse ΔV requirement is ≈12 m/sec as compared to 77 m/sec for the Thor/Delta. The reduced propellant requirement makes the vector mode (correction in cruise attitude) more attractive for the first midcourse maneuver, since the increase in propellant (maximum 40 percent) for this mode is comparable to the maximum precession propellant required by the axial jet mode. Execution of all midcourse maneuvers with the vector mode relaxes any time constaint caused by thermal considerations. This, in turn, allows the 4.5 N thruster to once again become a viable candidate, with the resultant advantage of smaller attitude disturbance at low spin speeds. The 22 N thruster has been retained for the Atlas/Centaur baseline study; however, the option to select the 4.5 N thruster is retained pending an updated Atlas/Centaur configuration that meets contract performance requirements.

Since the 1978 probe mission occurs during a different part of earth year than the 1977 mission, the inertial transit trajectory and star visibility is different. Evaluation of star sensor coverage in the southern ecliptic hemisphere shows that attitude determination capability and performance at the cruise attitude are as good as the Thor/Delta baseline. Star sensor boresight and cant angles are common with those employed on the Atlas/Centaur orbiter baseline discussed in the following paragraphs. Space axis attitudes

required for large probe separation, small probe targeting and separation, as well as probe bus targeting and entry, can be determined using the available stars. The encounter timeline is identical to that for the Thor/Delta baseline. The small probe separation will nominally take place at 47.5 rpm.

Orbiter Mission

Remarks for the probe mission separation, reorientation and initial spinup are identical for the orbiter mission. After ground station acquisition, however, the spin speed will be trimmed, if necessary, to 5 ±1 rpm for magnetometer boom deployment. The boom design utilizes centrifugal force to deploy the sensor 4.42 m (14.5 ft) radially out-board of the solar panel drum. Restraint springs and latching mechanisms at each of the three hinges provide energy storage and dissipation to soften dynamic interaction with the orbiter bus during deployment. After deployment, the orbiter spin axis attitude and spin rate will be adjusted for cruise; spin axis parallel to south ecliptic pole, spin speed ≈25 rpm. Remarks on the orbiter midcourse maneuver requirements, required propellant, vector mode and the 4.5 N thruster are identical to those for the probe bus.

The Type II trajectory, south periapsis (56 deg) polar orbit has been chosen for the Atlas/Centaur baseline. The required precession to the orbit insertion attitude from the nominal is ≈34 deg; no inversion maneuver of the type required for the Thor/Delta is necessary. However, the sun angle at insertion will generate more solar input to the aft end of the spacecraft and thus limit the time allowed at this attitude. To reduce thermal problems after insertion, a small reorientation normal to the sun line will be executed 20 minutes after insertion (initiated by the command memory). Upon reacquisition of the ground station, the attitude, spin rate and general spacecraft status will be ascertained. A precession of the forward end to the north ecliptic pole will then be executed in order to locate velocity sensitive instruments in the direction of orbiter velocity at periapsis. The Thor/Delta Type II, north periapsis (27 deg) baseline required the spin axis at the south ecliptic pole for orbiter science. However, orbiter corrections for the Atlas/Centaur baseline still require exclusive use of axial thrusters at the retro end of the spacecraft so that thruster configuration rationale for the orbiter is identical.

Since the Atlas/Centaur orbiter mission occurs at the same part of the earth year as the Thor/Delta mission, the inertial transit trajectory and star visibility during cruise is nearly identical. However, the star sensor for the Atlas/Centaur orbiter is required to scan the northern ecliptic hemisphere in orbit. Since there are fewer stars in this hemisphere than in the southern one, all having lower declination, star sensor parameter changes from the Thor/Delta orbiter are required. It was determined that the optimum star sensor boresight angle should be 32 deg from the ecliptical plane for spin axis at the south ecliptic pole during cruise and at the north ecliptic pole in orbit. In addition, the second star sensor slit should be canted +20 deg (instead of -20 deg for the Thor/Delta) in order to insure slit redundancy during the entire mission. (See Appendix A for explanation of cant effects on attitude determination). Attitude visibility for orbit

insertion is also assured for this choice of parameters. In the interest of commonality, this choice was also made for the probe bus with the resulting performance more than adequate for that mission.

6.3 MAGNETOMETER BOOM

For reasons of magnetic cleanliness at reduced system costs, it is desirable to deploy the magnetometer sensor package well out-board of the spacecraft residual magnetic field. The larger payload capability of the Atlas/Centaur booster permits consideration of devices capable of such deployment. The orbiter configuration design requires that a magnetometer sensor weighing about 0.54 kg (1.2 lb) be deployed to a position 4.42 m (14.5 ft) (18 ft from the spin axis) radially out-board of the bus solar array. Furthermore, the instrument cable, consisting of nine pairs of twisted, shielded leads, must also be deployed with the sensor. The three candidate devices studied are presented below.

Storable Tubular Extendible Member

With minimum restraints on weight and power, a power driven extensible boom of the SPAR bistem type is a possible candidate. The retracted boom is reeled up as a flat ribbon in a cassette/mechanism. Ideally, the instrument harness would also be a ribbon type cable which is easily stacked in an accordian-fashion and simply deployed. This type of design offers the advantages of controlled rate deployment, retraction, if necessary, and optional extension positioning. It also eliminates the requirement for velocity controls and/or impact damping mechanisms. The devices are available as almost off-the-shelf packages and have been used extensively in space applications. In this application, however, there are two serious drawbacks to the use of this design, both of which concern, or are caused by, the instrument electrical cable. The cable is required to be nine pair of stranded twisted shield type for magnetic considerations. This cable is extremely difficult to stow as a coil and is even more difficult to deploy from the coil position. Recorded failures of the extensible boom type of device on the Apollo program have been associated primarily with cable stowage or cable deployment problems. Furthermore, the alignment requirement between the spacecraft spin axis and the sensor axis in the deployed position cannot be assured because of the twisting moment executed on the boom by the cable and the inability to control tip rotation during the unreeling/tube formation sequence.

Coilable Lattice Extendible Boom (Astromast®)

The Astromast® is a linear lattice structure, or boom, which is deployed from the retracted into a compact stowage volume. The mast is constructed of thin, epoxy-glass longerons arranged in an equilateral triangle. The lattice structure is retracted by forcibly twisting it about its axis. This twisting causes the "batten" members to buckle. With the battens so shortened by buckling, the mast can be retracted into a compact configuration. The distortions that the longerons and battens undergo during retraction and deployment are elastic so that deployment and retraction can be repeated.

This design provides a convenient and reliable method for storing and deploying the sensor cables. The nine twisted and shielded pairs will be split into three wiring bundles, each bundle being attached to a longeron. The wiring harness therefore will deploy and retract in unison with the boom.

The boom is deployed by actuating a pyrotechnic cable cutter contained within the boom canister.

This boom design, in the deployed position, will not withstand the g-forces associated with orbit insertion motor firing. Therefore, the boom must be retracted for this maneuver, and redeployed following completion of the orbit insertion sequence.

Segmented Boom

The segmented hinged boom that can be centrifugally extended and can carry the cable within the boom represents the third possible candidate studied. The boom supports the magnetometer sensor package at the end of the last member of a three segment assembly as shown in Figure 6-1. The three segment assembly is mounted on the orbiter shelf, folded in accordian-fashion in the stowed position during launch and secured by pyrotechnic pin pullers which divert launch loads from the assembly and sensor. Deployment occurs upon ground command when the two pin pullers (wired in parallel) are actuated releasing the assembly to take advantage of the orbiter's spin rate in driving the three segments into a straight, rod-like configuration which locks after all of the deployment energy has been absorbed at the hinge points. This results in a predetermined sensor position sufficiently beyond the solar array to minimize shadowing effects on solar cells, as well as magnetic effects of the orbiter on the magnetometer. A brief discussion on the key elements of magnetometer boom is given in the following paragraphs:

- The boom assembly consists of three tubular beryllium members containing the electrical interface cable (nine twisted and shielded pairs) having adequate service loops at each hinge point. Beryllium material provides excellent weight/stiffness ratio and nonmagnetic properties.

- The assembly is mounted on the orbiter shelf with its main pivot assembly and all hinge axes in the plane perpendicular to the spin axis. The pivot and hinges contain energy absorption springs (at each of the three hinges) to soften dynamic interaction with the orbiter bus during deployment and to insure positive latching with adequate margin.

- Release of the pin pullers (wired in parallel for simultaneous firing) deploys the hinged boom radially, assisted by a kickoff spring and the rotor spin rate. Positive locking occurs at each hinge point and at the main pivot by means of a caming surface and deformation latch blade.

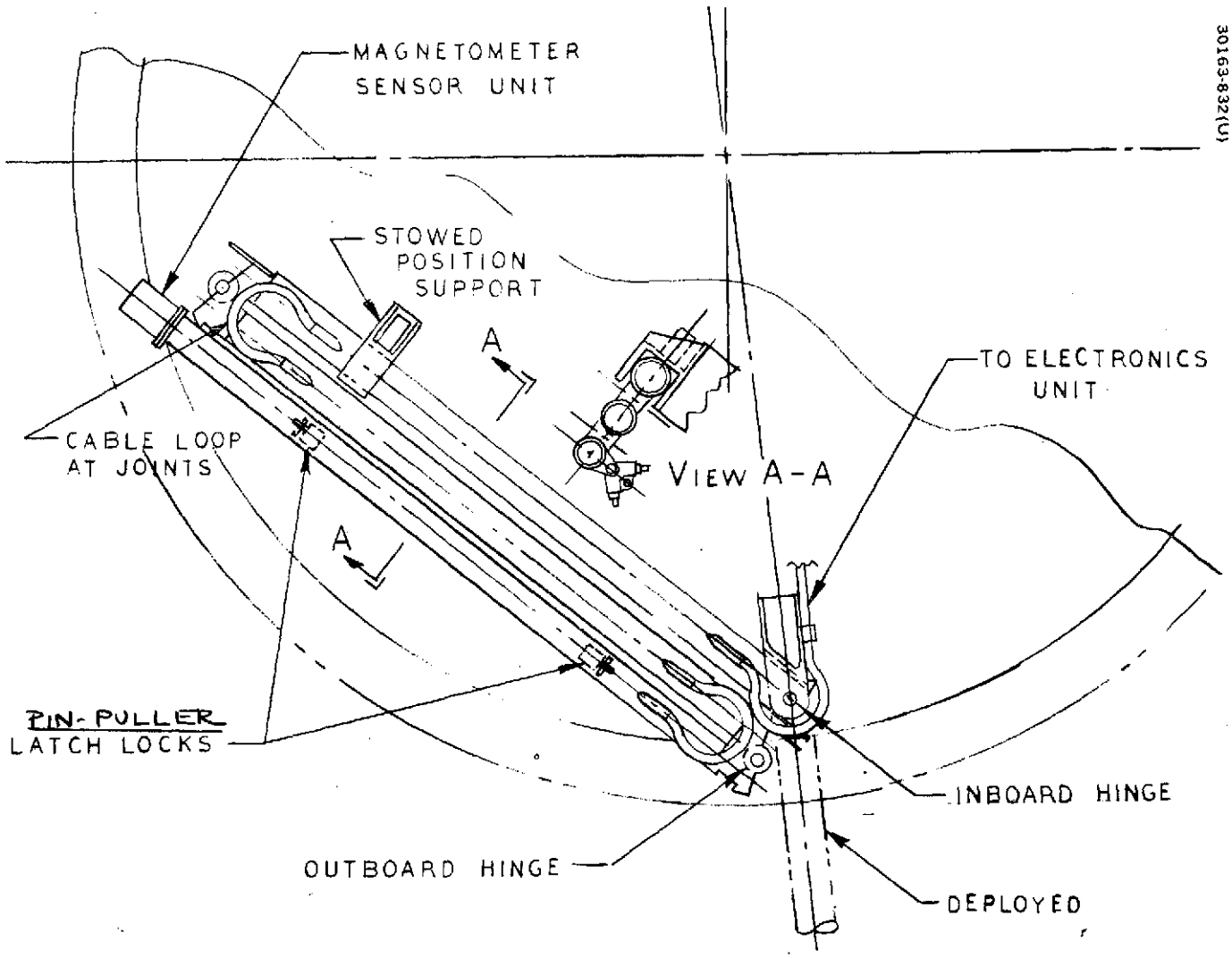

30163-832(U)

FIGURE 6-1. MAGNETOMETER BOOM IN STOWED POSITION

- A simulation model of the magnetometer boom deployment has been generated to show the deployment dynamics and to size the restraining springs. A typical boom deployment dynamics sequence is shown in Figure 6-2.

Design Selection

A summary of the design tradeoff characteristics for the three designs considered is presented in Table 6-1. The selection of the segmented boom as the baseline design is based upon minimum weight, complexity and the least impact on mission success if deployment fails.

6.4 BAPTA DESIGN CHANGES

The selection of a brush motor for the Thor/Delta was significantly influenced by the weight constraint and the inclusion in the BAPTA of a 2.54 cm (1.0 in.) diameter single S band rf rotary coaxial joint. The off-the-shelf Telesat BAPTA considered for the Pioneer Venus required modification to accept the rotary coax joint. The modification, as well as the oversized motor design (for the Pioneer Venus mission), resulted in the selection of a new scaled down BAPTA with the incorporation of a brush motor instead of a brushless motor for the baseline Thor/Delta design. The brush motor simplified the drive electronics, resulting in less weight.

The advent of the radio occultation experiment has resulted in a larger rotary coax joint required for the BAPTA to accept both an S band and X band signals. The larger dual frequency rotary coaxial joint (4.6 cm diameter) is associated with a bigger BAPTA than the one proposed for the Thor/Delta. The required size of the BAPTA proposed for the Atlas/Centaur allows use of the basic Telesat unit as the most cost effective approach. For this reason, the Telesat BAPTA modified to accept X band and S band rf rotary coaxial joint and employing a brushless motor was chosen as the baseline design.

The assembly, shown in cross section (Figure 6-3), consists of four major subassemblies:

1) The brushless motor assembly (provides despin control torque)

2) The main bearing assembly (provides relative rotation)

3) The encoder (provides a master index pulse, a rotation sense pulse, and 128 angular rate pulses each revolution)

4) The electrical contact ring assembly (ECRA) (provides for power and signal transfer across the spinning/despun interface)

The BAPTA design is the result of extensive experience in the design, fabrication, test, and successful orbital operation of high reliability despin bearing assemblies for Hughes Tacsat, Intelsat IV, Telesat Domestic, and

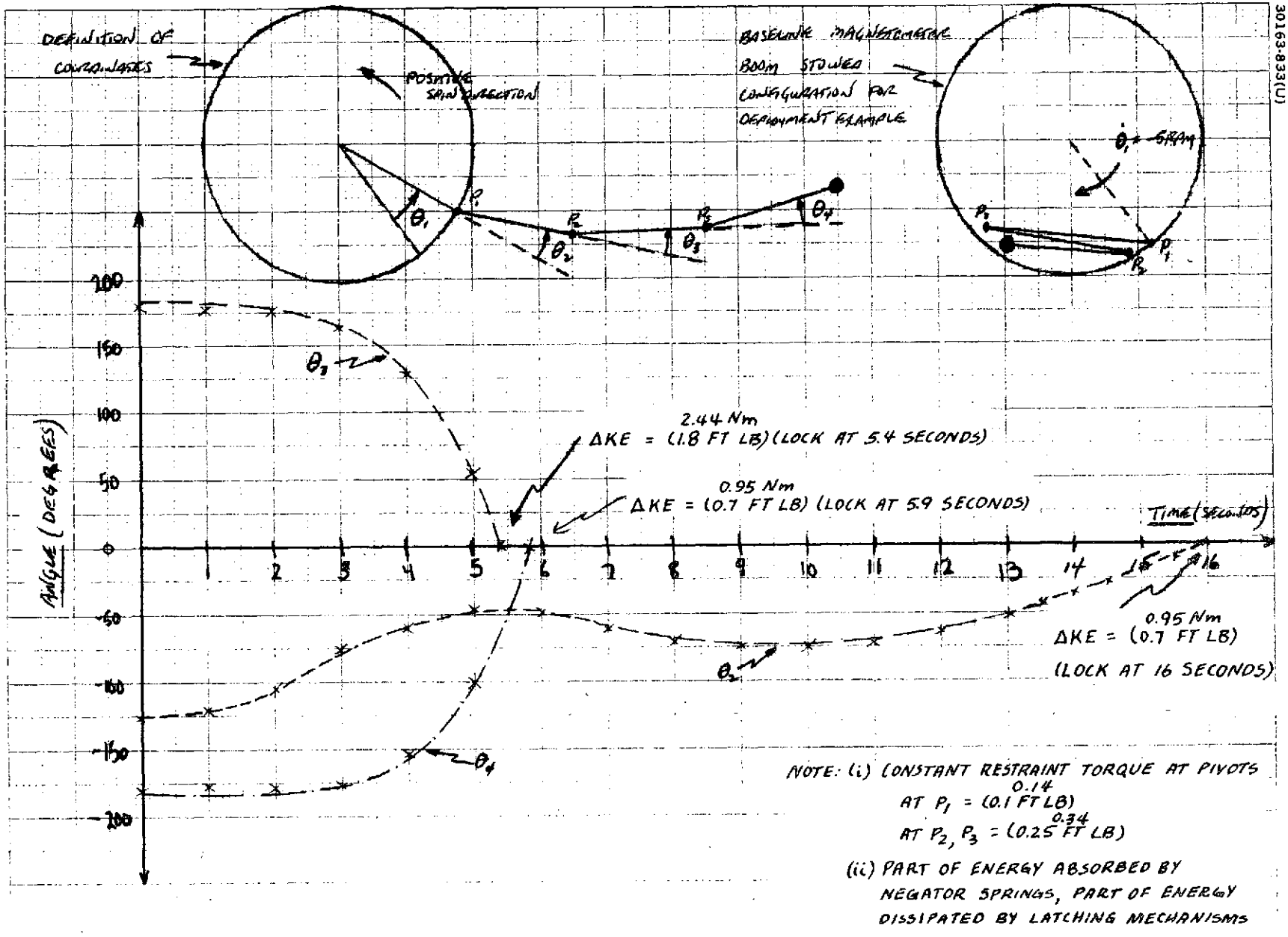

FIGURE 6-2. TYPICAL BASELINE MAGNETOMETER BOOM DEPLOYMENT DYNAMICS

30163-833(U)

TABLE 6-1. MAGNETOMETER BOOM DESIGN TRADEOFF SUMMARY

Parameter	Boom Type		
	Storable Tubular Extendible Member (Star Bistem)	Coilable Lattice Extendible Boom (Astromast)	Segmented Boom
Weight mass (excluding sensor) kg (lb)	4.54 (10.0)	4.13 (9.1)	3.27 (7.2)
Power, watts	Motor = 20	Motor = 21 Cable cutter (squib)	Two pin pullers
Number of times necessary to deploy or retract	Deploy twice Retract once	Deploy twice Retract once	Deploy once No retraction required
Failure Mode Effects	Boom Fails to Extend		
	Cruise wobble ≈4.1 deg Orbit wobble ≈1.6 deg	Cruise wobble ≈3.8 deg Orbit wobble ≈1.4 deg	Cruise wobble ≈5.1 deg Orbit wobble ≈1.9 deg
	Boom Fails to Retract		
	8 to 17 deg wobble during retro firing can result in mission failure	8 to 17 deg wobble during retro firing can result in mission failure	No impact

Notes: 1) For segmented boom, spacecraft dynamically and statically balanced with boom deployed.

2) For retractible boom, spacecraft statically balanced with boom stowed and dynamically balanced with boom deployed.

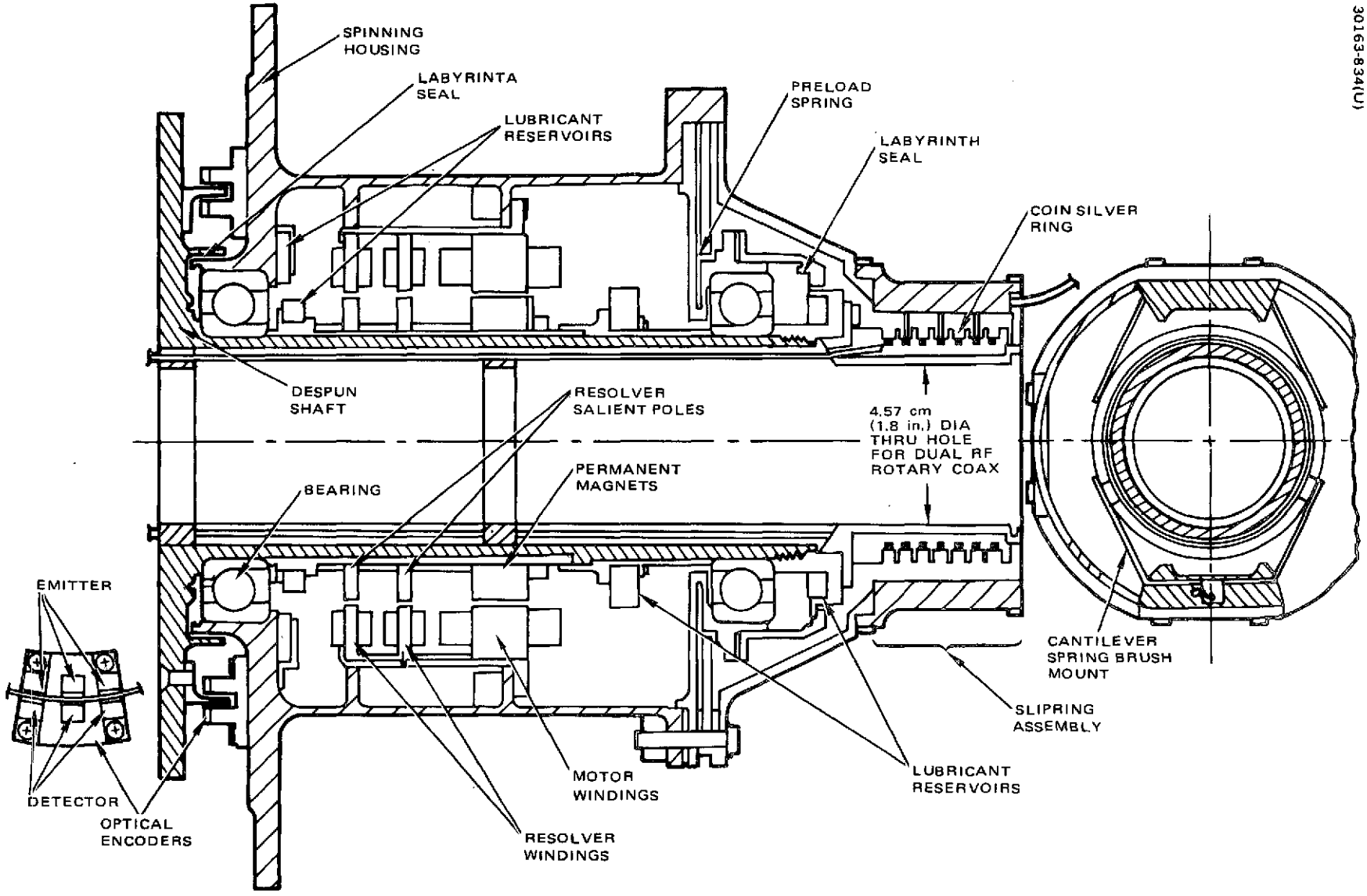

FIGURE 6-3. BAPTA ASSEMBLY CROSS SECTION

military satellites. The motor and bearing portion of the BAPTA is identical to that flown successfully on Telesat. The ECRA design is new, but the essential features of lubrication and brush and ring design and geometry are borrowed directly from previous flight proven despin assemblies. Design characteristics of the BAPTA are summarized in Table 6-2.

The BAPTA design minimizes the use of screw threads, screws, and lock wire within the spinning housing structure. Where their use is unavoidable, integrally machined bosses are employed to ensure entrapment of metallic chip debris in blind (non-thru) threaded holes.

The bearings, preload spring and assembly housing/shaft are designed for adequate structural stiffness to attain acceptable dynamic response of the supported spacecraft sections during launch accelerations. Bearing suspension and preload design compensate for local thermal gradients over the mission operating temperature range, to minimize frictional torque variation. Key elements in the BAPTA design changes for the Atlas/Centaur baseline are described in the following paragraphs.

Brushless Motor Design Description

The motor selected for Pioneer Venus is a fully redundant, resolver commutated brushless dc torque motor, identical to the Telesat, Western Union, and AMSAT despin assembly motors. The motor is shown schematically in Figure 6-4, and consists of two redundant sets of motor windings, segment wound on a common lamination stack (motor A windings occupy half of the circle, and motor B windings the other half), and two fully redundant, physically separated resolvers, mounted in a common housing. The physical segregation of the resolvers, motor windings, lead harnesses, and connectors to each motor/resolver pair eliminates the possibility of a single failure affecting both sets simultaneously, thereby maximizing reliability. The motor stator contains the magnets and two sets of resolver salient poles on a common sleeve. The motor redundancy features extend to the electronics where one of the two electronic sets drive 4 specific sets of motor winding.

Commutation control of the dual wound brushless motor is provided by a redundant pair of electromagnetic resolvers, one for each set of motor windings. Each resolver consists of a stator and rotor, rigidly mounted and precisely aligned to the structure that support the motor stator and rotor, respectively. The stator is built of high permeability iron laminations and has eight poles. The rotor contains a primary (excitation) coil and pair of secondary (sine and cosine output) windings on a laminated iron structure.

Functional operation of the resolver is shown in Figure 6-5. The primary (excitation) coil is magnetically coupled to each secondary (output) coil via the air gap and the poles of the stator. When an excitation voltage is applied to the primary windings, rotation of the rotor relative to the stator causes sinusoidal variations in the output voltage of each secondary winding as the pole pieces pass the rotor coils. The angular spacing of the

TABLE 6-2. BAPTA DESIGN CHARACTERISTICS

BAPTA type	Basic Telesat design Add on slipring and optical encoder Use beryllium shaft and housing
Bearings	
Size	6.0 cm (60 mm) bore 9.5 cm (95 mm) O.D.
Type	Angular contact, 25 deg C.A.
Tolerances	AFBMA Class 9
Material	440C CEVM
Balls	19 each, 1.02 cm (13/32)diameter, Grade 5
Retainer	Cotton phenolic, outer race riding
Lubrication	HMS 20-1727, vacuum impregnated
Encoder	
Type	Optical (gallium arsenide)
No. of sensors	6 (2 fully redundant sensors for each function
Master pulse	1 per revolution (two redundant sensors)
Rotation sense pulse	1 per revolution (two redundant sensors)
Angular rate pulse	128 per revolution (two redundant sensors)
Output voltage	2 V across 10 KΩ
BAPTA friction torque	
Maximum 4°C (40°F, 35 rpm)	0.20 Nm (0.15 ft-lbs)
4°C (40°F, 5 rpm)	0.16 Nm (0.115 ft-lbs)
Nominal 21°C (70°F, 35 rpm)	0.14 Nm (0.10 ft-lbs)
21°C (70°F, 5 rpm)	0.115 Nm (0.085 ft-lbs)
Torque margin, single motor	
Worst case 4°C (40°F, 35 rpm)	0.72 0.15 4.8 to 1
Nominal 21°C (70°F, 35 rpm)	0.72 0.10 7.2 to 1
BAPTA weight	14.50 lbs
Motor parameters	
Type	Brushless, resolve commutated
No. of motors	Two, segmented on common lamination
No. of resolvers	Two, separate laminations
Torque constant	0.87 ± 5 percent ft-lbs amp
Back EMF	1.18 ± 5 percent V rad/sec
Winding resistance	24 ± 5 percent ohms
Minimum torque output:	
One motor, 24 volts applied:	
35 rpm 0.95 Nm (0.72 ft-lbs)	
Stall 1.17 Nm (0.87 ft-lbs)	
Slipring parameters	
Ring material	Coin silver
Brush material	SM 476 (85 percent Ag, 3 percent C, 12 percent M_oS_2)
Ring diameter	5.84 Cm (2.3 in.)
Signal type circuits	
No. of rings	7
No. of brushes ring	2, common wear track
Brush type	Cantilever spring (MILSAT signal design)
Brush tip area	(0.060 x 0.245 0.0147 $in.^2$), 0.098 cm^2
Brush force	25 g
Current rating (at circuit)	
Continuous duty	0.22 A (75 A $in.^2$)
10 percent duty	2.2 A
Intermittent duty	20 A (20 ms pulse)
Friction torque (M = 0.25)	0.04 Nm (0.03 ft-lbs)
Brushwear life (@ 35 rpm)	>20 years

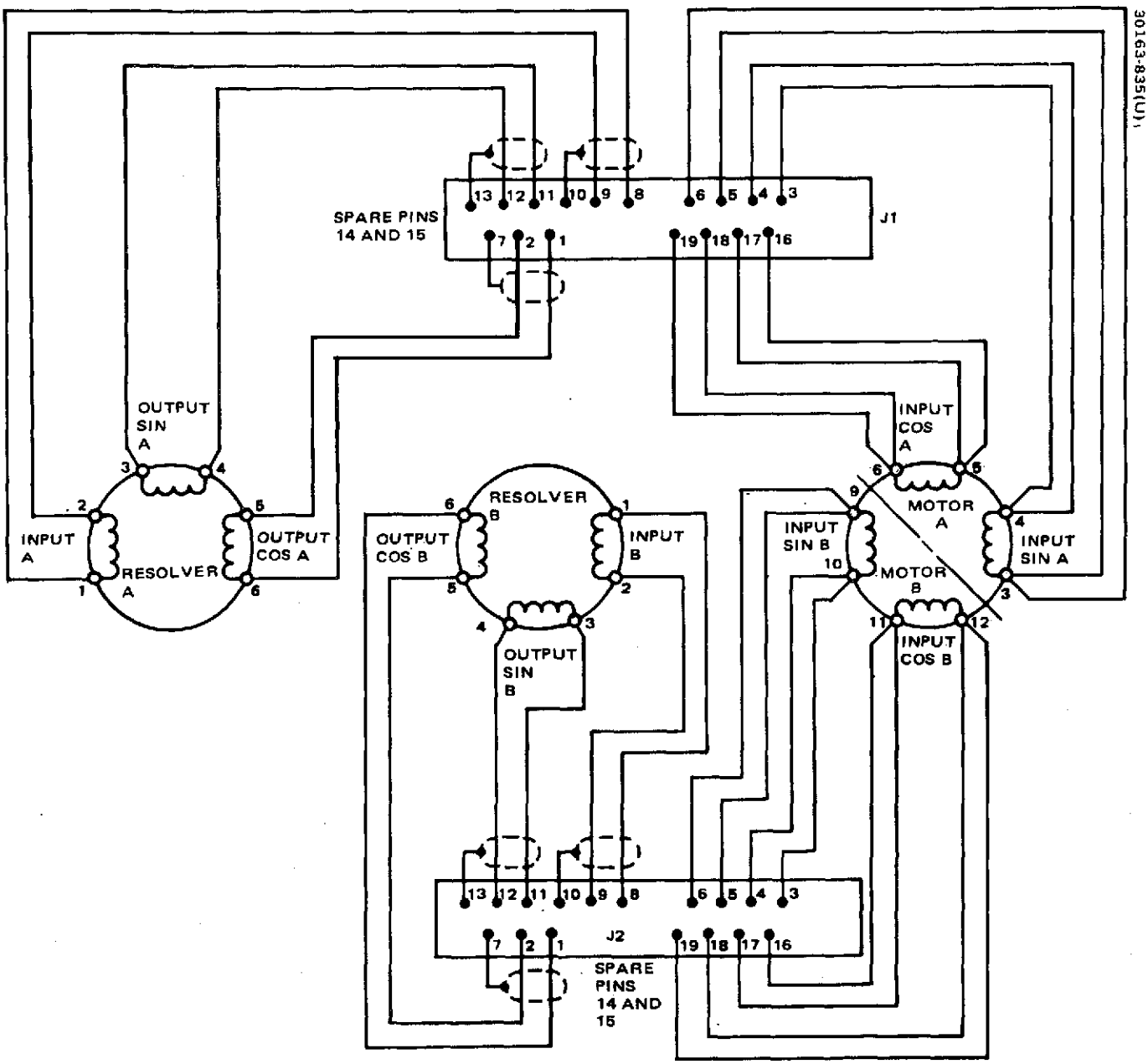

FIGURE 6-4. BRUSHLESS MOTOR ASSEMBLY SCHEMATIC

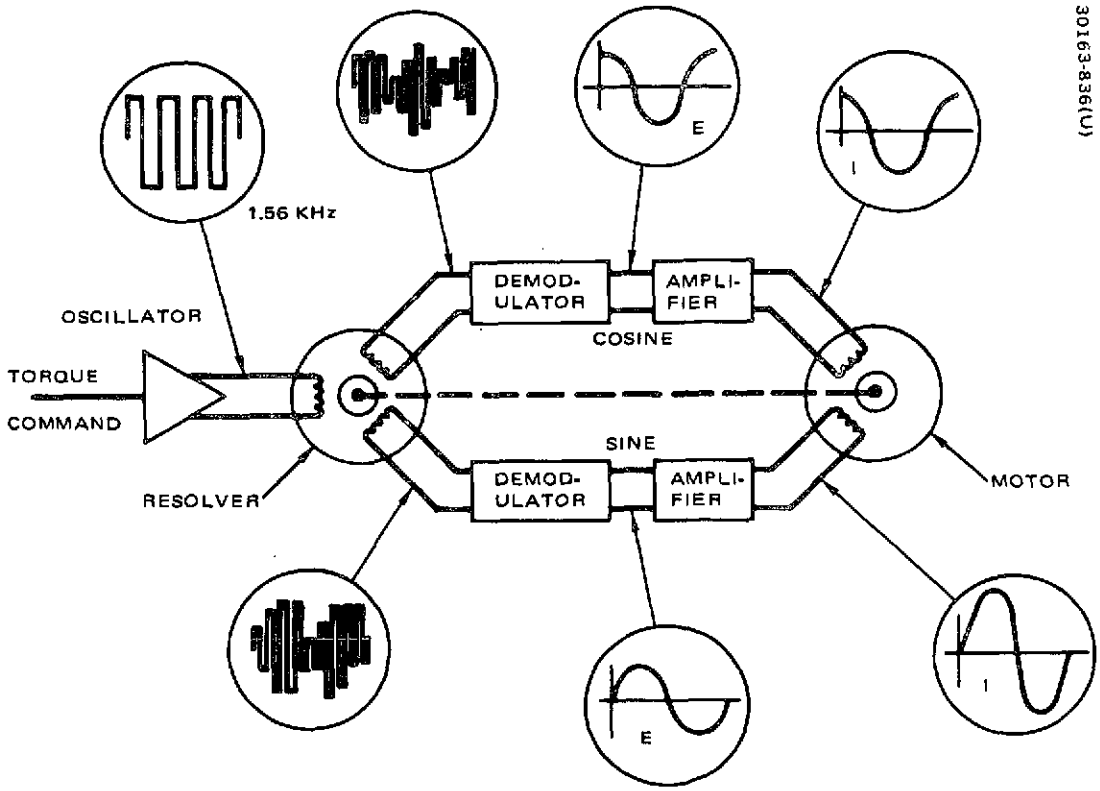

FIGURE 6-5. RESOLVER INPUT AND OUTPUT WAVEFORMS

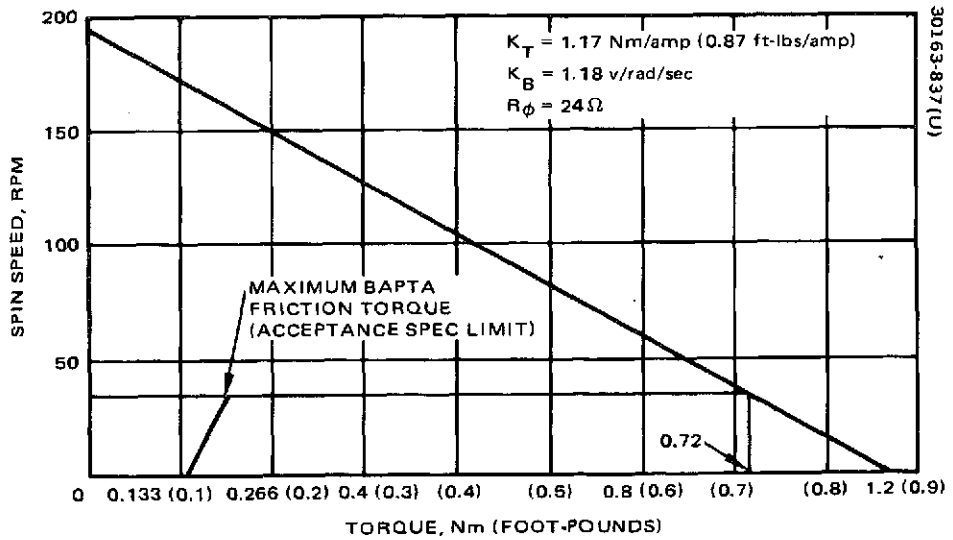

FIGURE 6-6. MOTOR OUTPUT TORQUE CAPABILITY VERSUS SPIN SPEED

secondary coils relative to the spacing of the pole pieces is such that the voltage produced in the two secondary coils is 90 deg out of phase electrically. The sine and cosine resolver outputs are demodulated and operate on the despin motor drive electronics such that current is applied to the motor sine and cosine windings in the same phase.

The output torque capability of one motor winding set is illustrated in Figure 6-6, for the minimum bus voltage condition (24 V available to the motor). Also shown is the worst case BAPTA torque, as allowed by the flight acceptance test specification. The margin of available motor torque above BAPTA friction reduces as spin speed increases. At the maximum spin speed of 35 rpm, the torque margin is 4.8 to 1. At lower spin speeds, the margin increases.

Features of the motor internal construction include firmly anchored and potted lead wires, sealed protective covers over motor, and resolver windings, potted laminations to provide lamination support and good heat dissipation characteristics, and a metal sleeve over the magnets to provide a smooth polished surface at the air gap. A final grinding of all critical diameters is performed after assembly of the rotor and stator. This provides a continuous, smooth, highly concentric air gap, and facilitates final cleaning and inspection operations. Alnico IX magnets are used for maximum field strength and high coercive force to preclude demagnetization due to any conceivable electronic transient.

6.5 RADIO OCCULTATION EXPERIMENT INTEGRATION TRADEOFF IMPACTS

A system design tradeoff was made to assess the impact of integrating the S and X band radio frequency occultation experiment into the spacecraft. (See final report, Volume 4). The basic requirement for the experiment was to maintain the spacecraft S and X band transmitter antenna beams pointing at the "virtual" earth for 2 to 3 minutes during the start and termination of an occultation period. Two schemes were considered which would impact the design of the ACMS. These were:

1) Use of the orbiter high gain antenna as a steerable antenna by providing azimuth slewing of the antenna assembly and elevation slewing of the reflector (fixed feed) at rates up to 5 deg/min.

2) Precession of the spacecraft spin axis to effect inertial slewing of the orbiter despun antenna over the range of ± 10 deg at rates up to 7 deg/min.

Steerable Antenna Tradeoffs

Providing the steerable antenna capability involves the addition of an elevation drive positioner mechanism on despun antenna assembly and associated control electronics on the rotor. The control signals from electronics to the positioner would be transferred via slip rings on the BAPTA from the

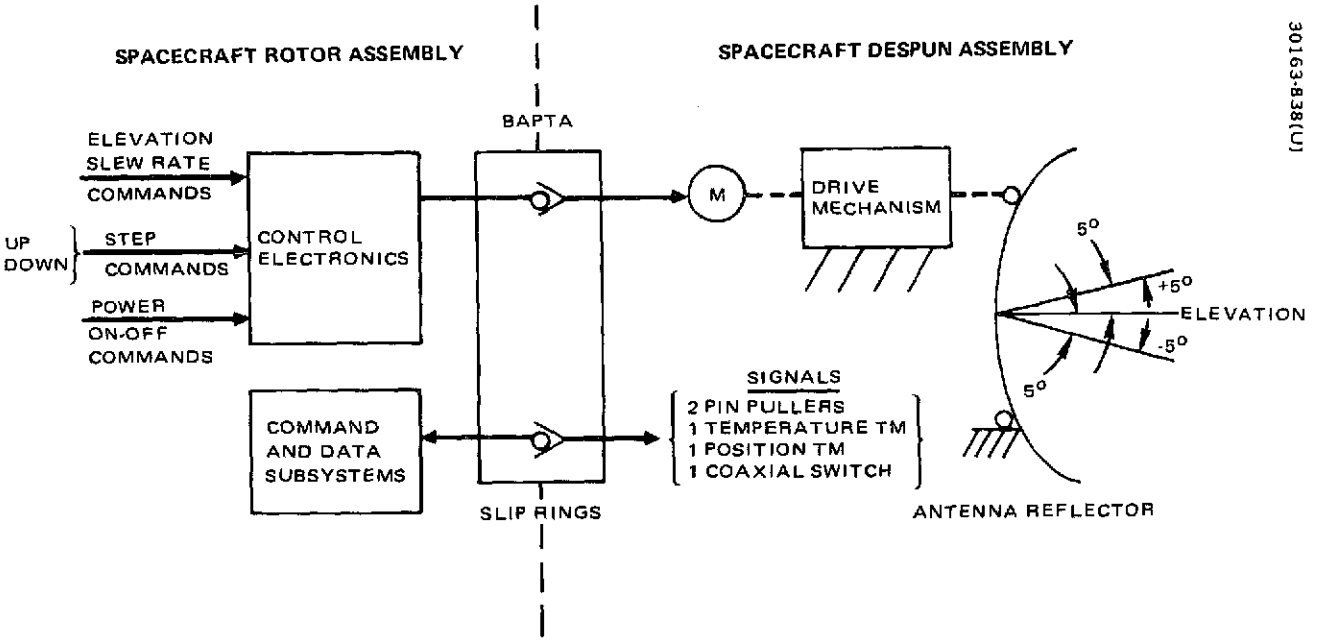

FIGURE 6-7. HIGH GAIN ANTENNA ELEVATION POSITIONER FUNCTIONAL BLOCK DIAGRAM

rotor to the despun assembly as illustrated in Figure 6-7. The positioner assembly supports and positions the antenna reflector on a single axis gimbal assembly such that the antenna dish centerline may be elevated through an arc of +5 deg at a rate of 0 to 5.0 deg/min, while the antenna feed remains fixed. The orientation will be set prior to launch and locked in position by ground launch. In orbit the antenna will be released and reorientated in orbit by ground command. Gimbal angle positions relative to spacecraft coordination system are telemetered to provide antenna orientation information.

Two methods for positioning the antenna dish were considered as possible candidates to perform the antenna positioning. These were a jackscrew drive mechanism and an on-axis drive mechanism.

Jackscrew Drive

The jackscrew drive design consists of a single axis gimbal and structure mounting subassembly and an actuator subassembly. The gimbal and structure support the antenna, provide the angular excursion freedom and attachment interface with the antenna support mast. The actuator is installed on the gimbal assembly such that linear motion of the actuator, acting at a radius arm, produces the antenna angular orientation. (See Figure 6-8).

The gimbal axis utilizes anodized and dry film lubricated bushings. Structural elements are designed of high strength aluminum alloy material.

The linear jackscrew actuator consists of an aluminum leadscrew and an aluminum spherical nut, a redundant stepper motor, and a rectilinear conductive plastic potentiometer. The motor operates through a spur gear reduction stage to drive the jackscrew in rotation. The nut is constrained to linear motion as the screw rotates. The irreversibility of the linear actuator is obtained through the jackscrew nut and motor detent load. This permits the actuator to hold the antenna rigidly when not being commanded.

The motor utilized is a four phase permanent magnet stepper type. This motor produces up to 0.2 Nm (30 in-oz) of running torque with a 90 deg step angle in a size 15 configuration. Motor mass is 0.21 kg (9 oz) and the operating power is approximately 15 W at 4°C (72°F). The required operational output torque is calculated on the basis of the imbalance moment produced by the combined antenna and positioner structure weight (on earth). This total force requirement is approximately 2.0 Nm (18 in-lb). The calculated torque provided by the gear box/motor subassembly is 5.95 Nm (53.0 in-lb).

Postulating an improbable but possible failure mode of the drive mechanism, provision has been made to effect a return of the antenna to zero elevation angle. This is accomplished by attaching springs (see Figure 6-8) to the antenna mounting structure which will drive the antenna to its zero position if the jackscrew drive is decoupled from the antenna. Decoupling is effected by actuating a pin puller, which separates the lead nut of the jackscrew drive from the antenna structure.

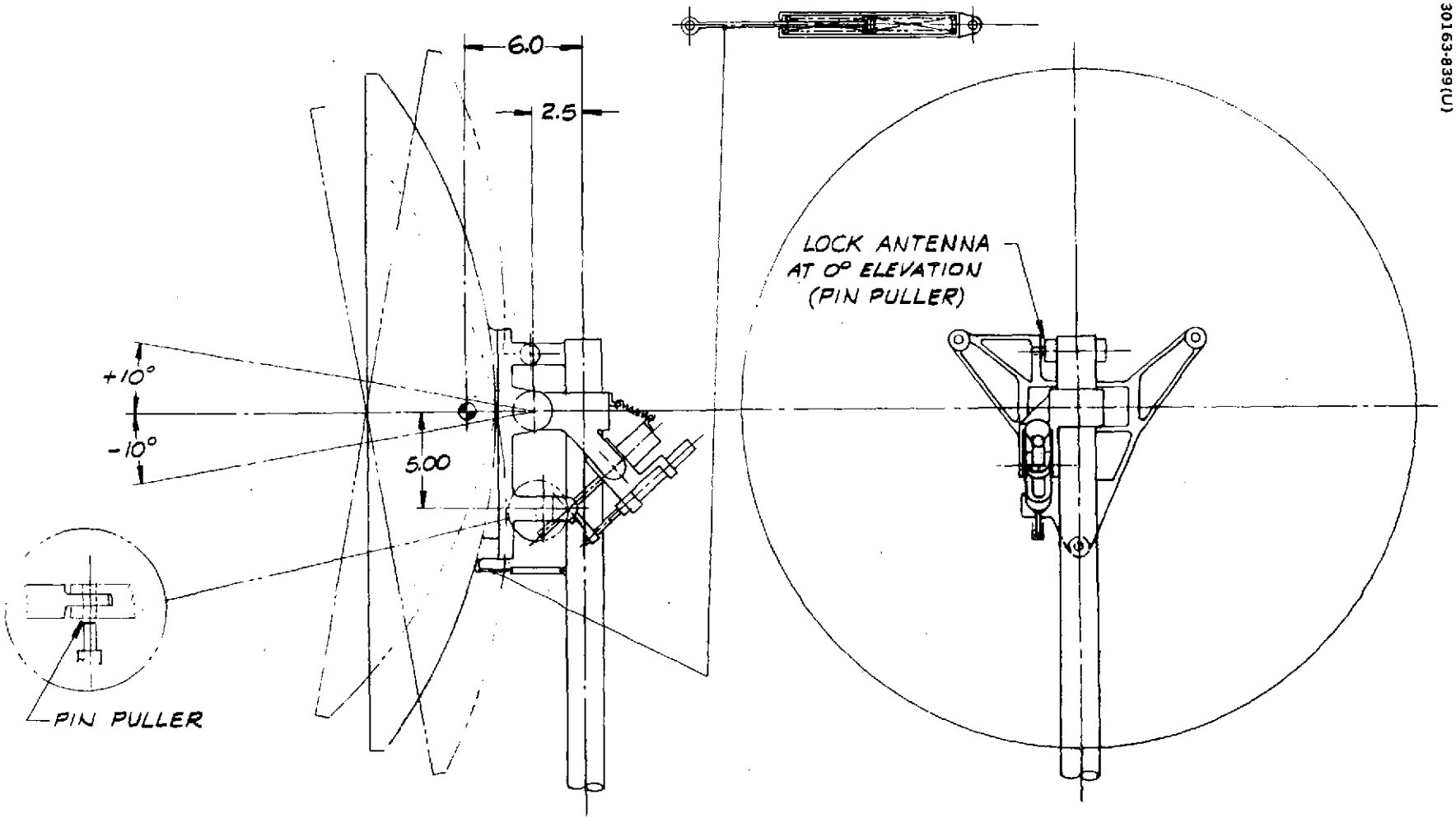

ANTENNA DIA 81.28 cm (32.00 in.)
ANTENNA WT 1.77 kg (3.9 lb)

GEAR BOX RATIO 6:1
MOTOR: 4 PHASE, 90° STEP, (1-50 PP)
OUTPUT TORQUE 0.0133 Nm (2.0 in.-lb)
SIZE 15 PM MOTOR

FIGURE 6-8. JACKSCREW DRIVE

30163-839(U)

On-Axis Drive

The on-axis drive mechanism design considered is similar in structural design and attachment interface to the jackscrew drive. The drive mechanism which produces the antenna interface orientation consists of a gear box subassembly and a large spur sector gear. The sector gear is attached to the gimbal assembly such that rotational motion of the gear box output pinion drives the sector gear to produce antenna angular motion.

The actuator subassembly consists of an aluminum housing and aluminum gears, aluminum sector gear and redundant stepper motors. The same motor is used as in the jackscrew drive. A servo mounted, wire wound, cermet, conductive plastic potentiometer is used to provide gimbal angle data.

In this design, the motor detent load provided by each motor is the only means of preventing the antenna dish from back driving through the gear box, therefore making it necessary to attach a pin puller to prevent irreversibility of the actuator during launch and boost stages, and a brake device to prevent back driving through the gear box after the pin puller is released. Such a device will necessarily reduce the torque margin in the system.

The attachment of the gear box subassembly to the gimbal structure must be carefully analyzed to prevent the gear teeth of the output gear of the gear box and the sector gear from impacting each other during the launch vibration environment. To prevent gear damage, it may prove necessary to "float" the gear box with respect to the sector gear which would increase the design complexity and weight. Without floating the gear box, the weight of this unit is estimated at 3.06 kg (6.75 lb), and with the float feature, the weight could exceed 3.7 kg (8 lb).

A "return to zero" feature in the event of a drive mechanism failure can be accomplished with a pin puller and spring arrangement to decouple the drive gear from the sector gear. The complexity would be slightly greater than that required for the jackscrew design.

Conclusions

Table 6-3 summarizes the key tradeoff considerations in selecting the proposed elevation drive mechanisms. The jackscrew mechanism was selected for the lower weight, cost, and complexity of the design. Reliable in-flight performance of the mechanism has been demonstrated on four Intelsat IV satellites.

In addition to providing the elevation drive capability, an azimuth slew rate capability must be added to the hi-gain antenna despin control system. This requires the addition of a rate command hold register and counter to the despin control electronics (DCE) to provide stepping of the antenna azimuth position at a rate of 0 to 5 deg/min. Table 6-3 includes the impact of this change on the DCE along with the elevation drive electronics.

TABLE 6-3. HIGH GAIN ANTENNA POSITIONER (ELEVATION DRIVE) TRADEOFFS

Item	Jackscrew Drive	On-Axis (Sector Gear) Drive
Accuracy, deg	±0.5	±0.5
Mass		
Elevation mechanism, kg (lb)	2.49 (5.5)	3.06 to 3.63 (6.75 - 8.0)
Electronics, kg (lb)	0.27 (0.6)	0.27 (0.6)
BAPTA sliprings, kg (lb)	0.45 (1.0)	0.45 (1.0)
Driving element	One required - 15 W stepper motor; four phase	One required - 15 W stepper motor; four phase
	Permanent magnet	Permanent magnet
Pin pullers	Two required	Three required
State of development	Motor and mechanism qualified on Intelsat IV	Motor only qualified on Intelsat IV
Cost factor	1.0	1.2
Failure mode		
Return to zero mechanization complexity factor	1.0	1.2

Spin Axis Precession Tradeoffs

Precession of the spin axis to maintain the S and X band despun antenna pointing at the "virtual" earth during occultation was investigated as an alternative to the "steerable" antenna approach. The guidelines used to study this approach were: spin rate of 5 rpm, spin axis precession of average rates up to 7 deg/min, nutation limited to ≈1 deg (with passive nutation damping negligible), propellant requirements not excessive, and compatibility with current jet control scheme desirable.

The fundamental problem area associated with this approach is pointing accuracy. The spin angular momentum is low implying that it is easy to precess the angular momentum vector. However, the combination of large precession rates and a long spin period (jet pulse interval) also imply a large precession per pulse. This, in turn, leads to a large residual nutation during the precession. Since nutation damping is negligible and the nutation occurs at a low frequency (≈7.5 cpm for a roll to pitch moment of inertia ratio of 1.5), the attitude error due to initial uncertainty and open loop precession must be added to residual nutation to evaluate the instantaneous spin axis pointing error.

Two spin axis precession modes illustrated in Figure 6-9 were considered. The first mode is the standard pulse mode of firing any one of three axial jets (or the pair of jets that generates a pure couple) at spin frequency. The second mode is the alternate fire mode of pulsing axial jets (1 and 2) on the retro end of the spacecraft alternately at twice spin frequency or pulsing the axial jets (2 and 3) that thrust opposite one another alternately at twice spin frequency. Both modes require a total of 1.8 kg (4 lb) of propellant to execute 4 deg of precession each day for the 40 days of the occultation experiment. The principal advantage of the alternate fire mode is that it can generate twice the precession rate as the standard mode for a 57 percent increase in maximum nutation at the Atlas/Centaur orbiter roll to pitch ratio of 1.6. Therefore, the alternate fire mode will generate ≈27 percent less nutation at any precession rate required. The instantaneous spin axis pointing error is estimated to be ≤2.5 deg at precession rates of 7 deg/min with the alternate fire mode where nutation contributes ≈1 deg to this error. The implementation of the alternate fire mode requires a logic and timing change in the jet control electronics. Spin axis precession employing either mode does introduce some operational complexity. Multiple maneuver commands must be stored for each segment of occultation precession. Attitude correction frequency would increase. Orbit disturbances would be generated if the standard mode couple or alternate mode "opposite thruster pair" were not employed. Radar altimetry pointing performance would probably be degraded during the early part of the mission. The additional thruster operations required could impact thruster reliability and thus potentially introduce mission operational complexity. In summary, the spin axis precession approach to implementation of rf occultation is subject to questionable pointing accuracy, increase propellant requirements and significant increase in operational complexity.

Occultation Integration Conclusions

The impact of providing either a steerable antenna or spin axis precession on the design of the ACMS for the occultation experiment integration is summarized in Table 6-4. The rf beam pointing error inherent in precessing the spin axis is approximately 2.5 deg for a 40 deg maneuver (+10, -20, +10 deg precession profile) versus ≤0.5 deg for the steerable antenna. The penalty to the ACMS for the improved performance of a steerable antenna is approximately 1.2 kg (2.7 lb) and $350K. The steerable antenna has the capability of slewing over the range of ±20 deg without disturbing the spacecraft attitude or orbit period.

The pertinent data summarized herein was used as a part of an overall system study related to "Dual frequency occultation experiment" tradeoff summarized in Volume 4. Neither of the alternatives studied above were utilized in the baseline design.

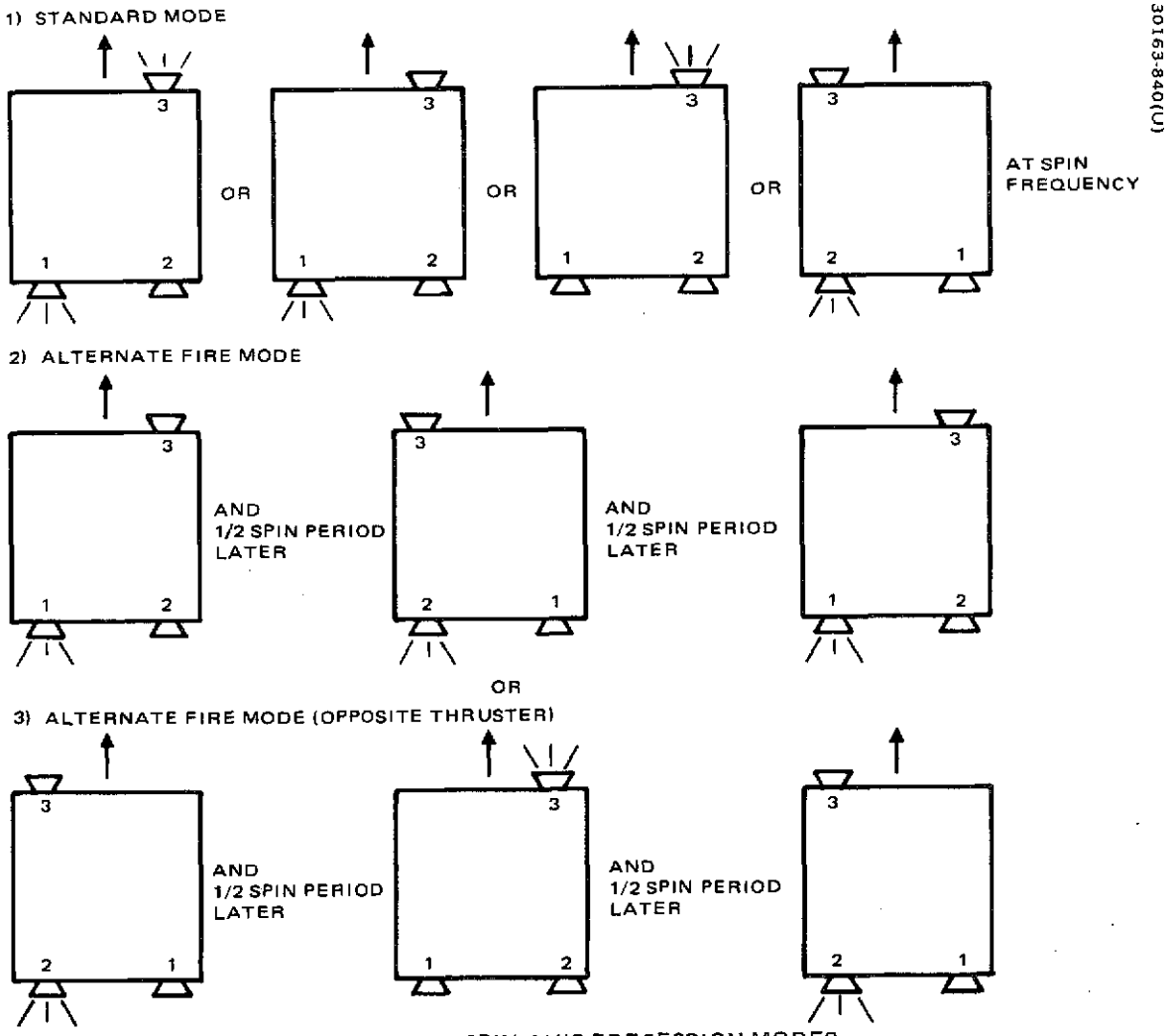

FIGURE 6-9. SPIN AXIS PRECESSION MODES

TABLE 6-4. TRADEOFFS OF OCCULTATION EXPERIMENT ON ATTITUDE CONTROL

Tradeoff	Steerable Antenna Approach	Spin Axis Precession Approach
1) Design mechanization	• Add elevation drive mechanism and electronics • Add azimuth rate control to DCE	• Add alternate axial jet firing mode to electronics
2) Mass, kg (lb)	• Mechanism ~2.49 (5.5) • Electronics 0.36 (0.8) • BAPTA 0.36 (0.8)	• Fuel 1.9 (4.2) (40 deg/day) • Electronics 0.1 (0.2)
3) Operational Complexity	• Stored slew command each orbit	• Stored multiple maneuver commands each orbit • Daily attitude correction • Daily orbital period disturbance • Science operations interference
4) Reliability Considerations	• Design must include "return to zero" elevation position in event of elevation drive mechanism failure	• Additional thruster operations in the "blind"
5) Beam pointing accuracy, deg	• Error ≤0.5	• Error ≤2.5
6) Growth potential	• Can increase elevation slew range to ±20 deg with no impact on design	• Can increase precession range to ±20 deg with ~double weight and pointing error increase
7) Cost factor (hardware), dollars	• 400 K	• 50 K

APPENDIX A. MODELS AND ANALYSIS FOR ATTITUDE DETERMINATION, ATTITUDE AND VELOCITY CONTROL

ATTITUDE DETERMINATION

Attitude Determination Analysis Model

The spin axis attitude is determined by the use of dual fan sun and star sensors (Figure A-1). The sun sensors (3) ψ fans and star sensor ψ^* fan can be assumed to be coplanar with the spacecraft fixed $X_S Z_S$ plane. The intersection of the i^{th} ψ and ψ_2 fan is declinated by the angle e_i. The intersection of the ψ^* fan and the ψ_2^* fan is declinated an angle α. The sun sensor ψ_2 fan and star sensor ψ_2^* fan are rotated about their respective boresights through angles β and β^*. When the sunline or star line of sight is coincident with the appropriate fan, a ψ, ψ_2, ψ^*, or ψ_2^* pulse occurs. Measurement of the $\psi\psi_2$, $\psi\psi^*$ and $\psi\psi_2^*$ pulse intervals provides the required information to determine spin axis attitude. Figure A-2 illustrates spacecraft-centered inertial coordinates $X_I Y_I Z_I$ with Aries (γ) along X_I and the ecliptic pole (north or south) along $+Z_I$. The Euler angles ϕ and θ define spin axis attitude and together with the spin angle ψ, they define the inertial location of the ψ fan or equivalently any point on the spacecraft. From this geometry, eight general relationships can be derived by a sequence of Euler angle rotations, i.e., ϕ rotation of the $Z_I Z_S$ plane about Z_I, θ rotation of Z_S in the $Z_I Z_S$ plane and ψ rotation of X_S about Z_S. The angle A_S defines the right ascension of the sunline. To simplify notation somewhat, A_S will be assumed zero; however, in practice the angles ϕ and A will be set equal to $\phi + A_S$ and $A + A_S$, respectively. The angles A and E are the star right ascension and declination angles, respectively.

When the sunline is coincident with the ψ fan, the Euler angles are defined by:

$$\tan \phi = -\tan \psi \cos \theta \tag{1}$$

The equation which defines the Euler angle relationships for sunline coincidence with the ψ_2 fan is:

$$\tan \theta \cos \psi = \sin (\psi_2 - \psi) \operatorname{ctn} \beta \csc e_i + \cos (\psi_2 - \psi) \cot e_i \tag{2}$$

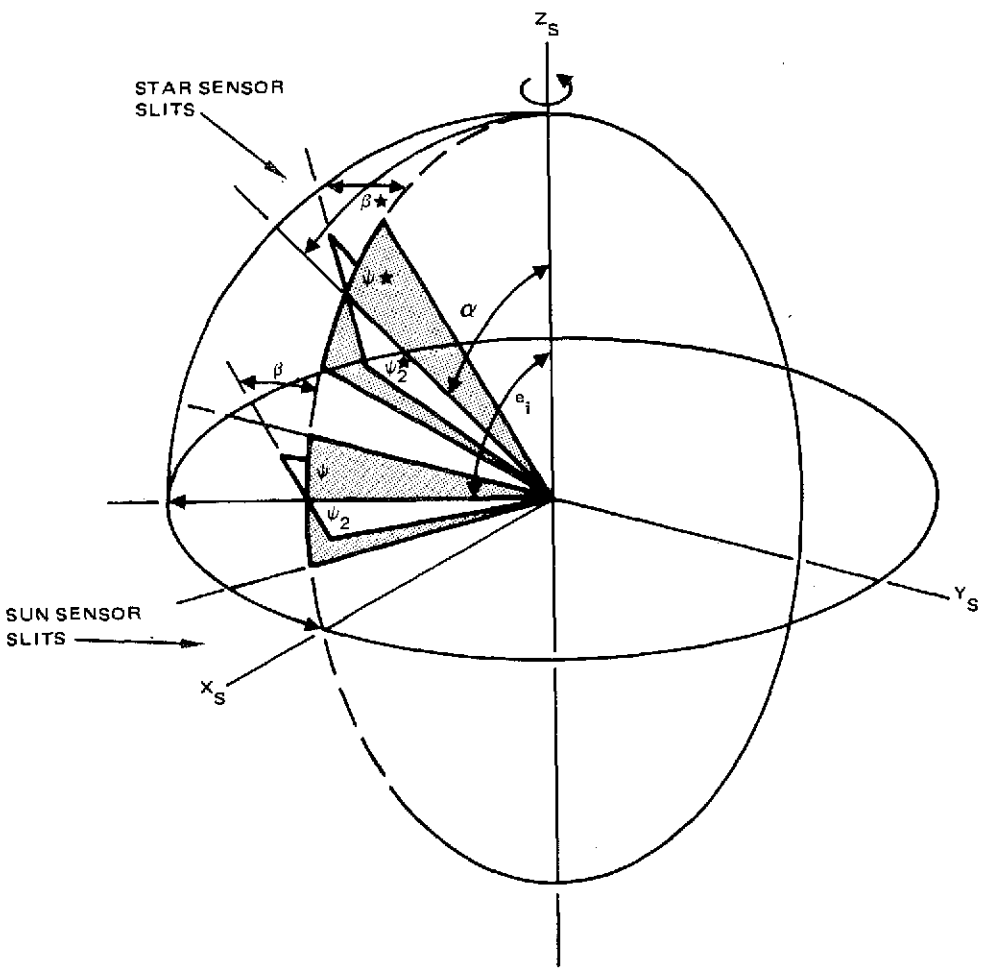

Z_S = SPACECRAFT SPIN AXIS

X_S, Y_S = ORTHOGONAL AXIS IN SPIN PLANE

α = DECLINATION ANGLE OF STAR SENSOR BORESIGHT FROM SPIN AXIS

e_i = DECLINATION ANGLE OF SUN SENSOR BORESIGHT FROM SPIN AXIS

ψ, ψ_2 = SUN SENSOR SLIT PLANES

$\psi\bigstar$, $\psi_2^{\bigstar}$ = STAR SENSOR SLIT PLANES

FIGURE A-1. SUN-STAR SENSOR GEOMETRY

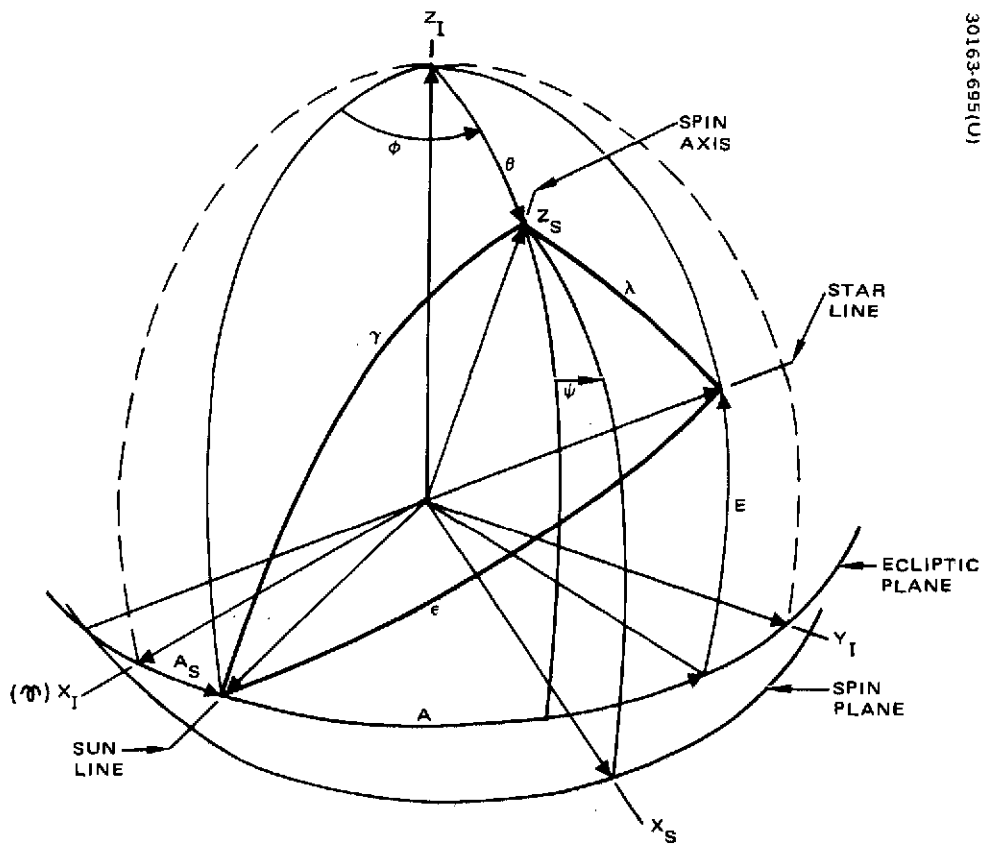

30163-695(U)

FIGURE A-2. SPIN AXIS INERTIAL GEOMETRY

A condition for Equation (2) is that the sun be in the field of view (FOV) of the ψ and ψ_2 fans. This condition is given in the following equation:

$$\sin e_i \cos\theta \cos(\psi_2 - \psi) + \cos e_i \sin\theta \geq \cos\left(\frac{FOV}{2}\right) \tag{3}$$

Equations (2) and (3) may also be used to define the star sensor FOV relationships by equating $\psi=\psi^*$, $\psi_2=\psi_2^*$, $\beta=\beta^*$ and $e_i=\alpha$. Using this set of sun and star equations with measurements of $\psi\psi_2$ and $\psi^*\psi_2^*$ angles, Equations (1), (2) and (2*) can be solved simultaneously for the Euler angles. This is the dual slit star sensor attitude determination scheme (measure aspect angles of two inertial targets).

For the case of a single star sensor slit using measurements of $\psi\psi_2^*$ angles, Euler angle relations are defined by the following equation:

$$\begin{aligned}
&\cos\psi\Big\{\cos(\psi_2^*-\psi)\Big(\sin\theta\tan E\cos\alpha\tan\beta^*-\cos\theta\cos(\varphi-A)\cos\alpha\tan\beta^*-\sin(\varphi-A)\Big)\\
&\quad+\sin(\psi_2^*-\psi)\Big(\sin\theta\tan E-\cos\theta\cos(\varphi-A)+\cos\alpha\tan\beta^*\sin(\varphi-A)\Big)\Big\}\\
&+\sin\psi\Big\{\cos(\psi_2^*-\psi)\Big(\sin\theta\tan E-\cos\theta\cos(\varphi-A)+\cos\alpha\tan\beta^*\sin(\varphi-A)\Big)\\
&-\sin(\psi_2^*-\psi)\Big(\sin\theta\tan E\cos\alpha\tan\beta^*-\cos\theta\cos(\varphi-A)\cos\alpha\tan\beta^*-\sin(\varphi-A)\Big)\Big\}\\
&+\sin\theta\cos(\varphi-A)\sin\alpha\tan\beta^*+\cos\theta\tan E\sin\alpha\tan\beta^*=0
\end{aligned} \tag{4}$$

The condition for the star being in the FOV of the ψ_2^* slit is given by the following equation:

$$\begin{aligned}
&\sin\alpha(\cos\theta\cos E\cos\psi_2^*\cos(\varphi-A)-\cos E\sin\psi_2^*\sin(\varphi-A)-\sin\theta\sin E\cos\psi_2^*)\\
&\quad+\cos\alpha(\sin\theta\cos E\cos(\varphi-A)+\cos\theta\sin E)\geq\cos\left(\frac{FOV}{2}\right)
\end{aligned} \tag{5}$$

Using Equations (1), (2), and (4) with measurements of $\psi\psi_2$ and $\psi\psi_2^*$ angles, the Euler angles can be derived for certain geometry conditions discussed in the visibility section of this report. This is the single canted slit star sensor attitude determination scheme (measure aspect angle of one inertial target and spin angle between two inertial targets).

By equating $\beta^*=0$ deg and $\psi_2^*=\psi^*$ in Equations (4) and (5), and using measurements of $\psi\psi^*$ angles the Euler angle relations are defined by the following equation:

$$\tan\psi = \frac{[\sin\theta \tan E - \cos\theta \cos(\varphi-A)]\tan(\psi^*-\psi) - \sin(\varphi-A)}{[\cos\theta\cos(\varphi-A) - \sin\theta\tan E] - \tan(\psi^*-\psi)\sin(\varphi-A)} \qquad (6)$$

Using Equations (1), (2), and (6) with measurements of $\psi\psi_2$ and $\psi\psi^*$ angles the Euler angles can be derived for certain geometry conditions. This is the single straight slit star sensor attitude determination scheme.

In summary, Equations (1) thru (6) and (2*) and (3*) are eight equations which implicitly define the spacecraft Euler angles ϕ, θ, ψ in three independent ways on the basis of four measurements; $\psi\psi_2$, $\psi\psi^*$, $\psi\psi_2^*$ and $\psi^*\psi_2^*$ spin angles.

Methodology for the Sun and Stars Visibility Study

In order to completely define spin axis attitude from sun and star sensor data, the fundamental questions of inertial target visibility and data sensitivity must be addressed.

The sun sensors (3) FOV will cover the range of 90 ± 75 deg from the + spin axis (Z_S). Therefore, the sun aspect angle can be measured for all spin axis angles of rotation to within 15 deg of the sunline.

The spin axis attitudes where the star is in the sensor FOV can be derived by pointing the centerline of the sensor FOV at the star and rotating the spin axis (Z_S) around the starline at a constant angle (α). Figure A-3 illustrates the resulting cone created by the spin axis. The thickness of the conical annulus (defining the allowable spin axis attitudes for star crossings of the fan) is determined by the elevation field of view of the star sensor fan. Referring to Figure A-3, the sun sensor is used to measure the angle λ and the star sensor is required to measure either the angle λ or the spin angle (A). Given the angle ϵ (angle between the sunline and the starline), and the above measured angles, the spin axis attitude can be determined using spherical triangle geometry assuming certain geometry and measurement error limitations. Basically, the star sensor measurements must be used to determine the spin axis position about the spacecraft sunline; i.e., the angle (B), in order to determine the spacecraft attitude.

Using the dual slits (ψ_2^*,ψ^*) of the star sensor, a change in the star declination angle λ will be detected for spin axis motions in the starline-spin axis plane. When the spin axis is near the sun-star-spacecraft plane, the detected motion about the sunline will be minimum; i.e., $\partial\lambda/\partial\beta$ will be small. Likewise, the maximum sensitivity of $\partial\lambda/\partial\beta$ will occur when the angle (A) is near 90 deg.

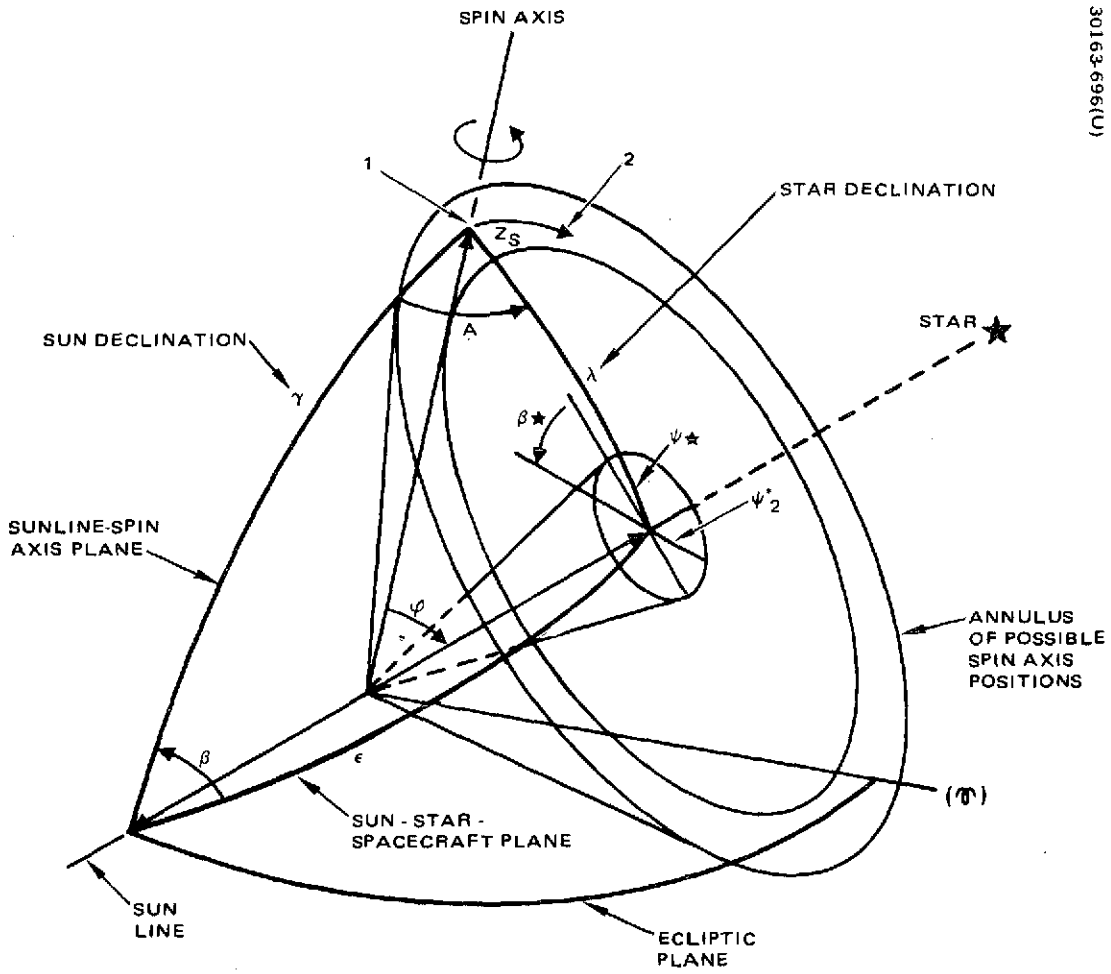

30163-696(U)

FIGURE A-3. SPIN AXIS ATTITUDES FOR STAR IN FIELD OF VIEW

To determine the attitude using only a single (ψ^* or ψ_2^*) star sensor slit becomes a little more complicated. Since the star angle, λ, cannot be measured directly using a single star sensor slit, the motions of the spin axis about the sunline must be determined from measurements of the spin angle (A) between the sunline (ψ) and the starline (ψ^* or ψ_2^*). However, when the plane of the ψ^* or ψ_2^* slit is normal to the sunline, at the time of a star pulse, no change in spin angle (A) will be detected for rotations of the spin axis about the sunline; i.e., $\partial A/\partial B$ will be zero. Looking at Figure A-3, this condition will exist at spin axis position (1) for the ψ^* slit. When the spin axis is rotated through an angle β^* about the starline to position (2), the same condition will exist for the ψ_2^* slit. At all other spin axis positions in the annulus, a change in spin axis position about the sunline will result in a change in spin angle between the sunline and the starline; i.e., $\partial A/\partial B \neq$ zero.

The general rule that can be derived from this example is that motions about the sunline are not detectable when one of the ψ^* fans is orthogonal to this line at the time of the star pulse. The location of the spin axis in the conical annulus will define when one of the two star slits will not be sensitive to this motion. Two locations displaced 180 deg on the annulus exist for each slit. It is here that the capability of independently using either sensor slit for attitude determination is lost. When this condition exists, the latter process reduces to the standard technique of using a dual slit sensor to define the star declination angle and a dual slit sun sensor to define the sun declination angle.

To demonstrate the above analytically, one can show for certain combinations of spin axis ϕ angle and star azimuth angle A, the ψ^* fan provides no useful information; i.e., Equation (4) becomes a trivial. Consider spacecraft-sun-star geometry for star azimuth angles of 0 and 90 deg with the spin axis nominally perpendicular to the ecliptic. For each of these two cases, the Euler angle equations above can be used to determine sensor's response to spin rotation, θ, toward the sunline (ϕ = 0 deg) and about the sunline (ϕ = 90 deg).

<u>ψ^* Case 1: A = 0° (Figure A-4)</u>

Using Equations (1), (2), and (6):

(a) when

$$\phi = 0^\circ \rightarrow \psi = 0^\circ;\ \sin(\psi_2-\psi) = \tan\theta/\cot\beta^*;\ \psi^*-\psi = 0$$

(b) when

$$\phi = 90^\circ \rightarrow \psi = -90^\circ;\ \psi_2-\psi = 0;\ \tan(\psi^*-\psi) = -\sin\theta\tan E$$

<u>ψ^* Case 2: A = 90° (Figure A-4)</u>

Using Equations (1), (2), and (6):

(a) when

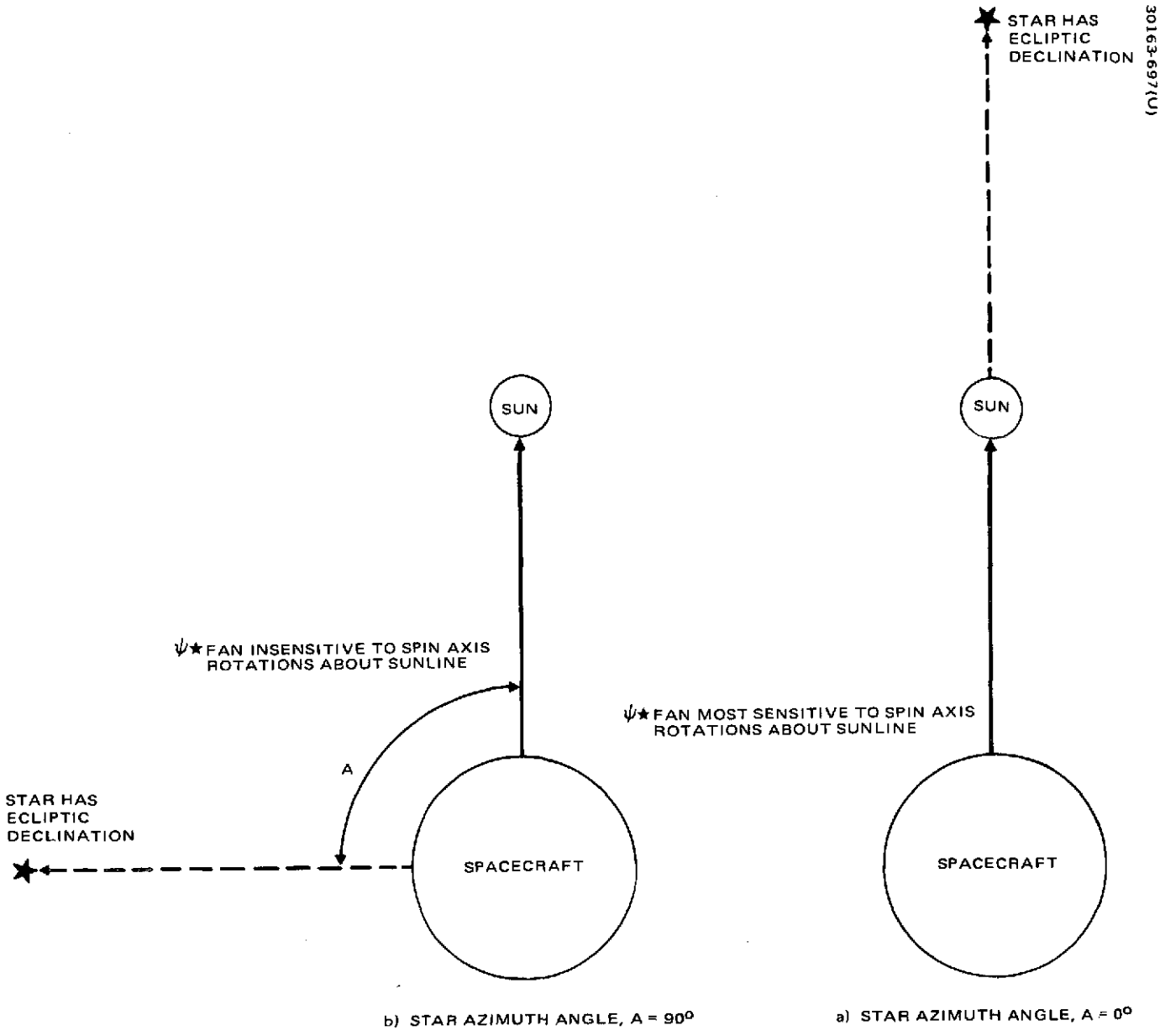

FIGURE A-4. SPACECRAFT-SUN-STAR GEOMETRY IN ECLIPTIC PLANE

$$\phi = 0^{o} \rightarrow \psi = 0^{o};\ \sin(\psi_2 - \psi) = \tan\phi/\cot\beta^{*};$$

$$\tan(\psi^{*} - \psi) = -1/\sin\theta \tan E$$

(b) when

$$\phi = 90^{o} \rightarrow \psi = -90^{o};\ \psi_2 - \psi = 0;\ \psi^{*} - \psi = 90^{o}$$

Note that for Case 2-b, star azimuth angle (A) of 90 deg, the spin axis rotations about the sunline, θ, are undefined by star sensor measurements. It is evident from Equation (6) that the most favorable geometry for the sun-sensor-star sensor ψ^{*} fan measurements occurs when A = 0 deg or the spacecraft, sun and star are coplanar. For this geometry, the $\psi_2 - \psi$ spin angle is most sensitive to spin axis rotations toward the sunline and the $\psi^{*} - \psi$ spin angle is most sensitive to spin axis rotations about the sunline.

In order to easily check star-sun sensor coverage of all possible Pioneer Venus mission maneuvers and cruise-orbit history, a series of attitude determination charts were developed. The first of these charts employs the use of Equations (1), (2) and (6) to generate values of ϕ and θ when the starline is on the edge of a sensor fan. Plotting ϕ and θ on polar graph paper (spacecraft at the origin) produces an annulus simulating possible spin axis attitudes with the star in the field of view of the ψ^{*} fan at some point in the spin cycle. Figure A-5 illustrates a typical annulus for the star Sirius and a straight slit. θ is measured in the radial direction and in the circumferential direction. The ecliptic normal is located at the center θ = 0 deg and the ecliptic plane at θ = 90 deg. ϕ (ecliptic right ascension) is measured in a counterclockwise (clockwise) direction in the north (south) ecliptic hemisphere with the spin axis coming out of the page. With this definition of coordinates, one is able to represent either the southern or northern ecliptic hemisphere on the graph where star declination is measured by θ and sun and star right ascension is measured by ϕ. Aries (γ) is located at θ = 90 deg, ϕ = 0 deg. As before, if an attitude lies in the annulus of a particular star, then the star sensor can see that star. The width of the annulus is directly analogous to the width of the star fan FOV (~ 25 deg). The angular distance (D) from the star to the inner and outer edge of the annulus is obtained from

$$D = \alpha \pm \frac{(\text{star FOV})}{2} \text{ (deg)}$$

where α is the declination angle from the spin axis to center of the sensor FOV.

The effective area of the polar annulus is reduced (unshared are in Figure A-5) due to the measurement error sensitivity problem associated with sun-star-spacecraft geometry discussed above. This area of error sensitivity on the annulus can be illustrated from plots of $(\psi^{*} - \psi)$ measurements versus $(\psi_2 - \psi)$ measurements with ϕ and θ as dependent parameters. These values are obtained from Equations (1), (2), and (6) with e = 90 deg, and values of ϕ and θ that lie within the conical annulus of interest. An example of how such charts are used to visualize the unshaded annulus region can be

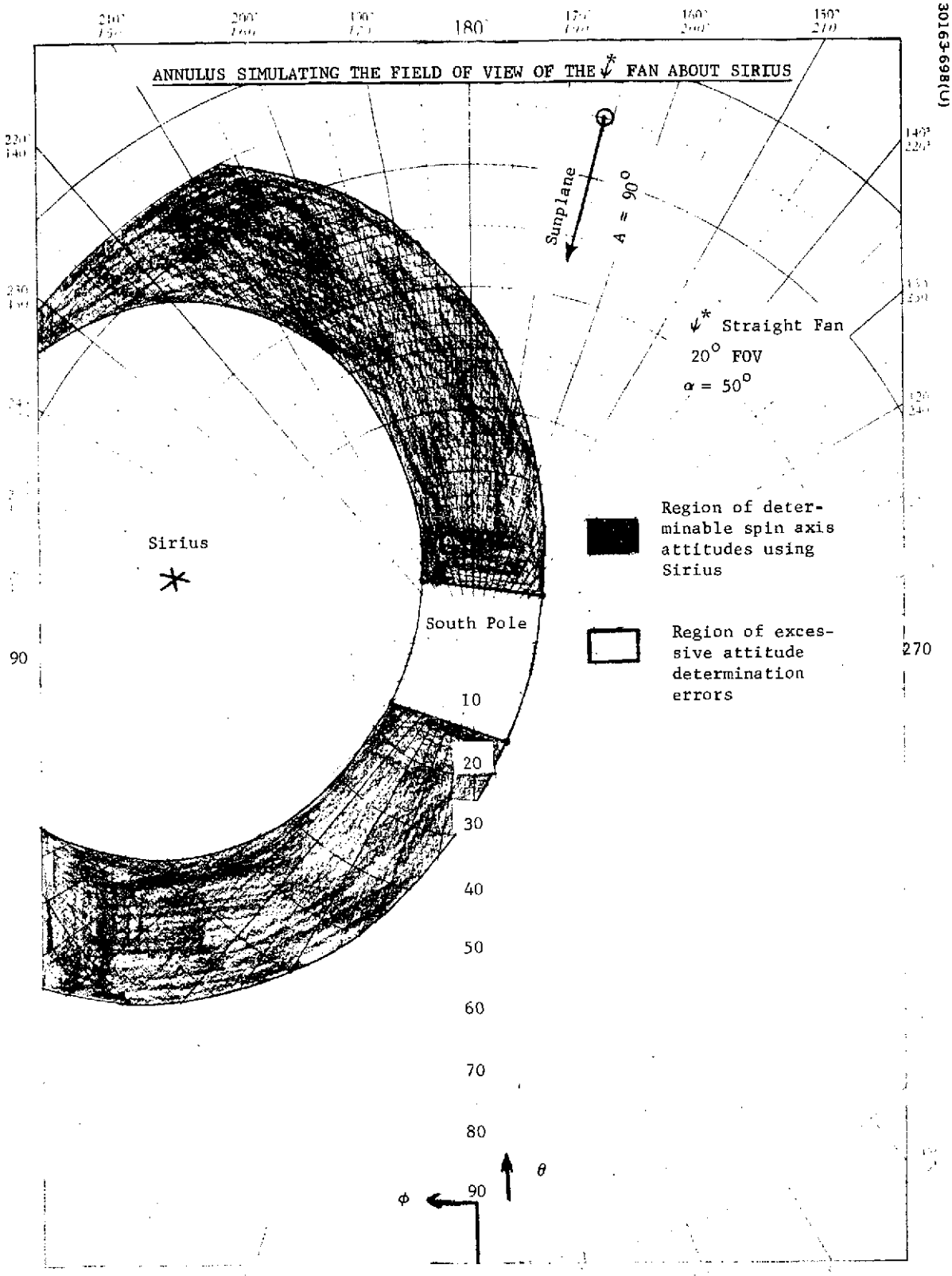

FIGURE A-5. ANNULUS SIMULATING FIELD OF VIEW OF Ψ* FAN ABOUT SIRIUS

seen from Figure A-6 where Sirius azimuth angle A = 90 and $\beta^* = 0$. Values of ϕ and θ are read from the figure given $(\psi^*-\psi)$ and $(\psi_2-\psi)$ spin angles. As can be seen from the figure, there exists a point corresponding to the south ecliptic pole where all the curves cross, implying an indeterminate condition. This corresponds to Case 2-b in the previous discussion. Small measurement errors ($\geq$0.1 deg) will result in large attitude uncertainties for $\theta < 15$ deg and $-20 \text{ deg} < \phi < 50$ deg, $145 \text{ deg} < \phi < 230$ deg. Removing these values of ϕ and θ as possible spin axis attitudes from Figure A- produces the unshaded area. Only in the shaded area can we determine attitude with reasonable accuracy.

Direct or reflected stray sun light will also reduce the effective visibility of the star sensor. For the purpose of this study the sun interference with the star sensor is assumed to occur if the sunline is within 60 deg in elevation and within 50 deg in azimuth of the center of the star sensor FOV. Treating the sun as a star (0 deg) declination and assigning the star sensor a 120-deg field of view (for the sun), one can use Equation (5) to determine the attitude when the sunline is within 60 deg of the boresight in elevation. Superimposing this 120-deg-wide annulus on the annulus plots, one can locate those star annuli which are potentially reduced by sun interference. If attitudes within a given star annulus also have $\psi^*-\psi$ pulses such that $-50 \text{ deg} \leq (\psi^*-\psi) \leq 50$ deg, the sun interferes with the star. Generally speaking, any star with a declination less than 70 deg ($\theta \geq 20$ deg) and with right ascension within 50 deg of the sunline will suffer seriously from sun interference.

The second kind of interference with the star sensor is reflected stray light from Venus. This occurs only during Venus approach and Venus orbit. The level of interference depends on distance of the spacecraft from the planet, orbit position, and spin axis direction (south or north). To facilitate the study of Venus interference, the minimum angle between the limb of Venus and the star sensor boresight at some point in the spincycle was graphed versus the true anomaly and the time from perigee passage. Venus is assumed to interfere with the star sensor if the angle between the limb of Venus and the star sensor boresight is less than 50 deg at the time of a star pulse. Figure A-7 gives a general picture of regions of no interference and possible interference for the baseline Venus orbit. A summary of the results of these studies is presented in the orbiter mission attitude determination study in a following section.

While the polar chart provides attitude determination information at discrete periods during the probe and orbiter missions, they become burdensome when used to generate a continuous mission history. Their prime usefulness is for attitude determination during midcourse corrections, probe release, orbit injection, etc. During cruise and Venus orbit, only attitude determination around the ecliptic normal is needed. Summary charts of available stars and allowable deviation from ecliptic normal for attitude coverage versus time in transit or orbit are clearly desirable.

One can generate orbit history bar charts indicating the exact coverage given around the ecliptic pole for each slit and by what star(s) (see Figure A-9). The types of slits considered were a zero cant ($\beta^*=0$ deg), a -20 deg cant, and a

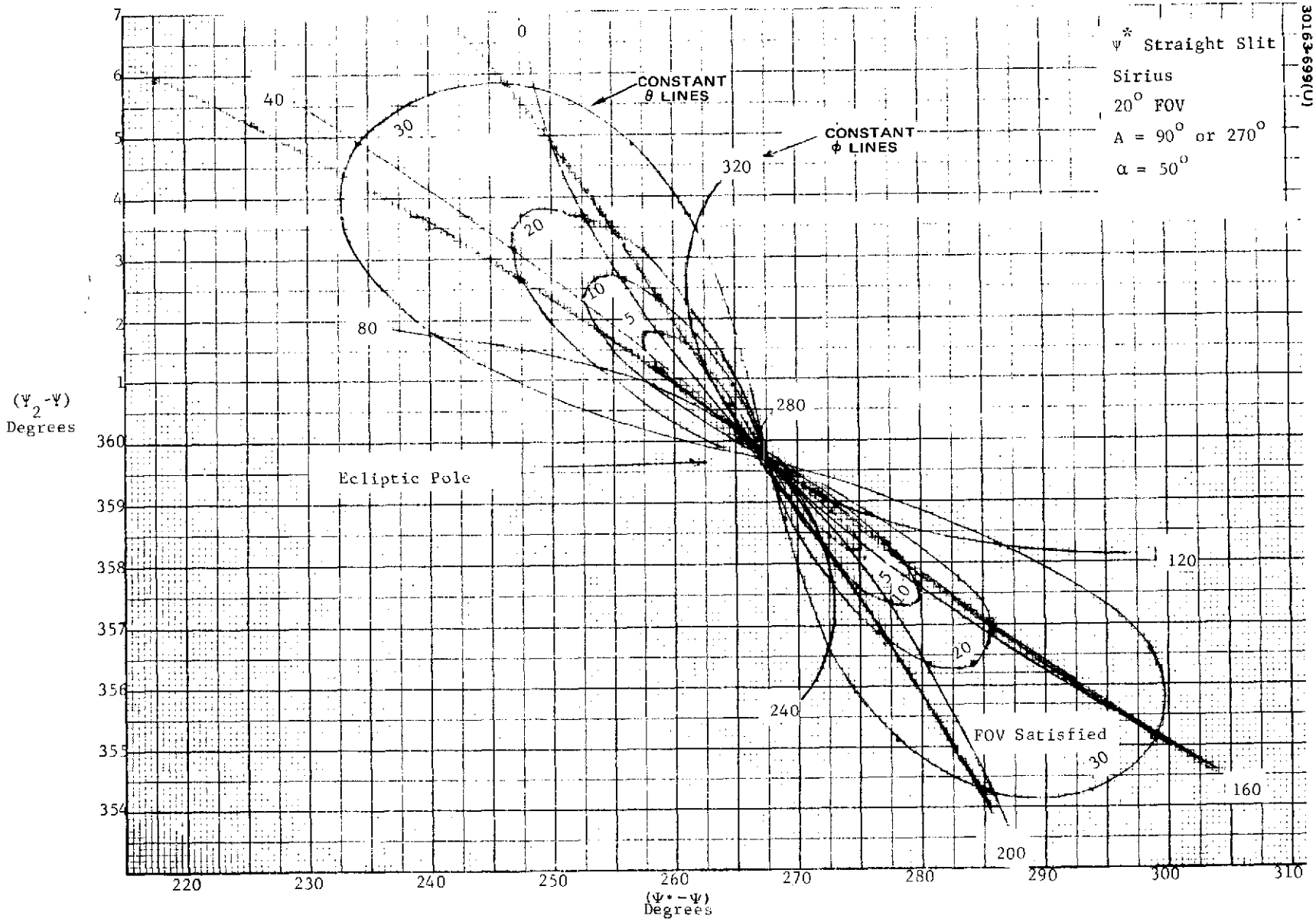

FIGURE A-6. ATTITUDE DETERMINATION CHART USING (ψ^*- ψ) VERSUS (Ψ_2 - Ψ) WITH PARAMETERS ϕ AND θ

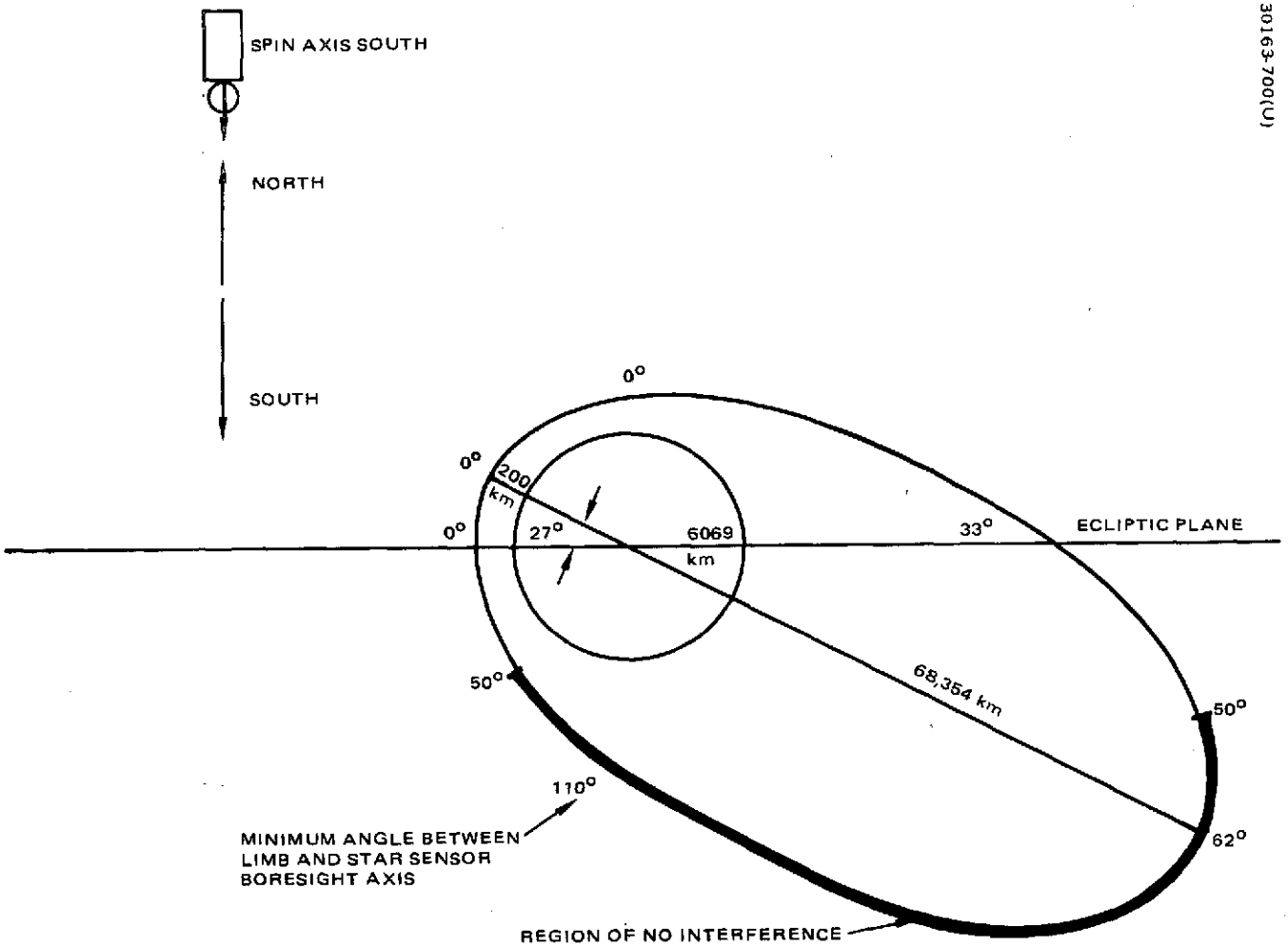

30163-700(U)

FIGURE A-7. BASELINE VENUS INTERFERENCE

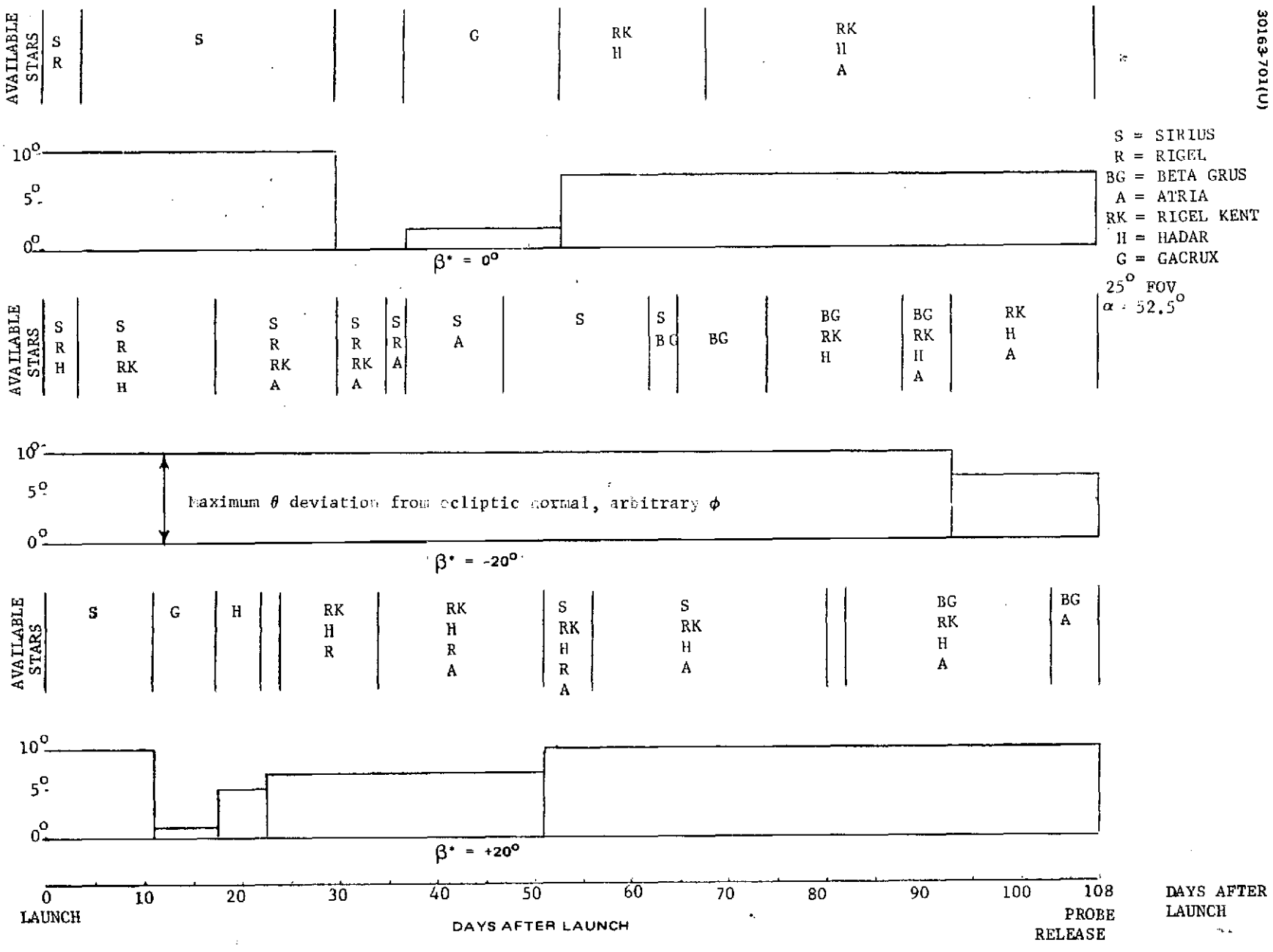

FIGURE A-8. PROBE CRUISE STAR VISIBILITY – SPIN AXIS SOUTH

+20 deg canted star slit. The length of the time in orbit in earth days corresponding to sun right ascension is used as the abscissa and the θ deviation from ecliptic normal is used as the ordinate. Only the worst case, maxumum θ deviation from zero (arbitrary ϕ), is used to construct the bar, with the most useful star listed first above the bar. Other stars listed provide at least 5 deg radius of coverage. For example, during the first 44 days after orbit injection, one is able to monitor attitude with a straight slit within 10 deg of the ecliptic normal using Sirius. One can check for coverage of the ecliptic normal, by how much, by what star(s), and by what kind of star slit (β^*=0 deg, -20 deg, +2- deg) for any period of the mission.

In review, the star sensor FOV polar charts show whether attitude determination is possible for any specific attitude maneuvers and the cruise and orbit star visibility history charts show how far the spin axis can deviate from ecliptic normal at any time and still allow attitude to be determined with some star and slit combination. Moreover, these charts can also be used to determine star sensor geometric parameters (β^*, α, star FOV) for optimum attitude determination during the particular attitude profiles of the probe and orbiter missions. The specifics of these trades are summarized in the following paragraphs.

Sun and Star Visibility for 1977-1978 Pioneer Venus Missions

Probe Mission (1977)

Primary probe bus attitude maneuvers are: spin axis reorientation to south ecliptic normal after third stage separation (launch); the first midcourse maneuver some 5 days after launch; probe release (L + 108 days); and Venus encounter (L + 128 days). For the first midcourse maneuver, where the spin axis could be anywhere in the southern ecliptic hemisphere, at least 90 percent of all possible attitudes can be determined with either a straight ψ^* fan or a canted ψ_2^* fan. The initial reorientation following third stage separation can be monitored by using the sun and stars Atria and Sirius. The various attitudes associated with large probe separation, small probe targeting, separation and probe bus retardation and entry can be determined by using the sun and stars Beta Grus, Vega and Alpha Hercules.

For coverage of the south ecliptic normal (cruise) attitude, the -20 deg canted ψ_2^* slit will provide useful information with 7 deg of ecliptic normal during the entire cruise phase. This is illustrated in Figure A-8 where angular deviation from the pole and usable stars are plotted versus transit time for each type of slit considered. Note that with a straight ψ^* slit, there is no ecliptic normal coverage during the L + 30 to L + 37-day interval. Sensor redundancy is lost during this interval for the straight slit configuration, however, no mission requirements are sacrificed. While the straight slit is somewhat inferior to either canted slit during cruise, it has been selected on the basis of superior coverage at encounter.

The straight slit provides the best coverage of attitudes for small probe targeting, separation and probe bus retardation, respectively. This observation together with the previous one on the superiority of the -20 deg

canted ψ_2^* fan during cruise are the basis for selecting these two slit cant angles for the probe mission. By selecting α = 55 deg, better coverage will be provided for the small probe release and retardation maneuver. Therefore, the preferred parameters for the probe mission are:

1) FOV = 25 deg

2) α = 55 deg

3) β^* = -20 and 0 deg

An alternate attitude for the cruise phase of the mission would be to point the star sensor in the northern ecliptic hemisphere. For the first midcourse maneuver, where the spin axis could be anywhere in the northern hemisphere, at least 75 percent of all possible attitudes can be determined with either a straight ψ^* slit or a canted ψ_2^* slit. Given a boresight angle (α) of 60 deg, one can monitor all midcourse maneuvers and the reorientation maneuver to ecliptic normal after third stage separation with ψ^*, ψ_2^* redundancy. During the cruise phase (ecliptic normal), ψ^* information is not usable for days L + 11 to L + 20 or 8 percent of the mission. The ψ_2^* slit provides useful information during the entire mission within 4 deg of the ecliptic normal. The alternate scheme, however, does provide "cleaner" coverage of all probe encounter maneuvers by positioning the associated attitudes more toward the center of the annuli surrounding Beta Grus and Vega.

If one constrains the spin axis north orientation to the baseline set of parameters (ψ^* and ψ_2^* slit FOV = 25 deg, α = 55 deg, β^* = -20 and 0 deg), the ability to determine attitude will be more difficult. ψ^*, ψ_2^* slit redundancy around the ecliptic pole is not available for the midcourse maneuvers and the reorientation to ecliptic normal after third stage separation. In general, cruise phase (ecliptic normal) ψ^* information is useless for days L + 0 L + 31 or 29 percent of the mission. However, the ψ_2^* fan provides useful information during the entire mission within 5 deg of the ecliptic normal. In summary, the set of star sensor parameters selected is significantly affected by the spin axis orientation during cruise. The latter has been selected to be the south ecliptic pole because of its general overall star coverage superiority and commonality with the orbiter mission choice discussed below.

Orbiter Mission (North Periapsis Baseline 1978)

Transit to Venus. For the orbiter mission, the primary attitude maneuvers during transit are associated with spin axis reorientation after third stage separation, and the first midcourse correction some 5 days after launch. Spacecraft cruise to Venus requires 187 days with the spin axis nominally parallel to the south ecliptic pole

Initial reorientation after third stage separation can be monitored using ψ^* slit and stars Al Suhail and Hadar. Reorientation during the first midcourse ΔV correction can also be monitored with this slit for 85 to 90 percent of the possible spin axis attitudes in the southern hemisphere. The

subsequent midcourse maneuvers are similarly covered by the ψ^* slit if precession to some attitude for a ΔV maneuver is required. The ψ_2^* slit ($\beta^* = -20$ deg) is equally useful for all of these maneuvers.

For coverage of the south ecliptic normal (cruise) attitude, either the ψ^* or ψ_2^* slit will provide useful information within 5 deg of the ecliptic normal during the entire cruise phase. This was illustrated in Figure A-9 where angular deviation from the pole and usable stars are plotted versus transit time for each type of slit considered.

An alternate scheme to the baseline cruise attitude is to position the spin axis parallel to the north ecliptic pole. For this choice, the primary orbiter attitude maneuvers and steady state attitudes around the north ecliptic pole can be covered. However, ψ^*, ψ_2^* slit redundancy for the cruise attitude and midcourse maneuver coverage in the north ecliptic hemisphere (65 to 70 percent) is decidedly less than the baseline scheme. Changing the boresight angle (α) to 60 deg improves the cruise attitude coverage but does not improve the midcourse maneuver coverage in the north. The fact that the midcourse maneuver coverage in the north does not improve and is less than the baseline, together with the mounting constraint of the star sensor (top of spacecraft), are significant inputs for the choice of the south ecliptic pole as the cruise attitude.

Venus Orbit Injection. Prior to retro firing, the spin axis is precessed from the south ecliptic pole to the insertion attitude in the northern hemisphere. Minimum coverage in the southern hemisphere is provided by Sirius and Betelgeux, while the northern hemisphere minimum coverage is provided by Capaella. Redundant coverage in the south is provided by Rigel, Beta Grus, Achernar, Canopus, Mirach, Al Suhail and Aldebaran. Redundant coverage in the north may be provided by Mira.

After the spacecraft has been inserted into orbit, the spin axis is precessed from the northern hemisphere to the south ecliptic normal for the duration of the orbit mission. The path is similar to the preinsertion maneuver and, as would be expected, the coverage is the same. This coverage is provided by the ψ^* slit (straight); a ψ_2^* slit ($\beta^* = -20$ deg) provides similar coverage with acceptable accuracy yielding ψ^*, ψ_2^* fan redundancy.

Venus Polar Orbit. During Venus orbit, the spin axis is maintained at the south ecliptic normal. The orbiter will orbit Venus for one Venus year (225 days) after insertion. Figure A-9 defines ecliptic normal coverage for this period for a ψ^* and ψ_2^* slit. Spacecraft position in orbit for this coverage is such that there is no Venus interference; i.e., the boresight of the star slit is >50 deg from the limb of the planet. Generally speaking, this implies that the spacecraft is "beneath" the planet; this will always occur every 24 hours. As can be seen in the figure, the ψ_2^* slit ($\beta^* = -20$ deg) always yields coverage for the spin axis attitudes within 5 deg of the south ecliptic pole. For the ψ^* slit ($\beta^* = 0$ deg), coverage is similar except for the period I + 44 to I + 49 days, where the ψ^* slit provides no useful information for attitudes around the pole; however, a slight change in spin axis attitude will allow Al Suhail to be used if required. Therefore, ψ^*, ψ_2^* redundancy is lost during this period (i.e., 2.2 percent of the orbit history).

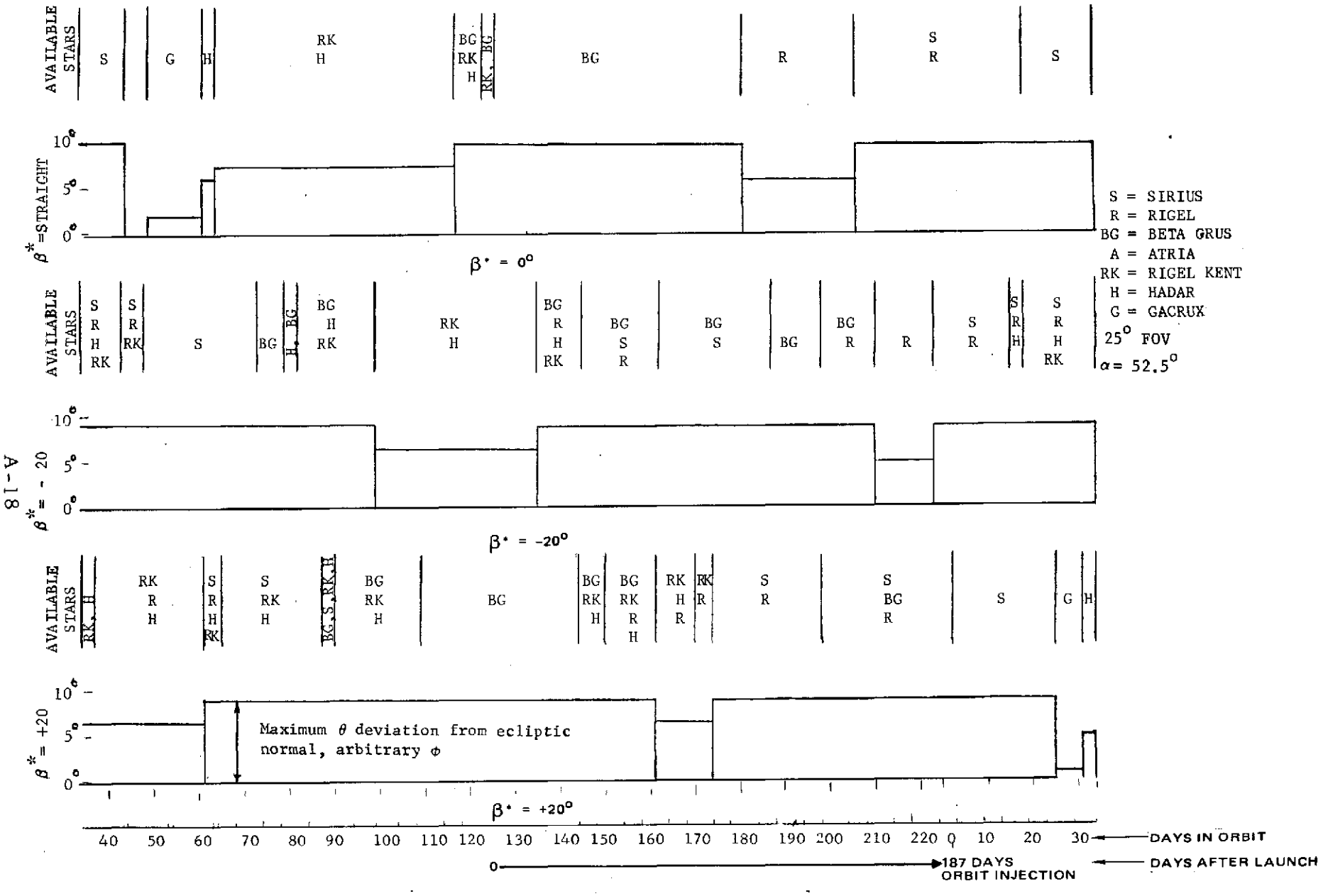

FIGURE A-9. ORBITER CRUISE STAR VISIBILITY - SPIN AXIS NORTH

Since it is not always desirable to check or change the attitude beneath the planet, it is important to know the extent of Venus interference during all phases of the 24-hour orbit. As mentioned previously, one can use standard orbital equations to generate the elevation angle between the planet limb and the star sensor boresight. This angle is graphed versus the true anomaly and time from periapsis passage in Figure A-10.

Note that the Venus limb elevation angle is greater than 50 deg for 15.5 h, with the peak at TA = 117 deg (when the spacecraft lies underneath the planet). This implies that Venus can interfere with attitude determination for less than half of the orbit. In fact, the period when Venus is actually in the star sensor FOV (minimum angle = 0 deg) during some phase of the spin cycle is about 1 h. Therefore, Venus interference with star visibility must be investigated for 190 deg $\leq$ TA $\leq$ 78 deg.

With these observations and the knowledge of the orbit plane position with respect to Aries and the star right ascension and declination, it is a straightforward matter to tell when Venus interferes with a star. Note that even though Venus is within 50 deg in elevation of the star sensor boresight during some phase of the spin cycle, it is not necessarily within 50 deg in azimuth during the entire spin cycle. Given this knowledge, one can construct new star visibility charts (subsets of Figure A-9) for those periods when Venus is within 50 deg in azimuth of the star sensor boresight at some phase of the spin cycle. These charts have been used to determine attitude determination windows throughout the mission.

Despin Reference at Periapsis. It is necessary to have at least one star for a despin reference during the eclipse periods at periapsis. The orbiter descending node (crossing of the ecliptic plane after periapsis) occurs at an ecliptic right ascension of 207 deg. Since Venus subtends a maximum angle of 150 deg at periapsis and Venus interference occurs when the star is less than 50 deg in right ascension from the limb, candidate stars for a despin reference must have a right ascension between 152 and 262 deg.

Periapsis eclipses start to occur $\approx$33 days after insertion. Three stars (Hadar, Gacrux and Rigel Kentaurus) are available as despin references for spin axis attitudes within 5 deg of ecliptic normal. In the absence of solar eclipses, one of these stars can also be used as a backup despin reference at periapsis from 2 through 187 days after orbital insertion. In other words, the sun does not interfere with star pulse generation in this time period.

If, perchance, the antenna need be despun during apoapsis eclipses some 186 to 191 days after orbit insertion, Sirius is available (as well as other stars). Since the sun sensor is redundant, a backup despin reference or sensor is always available for any orbital phase of the baseline orbit.

In conclusion, for the orbiter mission, the best star sensor coverage will be provided with the sensor scanning in the southern hemisphere with α = 51 deg. Therefore, the preferred parameters are:

1) $\psi*$, ψ_2^* FOV = 25 deg

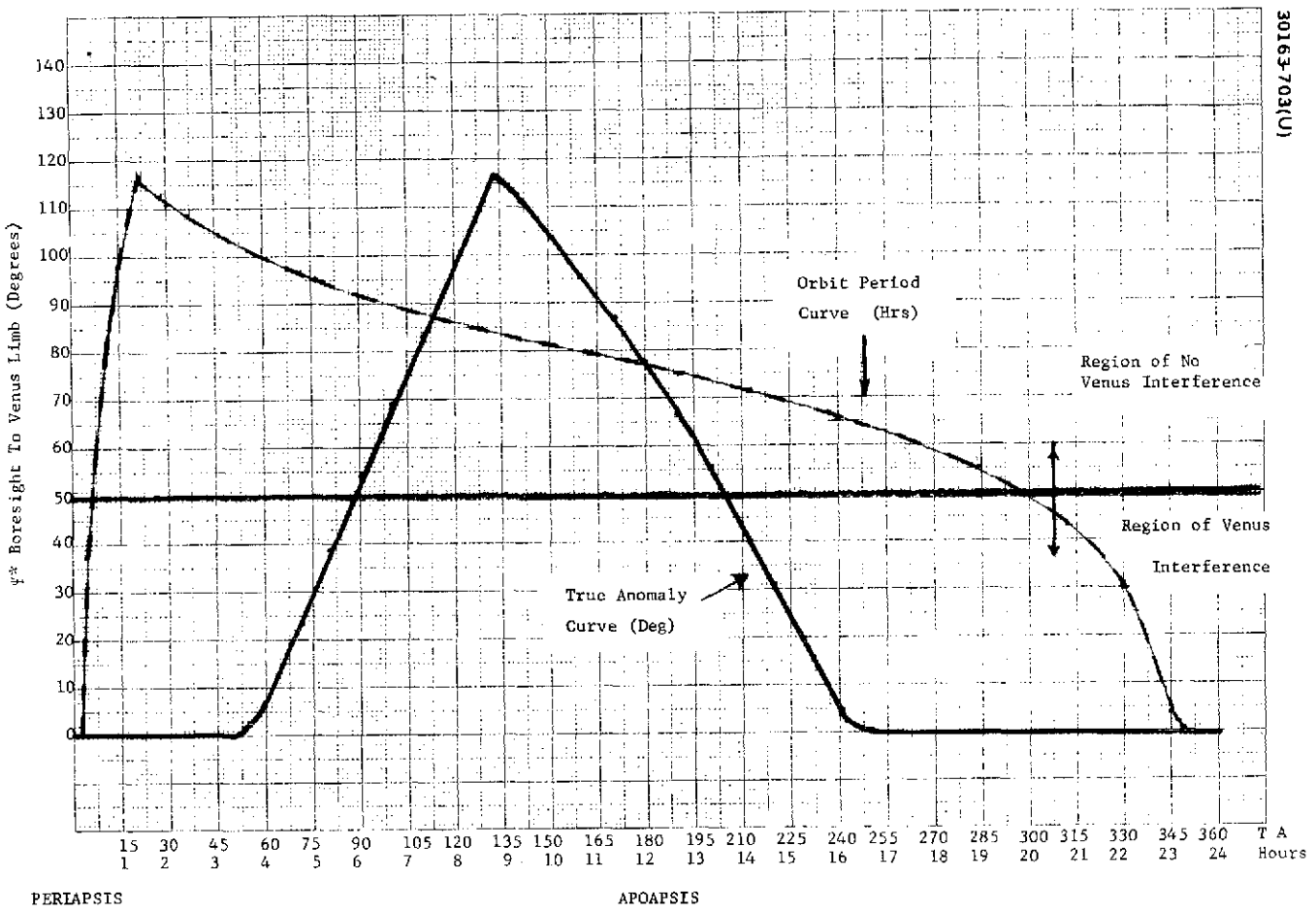

FIGURE A-10. VENUS INTERFERENCE DURING 24-HOUR ORBIT

2) α = 51 deg

3) β^* = 0 and -20 deg

The choice of south ecliptic pole as the cruise attitude is clinched by the requirement that the star sensor scan in the southern hemisphere during orbital operations. Since the sensor is mounted on the top of the spacecraft and the top must point south for science measurements at periapsis for the baseline orbit, the choice of sensor parameters is biased. With this set of parameters, cruise as well as midcourse star visibility coverage would be significantly decreased for a north ecliptic spin axis cruise attitude (as discussed above).

Alternate Orbiter Mission (South Periapsis 1978)

One of the orbiter missions being considered is to place periapsis at 43 deg south latitude. For this mission the spin axis would be pointing in the southern hemisphere during the cruise phase (same as baseline). However, the spin axis would be pointed in the northern hemisphere during orbit.

Orbit Insertion. The encounter date for the alternate scheme is the same as the baseline; the primary difference being that insertion is at 43 deg south latitude instead of 27 deg north latitude. Since the cruise attitude is at the south ecliptic pole, a precession maneuver of 43 deg positions the spacecraft for orbit injection.

This maneuver and the actual insertion attitude can be monitored using Betelgeux. After the spacecraft has been injected into orbit, the spin axis is precessed to the north ecliptic pole for the remainder of the orbit phase of the mission. During this maneuver, Betelgeux provides coverage in the south, while Capella provides coverage in the north.

Venus Polar Orbit. North ecliptic normal coverage during the period of the orbit when Venus does not interfere is decidedly less than in the north 27 deg periapsis baseline. Between I + 25 → I + 28 days no coverage is given by a +20 deg cant ψ_2^* slit or a straight ψ^* slit. The -20 deg cant ψ_2^* slit has an 8-day period when it provides no useful information and is generally inferior to the +20 deg cant ψ_2^* slit. The straight ψ^* slit, although inferior to either canted ψ_2^* slits, is maintained in the star sensor because of despin considerations. The period of no Venus interference (above 50 deg line) lasts 19.5 h. This is 4 h longer than the baseline. Due to the greater availability of stars in the southern hemisphere to cover the ecliptic pole, these extra 4 h (190 deg ≤ TA ≤ 206 deg) do not in general result in an advantage to the south periapsis over the baseline north periapsis.

Despin Reference at Periapsis. The right ascension of the orbit plane is the same as the baseline; the candidate stars are subject to the same constraint in right ascension but now lie in the northern ecliptic hemisphere. Arcturus is the primary despin reference during periapsis eclipses, with Alpha Hercules being a marginal backup. Apoapsis eclipses are covered by

Mirach with Altair and Scheat as backups. In general, the number of stars available for despin reference is more limited for the alternate choice of orbit.

ATTITUDE CONTROL, VELOCITY CONTROL, AND SPIN SPEED CONTROL ANALYSIS MODELS

The spin stabilized Pioneer Venus spacecraft typically execute two types of maneuvers: ΔV maneuvers and attitude (spin axis orientation) maneuvers. ΔV maneuvers are required for trajectory corrections and orbital touchups; these maneuvers are conveniently divided into radial and axial ΔV maneuvers. Axial ΔV refers to velocity increments parallel to the nominal spin axis, while radial ΔV refers to velocity increments perpendicular to the nominal spin axis. Attitude maneuvers are required to obtain the proper inertial orientation for the ΔV maneuvers, to orient antennae for communications, and to maintain the proper sunline orientation for power and thermal considerations. In addition to these maneuvers, spin speed control is also required. For convenience, spin control will also be classified as a maneuver. For the Pioneer Venus, orientation and spin control maneuvers are also required for experiments and for probe separation.

The Pioneer Venus probe bus is provided with six control jets or thrusters -- four that thrust radially and two that thrust axially; the Pioneer Venus orbiter bus is provided with seven control jets -- four radial and three axial. These jets nominally perform the previously mentioned four maneuvers with some redundancy; that is, each maneuver can be performed with more than one jet or combination of jets. Because of uncertainties in the mass and geometric properties of the spacecraft, in timing, and in the impulse and alignment of the thrusters, the executed maneuver will deviate from the nominal maneuver; in addition, these uncertainties will, in general, induce crosstalk or coupled maneuvers. As an example of crosstalk, the generation of an axial ΔV maneuver will cause incremental changes in attitude, spin speed, and radial ΔV. Furthermore, spacecraft nutation is generally induced.

This appendix summarizes the error block diagrams and algorithms for estimating performance parameters of the nominal maneuvers, the associated uncertainties, and crosscoupling effects. The first four flow charts A-11 through A-14 (corresponding to each nominal maneuver) display, for each jet control mode, the first-order error sources that contribute to the random deviation of the actual from the nominal maneuver as well as crosstalk between maneuvers; the following seven flow charts, A-15 through A-21, display the algorithms necessary to evaluate maneuver errors.

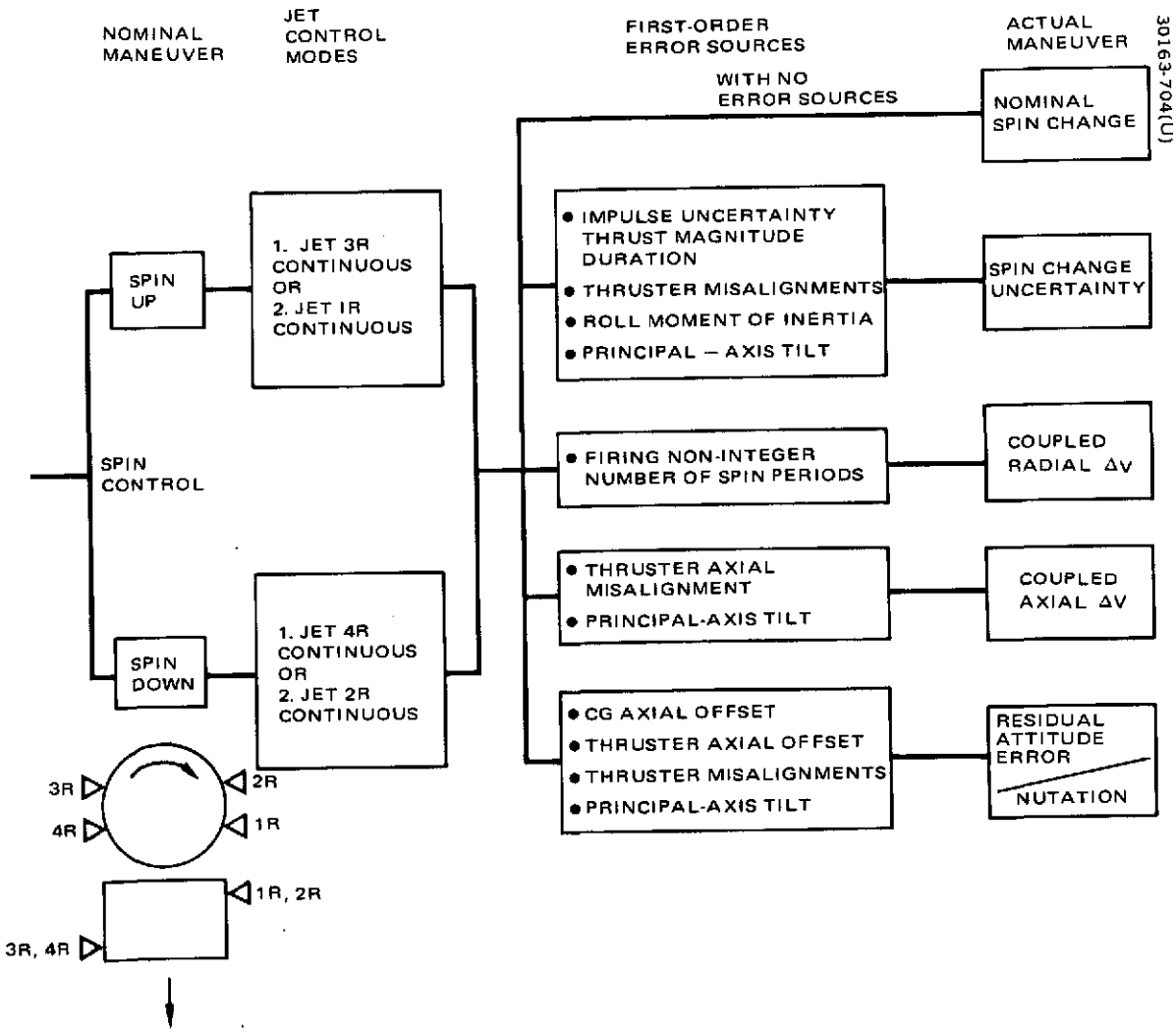

FIGURE A-11. SPIN CONTROL MANEUVER WITH FIRST ORDER ERROR SOURCES CONTRIBUTING TO UNCERTAINTY AND TO COUPLED MANEUVERS

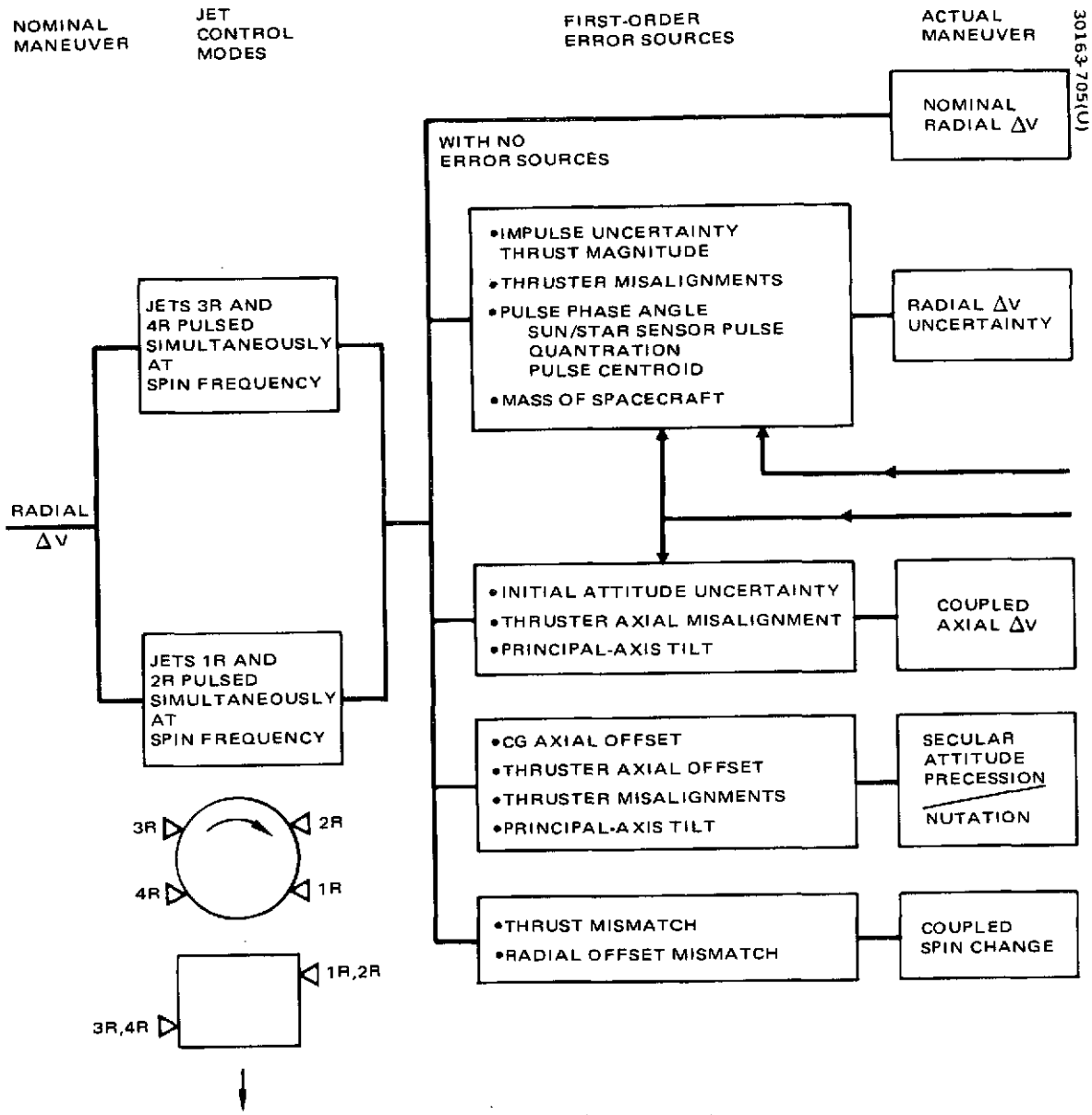

FIGURE A-12. RADIAL ΔV MANEUVER WITH FIRST ORDER ERROR SOURCES CONTRIBUTING TO UNCERTAINTY AND TO COUPLED MANEUVERS

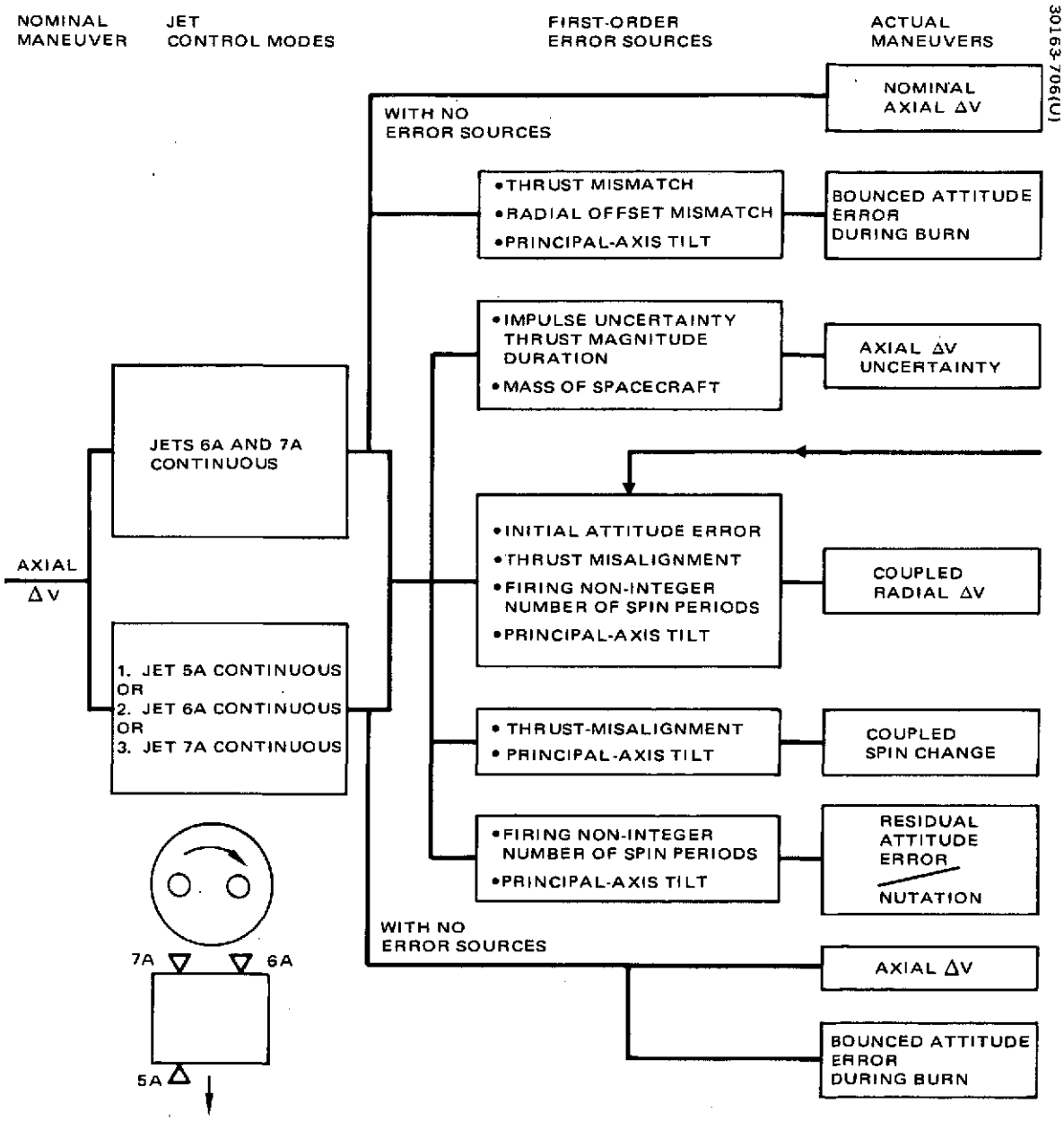

FIGURE A-13. AXIAL ΔV MANEUVER WITH FIRST ORDER ERROR SOURCES CONTRIBUTING TO UNCERTAINTY AND TO COUPLED MANEUVERS

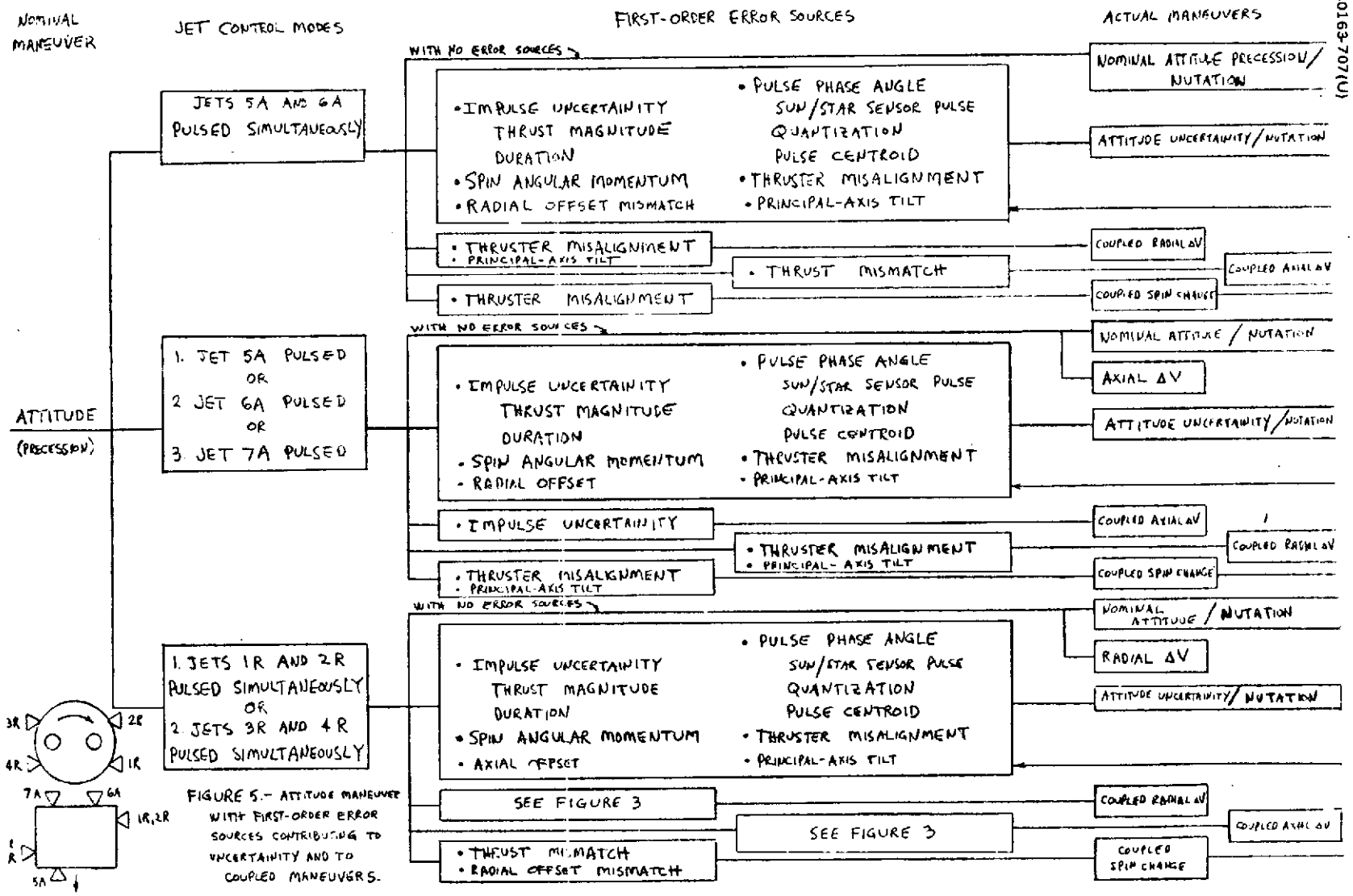

FIGURE 5.- ATTITUDE MANEUVER WITH FIRST-ORDER ERROR SOURCES CONTRIBUTING TO UNCERTAINTY AND TO COUPLED MANEUVERS.

FIGURE A-14. ATTITUDE PRECESSION MANEUVER WITH FIRST ORDER ERROR SOURCES

30163-707(U)

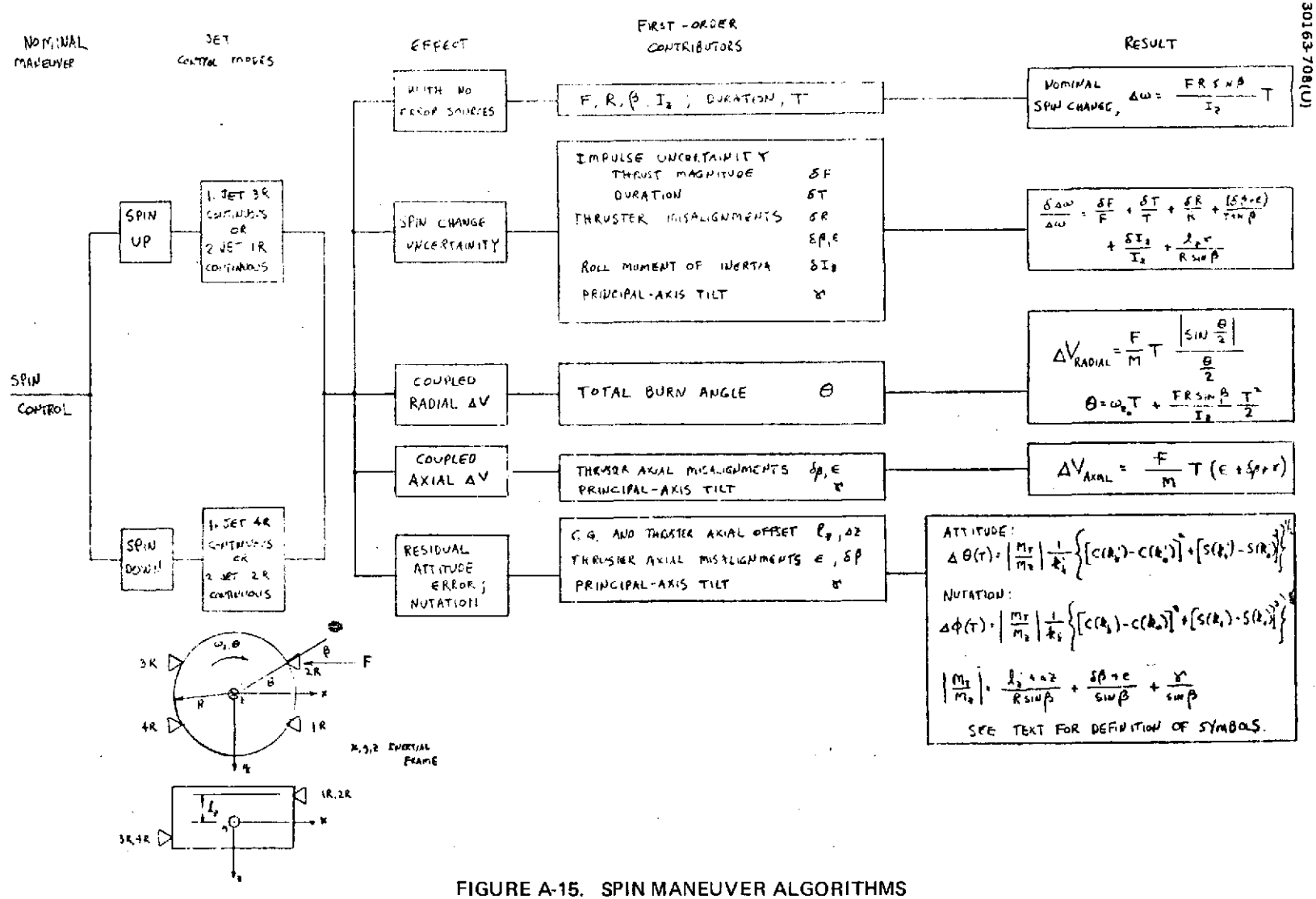

FIGURE A-15. SPIN MANEUVER ALGORITHMS

30163-708(U)

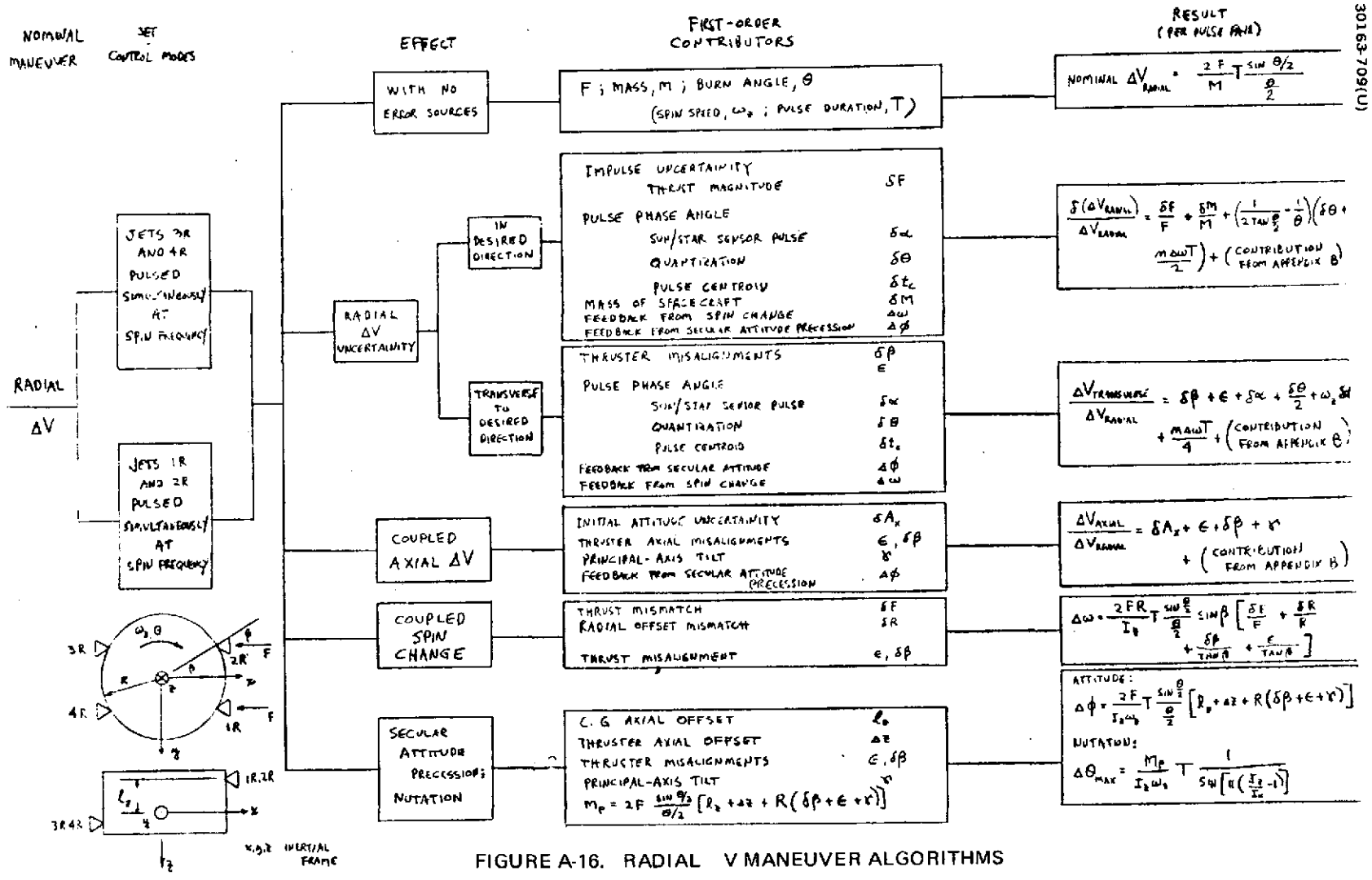

FIGURE A-16. RADIAL V MANEUVER ALGORITHMS

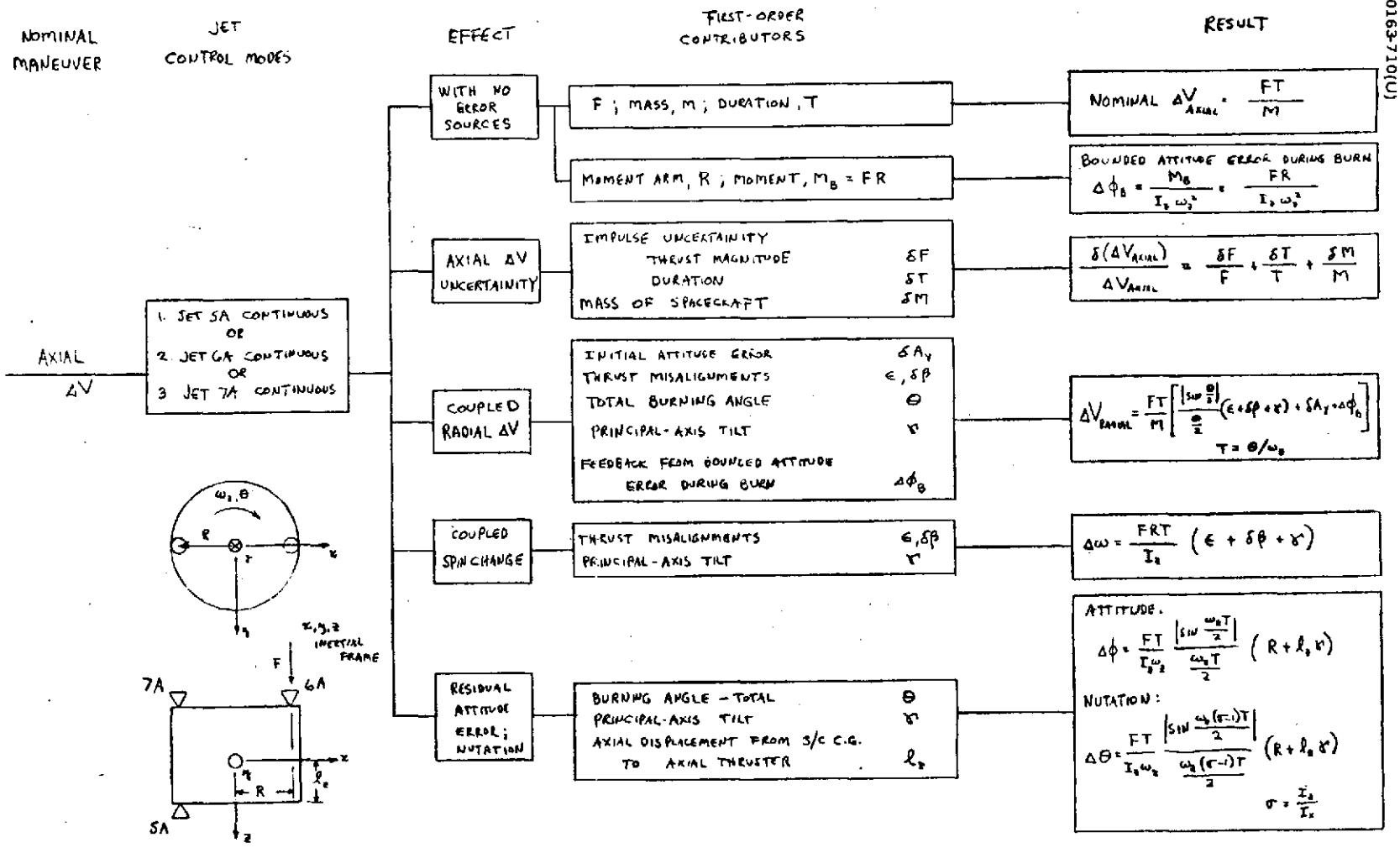

FIGURE A-17. AXIAL V MANEUVER ALGORITHMS – ONE AXIAL JET MODE

30163-710(U)

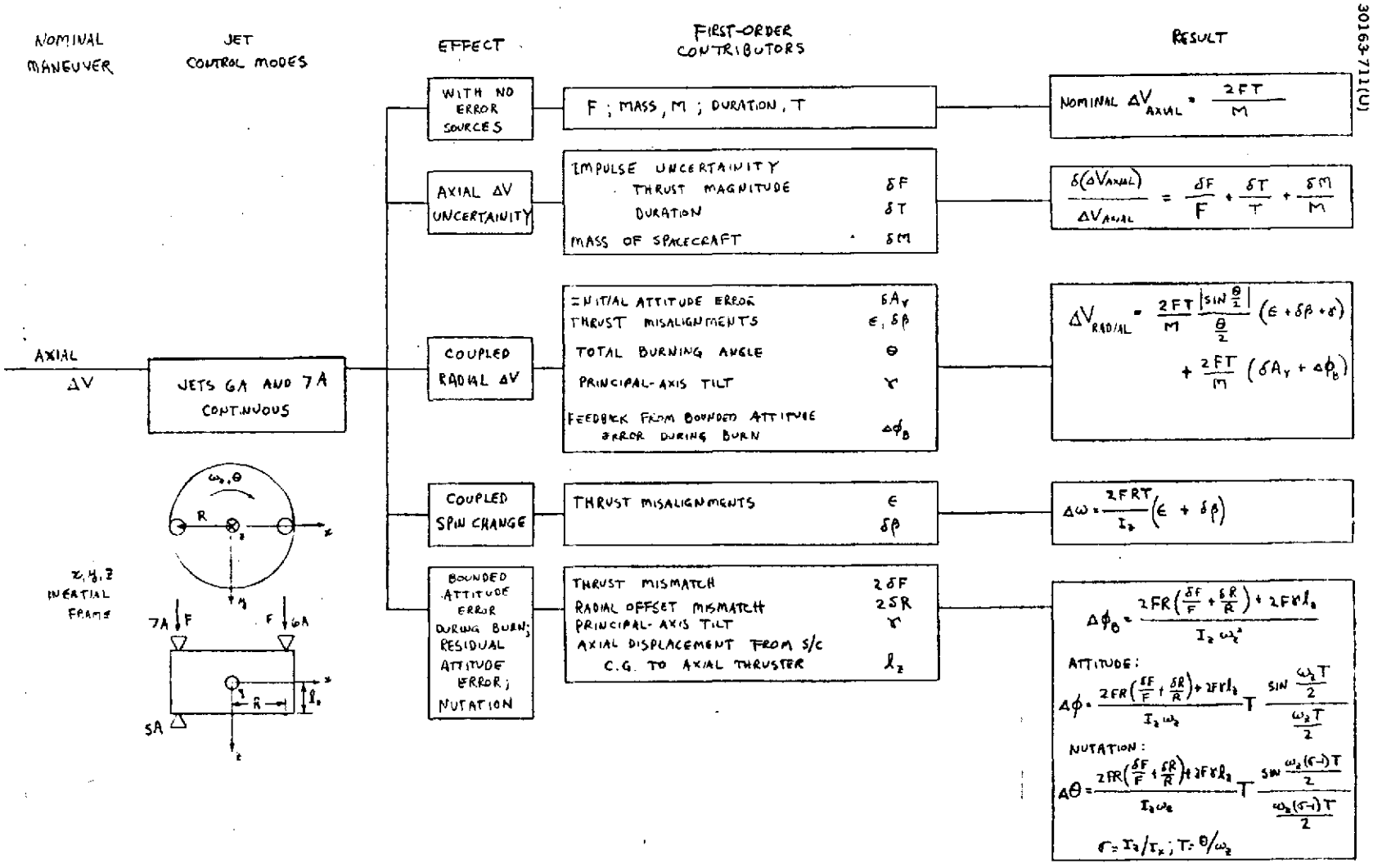

FIGURE A-18. AXIAL V MANEUVER ALGORITHMS – TWO AXIAL JET MODE

30163-711(U)

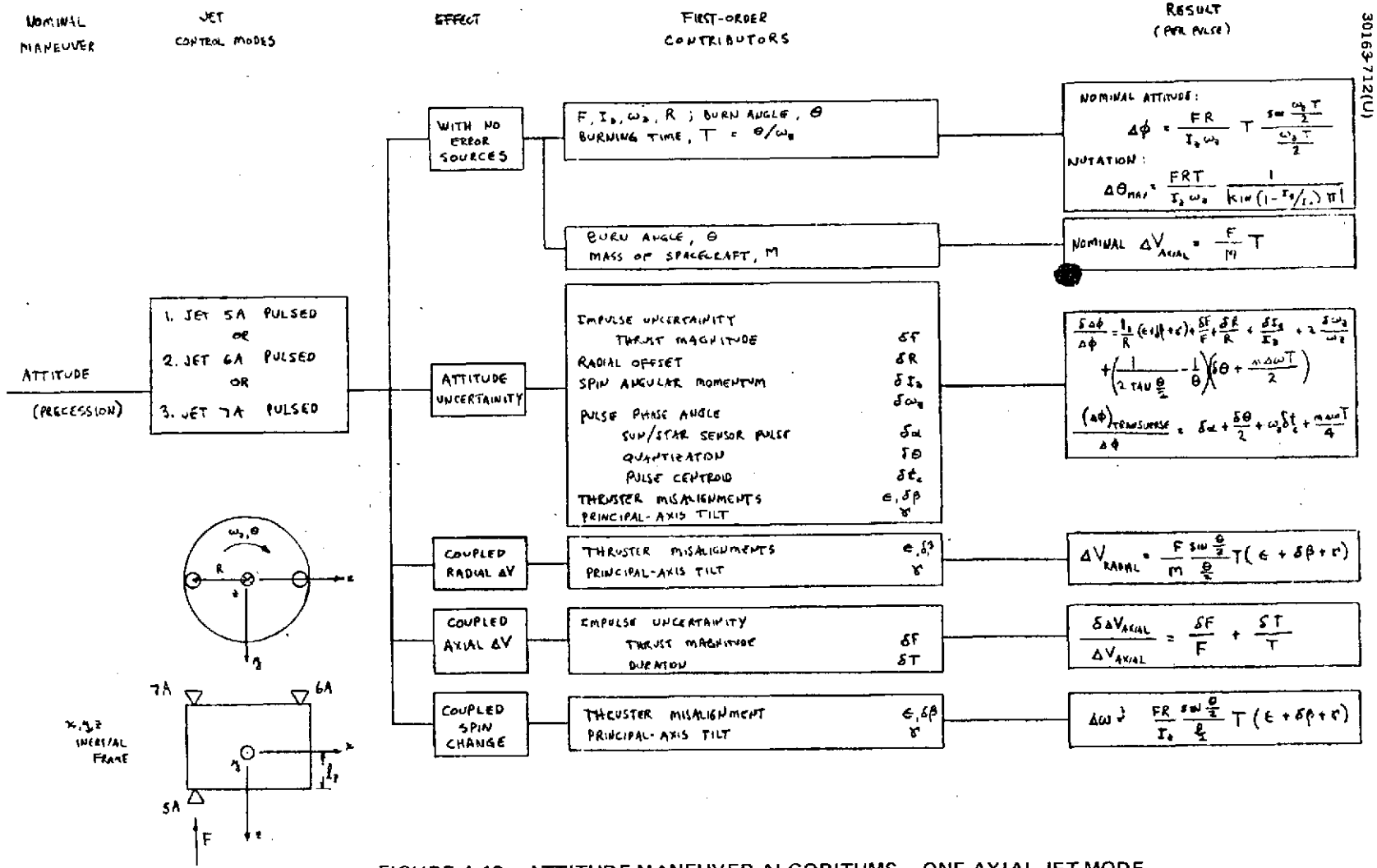

FIGURE A-19. ATTITUDE MANEUVER ALGORITHMS – ONE AXIAL JET MODE

30163-712(U)

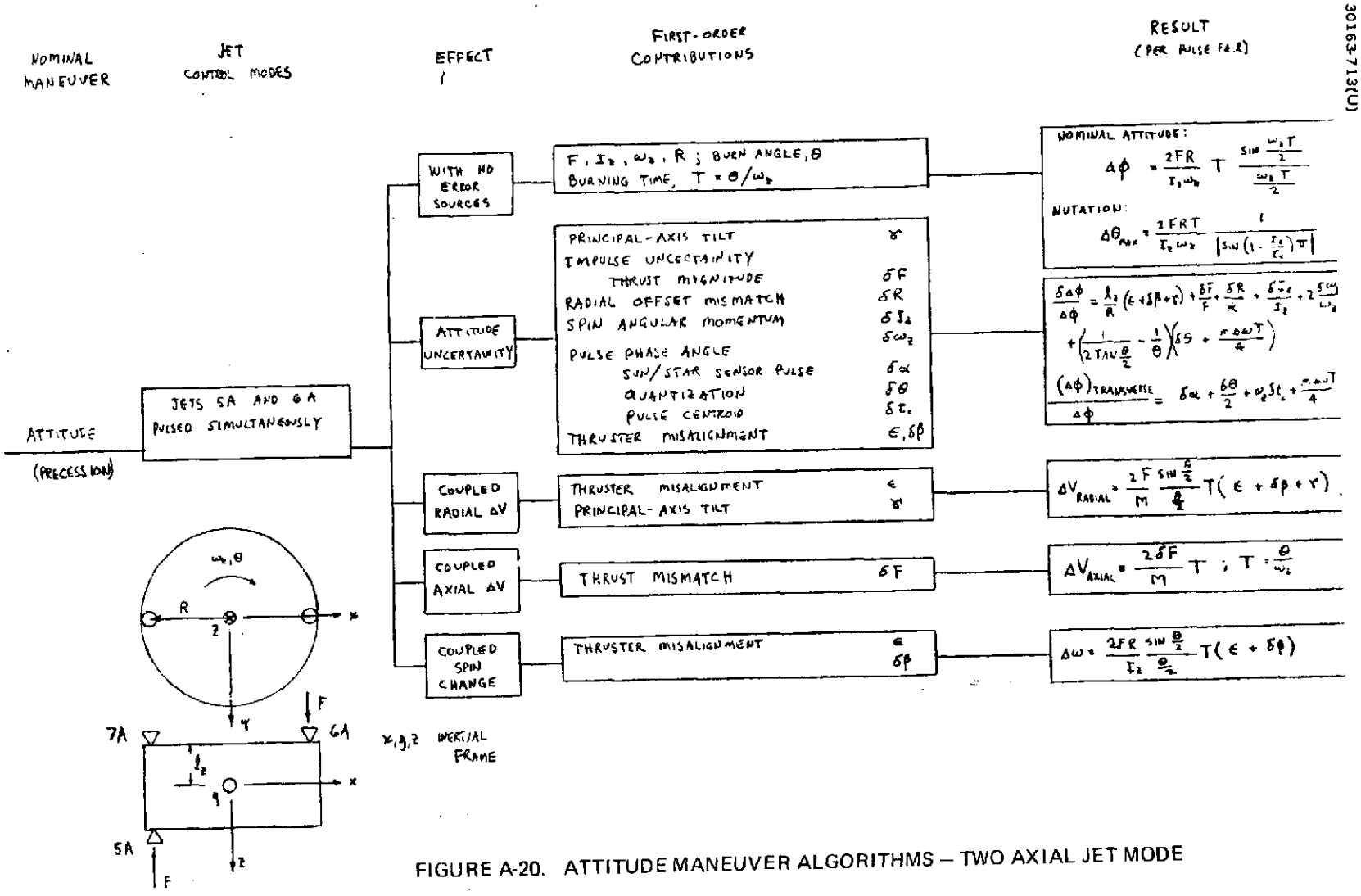

FIGURE A-20. ATTITUDE MANEUVER ALGORITHMS – TWO AXIAL JET MODE

30163-713(U)

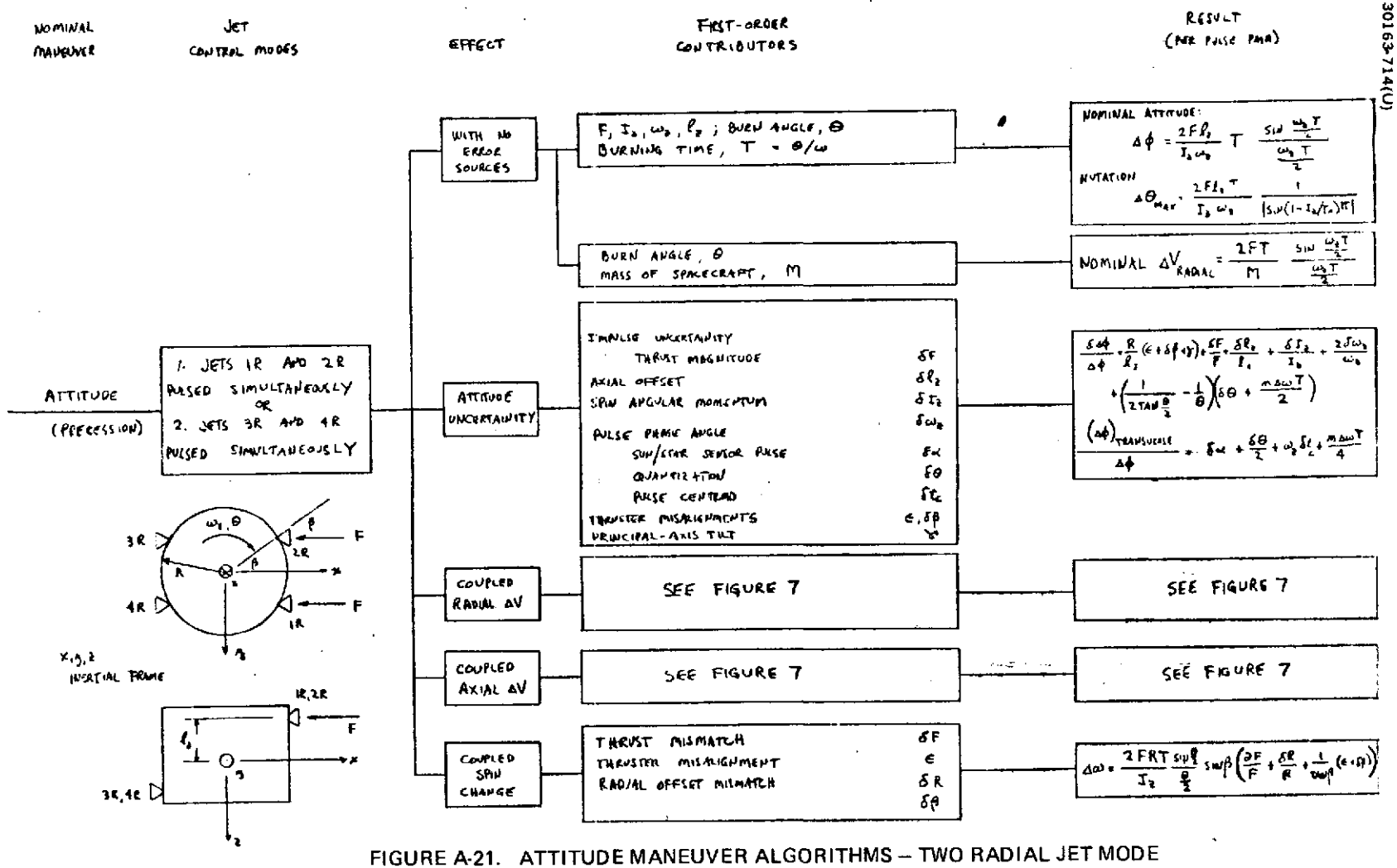

FIGURE A-21. ATTITUDE MANEUVER ALGORITHMS – TWO RADIAL JET MODE

APPENDIX B. MODES AND ANALYSIS FOR HIGH GAIN ANTENNA DESPIN CONTROL

CONTROL LOOP ANALYSIS MODEL

The analytical model used in the analysis of the despin control system (DCS) is shown in Figure B-1. In the tracking mode of operation, inertial platform error is sampled and held 16 times per rotor spin revolution, while the first order approximation to platform rate is sampled and held 128 or 2^7 times per rotor spin revolution. The line of sight (LOS) error is processed through a proportional and an integral path to obtain a control position torque to drive the bearing and power transfer assembly (BAPTA) motor. The commanded torque is summed with a ground commandable bias and a rate loop torque to form a net commanded torque signal. The net torque (friction plus motor) controls the platform dynamics in azimuth to maintain the despun antenna pointing at the Earth. Thus, in the steady state condition, the net commanded torque will be equal and opposite to bearing friction torque.

The first order approximation to platform rate is determined by measuring the angle subtended by two consecutive shaft encoder pulses. By comparing this angular measurement to a zero platform rate angle measurement or $360/2^7$; 3.045 deg, the first-back-difference of position is obtained. Any error between the two measurements indicates a change in platform position over a fixed time, or a non-zero platform rate. The derived platform rate is used to provide the required system damping for both tracking and acquisition modes of operation.

As mentioned previously, the tracking mode position sample rate of 16 times per spin period results in a stable null in any one of the 16 sectors. To assure automatic acquisition of the appropriate sector, the 16 times per spin period sample rate is disabled during acquisition mode control. A once per spin period sample of the inertial platform error is determined and a pulse of torque is applied through a proportional and integral path to drive the BAPTA motor. This command pulse of torque is once again summed with a ground commandable bias and a rate loop torque to form a net command torque. This mode of control will continue until the LOS error is less than one half a sector, at which time the tracking loop control is enabled and final LOS error is nulled. Simulated performance detailed in the latter portions of this text illustrate the acquisition technique.

The analytical model has been implemented on an analog computer with single axis vehicle dynamics. The simulation has been utilized

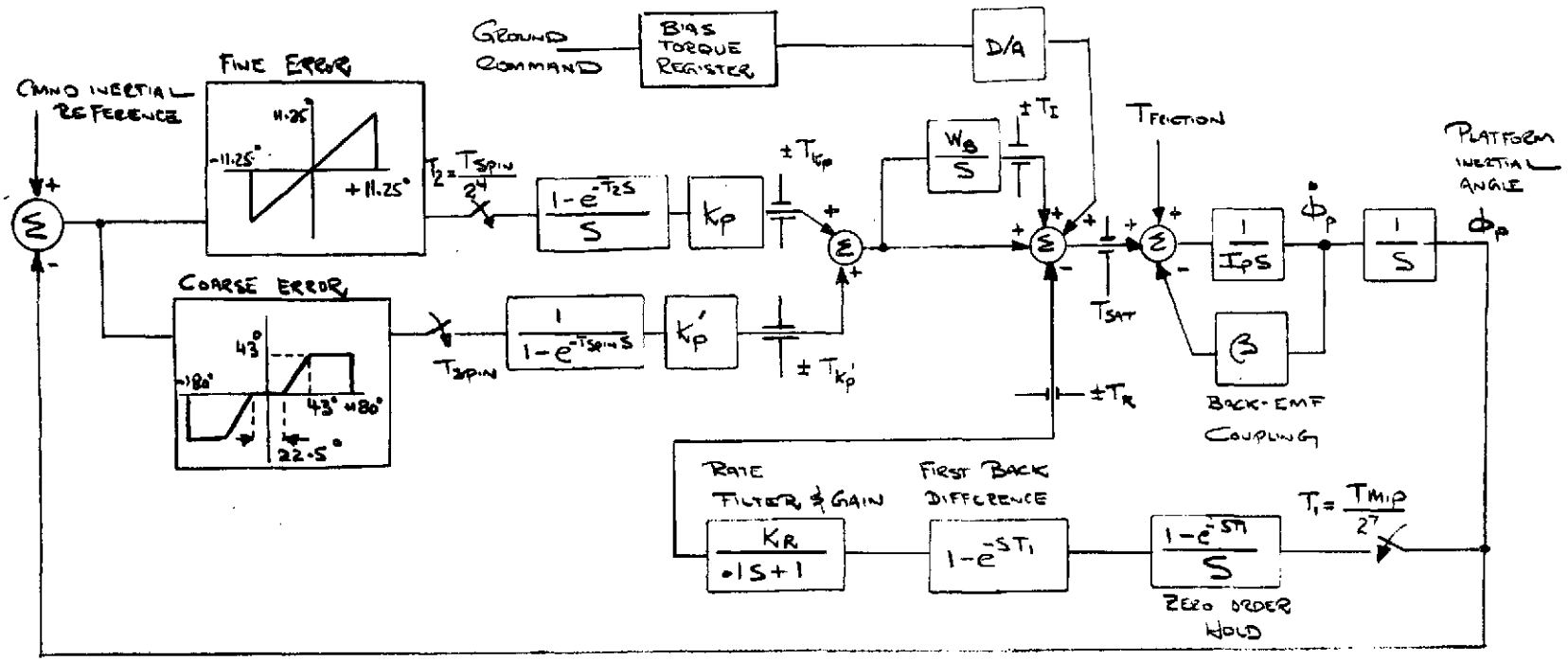

NOMINAL S/C INERTIAS

I_P (PLATFORM) = .08 SLUG-FT²

I_R (ROLL) = 80. SLUG-FT²

I_T (TRANSVERSE) = 49 SLUG-FT²

I_{xy} (PLATFORM TRANSVERSE) ≤ .2 SLUG-FT²

CONTROL LOOP GAINS

W_B = 0.1 SEC⁻¹

K_p = .5 FT-LB/RAD

K_p' = .2 FT-LB/RAD

K_R = 3.0 FT-LB/RAD/SAMPLE OR 6.0 FT-LB/RAD/SAMPLE

$\beta = \frac{K_T K_V}{R_m}$ = .025 FT-LB/RAD/SEC

CONTROL LIMITS

T_{SAT} = ± .5 FT-LBS

T_R = ± .15 FT-LBS

T_I = ± .15 FT-LBS

T_{K_D} = ± .10 FT-LBS

T_{K_P}' = ± .15 FT-LBS

FIGURE B-1. DESPIN CONTROL SYSTEM MODEL

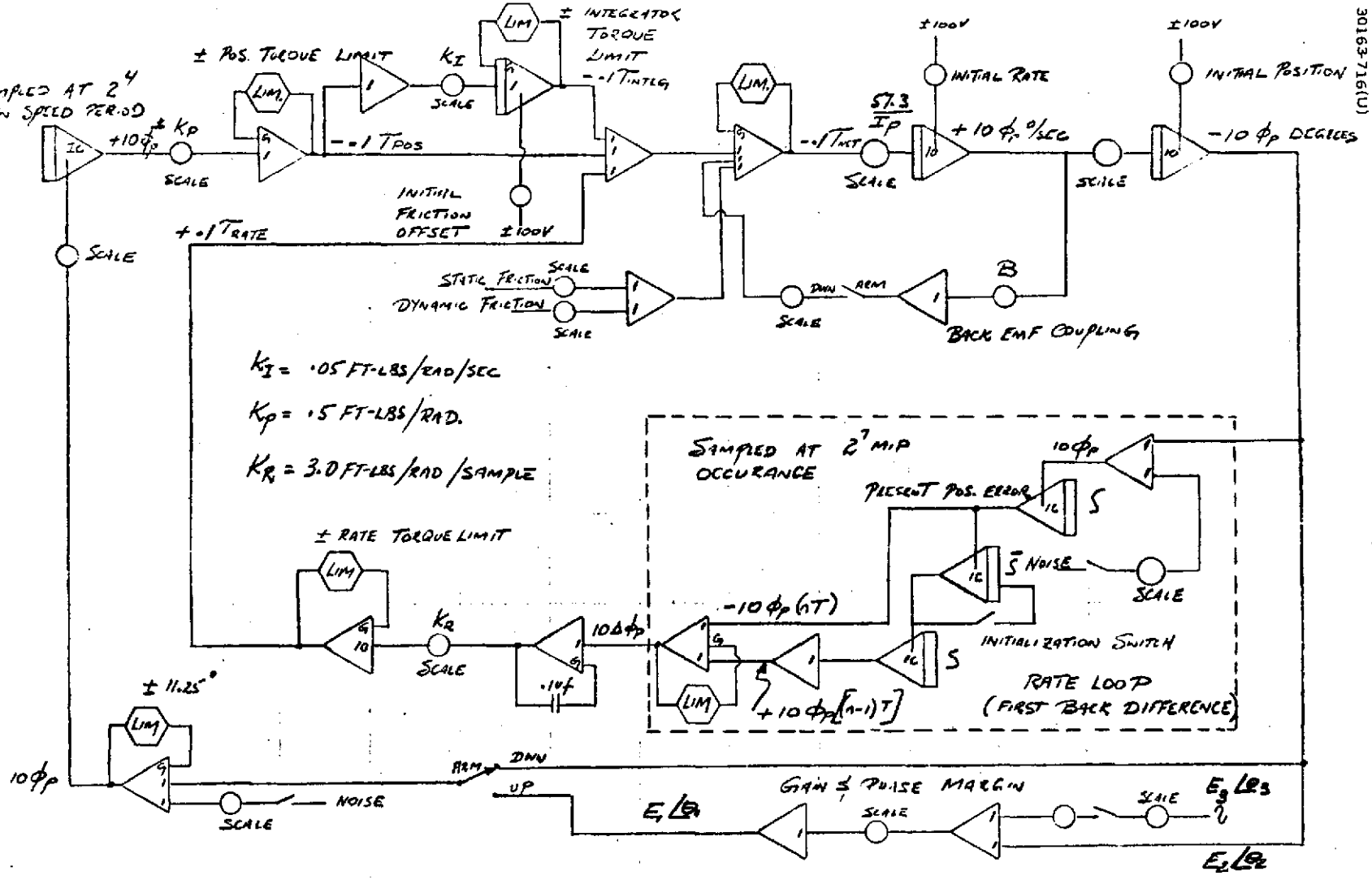

30163-716(U)

FIGURE B-2. SIMULATION MODEL IMPLEMENTATION - SMALL ANGLE SIMULATION (TRACKING MODE)

extensively to evaluate the effects of system nonlinearities, to verify performance predictions based on frequency domain analyses, and to generate performance prediction data. Figure B-2 shows the implementation of the simulation model for the tracking mode, while Figure B-3 shows the implementation of the simulation for the acquisition mode.

Using frequency-domain analyses, for the configuration proposed, the system gains were optimized to provide the desired gain and phase margins over the operating range of spin speeds. The frequency analyses were performed from the analog simulation using the technique illustrated in Figure B-2. The control system is operated as a closed-loop with a sine-wave forcing function input given by $E_3 \angle \theta_3$. By observing the instantaneous amplitude and phase shift of signal $E_1 \angle \theta_1$ and $E_2 \angle \theta_2$, the open loop transfer function $G^*_{OL}(S)$ can be determined. The principal results of this technique are given in Figures B-4 and B-5. These results have been verified by a digital simulation using sample data control theory.

Friction Torque Sensitivity

Figures B-6 and B-7 are plots of the transmission factor from bearing friction to platform error as a function of frequency for the selected control loop configuration. Figure B-6 shows that the most sensitive region for operation at 5 rpm occurs for friction variations on the order of 0.05 to 0.3 Hz.

Maximum system sensitivity at 5 rpm is 2.2 rad/ft-lb. Figure B-7 shows that the most sensitive region for operations at 30 rpm occurs for friction variations on the order of 0.4 to 0.8 Hz. Maximum system sensitivity at 30 rpm is 1.53 rad/ft-lb.

For performance evaluation, a nominal friction value of 0.075 ft-lb and a maximum peak to peak torque variation of 0.014 ft-lb has been adopted as a standard. These assumed short term friction torque estimates are based on Intelsat IV BAPTA design data. Therefore, worst case steady state platform motion due to short term torque ripple in the most sensitive frequency range will be ±0.9 deg at 5 rpm and 0.62 deg at 30 rpm. For lower frequencies, the integrator effectively nulls pointing error due to friction variations, while at higher frequency the torque variations are outside the bandpass of the control system.

Sensor Noise Sensitivity

The principal disturbance to platform pointing is the random error on sun or star reference pulses, PLL limit cycle effects, MIP pulse jitter and shaft encoder pulse jitter (rate loop).

Figures B-8 and B-9 show the closed loop transfer function from sensor noise to platform pointing as a function of frequency for the proposed design at 5 rpm and 30 rpm, respectively. Figures B-10 and B-11 shows

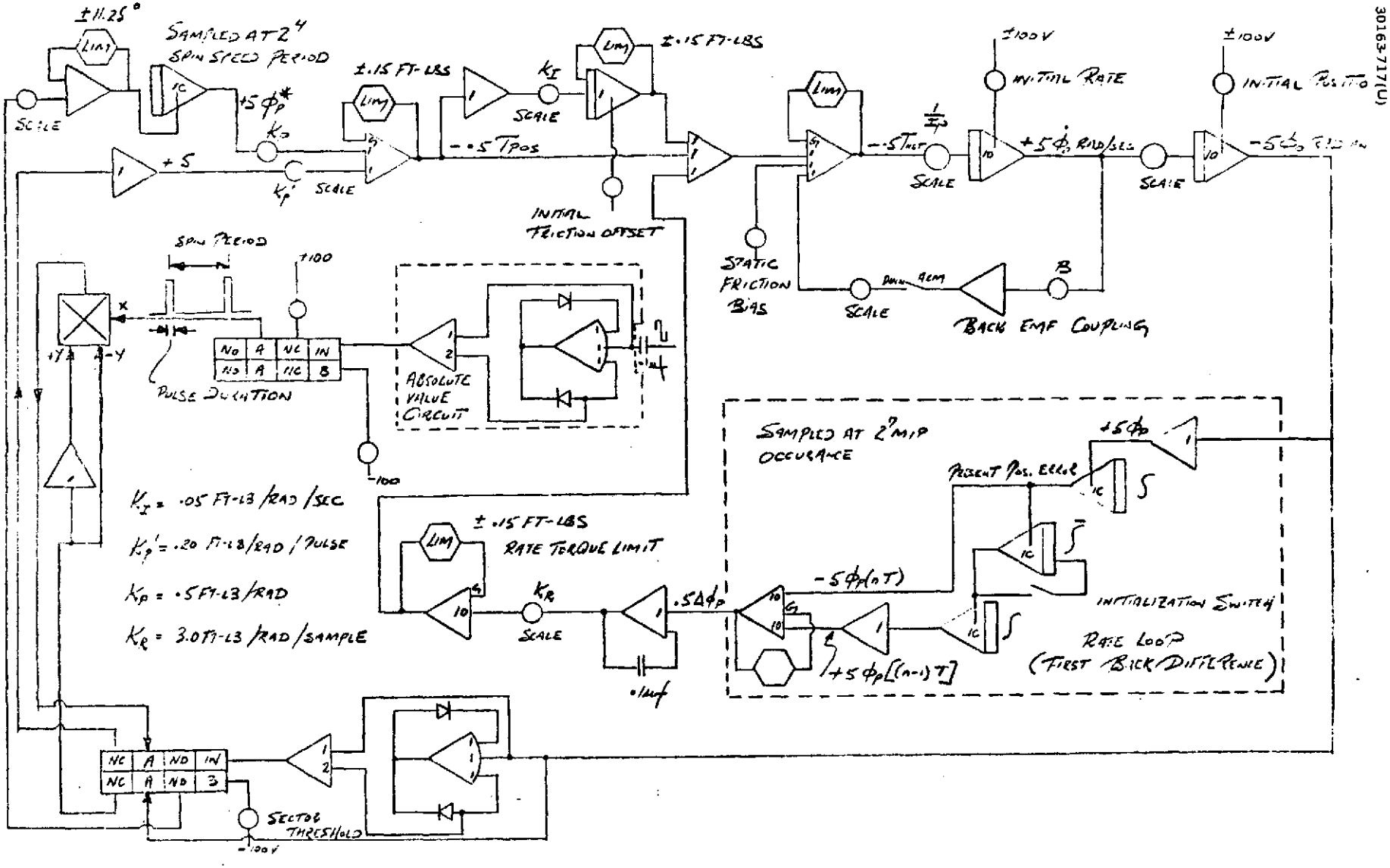

FIGURE B-3. SIMULATION MODEL IMPLEMENTATION - LARGE ANGLE SIMULATION (ACQUISITION MODE)

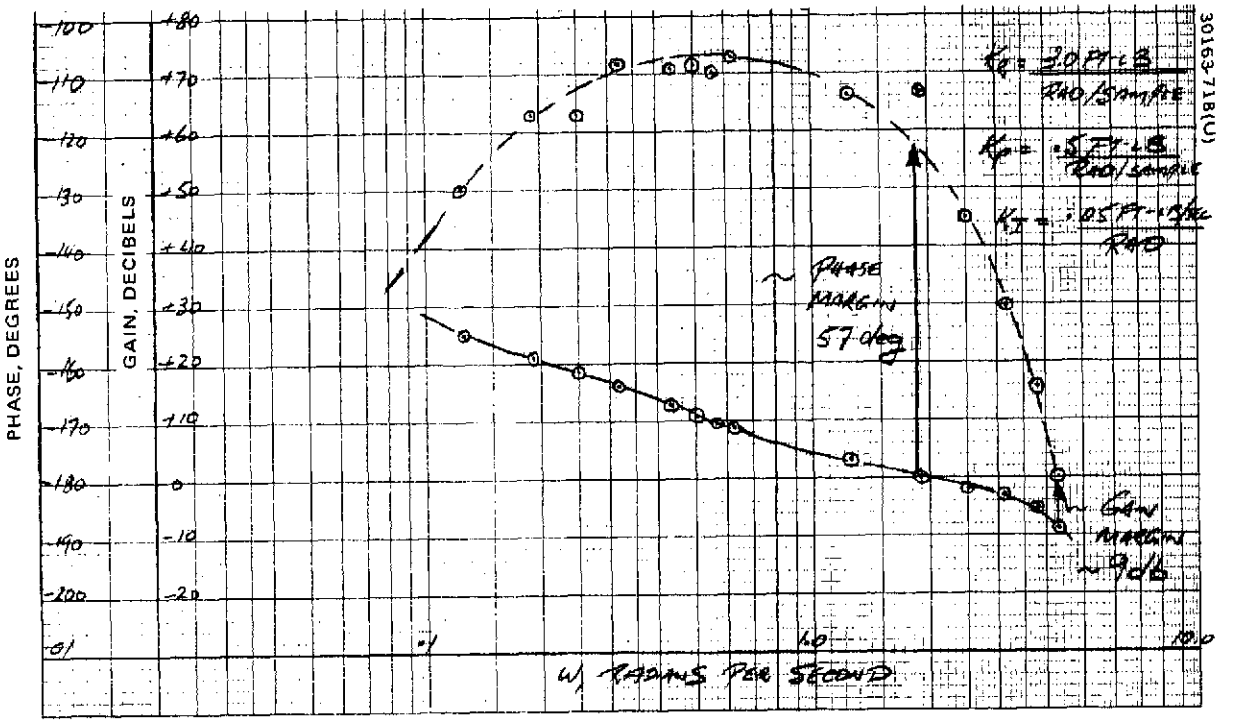

FIGURE B-4. OPEN LOOP FREQUENCY RESPONSE (5 RPM) OBTAINED FROM ANALOG SIMULATION

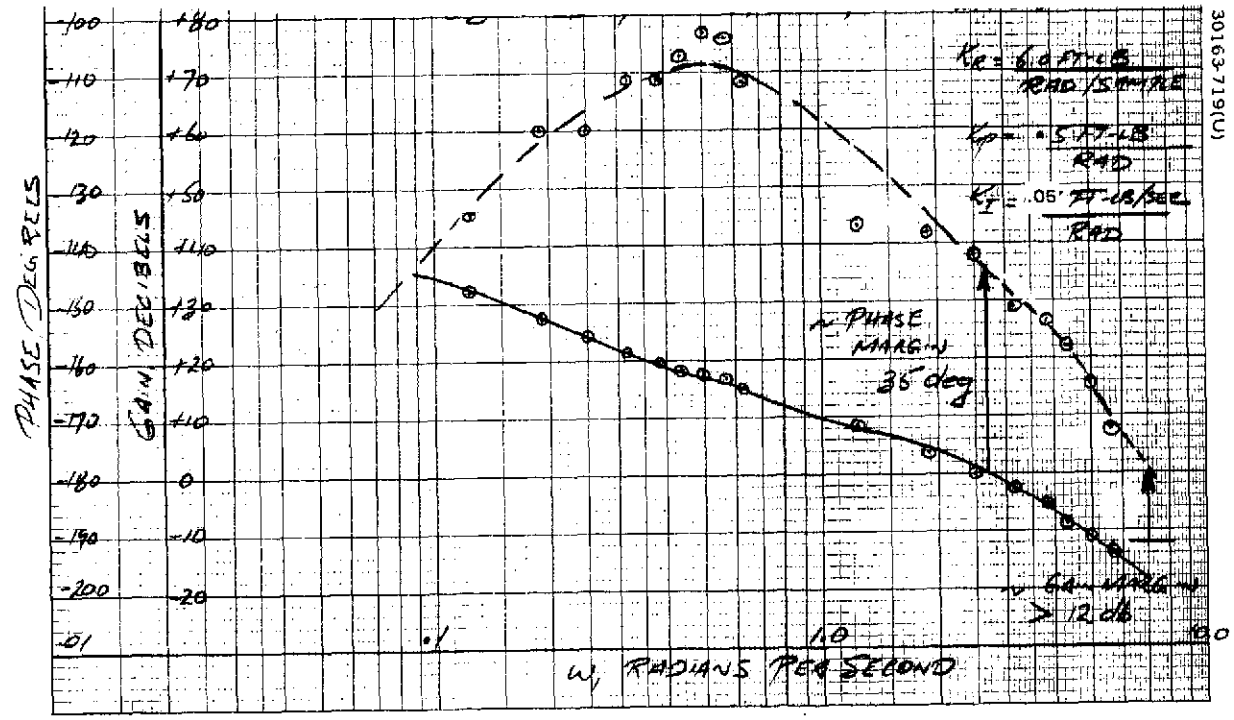

FIGURE B-5. OPEN LOOP FREQUENCY RESPONSE (30 RPM) OBTAINED FROM ANALOG SIMULATION

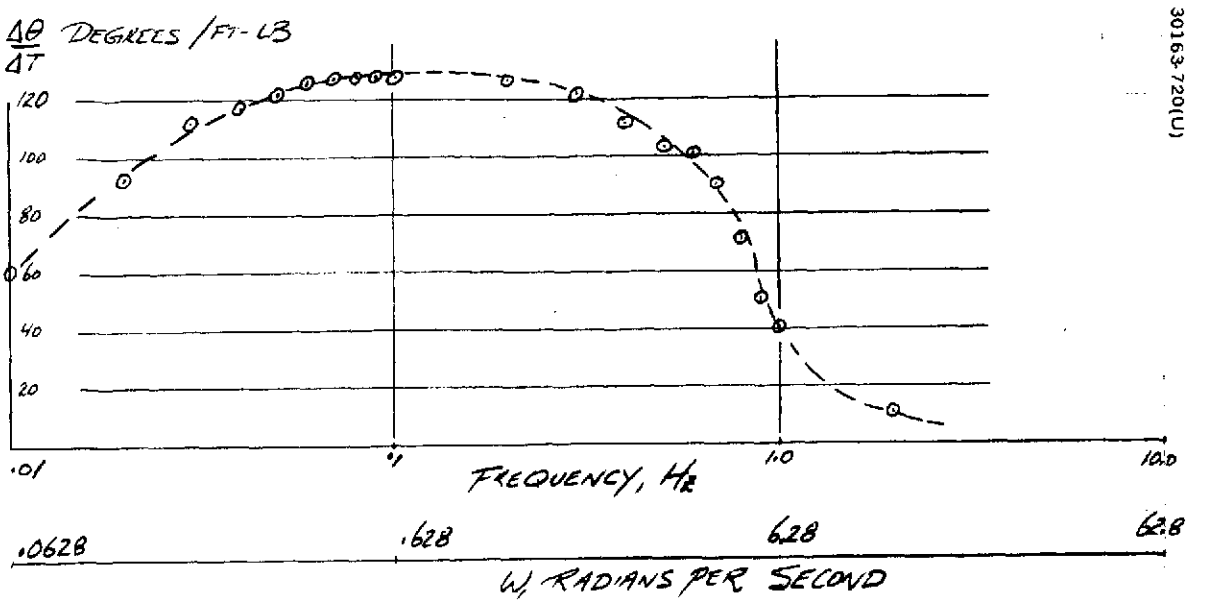

FIGURE B-6. TRACKING LOOP RESPONSE TO BEARING FRICTION TORQUE VARIATIONS AT 5 RPM

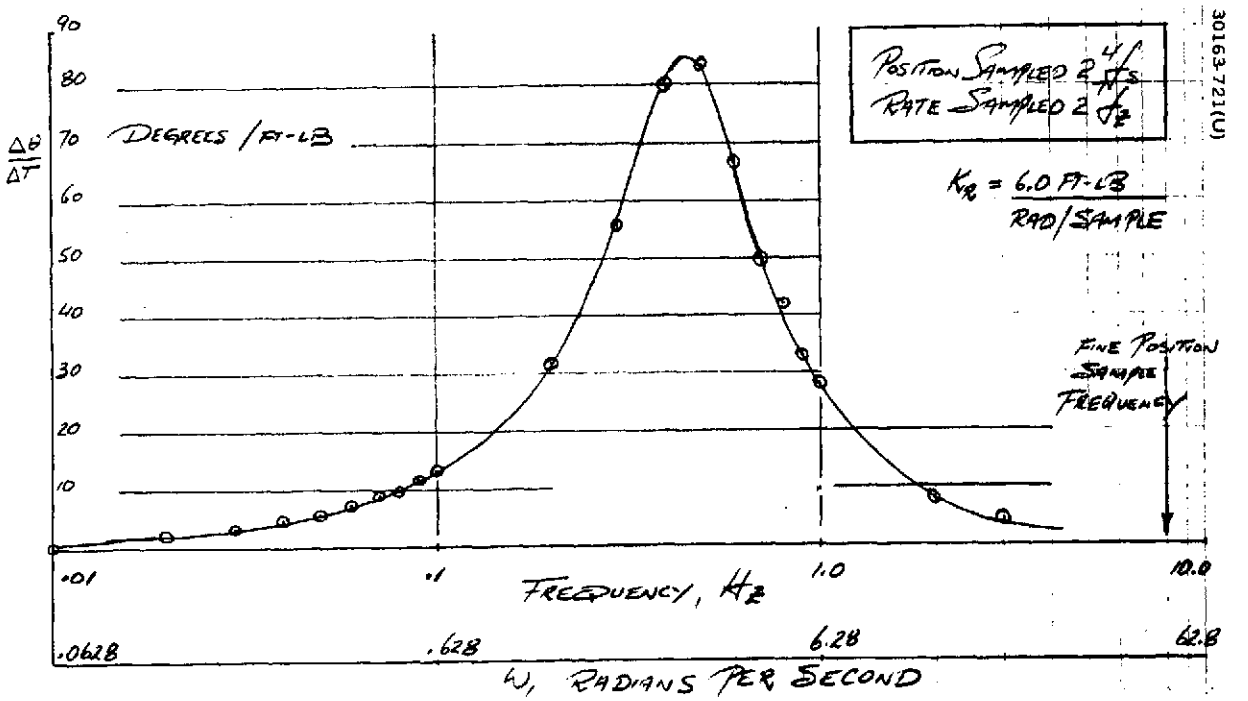

FIGURE B-7. TRACKING LOOP RESPONSE TO BEARING FRICTION TORQUE VARIATIONS AT 30 RPM

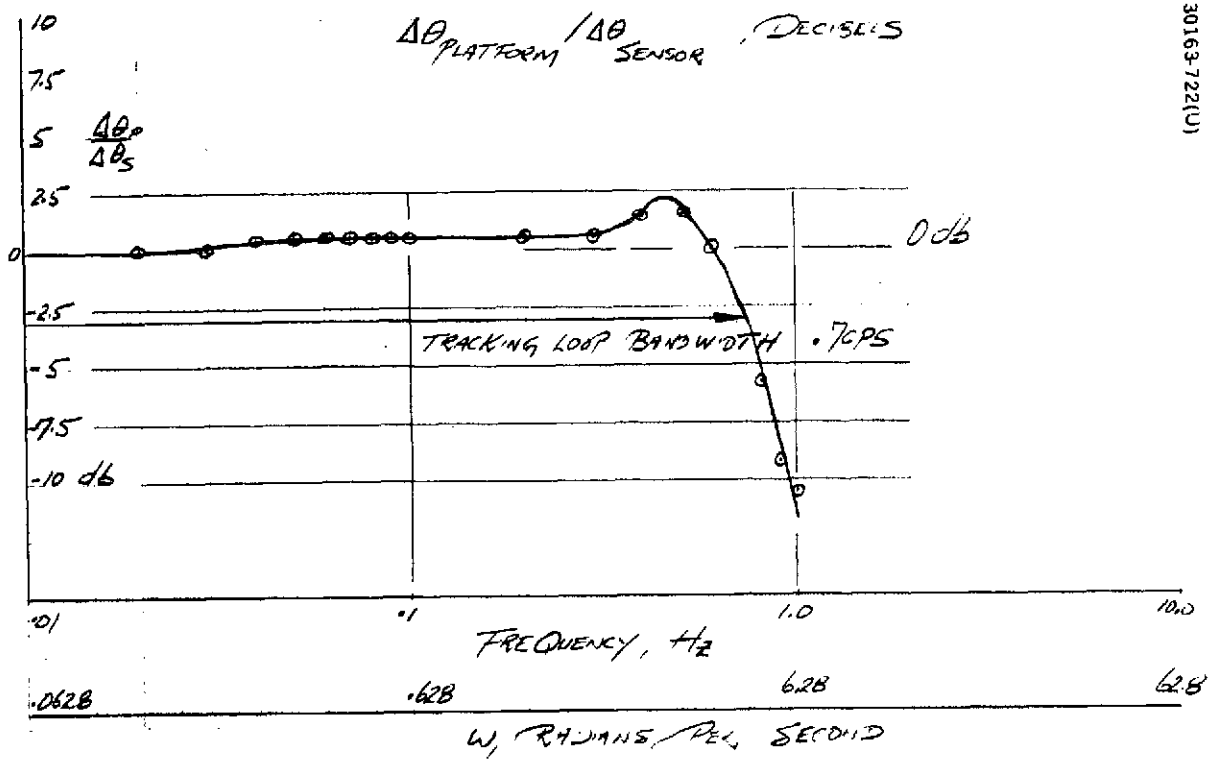

FIGURE B-8. TRACKING LOOP RESPONSE – CLOSED LOOP FREQUENCY RESPONSE AT 5 RPM

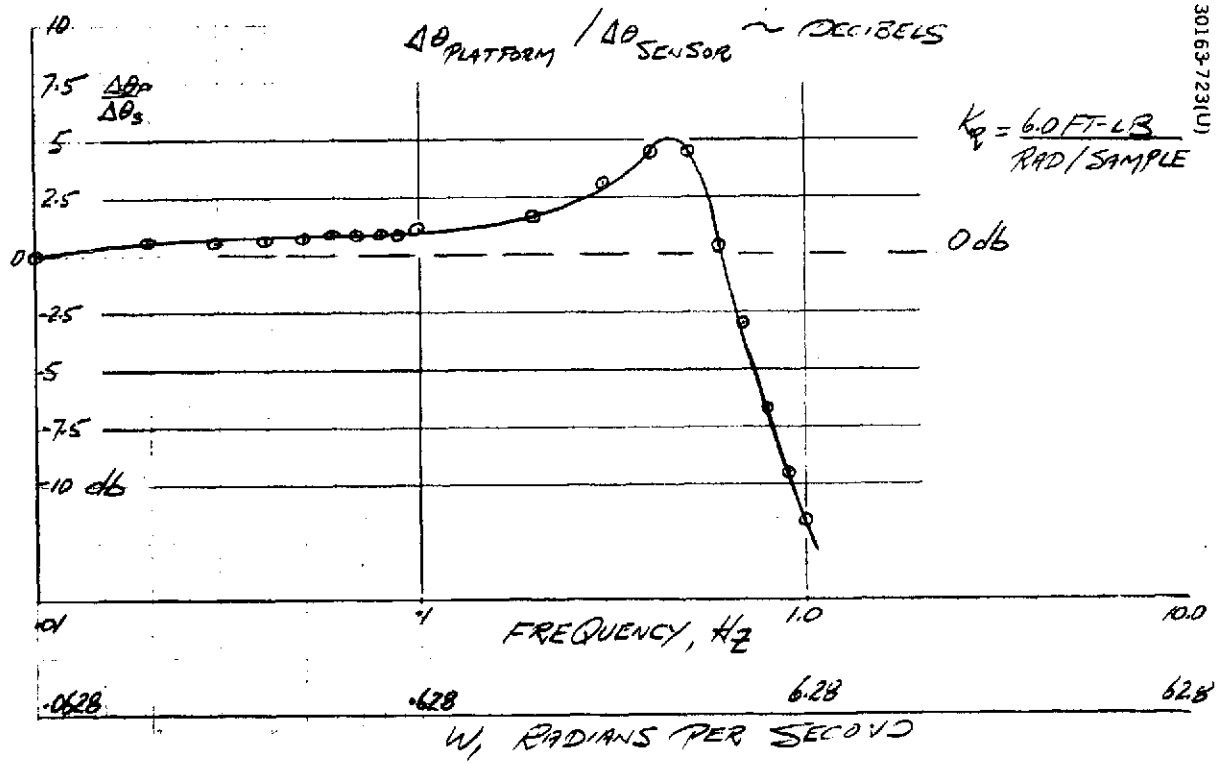

FIGURE B-9. TRACKING LOOP RESPONSE – CLOSED LOOP FREQUENCY RESPONSE AT 30 RPM

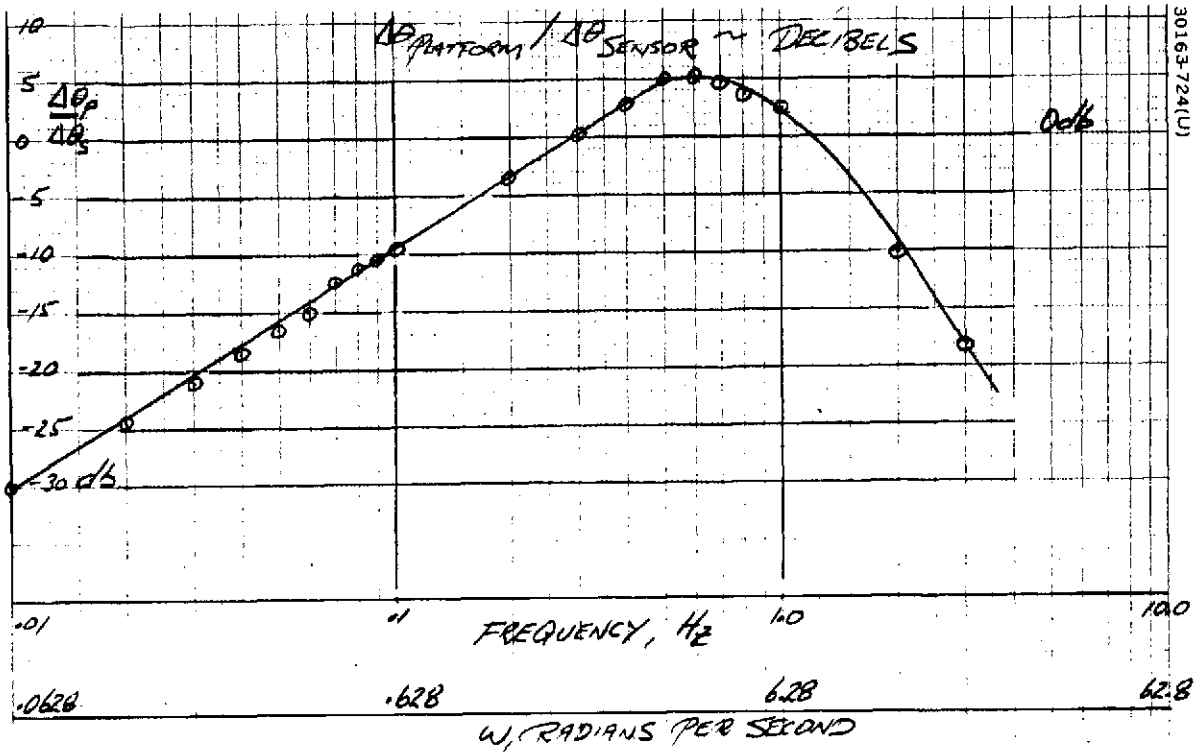

FIGURE B-10. SHAFT ENCODER NOISE RESPONSE – CLOSED LOOP FREQUENCY RESPONSE AT 5 RPM

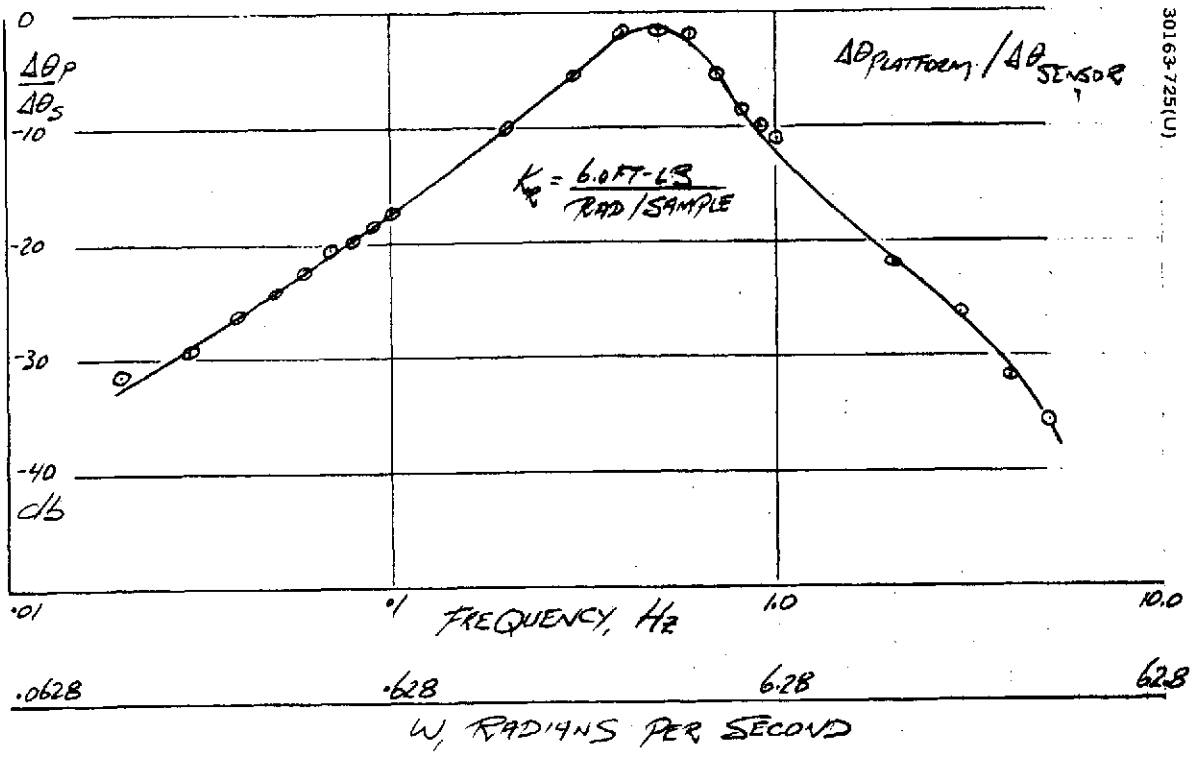

FIGURE B-11. SHAFT ENCODER NOISE RESPONSE – CLOSED LOOP FREQUENCY RESPONSE AT 30 RPM

the closed loop transfer function from shaft encoder noise (rate loop) to platform pointing as a function of frequency for 5 rpm and 30 rpm system operation. Since the MIP pulse jitter is an order of magnitude smaller than the sensor noise, it can be neglected. Similarly the frequency and amplitude of the shaft encoder MIP pulse jitter results in a negligible platform error. Therefore, the net 3σ platform pointing inaccuracy due to pulse jitter in the despin control system is associated with sensor noise and PLL limit cycle effects. The total random error associated with short term azimuth pointing error is an rss of sensor noise, PLL jitter and platform motion due to friction torque variations. This information is summarized in Table B-1.

Kinematic Coupling

If the despin reference is not orthogonal to the spin axis, nutation motion of the spacecraft spin axis will cause a phase error in the azimuth reference pulse from the star. The principal result gives rise to an apparent error in measuring rotor spin phase given by

$$\Delta \phi_R = \tan \gamma \left[\psi \sin \beta - \theta \cos \beta \right]$$

where

$\Delta \phi_R$ = error in measuring phase due to kinematic coupling

γ = reference source elevation relative to spin axis normal

β = inertial pointing angle

ψ, θ = nutation angles

Assuming a maximum source elevation relative to spin axis normal of 51.5 deg and sin β or cos β = 1, the maximum rotor phase error shall be equal to 1.3 times the amplitude of the nutation. Based upon a worst case steady state residual nutation of 0.2 deg, the total azimuth pointing inaccuracy shall then be 1.22 deg for 5 rpm operation and 0.96 deg for 30 rpm operation using the star despin reference.

Simulated Performance

In order to investigate the overall DCS performance and acquisition in particular, the analog simulation has been used to generate representative performance data. The analog simulation has the advantage of giving instantaneous, real-time system response with ease in variation of pertinent control loop parameters. The elements included in this simulation are as listed below and graphically depicted in Figures B-2 and B-3.

TABLE B-1. SHORT TERM AZIMUTH POINTING STABILITY

Random Error Sources	Azimuth Pointing Error (3σ)	
	5 rpm	30 rpm
Sensor Noise (Star Sensor)	0.3°	0.3°
PLL Jitter	0.1°	0.1°
Friction Torque Variations	0.9°	0.62°
Total Random Error (rss)	0.96	0.7

1) Single axis dynamics, BAPTA dynamics

2) Nonlinear error detector (fine position)

3) Coarse and fine position control logic selection

4) Multirate sampling

   a) Rate

   b) Fine position control

   c) Coarse position control

5) DCE shaping

6) Coarse position pulse control mechanization

7) Bearing friction

8) Sensor noise

Acquisition for Azimuth Pointing

Figure B-12 shows typical time histories of the system performance at 5 rpm using the coarse positioning control only. The coarse positioning loop gain of 0.20 ft-lb/rad/pulse is used to show acquisition control system speed of response and stability characteristics. It is noteworthy to point out that the concept of pulse torque was formulated to achieve automatic sector acquisition for low spin speed and small platform inertia. The pulse torque method allows a high position loop gain control for a fraction of the total spin period, while for the remainder of the spin period system stability is provided by the rate loop.

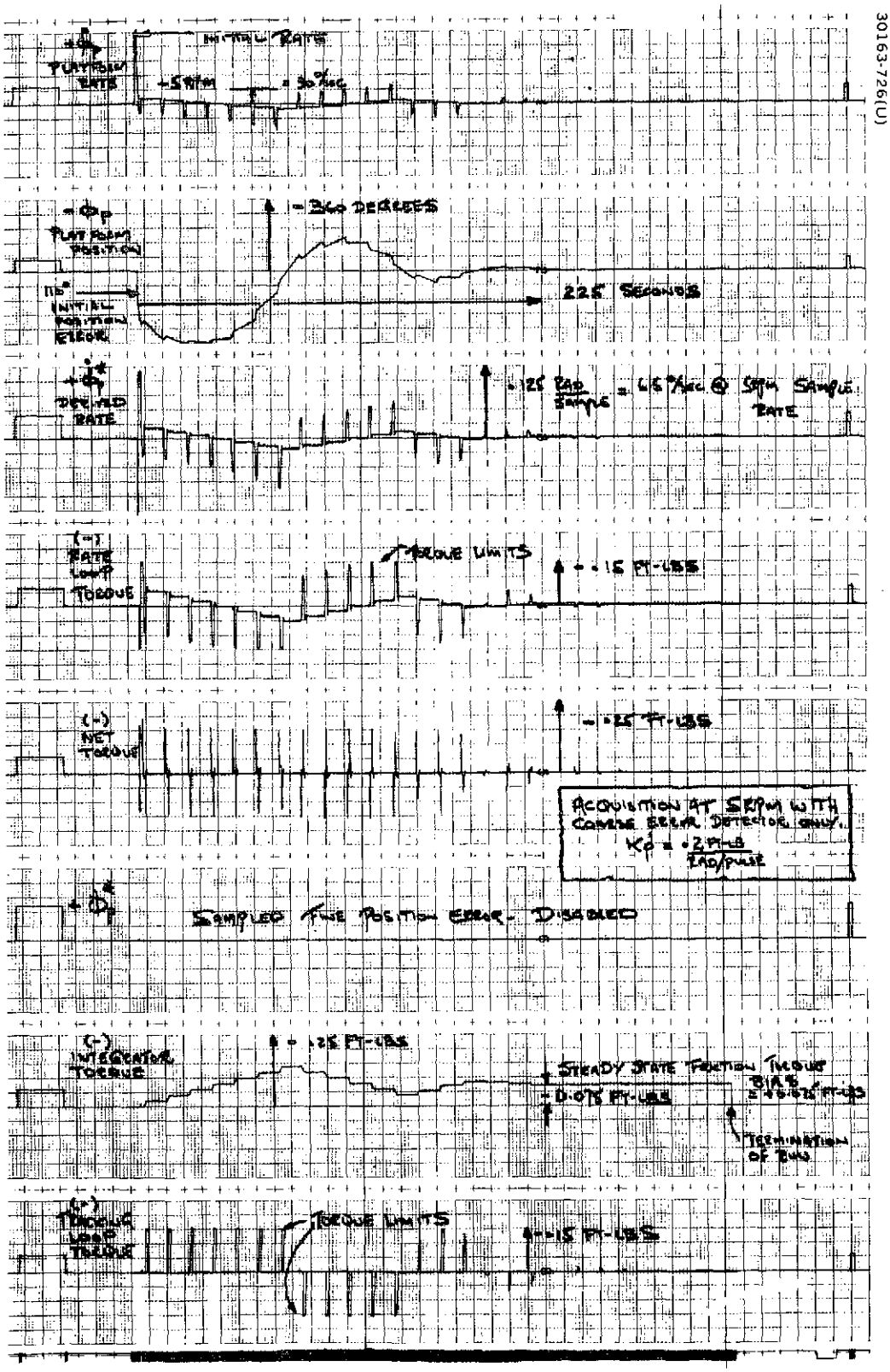

FIGURE B-12. ACQUISITION AT 5 RPM WITH COARSE ERROR DETECTOR ONLY

Each acquisition sequence begins with the despin control electronics in the OFF position. Thus, the platform is spunup in relationship to the rotor (defined as a positive rate) by bearing friction and back EMF. In steady state, with the DCE OFF for a long duration the platform rate and rotor rate will be identical. Notice though, that at the beginning of these runs a much larger platform rate (25 rpm) is introduced. The large platform rate is introduced to illustrate the system dynamics and to provide additional rationale for the pulse torque scheme. Once the initial platform rate bias is nulled, the instantaneous platform rate (with the position loop open) is defined by

$$\dot{\phi}_P = \frac{\tau_F - \tau_I}{K_R}$$

where

τ_F = friction torque bias

τ_I = integrated friction torque

K_R = rate gain

The system then continues to null both position and rate errors for acquisition of the proper sector. Again, it is germane to note that the analog simulation does not differentiate between ±360 and ±0 deg. However, in the actual spacecraft despin control electronics logic will be provided to prevent an idiot mode of operation.

Acquisition with both coarse and fine position control is shown in Figure B-13 for 5 rpm operation and Figure B-14 for 25 rpm operation. Note that during the acquisition cycle, the fine position control is disabled until the coarse control brings the platform to with ±11.25 deg (or 1/2 of a sector) of the desired position.

Steady State Pointing

The principal disturbance for steady state pointing is bearing friction and motor torque variations. Sensor noise, PPL limit cycle, and SAE/MIP jitter have a second-order disturbing effect. Random type errors characteristic of sensor noise are simulated by a white noise input. Frequency depended errors characteristic of bearing and motor torque variations are simulated by a peak-to-peak variation at a once per spin speed frequency. Figure B-15 shows the system response at 5 rpm with random errors characterized by white noise and bearing friction variations characterized by a frequency dependent component. Sensor noise and PPL limit cycle effects are simulated by 0.3 deg amplitude, SAE/MIP jitter by 0.15 deg amplitude and bearing friction by 0.014 ft-lb peak-to-peak at 0.0835 cps. The worst case pointing error is generally below 0.6 deg with infrequent peaks as high as 0.75 deg. This level is well below the allocated amount of 1.0 deg (3σ).

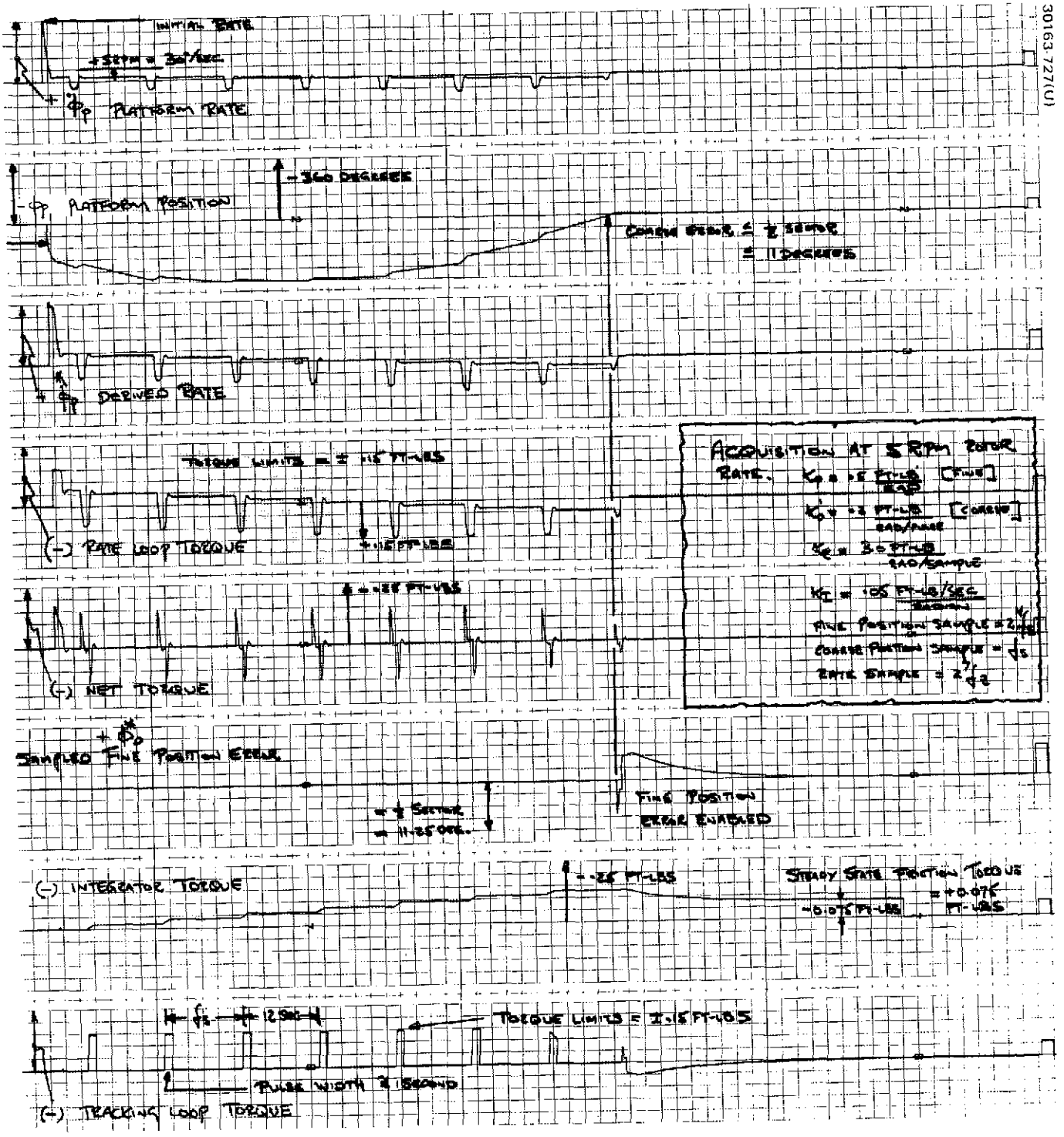

FIGURE B-13. ACQUISITION AT 5 RPM ROTOR RATE

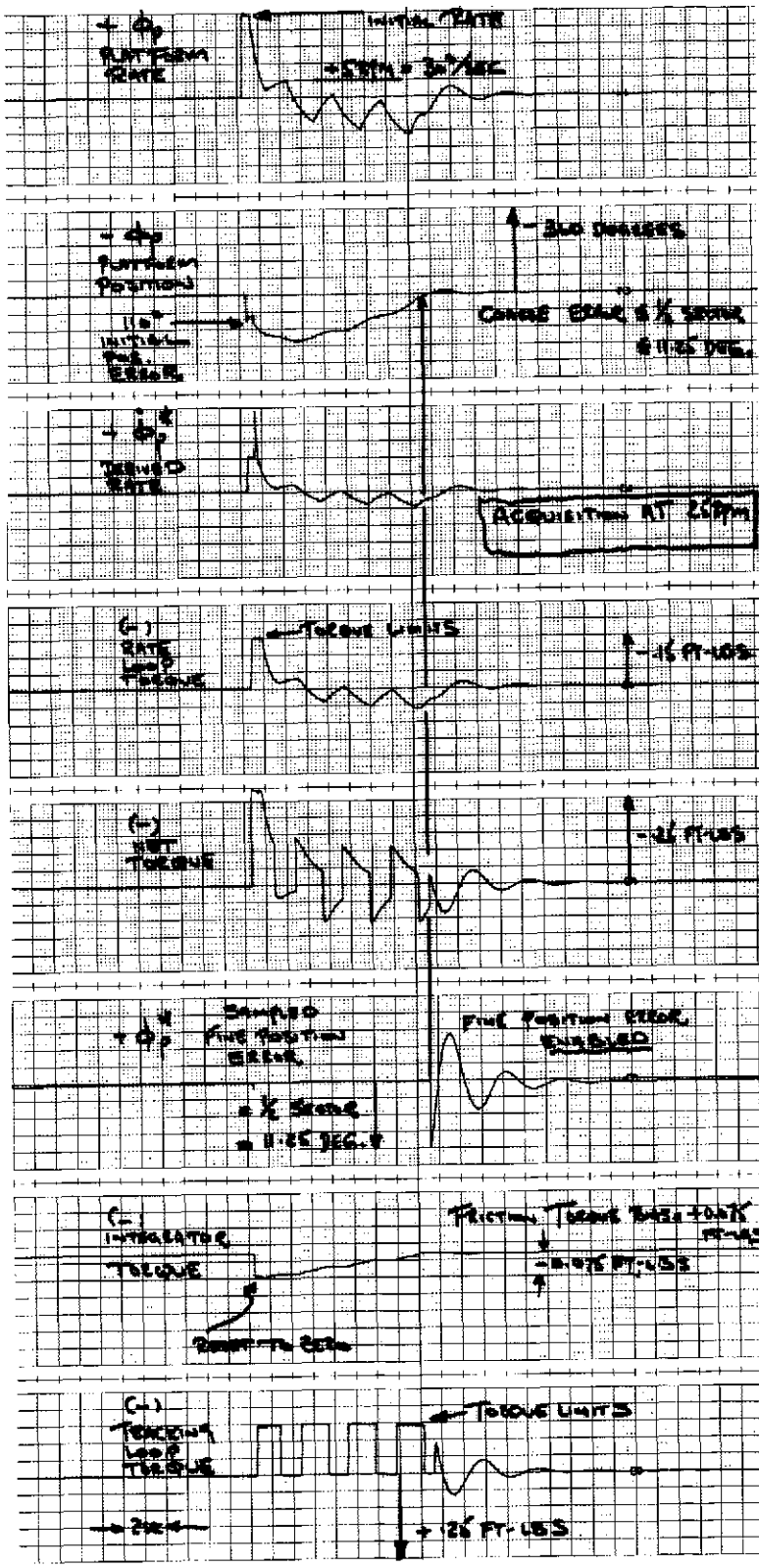

FIGURE B-14. ACQUISITION AT 25 RPM ROTOR RATE

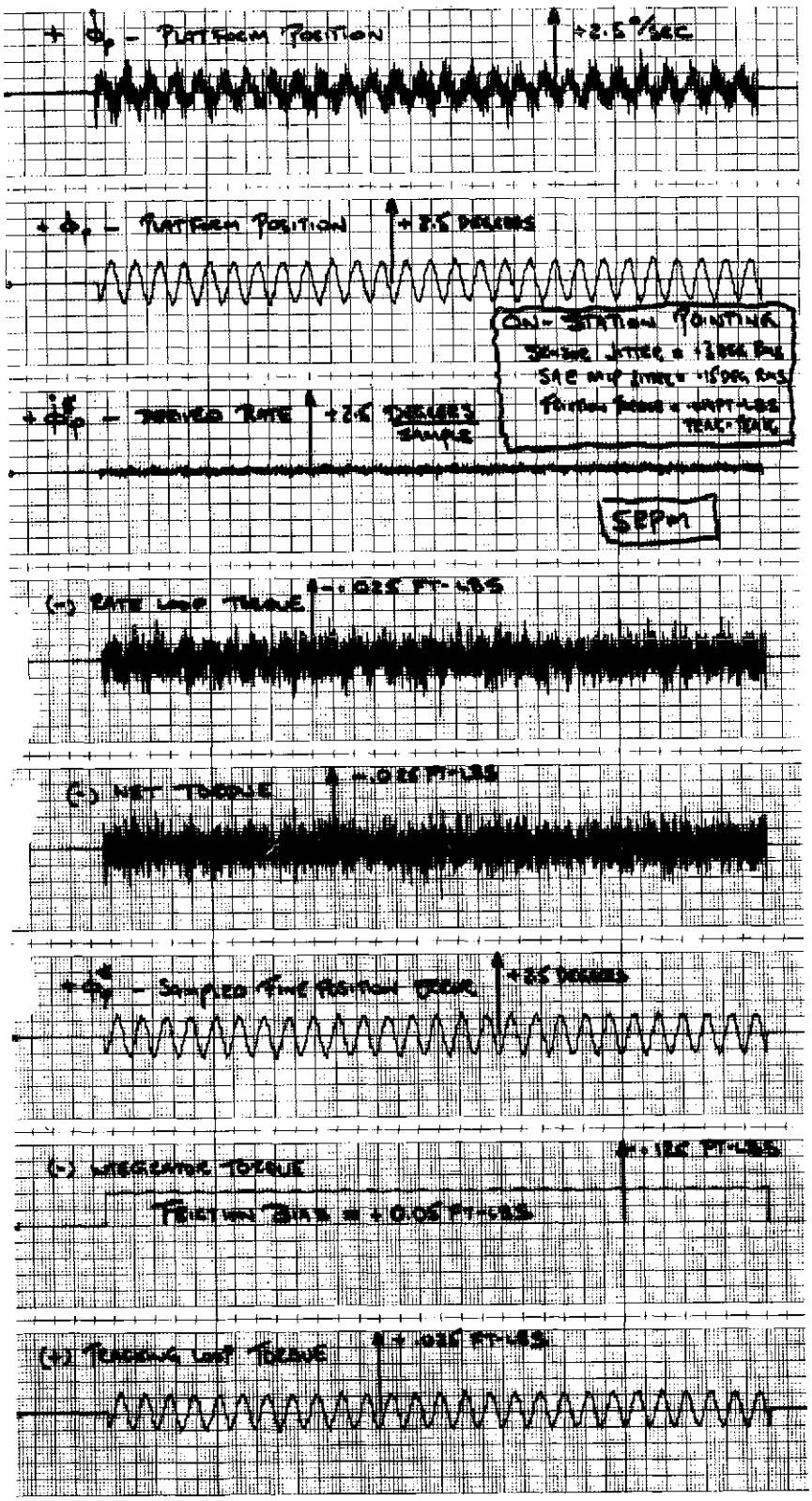

FIGURE B-15. ON STATION POINTING

Despin Control System Tradeoffs

The principal tradeoffs considered in deriving the system design were the BAPTA design, the type of control electronics, and the control law mechanization. A summary of the tradeoffs considered is presented in Table B-2. The detail tradeoff rationale for the BAPTA and control electronics is presented under the appropriate hardware section (Appendix C). The control law mechanization tradeoff is presented herein.

There are a number of considerations in selecting system gains or tracking loop shaping transfer functions. These include: 1) adequate stability margin for azimuth pointing over the entire range of spin speed, 2) reduction of pointing errors and motor torque ripple, due to sensor noise and frequency variant friction torque variations, to an acceptable level, and 3) simplicity of design.

Both single loop (position only) and dual loop (position and rate) were considered for normal tracking operations. A quasi-continuous (high sample rate) rate loop eliminates a lower gain crossover (thus improving system stability margins) and provides additional damping of nutation via platform cross products of inertia. Additionally, the position loop dc gain and integrator gain are normally chosen as high as possible to minimize loop sensitivity to friction torque variations, while avoiding excessive gain to sensor noise. The need to choose a high position loop gain for the low spin speed and platform inertia system necessitated the use of the dual loop control. However, the implementation of the quasi-continuous rate loop having a suitable stable (noise free) output does require increased complexity in both mechanical and electronic design.

Integral or nonintegral shaping can be used in the position loop. In principle, integral shaping is somewhat more complex and yields smaller gain margins, although the resultant sensitivity to friction variations is very much less. The electronic complexity of integral versus nonintegral is approximately the same using the all analog shaping design approach. By implementing the integrator along with one of the lead terms as a proportional-plus-integrator stage, the potential problem of integrator windup is circumvented. The computed stability margins are adequate with the integral approach. In the configuration proposed, therefore, the integral shaping provides the desired insensitivity to friction variations without unduly compromising the remaining aspects of system performance.

Automatic versus manual acquisition of proper sector for azimuth pointing was considered. In principle, for near earth orbits a manual acquisition is desirable because of the inherent reduction in spacecraft electronic complexity, weight, and cost. However, for deep-space probes, where the communication time period becomes unduly long, the automatic acquisition becomes a necessity. Therefore, the proposed design provides automatic sector acquisition by means of the coarse and fine position control scheme.

TABLE B-2. DESPIN CONTROL SYSTEM TRADEOFF SUMMARY

Tradeoff	Considerations	Selected Approach and Rationale
Brush motor versus brushless motor	Brush-type requires fewer electronics parts but involves potential wearout mode due to brush contact. Brushless type has no contact, but requires two power amplifiers and resolver circuitry.	Brush type selected based on 1.5 lb weight saving; reduced power consumption, approximate cost saving of $30K per spacecraft and prior program experience. Infinite brush life capability for a 2 year mission.
Shaft angle encoder, optical, magnetic or mechanical	Magnetic encoders have been used successfully on previous Hughes spacecraft but are considerably heavier than optical encoders. Mechanical encoders are lighter than optical encoders, but have limited space flight history.	Tentatively selected optical encoder because this device is light weight and provides suitable noise free signal at 5 rpm. However, the mechanical encoder seems an attractive alternate that will be studied further.
BAPTA housing and shaft material selection	Titanium and beryllium materials were considered. Titanium for ease of manufacture and lower cost. Beryllium for superior stiffness to weight ratio.	Beryllium selected for superior stiffness to weight ratio. Total BAPTA weight savings of ≈ 3 lbs.
Analog vs. digital implementation	Analog is generally simpler but yields a loop gain inversely proportional to spin speed. Digital offers more design flexibility and is not spin speed sensitive.	Digital was selected to accommodate the wide spin speed requirements.
Automatic vs. manual sector acquisition	Manual sector acquisition is simpler and convenient for near-Earth orbit. Automatic sector acquisition requires more complex mechanization, but is essential for interplanetary mission.	Automatic sector acquisition selected because of the communications delays inherent in interplanetary missions
Voltage driver versus current drive	Voltage drive provides additional rate damping and acts as a speed control. Current drive delivers torque independent of speed.	Voltage drive selected since voltage mode rate damping is significant for the small platform inertia used.
Single loop (position only) versus dual loop (position and rate) for steady state pointing	Single loop requires more complex shaping but is typically less sensitive to sensor noise sources. Dual loop has larger stability margins but requires the addition of a more complex SAE and associated electronics. Dual loop is less sensitive to friction torque fluctuations.	Dual loop configuration chosen to provide the required stability at low spin speed and low platform inertia and to minimize platform jitter due to friction torque fluctuations.
Integral versus proportional compensation	Integral gives much better reduction in friction sensitivity for a low inertial platform but requires additional lead compensation. Integral compensation typically requires a separate command for offset pointing. Proportional shaping is conceptually simpler.	Integral compensation chosen to minimize friction sensitivity. Dual loop provides the needed stability margin. Offset pointing is also provided by summing torque ahead of the integrator stage.

The motor drive circuitry can be configured either as a voltage drive (which is effectively a speed control) or as a current drive (which is effectively a torque control). The voltage drive is an open-loop torque circuit, while current drive utilizes negative feedback to deliver a desired torque independent of speed and armature resistance variations (due to temperature changes). Voltage drive is potentially attractive (in spite of the speed and temperature dependence) when controlling a small inertia because it provides speed control of the load inertia which can be utilized for acquisition and extra damping. This additional damping and the inherent simplicity in the electronic design using the voltage drive mechanization adjudicates its use.

APPENDIX C. ATTITUDE CONTROLS AND MECHANISMS HARDWARE DESCRIPTION

EQUIPMENT CONFIGURATION

The spacecraft equipment configuration for the attitude control function will be comprised of three redundant dual slit sun sensors, one dual slit star sensor (each slit independent and functionally redundant), one redundant ADP electronics unit, one solenoid driver electronics unit (functionally redundant), one redundant DCE unit, one BAPTA, and one nutation damper. The only elements not redundant are the star sensor sun shade and optics, BAPTA bearings and motor magnetics, and the nutation damper. However, due to the high reliability of these elements, redundancy is not warranted (due to a significant weight penalty). The electrical cross-strapping scheme shown in Figure C-1 provides maximum flexibility and utilization of the proposed hardware. Table C-1 identifies the preliminary physical characteristics of the ACMS hardware.

RELIABILITY ASSESSMENT

ACMS achieves a predicted reliability of 0.9883 for the orbiter and 0.9995 for the probe bus (Table C-2) based on the estimated parts count and associated failures rates currently standard within Hughes and the mission life defined below. The failure rates for electronic components have been modified by the Hughes experience factor of 0.606. The "E" factor is an attempt to reflect the operational experience that Hughes satellites have in orbit, thereby compensating for the basic inaccuracy of most handbook data. It is calculated as the ratio of actual part failures in space to the expected number of failures using the handbook data. This factor is periodically updated to reflect additional flight experience. The "E" factor is currently 0.606.

Reliabilities have been calculated based upon the following mission times:

1) The operational life of the orbiter is 200 days in transit to Venus and 225 days in orbit

2) The operational life of the probe bus is 125 days; the operational life of the probes, both large and small, is 108 days inactive (launch to separation), 20 days low power mode, and 90 min high power mode (descent).

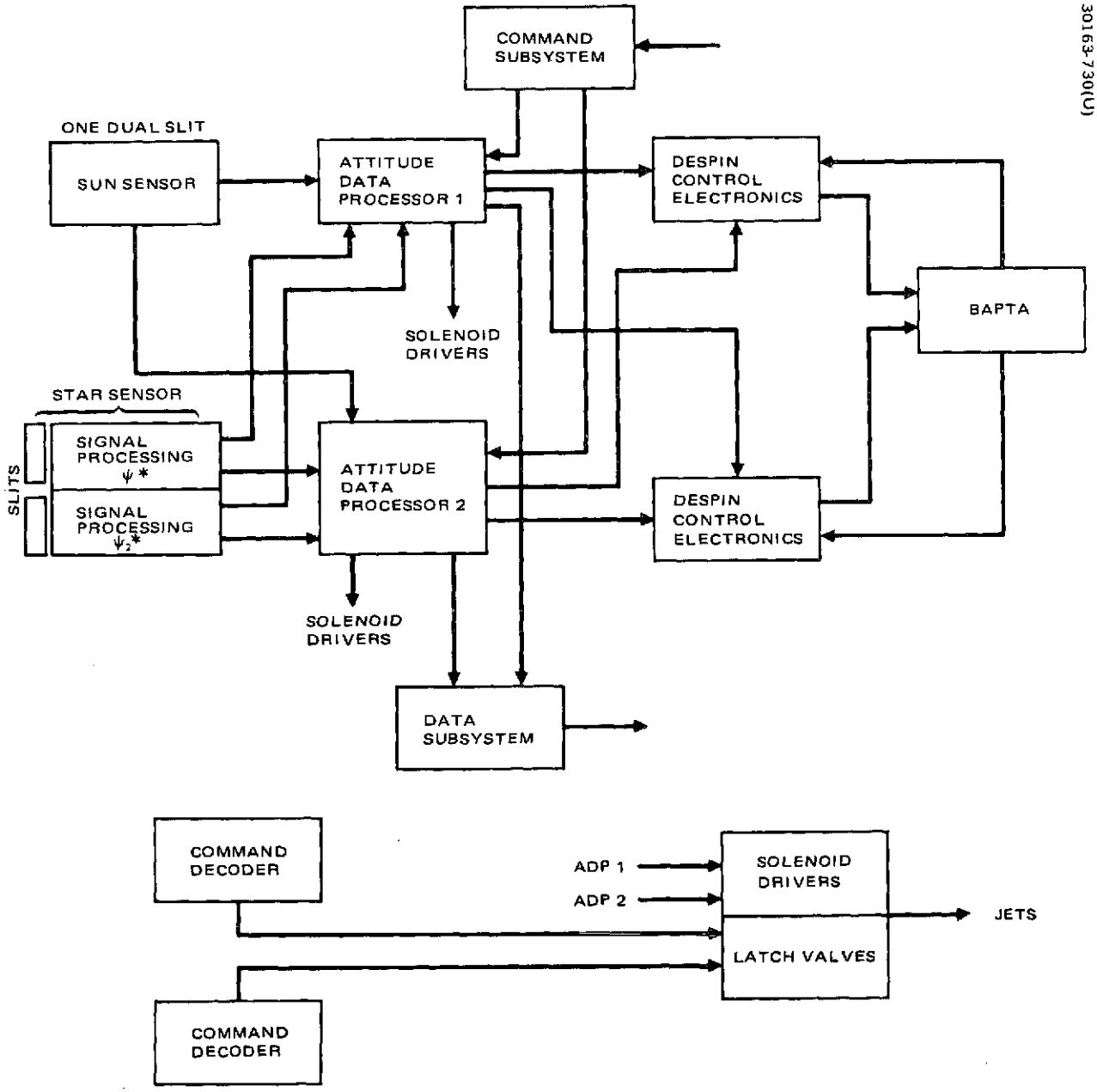

FIGURE C-1. ACMS ELECTRICAL CROSS STRAPPING DIAGRAM

TABLE C-1. ACMS EQUIPMENT LIST

Component	Number per Spacecraft	Mass, kg (lb)	Size, cm (in.) (L x W x H)	Power, W
Sun sensors	3	0.1 (0.2)/unit	4.1 x 7.1 x 4.8 (1.6 x 2.8 x 1.9)	—
Star sensors	1	2.5 (5.5)	44.5 x 30.5 x 30.5 (17.5 x 12 x 12)	1.0
Attitude data processor	2	1.6 (3.6)/unit	22.9 x 15.2 x 7.6 (9 x 6 x 3)	4.0
Solenoid drivers (jet and latch valves)	1	1.0 (2.2)	25.4 x 15.2 x 3.8 (10 x 6 x 1.5)	2.0 (1 percent duty cycle)
Nutation damper	1	0.9 (1.9	58.4 x 2.5 (23 x 1) diameter	—
BAPTA (orbital only)	1	5.1 (11.2)	15.2 dia 30.5 L (6 dia 12 L)	1.0
Despin control electronics (orbital only)	2	1.7 (3.7)/unit	25.4 x 15.2 x 7.6 (10 x 6 x 3)	5.0
Thermal louvers		0.29 (0.65)/unit	40.6 x 20.3 x 5.7 (16 x 8 x 2.25)	—
(probe bus)	6			
(orbiter)	8			
Pin pullers		0.06 (0.14)/unit		—
(probe bus)	2			
(orbiter)	1			
Bicone deployment mechanism (probe only)	1	0.9 (2.0)	62.2 x 2.5 (24.50 x 1) diameter and attachment structure	—
Magnetometer deployment mechanism	1	1.5 (3.2)	106.7 x 2.5 (42 x 1) diameter and pivot joint	—

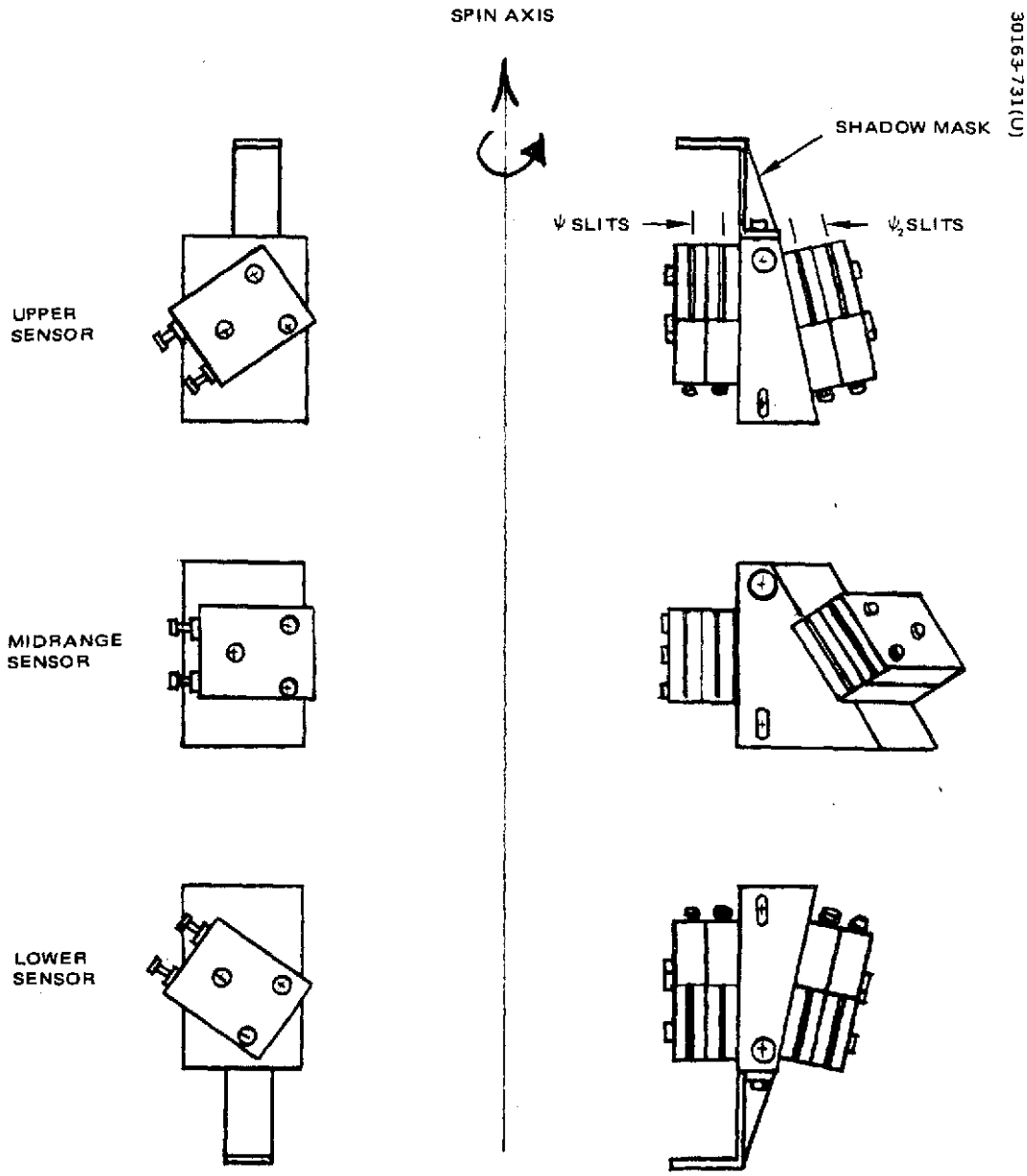

FIGURE C-2. SUN SENSOR CONFIGURATIONS

TABLE C-2. ATTITUDE CONTROL SUBSYSTEM RELIABILITY

Unit	Estimated Reliability	
	Orbiter	Probe Bus
Star sensor	0.9984	0.9998
Sun sensor attitude data processor	0.9960	0.9996
Jet control electronics		
Despin control electronics	0.9963	
BAPTA	0.9976	
Nutation damper	0.99991	0.99997
Subsystem	0.9883	0.99946

Reliability is enhanced by redundancy, cross-strapping, duty cycling of equipment used periodically, and minimization of single point mission failures in the proposed design. All electronic units are functionally redundant and conform to the design criteria that no single failure should cause a mission failure. Where redundancy is not feasible, conservative design reduces the probability of a single point failure.

SUN SENSOR DESIGN

The sun sensor design for the Pioneer Venus spacecraft consists of three sun sensor assemblies: an upper sensor assembly, a midrange sensor assembly, and a lower sensor assembly. The sensor assemblies are arranged as shown in Figure C-2 to provide signals over the 10 to 170 deg range of sun elevation angles. Table C-3 summarizes the design.

Each sensor assembly consists of four sensor units (two pairs of redundant units) on a precision bracket. Each of the sensor units contains a silicon photovoltaic cell and has a narrow planar field of view of approximately 90 by 1.75 deg. Two of the viewing planes of each sensor (the ψ planes) are aligned parallel to the spin axis while the other two viewing planes (the ψ_2 planes) are inclined to the spin axis at an angle of β deg. A separation angle between the ψ and ψ_2 planes, θ_o, is used in some applications to ensure that the ψ pulses always precede the ψ_2 pulses. This simplifies the data processing.

TABLE C-3. SUN SENSOR CHARACTERISTICS

Parameter	Upper Sensor	Midrange Sensor	Lower Sensor
Configuration Three dual redundant sensor assemblies made up of fan beam sensor units with silicon photovoltaic cells	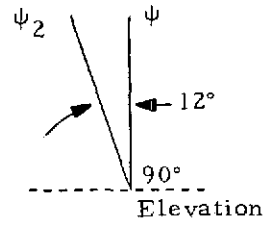	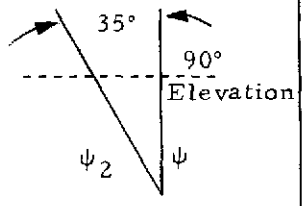	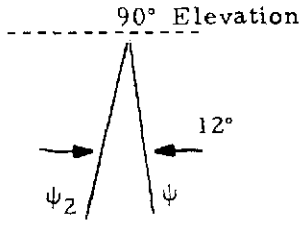
Field of View			
ψ, deg	10 to 90 (full FOV) 10 to 55 (required FOV)	45 to 135	90 to 170 (full FOV) 125 to 170 (required FOV)
ψ_2, deg	15 to 90 (full FOV) 15 to 55 (required FOV)	55 to 125	90 to 165 (full FOV) 125 to 165 (required FOV)
Accuracy			
Azimuth angle (ψ), deg	0.25 (3σ) at 55 to 0.5 (3σ) at 10	0.20 (3σ) at 90 ±35	0.25 (3σ) at 125 to 0.5 (3σ) at 170
Elevation angle, smoothed, deg	1.0 (3σ) at 55 to 0.5 (3σ) at 15	0.15 (3σ) at 90 ±35	1.0 (3σ) at 125 to 0.5 (3σ) at 165
Mass, kg (lb)	0.091 (0.2)	0.091 (0.2)	0.091 (0.2)

The construction details for a sensor unit are shown in Figure C-3. The narrow planar field of view is defined by inner and outer slits whose width is adjusted by means of shims. The sensor unit contains an integral 1000-ohm resistor which acts as a load to the silicon cell. The sensor pulses widen appreciably as the sunline nears the spin axis. An additional widening effect will be present on this mission as the spacecraft nears Venus and thus gets closer to the sun. The larger angular size and higher intensity will result in a larger amplitude and wider pulse. Although the sun intensity level at Venus is almost twice that at the earth, the resultant pulse amplitude will not double due to the diode loading effect of the non-illuminated parts of the cell. The pulse slope near the nominal trigger level of 100 mV will be more than adequate. The maximum sensor output voltage due to Venus albedo has been estimated to be 0.012 V. This level is well below the nominal trigger level of 100 mV and presents no threat to proper sensor operation.

The sun sensors design is based on utilizing an existing design developed for Hughes earth orbit satellites, such as the Intelsat IV and Telesat communication satellites. The only modification required for the Pioneer Venus spacecraft will be the mounting brackets.

Sun Sensor Tradeoffs

An analysis was made of sun sensor field of view requirements necessary to satisfy the mission attitude requirements. The basic conclusions were that the sun sensor system must accomplish the following:

1) Provide sun azimuth reference pulses over a range of sun elevation angles from 10 to 170 deg relative to the spacecraft spin axis

2) Provide information from which the sun elevation angle can be determined over a range of sun elevation angles from 15 to 165 deg

3) Provide full redundancy due to the critical nature of the sun sensor signals

Azimuth Reference Pulse Sensors

The azimuth reference pulse requirement is the simplest task to fulfill. The most straightforward method of producing the pulses is a fan beam field of view sensor using shadow mask techniques and a silicon photovoltaic cell. The fan beam is nominally parallel to the spin axis. The cell develops a signal whenever the sun passes through the field of view. For this type of sensor, the pulses get progressively wider as the sunline nears the spin axis for a practrical shadow mask size, and multiple cells must be used if large fields of view are required. There are many variations on the basic technique (such as designs using pinhole apertures, deposited reticles on glass blocks, lenses, etc.), but the basic principle of operation is the same. If it is necessary, the effects of the pulse widening on accuracy can be partially com-

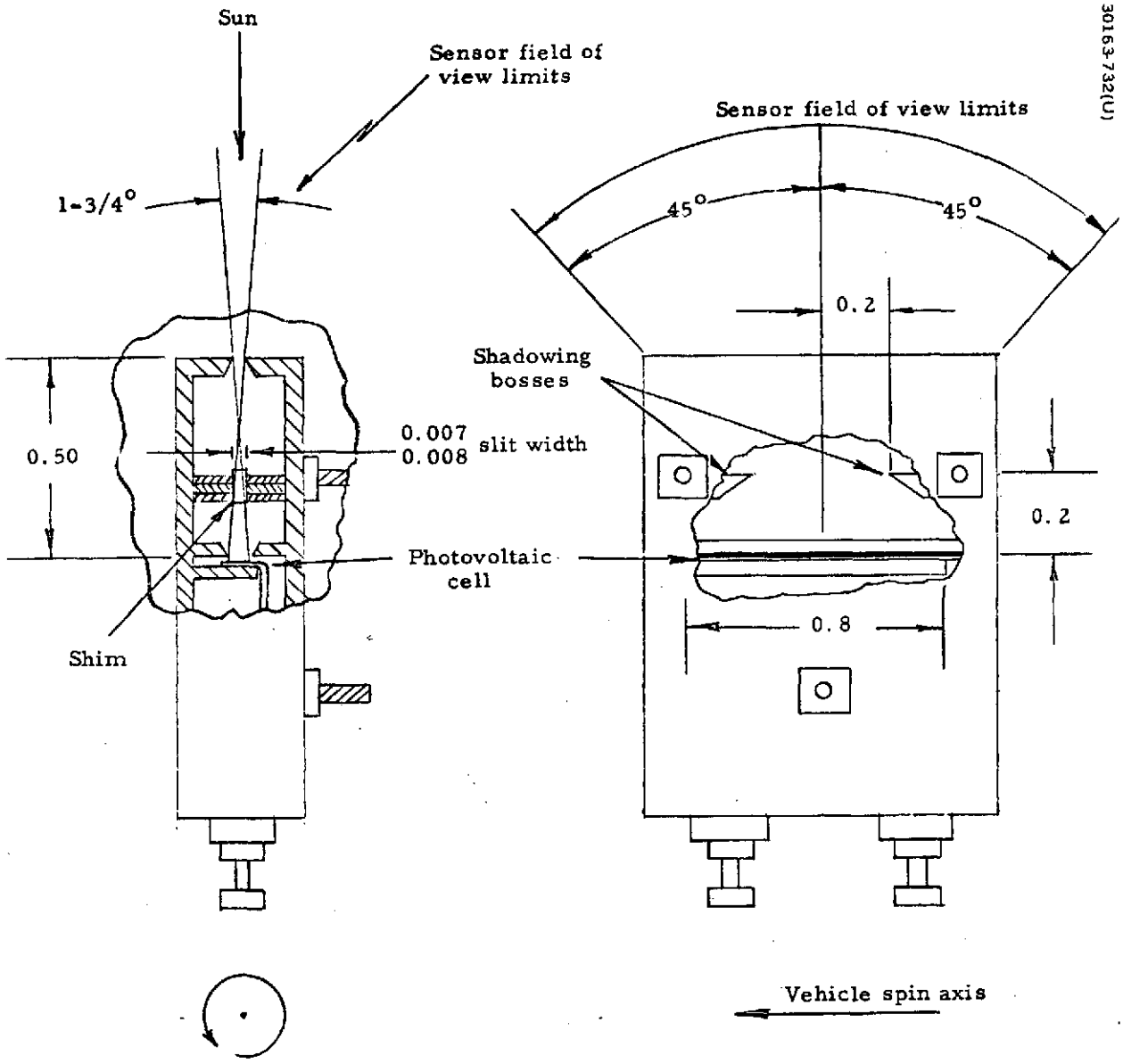

FIGURE C-3. INDIVIDUAL SUN SENSOR UNIT

pensated for by making use of ground calibration pulse data. Even better compensation can be obtained by incorporating an electronic processing scheme that provides both leading and trailing pulse edge data. This permits the center of the pulse to be determined and greatly reduces the effects of apparent sun size variations and space environment on ground calibration data.

Another variation on the basic fan beam field of view design is to use two detectors behind the slit and to sense the null crossing as the beam of light sweeps across the detectors. Again, there are many variations on the design involving the use of pinhole apertures, lenses, etc., but the basic technique is the same. The chief advantage of this null technique is that the zero crossing is quite insensitive to cosine law effects on amplitude, apparent sun size variations and other effects. It does, however, result in a slightly more complicated sensor and processing electronics configuration.

Elevation Angle Sensors

The sun elevation angle sensing requirement is slightly more difficult to meet than the azimuth pulse requirement, but a variety of methods exist to accomplish this task. The large field of view requirements make the use of analog techniques difficult. Simple energy balance types of sensors are not feasible to provide 0.25 to 1 deg accuracy over such a large angular range. Even if such a large linear range could be obtained, the problems of accurately predicting the output in orbit would be severe. There is one type of analog device which should be considered, however. It is a lateral effect photovoltaic cell. Such a cell can be designed to put out a signal proportional to the intensity and position of a light spot on its surface as well as a separate signal proportional only to the intensity. A long thin cell of this type could be used to provide position and intensity signals which could be used to determine elevation angle. However, the wide angular range requirements would still require very precise calibration to achieve the required accuracy.

There are two types of digital sensors which could be used to fulfill the sensing requirements. One is a true digital sensor which used an array of silicon cells and a reticle to produce an 8-bit digital word corresponding to sun position. The other type is really a quasi-digital sensor in that it produces two analog pulses whose separation in spin angle can be used to determine elevation angle.

The most suitable true digital sensor for this task is manufactured by Adcole Corporation and consists of a sensing head containing 8 digital detectors and one "command" detector in conjunction with an electronics package. It provides sun elevation angle information with a resolution of 0.5 deg and an accuracy of ±0.25 deg over an angular range of 128 deg. Thus, two sensor units would be needed to provide full coverage with a good overlap in the 90-deg region. The output of the command detector could also be used to provide the azimuth reference pulse in addition to its other function of commanding the digital detector readout time.

TABLE C-4. SUN SENSOR TRADEOFF TABLE

Parameter	Type of Sensor		
	Analog, Lateral Photo Effect	True Digital Coded Reticle	Quasi-Digital Fan Beam Field of View
Azimuth pulse output stability	Suitable, ≈0.25 deg with calibration	Suitable, ≈0.25 deg with calibration	Suitable, ≈0.25 deg with calibration
Elevation accuracy	Fair; requires extensive calibration and test. Affected by temperature and stray light sources.	Very good; can give resolution of 0.5 deg and accuracy of 0.25 deg over the entire field of view. Unaffected by stray light.	Good; central region accuracy very good. Less accurate than true digital in regions nearer the spin axis. Unaffected by stray light.
Sensor head complexity and number needed	Detector would require considerable development effort. Would probably use two redundant heads per spacecraft.	Sensor head somewhat complex but is well proven in flight. Would probably use two heads with redundancy in central 90 ±53 deg region.	Sensor head uncomplicated. Well proven in flight. Obtain full redundancy with three assemblies.
Electronic processing circuitry	Not too complex but would require analog to digital conversion for telemetry resolution.	Complex electronics per sensor head	Very simple. Uses essentially existing circuitry.
Development status	New	Well proven	Light
Weight	Light	Electronics processing heavy	Fairly light
Cost	Development moderate Recurring medium	Nonrecurring low Recurring fairly high	Nonrecurring low Recurring medium

The quasi-digital sensor uses two fan beam field of view sensors (identical to those described earlier in the discussion on azimuth reference pulse generation). One sensing plane is placed parallel to the spin axis (as in the azimuth reference case) while the other is inclined to the first plane by and angle β. The spin angle between the pulse produced by each of the sensor units is a function of the plane inclination angle, β, and the angle between the spin axis and sunline, γ. As in the case of the true digital sensor, one of the necessary signals produced for elevation angle determination can also be used as the azimuth reference pulse.

Sun Sensor Selection

The pertinent characteristics of the sun sensor configuration considered are shown in Table C-4. Any of the three elevation sensors considered also provide an analog azimuth reference pulse. Since the accuracy of such a pulse is adequate for the mission requirements (i.e., a more accurate method such as the null crossing type is not needed), the tradeoff reduces to a choice between the three elevation sensors. The most straightforward and simplest method is clearly the quasi-digital. It does not require the somewhat complex processing electronics used by the true digital nor does it have the calibration or development uncertainties of the lateral photo-effect device. Its electronics processing is essentially free, since the angular measurement between pulses uses circuitry which already exists for other tasks. It also has a very good flight history, having been flown on all Hughes-built spinning and dual spin satellites to date with no failures. Thus, this is the chosen configuration.

STAR SENSOR DESIGN

The star sensor design chosen for the Pioneer Venus missions is a passive star scanner with refractive optics and two long, narrow silicon photovoltaic detectors. Each detector, in conjunction with the optical system, forms a narrow fan-beam field of view 1.0 by 25 deg in size. One of the field of view planes is parallel to the vehicle spin axis while the other is canted at 20 deg to that field of view. The center of the field of view is aligned nominally at 53 deg to the spacecraft spin axis. Figure C-4 shows the sensor configuration and field of view orientation. The sensor will have a threshold detection level of +1.0 silicon magnitude stars giving it the capability to detect the 25 brightest silicon stars. Table C-5 summarizes the star sensor design.

The solid state sensor would be a new design, since no existing design is available which is capable of operating over the wide spin speed range of operation. The solid state sensor would have two independent detector channels (one channel for each slit) and each slit could be used for attitude determination (with the sun sensor).

The block diagram of the sensor electronics is shown in Figure C-5. Each of the two detector channels is completely redundant except for the optics and stray light shield. The inputs supplied to each channel of the sensor are:

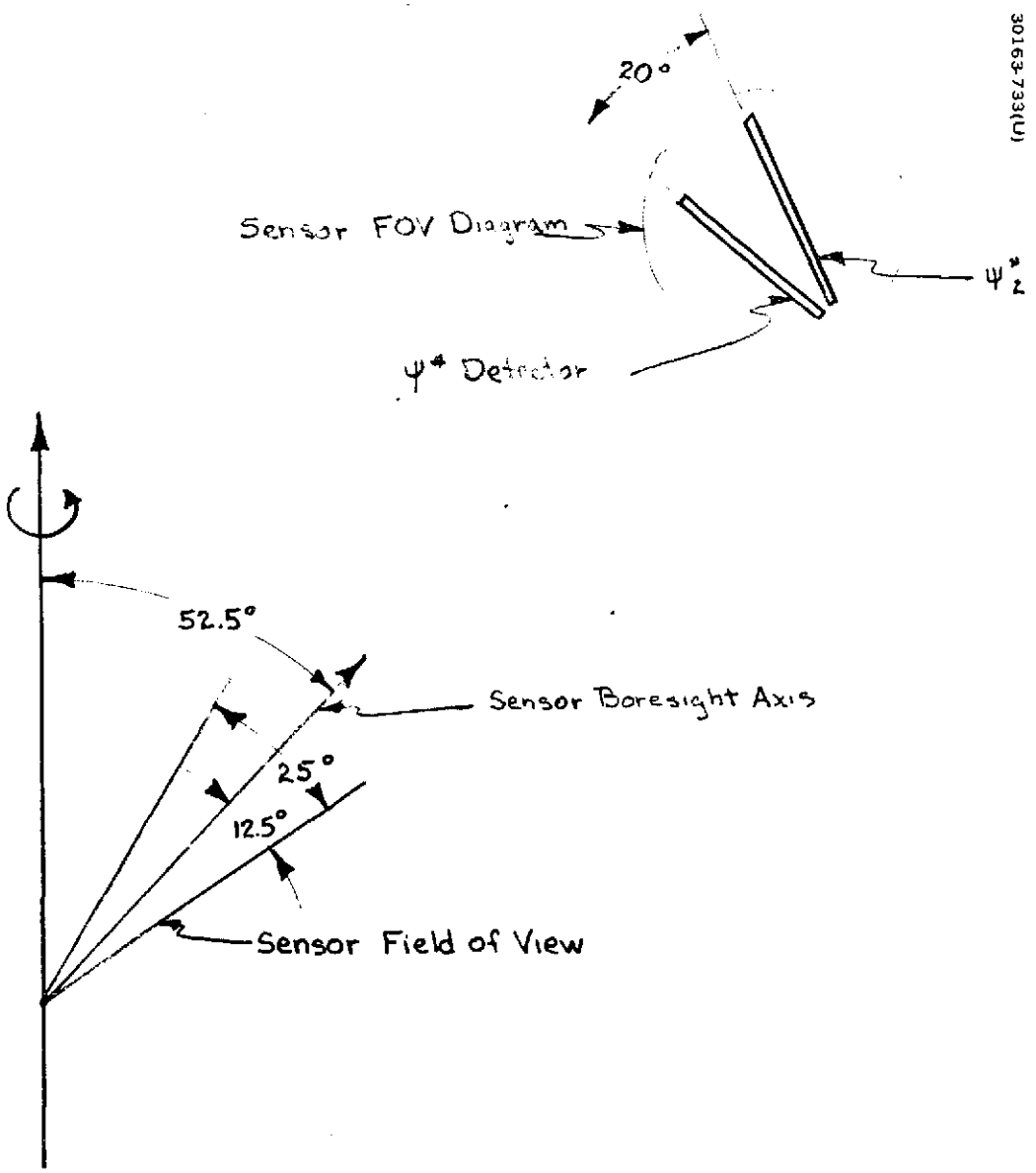

30163-733(U)

FIGURE C-4. STAR SENSOR FIELD OF VIEW ORIENTATION

TABLE C-5. STAR SENSOR CHARACTERISTICS

Parameter	Characteristics	Comments
Type of sensor	Passive, dual fan beam, beam field of view with silicon photovoltaic cell	Each field of view electrically independent for redundancy
Field of view and orientation	25 deg elevation field of view, 20 deg cant angle between field of view, optical axis 53 deg from spin axis	
Sensitivity	-1.5 to +1.0 magnitude (silicon) stars	
Outputs	Star crossing pulse when star exceeds threshold Star intensity signal proportional to intensity of brightest target	Eight step ground commandable threshold
Accuracy:		
Raw azimuth	±0.5 deg (3σ)	Smoothing is accomplished by ground data processing
Smoothed azimuth	±0.17 deg (3σ) includes bias errors	
Smoothed elevation	±0.7 deg (3σ)	
Sun rejection	For angles greater than 60 deg to the optical axis	
Earth and Venus rejection	For angles greater than 35 deg to the optical axis	
Power	Less than 1 W per channel	
Mass	Less than 2.5 kg (5.5 lb)	Includes sun shade

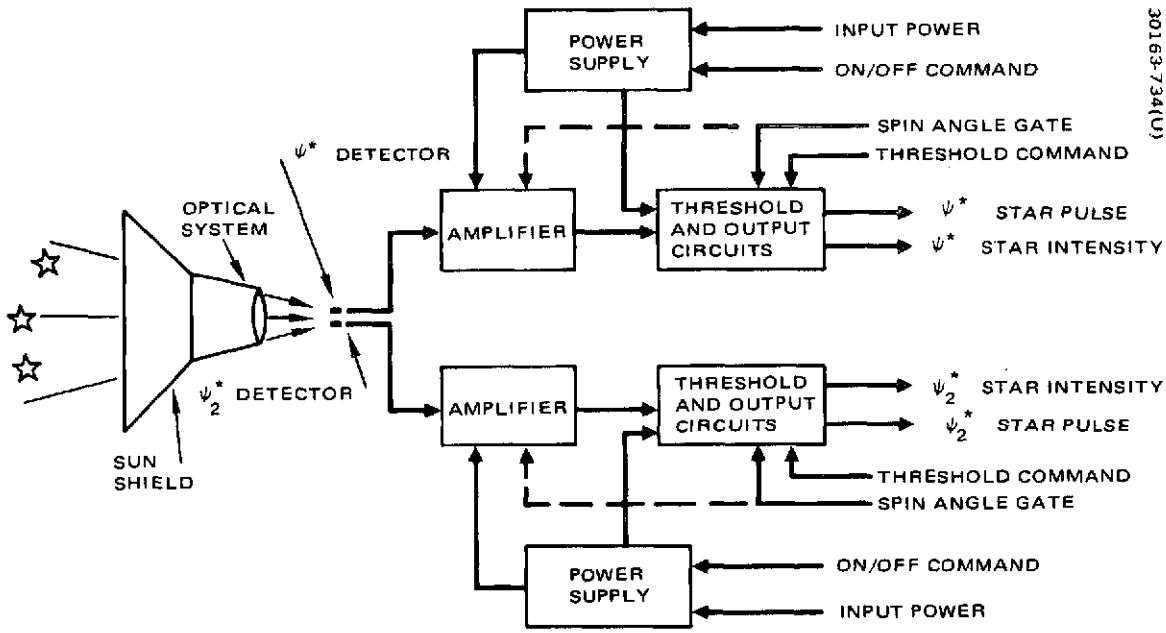

FIGURE C-5. STAR SENSOR BLOCK DIAGRAM

1) Power

2) On/off command

3) Star threshold command

4) Spin angle gate signal

The output signals supplied by each channel are:

1) Star pulse signal

2) Star intensity signal

Star Threshold Command

The star threshold command is a digital pulse command which is capable of being set at any one of 8 discrete levels which are proportionally spaced with respect to star intensity in the nominal sensitivity range of the sensor. This command will help ensure that output pulse are produced only on desired targets.

Spin Angle Gate Signal

The spin angle gate signal is a logic command which is ON for a predetermined portion of the rotor revolution. It is anticipated that the gate signal will be ON for no more than 10 deg of spacecraft revolution, allowing star signal detection during only this period. This command, in conjunction with the threshold command, will help ensure that output pulses are produced for the desired targets.

Star Pulse Signal

The leading edge of the star pulse signals will determine the azimuth and elevation of the measured star with respect to their nominal positions relative to the sensor alignment references. Crossing the slit parallel to the spin axis will give basic azimuth reference; the time interval between the crossings of the two slits will give the elevation reference.

Star Intensity Signals

Each channel will provide an analog star intensity signal whose level is proportional to the intensity of the brightest star above the threshold level which occurs during the ON time of the spin angle gate.

Baffle Design

A two-stage stray light sheild of the type shown in Figure C-6 is required to protect a sensor having a 25 deg field of view and a 2-in. diameter optical system from sun interference for θ_s = 60 deg and planet interference for θ_p = 33 deg. The shield must be 8.7 in. in overall length with the diameter of the inside edge of the last baffle of the outer stage equal to 9.2 in.

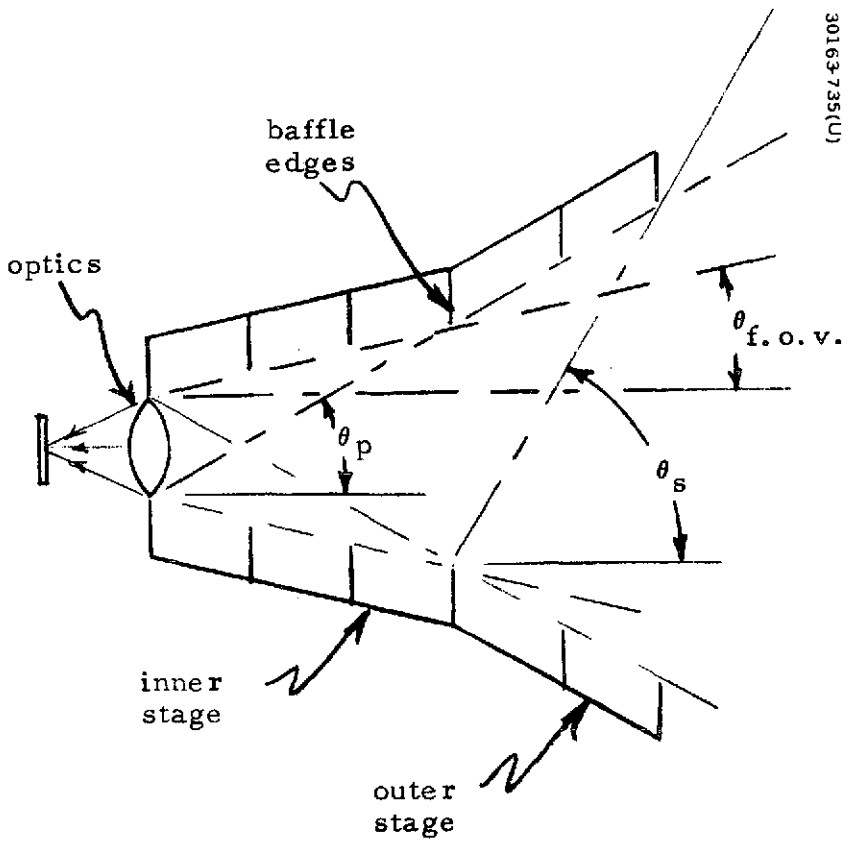

$\theta_{f.o.v.}$ = field-of-view half angle

θ_s = sun protection angle

θ_p = Planet protection angle

FIGURE C-6. DESIGN FEATURES OF TWO-STAGE STRAY LIGHT SHIELD

Detector Selection

The proposed detector for the solid state star sensor will be made of silicon photodiodes based on silicon planar diffused oxide passivation technology.

Star Sensor Tradeoffs

The basic functional requirements for the star sensor system are as listed below:

1) Provide star pulse information which can be used in conjunction with the sun sensor outputs to permit the attitude of the spacecraft to be determined (by use of ground-based computer operations).

2) Provide (with the aid of a spacecraft supplied spin angle gate) a once-per-revolution star output pulse to be used for on-board real time operations.

3) Provide appropriate sun, earth and Venus interference rejection.

4) Provide redundant operational modes for reliability purposes.

Since the spacecraft is a spinning vehicle, the obvious choice for the star sensor task is a static no-moving parts design. The tradeoff considerations then involve selecting the type of static configuration to be used.

The majority of static sensors flown to date have used a photomultiplier tube (PMT) detector. The basic configuration of such a sensor is shown in Figure C-7. It consists of a stray light shade, an optical system, a reticle, a PMT, and an electronics assembly containing the power supplies and the signal processing circuity. The reticle usually contains at least two slits (one inclined to the other) to provide both azimuth and elevation information on a target star. This type of sensor has generally been used to supply star pulse information for use on the ground (i.e., not in a real time sense). Several versions of this type of sensor have been flown. The sensor on the OSO-H satellite is a good example of this type of sensor. It uses a two-slit reticle and has an elevation field of view of 10 deg. It provides usuable information on stars down to +3.5 magnitude.

A static sensor can also be made using a solid state detector. In this case, the reticle used with the PMT is not needed, since the detectors themselves can be fabricated in narrow strips to define the field(s) of view (in fact, a reticle is not only not needed, but is not desirable since noise considerations make a small detector mandatory). A static sensor using a solid state detector is shown schematically in Figure C-8. It is, of course, very similar to the design using a PMT except for the absence of a reticle and a high voltage power supply and the use of dual signal processing circuitry. Solid state sensors of this type do not have the wide flight experience that the PMT devices have. The single field of view silicon detector sensor

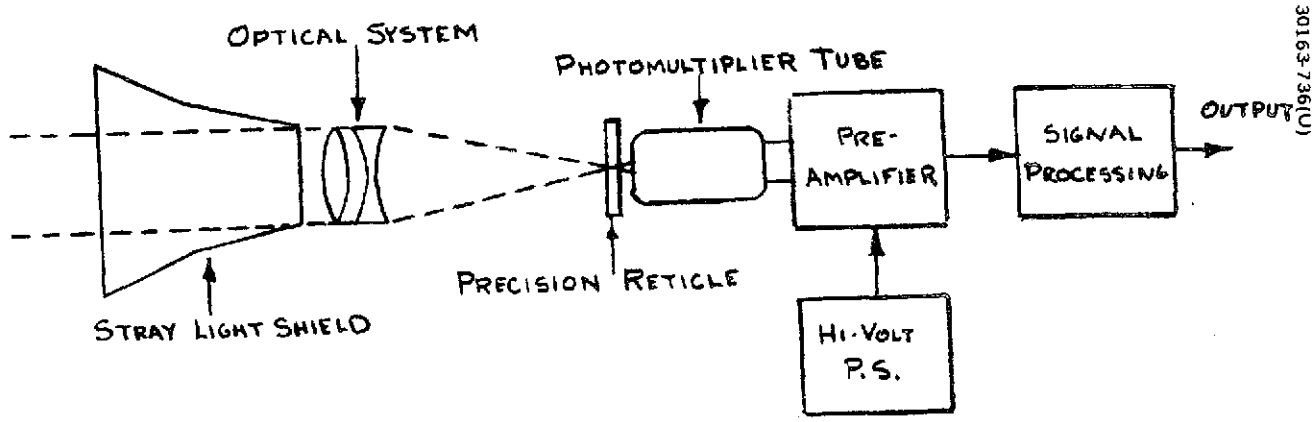

FIGURE C-7. PHOTOMULTIPLIER TUBE STAR SENSOR

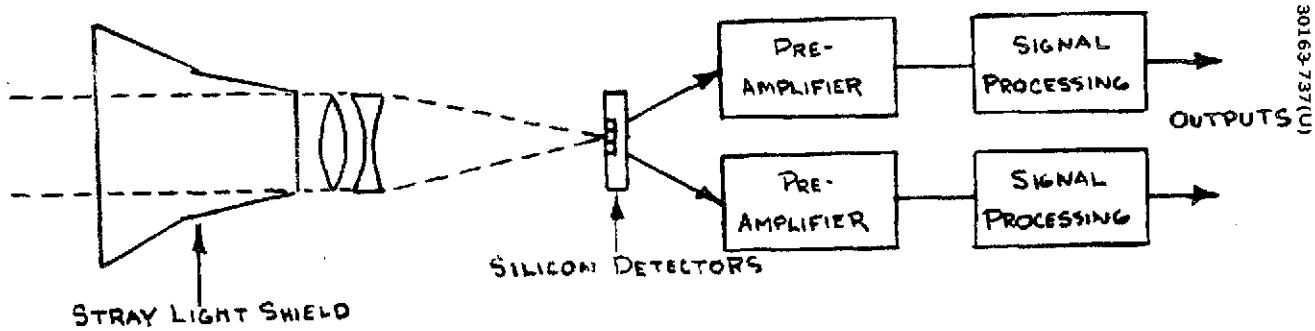

FIGURE C-8. SILICON SOLID STATE STAR SENSOR

on the Pioneer Jupiter mission and a multiple field of view, cadmium sulphide detector sensor used on the very slow rotation (i.e., orbital rate) SPARS payload are instances, however, where mission requirements have made their use feasible.

The first tradeoff decision to be made is between a PMT type or a solid state type system. At the present time, the silicon photovoltaic detector clearly appears to be the best choice* of the solid state types. It will, therefore, be used in the tradeoff comparison with the PMT detector. The pertinent features of the detectors are summarized in Table C-6.

As can be seen by Table C-6, the PMT has advantages in the areas of low internal noise, fast response, and experience. The silicon detector has advantages in the areas of size, lack of requirement for high voltage, quantum efficiency, and ruggedness. When comparing sensitivity of detectors, care should be taken with the spectral characteristics of the stars. The silicon sensor with its sensitivity in the infrared region will result in considerable brightening of cool stars while reducing the brightness of hot stars only slightly. This characteristic increases the number of stars that can be tracked with a silicon detector when compared to a PMT for any given magnitude. Specifically, to retain detection of 25 stars with a PMT would require 0.7 magnitude more sensitivity than that of the silicon detector (i.e., twice the sensitivity).

The way in which these factors interact with the requirements for a particular mission are somewhat complex. However, a first-order approximation to the types of sensor requirements each is suited for can be made. Sensors which must provide high accuracy on very dim stars on fairly rapid spinning vehicles will probably need to use PMT detectors. Sensors which have only moderate accuracy requirements on fairly slow spinning vehicles and do not have a sense very dim stars can use silicon detectors. There is quite a gray area in between where the choice is not at all clear. For instance, the use of multiple silicon detectors to divide up the field of view in small segments can offset many of the advantages of the PMT for some missions. There will obviously be a point, though, where the resultant electronics complexity becomes somewhat overwhelming. It is clear though that if a sensor using silicon detectors can fulfill the mission requirements without requiring too many detectors, it offers important advantages over a sensor using a PMT due to weight, power and reliability considerations.

For the Pioneer Venus mission, this is clearly the case. A design using silicon detectors is capable of meeting the desired performance. Although the performance with a PMT would give higher signal-to-noise levels without stray light, however, maintaining this improvement in the presence of stray sunlight would require a better stray light shield than is needed with the silicon detector. Since there can be two separate detectors for the field of view, the silicon detector design also easily lends itself to full electronics redundancy (i.e., each field of view channel is electrically independent).

*Discussed in the performance tradeoffs below

TABLE C-6. PMT VERSUS SILICON DETECTOR SENSOR TRADEOFF CONSIDERATIONS

Tradeoff Parameter	PMT Detector	Silicon Detector
Internally generated noise	Very low	Fairly high
Size	Fairly large - results in large, single detector sensors	Small and compact - results in medium size, multiple detector sensors
Response time	Very fast – microsecond range	Basic detector is fast – generally slow when coupled with high gain amplifier
Field of View (FOV)	Predetermined cathode configuration make FOV not as flexible as silicon detector	Has large FOV because detector can be shaped for each slit, therefore requires less sensitivity to obtain sufficient number of stars
Spectral range and quantum efficiency	Visual spectral range, quantum efficiency of approximately 20% at ≈0.45 microns for S-20	Spectral range in red portion of visual range and into the near infrared quantum efficiency of approximately 70% at ≈ 0.8 microns
Susceptability to damage from high intensity sources	Requires sun and possibly planet protection. Has slow recovery time (100 - 300 msec)	Requires no protection, has fast recovery time (<8 msec)
Redundancy considerations	Generally requires two complete sensors for redundancy	Redundancy (except for optics and light shield) can be achieved in single package
Reliability	Requires 1.5 - 2.5 KV power supply plus signal processing and pulse train separation electronics	Separate detectors for each slit make signal processing easier
Weight	> 10 lbs. per sensor	<5.5 lbs per sensor
Power	> 7 watts per sensor	<2 watts per sensor (<1 watt per channel)
Resistance to radiation and Magnetic fields	Low	Good
Stray light	High light levels can limit operation	Tolerant of high light levels with minimum degradation of signal to noise
Ruggedness	Fragile	Rugged
Previous space history	Extensive use in space instruments including star scanners	Limited use due to relatively recent development

Another important tradeoff consideration is field of view versus sensitivity. Related parameters are the angle between the field of view and the spin axis, and stray light shielding. Both small fields of view and small angles between the field of view and the spin axis will result in the star sensor seeing less of the celestial sphere during a revolution and thus having to sense dimmer stars in order to insure coverage for a given orientation. Small fields of view also improve signal-to-noise ratios and help the stray light shield design problem. However, detector noise increases roughly as the square root of the field of view area while the available targets of a given magnitude go up, on the average, in direct proportion to the elevation field of view. One of the most severe design problems with any detector system is its ability to reject targets dimmer than the target star. As sensitivity is increased, the number of detectable stars increases almost exponentially. A compromise must be reached between the system sensitivity, signal-to-noise ratio, and stray light shielding capabilities when selecting the field of view. Based upon the analysis and experience of the solid state sensor manufacturers contacted during this study, a single solid state detector can be designed which will reliably detect +1 silicon magnitude stars for fields of view up to 25 to 30 deg using present state-of-the-art detector and preamplifier technology. From the results of the visibility studies herein, a sensor capable of detecting 25 stars (+1 silicon magnitude sensitivity) with a 25 deg field of view will satisfy all of the mission attitude determination requirements. By using only a few of the brightest stars it becomes much easier to discriminate against dim background stars using an adjustable detection threshold setting. Therefore, a solid state detector having a wide field of view and adjustable detection threshold setting offers superior star discrimination capability over a narrow field of view PMT sensor which must detect dimmer stars to obtain the same spacecraft attitude coverage.

Star Sensor Selection

In summary, the solid state dual slit star sensor design (utilizing slit redundancy) will weigh approximately 15 lb less per spacecraft, require approximately 5 W less power, be more reliable (no high voltage stress), less susceptible to stray light interference, and provide easier dim background star discrimination than a PMT type sensor (two required). For these reasons, a solid state star sensor design has been selected for the baseline design of the Pioneer Venus spacecraft.

Optical Considerations

There are two basic optical systems to be considered: reflective and refractive. The reflective systems are generally limited in their field of view unless a curved focal plane can be accommodated. Curved detectors have been fabricated but these are strictly in the experimental stage and performance could be marginal. Fiber optics have been used to transmit the curved field to a flat diode, but light losses in the fiber bundle offset much of the weight advantage that might be gained by using reflective optics. A very low f/number must be used to reduce the detector size.

Considering the large field of view and low f/number, a refractive system was selected to take advantage of its large field of view and the absence

of spiders or other support structures in the field of view. The absence of support structures makes this system less susceptible to stray light impingement problems. The very low f/number (f/1.0) was selected to minimize the detector size thus reducing system electrical noise and improving signal-to-noise characteristics.

Stray Light Rejection/Baffle Design

Rejection of stray light is a major design problem. Stray light from bodies such as the sun, earth, and Venus entering the optical system is sensed by the detector and creates system noise seriously affecting star detection, false alarm rates, and accuracy. There are many different types of baffle designs which have been proposed and/or used for spacecraft. For this application, the two-stage baffle with recessed surfaces and baffle rings is required to assure satisfactory operation to within 60 deg of the sun and 35 deg from earth and Venus.

Figure C-6 shows the basic design features of such a baffle. All edges of both stages are, of course, outside the detector field of view so that they cannot be directly imaged on the detectors. The outer stage of the baffle is configured so that none of its edges can be seen by optics and so that no sunlight can impinge directly on the inner stage. The angle θ_s, which is defined by the outer stage, is usually considered to be the smallest angle the sun can make with the optical axis without causing performance degradation. The angle θ_p, which is defined by the inner stage, is usually considered to be the smallest angle the illuminated limb of a planet can make with the optical axis without causing performance degradation. Neither of these angles are exact limits, of course, but they do serve to indicate the rough criteria used to initially design a shield. Since each length of the inner shield produces a new size for the entire sheild, the usual design procedure is to lay out several configurations in order to select one with the best set of parameters. Large fields of view, large diameter optics and small sun protection angles all increase shield size with the sun protection angle being the strongest factor. To protect a sensor having a 25 deg field of view and a 2-in. diameter optical system from sun interference for θ_s = 60 deg and planet interference for θ_p = 33 deg, the shield must be 8.7 in. in overall length with the diameter of the inside edge of the last baffle of the outer stage equal to 9.2 in. In addition to the shield, careful attention must also be given to the optics and optics detector housing if good stray light rejection is to be achieved. Very smooth surfaces on the optics, good cleanliness and careful attention to sources of internal reflections are all very important.

Detector Selection

The proposed detector for the solid state star sensor will be made of silicon photodiodes based on silicon planar diffused oxide passivation technology. Compared with other candidate materials, the silicon photodiode offers the following advantages:

1) Low leakage current

2) Low noise

3) Fast response time

4) High quantum efficiency

5) High sensitivity

6) Excellent long-term stability

The silicon planar diffused, oxide passivated photodiode can be easily fabricated on a silicon wafer using standaridized photolithographic masking and etching procedures for the sequential metallizing techniques. Large area devices or a multiplicty of small area devices with suitable leads can be fabricated readily in the planar device on a single wafer.

The silicon photodiode proposed will be operated in the photovoltaic or zero biased mode. Operation in the photoconductive or reversed bias mode did not offer significantly improved performances for the proposed application. Although the reversed bias mode does reduce the junction capacitance, leakage currents increase with increasing bias. Guard ring technology is applied to reduce the leakage current problem at the cost of increased device complexity. In the photovoltaic mode, the only source of leakage currents is in the bulk of the device with no surface leakage. Guard rings and bias voltage supplies are not required.

A major noise source is the temperature dependent Johnson noise current. If a large load resistor is used with a large junction capacitance, it appears that the frequency response will be limited. However, the use of a detector with high junction resistance in combination with a feedback operational amplifier reduces the Johnson noise to a negligible level while preserving signal amplitude with adequate frequency response.

System Signal Level

The peak signal level at the detector is given by the expression:

$$I_{p.} = (2.512)^{-m} FA'R_s$$

where

F = filter factor at specific vehicle spin rate

A' = effective objective collecting area

m = magnitude of threshold star

R_s = response of detector to 0.0 magnitude AO star

The signal current generated in the detector for a 0.0 magnitude AO star was calculated to be 0.489×10^{-12} A/cm^2 of effective objective area. For an aperture diameter of 5.1 cm, optical efficiency of 75 percent and maximum off-axis operation of 16 deg (inclined slit), the effective collecting area is calculated to be 13.1 cm^2. A lower break of 1 Hz and an upper break of 120 Hz was selected as the best compromise of signal versus noise equivalent bandwidth (NEBW) for system operations over the spin speed range of 5 to 60 rpm. At 15 rpm and 60 rpm the filter attenuation factors are 0.91 and 0.70, respectively. The NEBW is 91 Hz.

The detector current produced by the dimmest star of interest (M = +1) at a vehicle spin rate of 60 rpm would reach a peak amplitude of:

$$Ip60 = 1.79 \times 10^{-12} \text{ A}$$

At a spin rate of 15 rpm, the detector peak current would increase to:

$$Ip15 = 2.32 \times 10^{-12} \text{ A}$$

System Noise Level

With a silicon detector the basic noise sources are: detector dark noise, amplifier and feedback resistor noise, detector short noise due to current flow and excess noise in the detector such as 1/f and popcorn noise. The total system noise is given by:

$$I_{NS} = \left[\Sigma\, i_n^2\right]^{1/2}$$

where

i_n = the noise current produced by the individual noise sources

The most serious type of system noise which must be considered in silicon star sensors is detector dark current noise. The dark noise current is the rss of the short noise and Johnson or thermal noise. As the bias voltage of the diode approaches zero (photovoltaic mode), the dark current of the detector decreases rapidly and the equivalent impedance of the diode decreases, which effectively results in a decrease in shot noise and an increase in thermal noise. There is a point, generally around 100 mv bias, where the combination of shot noise from the dark current and thermal noise of the diode is at its minimum. This point can have a noise level of 25 percent less than the zero bias photovoltaic mode. Extrapolation from detector (United Detector Technology) data yields an estimate of dark current noise = 0.198×10^{-12} A at 40° C with the 100 mV bias improvement.

The noise generally associated with the system amplifier is predominantly the Johnson noise of the feedback resistor used by the pre-amplifier operational amplifier. This noise can be reduced by increasing the value of the feedback resistor. Using a resistor value of 200 MΩ (no undue sacrifice in reliability or ease of manufacturing), the amplifier noise contributions is less than one-half the value of the dark current noise or 0.094×10^{-12} A.

Detector current is generated by the various sources of stray light impinging on the detector such as solar or planet albedo, star background and signal current. The two-stage baffle design will be configured to limit stray light current to that which would be produced by a -1.0 magnitude star. This light would be in the form of a very long time period light signal occurring one time each revolution. Because of the long time period, it is assumed that the condition is steady state and causes a shot noise effect in the photodiode. This stray light noise is calculated to be 0.021×10^{-12} A or 10 percent of the detector noise. Detector current due to star background energy can be calculated by assuming average densities for different parts of the celestial sphere. The sky background light level is usually expressed in terms of equivalent 10th magnitude stars per square degree. In the brightest part of the Milky Way the level can go as high as 700. Assuming this level for the entire 1.0 by 25 deg field of view gives 700 x 25 = 17,500 equivalent 10th magnitude stars. This worst case would produce a signal equal to a -0.6 magnitude star $\left(10 - \frac{\log 17,500}{4}\right)$ Since it was previously shown tht stray light equal to a -1.0 magnitude star had little effect, this lower value of noise will be neglected. The detector shot noise generated by the signal current from the minimum detected star, 1.0 magnitude, can be neglected for the same reason.

Two forms of excess noise are sometimes found in silicon photodiodes. One is burst (also known as popcorn, boxcar and bistable) noise and the other is flicker or 1/f noise. In burst noise, the current through the diode abruptly and randomly changes between two or more discrete values. This burst noise is seldom found in individual devices of the type proposed and can be eliminated by device selection. The 1/f noise is associated with the diode leakage current. Actual measurements on typical photodetectors show them to be 1/f noise free down to 0.1 - 1.0 Hz. To avoid this type of noise in the system, a lower frequency cutoff of 1 Hz was selected.

The total system noise is the rss of the detector noise, amplifier/feedback resistor noise and background noise, i.e., $I_{NS} = 0.220 \times 10^{-12}$ A.

System Signal-To-Noise

At a spin rate of 15 rpm, the peak signal-to-noise for a +1 magnitude star will be:

$$S/N_{15} = \frac{I_p 15}{I_{NS}}$$

$$S/N_{15} = \frac{2.32}{0.22} = 10.6$$

At a spin rate of 60 rpm, the peak signal-to-noise for a +1 magnitude star will be:

$$S/N_{60} = \frac{1.79}{0.22} = 8.2$$

Performance

There are three basic performance criteria: angular accuracy, probability of detection, and false alarm rates.

Angular Accuracy

Angular accuracy is associated with: alignment stability, threshold effects, elevation versus azimuth measurements, and angular jitter caused by noise. Alignment stability of well under 0.05 deg is easily maintained so this item is not a problem for this application. Threshold effects cause the apparent position of the star to move if a fixed threshold and a simple leading edge trigger method is used. This error is reduced to a reasonable level by triggering on a fixed percentage (usually 50 to 70 percent) of the peak star, since the sensor will generally be viewing isolated targets when high accuracy is of concern.

The azimuth angle measurement accuracy is a direct function of the measurement of when the star crosses the vertical detector. The elevation accuracy depends on the time measurement between the crossing of the canted and vertical detector. The ratio of the azimuth error of angular measurement to elevation error is approximately equal to the tangent of the cant angle. For the chosen configuration, this ratio is 0.364. Since there is uncorrelated random noise on each star crossing, the effect of noise on the two required star crossings used for elevation determination is $\sqrt{2}$ greater than for azimuth. Therefore, the error in elevation due to noise is 3.9* times the error in azimuth due to noise. Systematic bias errors can be determined by ground software and applied as correction factors to smoothed data. Noise on the raw star signal causes jitter on the star output pulse. The 3σ angular jitter can be related to the signal-to-noise ratio and input filter factors by the following:

$$3\sigma \text{ angular jitter} = \frac{\text{peak signal out of the filter}}{\text{peak signal-to-noise x signal slope}}$$

*

$$\text{Elevation error } (1\sigma) = \frac{\sqrt{2} \cdot \text{ Azimuth error } (1\sigma)}{\text{Tan } 20^\circ} = 3.9 \cdot \text{Az } (1\sigma)$$

For the selected break frequencies, filter factors and signal-to-noise ratios, the 3σ angular measurement errors at 15 rpm and 60 rpm are 0.15 and 0.36 deg, respectively.

The above calculations are for the 3σ angular error of a single sample of data. During the mission, at least 25 samples of data will be used in attitude determination calculations. This will result in a reduction of appoximately $\frac{1}{\sqrt{N}}$ in the 3σ dispersion; i.e., for 25 samples the 3σ azimuth errors at 15 rpm and 60 rpm are 0.03 and 0.07 deg, respectively. The corresponding elevation errors due to azimuth angular jitter would be 0.12 and 0.28 deg.

Probability of Detection and False Alarm Rates

The probability of detection is represented by the area under the right-hand curve minus the shaded area to the left of V_T in Figure C-9, while the probability of a false alarm is represented by the area of the left-hand curve which lies to the right of V_T. If the threshold is set at 70 percent of peak signal, the probability of detection under the worst case spin rate of 60 rpm (S/N = 8.2) would be 99.3 percent. At a spin rate of 15 rpm (S/N = 10.6) the probability of detection would be 99.93 percent. With the threshold set at 70 percent of peak signal under the worst case signal-to-noise (8.2), the false alarm rate (FAR) is less than one in every 10,000 revolutions. If the threshold is set at 50 percent of peak signal at 60 rpm, the FAR is ≈1 in a 100 revolutions. If the spin angle gate is set to allow signals for only 10 deg per revolution, the probability of any false alarm is further reduced.

Proposed Designs from Vendors

The proposed Honeywell system would use a 1.5 in. diameter f/0.86 refractive system with a single stage baffle. A V-slit silicon detector, 25 by 1.5 deg would feed the dual FET, operational amplifier combination. The system would weight 3.8 lb including the sunshield, and use approximately 1.0 W of power. All mission parameters will be fulfilled. Honeywell has designed and fabricated the Canopus tracker for the Mariner Mars '69 scientific flyby. This system is a photomultiplier type system. An operational silicon star sensor has been built under Honeywell funding with the capability of tracking 4th magnitude stars. This system has a 5 in. diameter objective and a total field of view of 6 deg. Presently they are under contract to supply solid state silicon star scanners with detection capabilities of 3.6 silicon magnitude and weighing 7.0 lb or less (including a 3.0 lb sun baffle).

Ball Brothers Proposal

The proposed Ball Brothers system would use a 2.0 in. (50 mm) f/1.0 refractive system with a two-stage sun shade. A V-slit silicon detector, 25 by 0.5 deg, would feed the systems dual preamplifiers. The system would weigh 5.2 lb including the sunshade, and use the proposed Pioneer Venus system. The field of view is similar, being 40 by 0.5 deg. The silicon detector was made of low resistivity bulk material to improve the system's resis-

tance to radiation. Because of the high radiation expected on the Jupiter mission, great effort was expended to protect against these radiation flares. The Pioneer Venus mission will not encounter the radiation level expected from the Pioneer Jupiter mission. Degradation of signal-to-noise from reflections off visual particles passing the spacecraft was very much less than expected and was not a major factor in the mission. The TRW system is designed to detect only the bright star Canopus (-1.0 silicon magnitude) A spin angle gate is used to reduce the false alarm rate. The TRW system uses a Cassegrain Bauers system with a 2.5 in. reflective objective. An optical fiber bundle is used in the spherical focal plane to bring the light to the silicon detector. The optical efficiency of the overall system is down around 30 to 40 percent. TRW felt that a solid state silicon detector is feasible, although the 4.0 lb weight limit will most likely have to be increased to include an adequate baffle to track within 60 deg of the sun and 35 deg from earth and Venus.

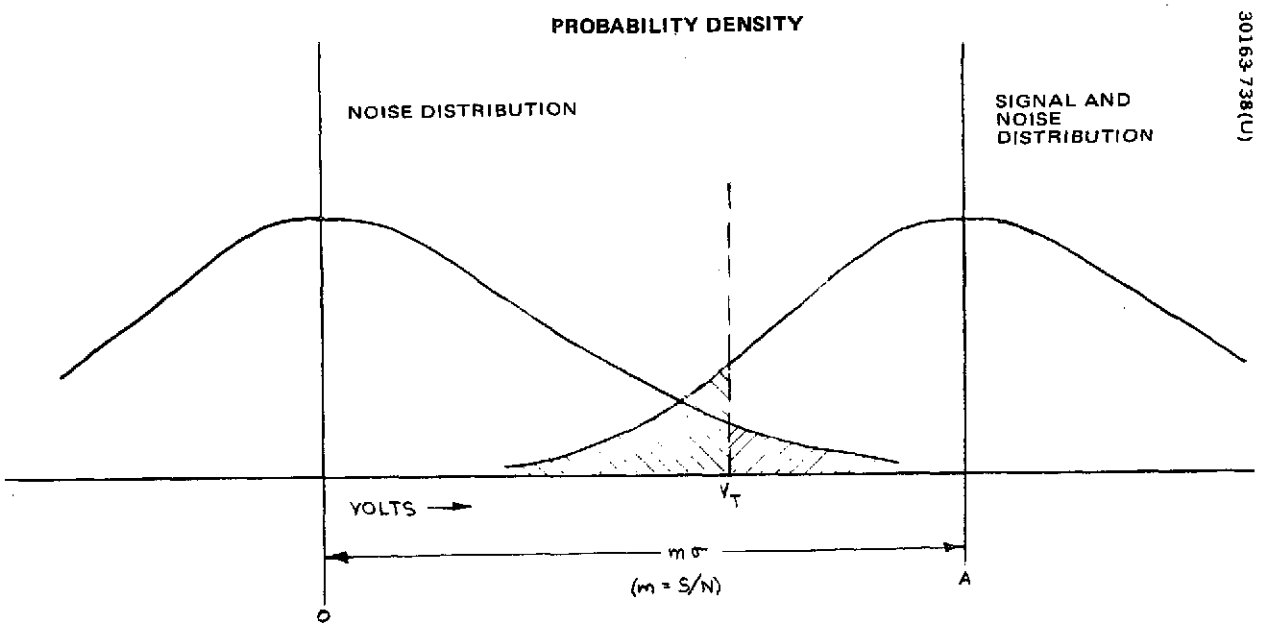

FIGURE C-9. PROBABILITY OF FALSE ALARM AND SIGNAL DETECTION

ATTITUDE DATA PROCESSOR DESIGN

The attitude data processor (ADP) is a digital electronics unit. Two redundant units are used in each spacecraft.

The ADP electronics unit will be a new design due to the particular operational requirements of the Pioneer Venus mission. However, the designs of many of the functional blocks, such as the sensor buffer circuits, phase lock loop, command decoder logic, crystal controlled clock and power supply, are derived from existing Hughes designs. The ADP provides the data processing for both the sun and star sensors. This eliminates duplication of time interval measurement electronics in each sensor; thus, resulting in a minimum cost design. Table C-7 summarizes the characteristics of the ADP unit. The ADP unit block diagram is shown in Figure C-10. It has been partitioned into the following subunits:

1) Inertial reference generator

2) Attitude sensor processor

3) Jet control electronics

4) Input/output electronics

Inertial Reference Generator

The inertial reference generator contains the following blocks:

1) Phase locked loop

2) Sun sensor buffering

3) Star sensor buffering

4) Star gate 1 logic

5) Star gate 2 and star advances logic

6) Angle delay generator

Phase Locked Loop

The phase locked loop (PLL) receives as its input the sun pulse or the star 1 pulse, as commanded, for use as the selected inertial reference (SIR). The following outputs are available from the PLL:

1) Fs (which is the PLL output at the SIR reference frequency and phase)

TABLE C-7. ATTITUDE DATA PROCESSING ELECTRONICS CHARACTERISTICS SUMMARY

Physical Characteristics	
Parts count	200 integrated circuits; 300 discretes
Weight	1.6 kg (3.6 lb)
Size	23.1 x 14.7 x 6.9 cm (9.1 x 5.8 x 2.7 in.)
Average power dissipation	4 W JCE ON; 3.7 W JCE OFF
Performance	
Inertial reference generator (phase lock loop)	
Phase locked loop maximum quantization	12 bits
RPM range	4.4 to 70 RPM (commandable in 4 ranges)
Delayed SIR range	0 to 360 deg
Delay quantization	10 bits
External outputs (fs = spin rate clock)	
To DCE	Fs, 2^{12}Fs
To science	Fs, 2^{10}Fs
To small probe release	Delayed SIR
Attitude determination (time interval measurements)	
Clock rate	2 kHz
Maximum range	16 bits
Inputs	Sun pulses, star pulses, MIP
Jet control electronics	
Number of axial jets	3
Number of radial jets	4
Firing modes	Angle, time
Angle mode pulse widths	30 ms ±1 and 117 ±3 ms
Countdown logic	12 bits
Angle mode	2^{12} revolutions
Time mode	2^{11} seconds
Command	
Magnitude word commands	6 words of 10 bits each
Pulse commands	7
Telemetry	
Digital telemetry	9 words of 8 bits each
Analog and bilevel	TBD

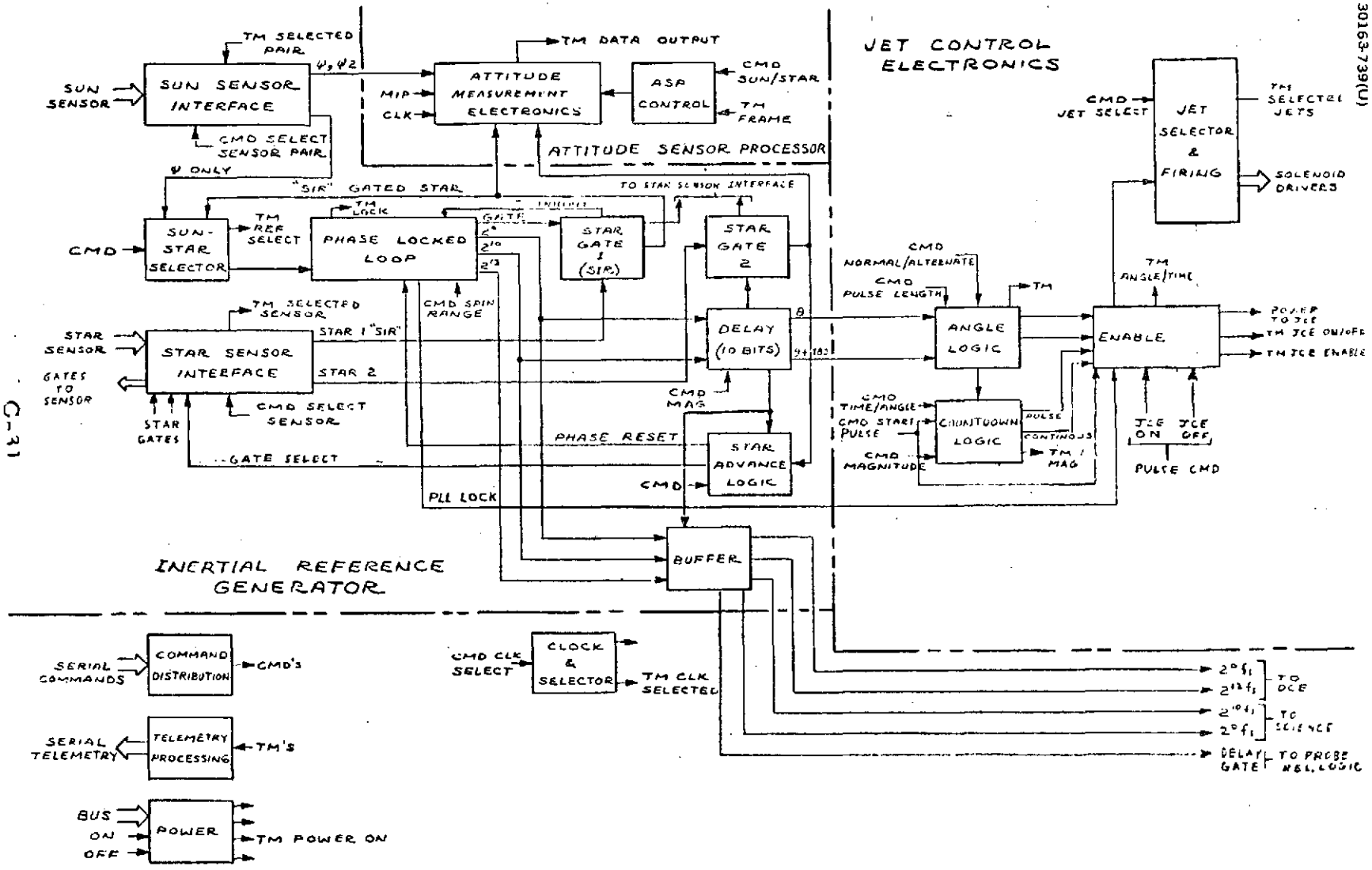

FIGURE C-10. ATTITUDE DATA PROCESSOR UNIT

30163-739(U)

2) 2^{10} Fs
3) 2^{12} Fs

} Multiples of the reference frequency

4) Gate output at the reference frequency starting at 355 deg and ending at 5 deg.

5) PLL loss of lock (when the phase lock is lost).

The PLL samples the error between the SIR and Fs pulses once per revolution. This voltage is held and applied to the loop shaping network for the complete revolution. The shaping network, in turn, drives a voltage controlled oscillator (VCO) which produces 2^{12} Fs. The 2^{12} is divided down to provide 2^{10} Fs and Fs. Any error between the Fs and SIR changes the VCO frequency until both signals are phased and frequency locked.

When the input reference is missing during a revolution, the error is set to zero for one more period as this absence can be caused by noise, particularly on stars of weak amplitude. Several consecutive misses will cause the loop to try to lock to any reference and produce the PLL loss of lock signal which, in turn, will stop any jet firing. The PLL loss of lock signal is provided to telemetry as is the count of the number of times SIR was missed since the last telemetry sample.

Sun Sensor Buffering

The sun sensor buffer circuits process the ψ and $\psi 2$ signals from any of the three pair of sun sensors by amplifying, shaping, and threshold detecting. Three bits of a magnitude command selects one of three available pairs of sun sensor slits.

Star Sensor Buffering

The star sensor buffer circuits selects the outputs of two star sensors slits (ψ^*, ψ^*2) for data processing. The star sensor buffer also provides gate 1 (SIR gate) to the ψ^* sensor slit. The sensor output occurring in gate 1 is called "Star 1." Gate 2 (delayed gate) is provided to either star sensor the ψ^* or ψ^*2 slit as selected by ground command. The sensor output occurring in gate 2 is called "Star 2."

Star Gate 1 Logic

The star gate 1 logic accepts the star 1 pulse and the gate signals to produce the gated star signal which may be used as selected inertial reference (SIR). The gate also produces an inhibit signal which prevents the PLL from updating its output frequency if no SIR is detected during the angular period of -5 to 5 deg. When the SIR is missing in several consecutive revolutions, the PLL loss of lock signal is produced, and the inhibit signal removed.

Star Gate 2 and Star Advance Logic

The star gate 2 logic accepts the delayed gate produced by the delay logic and the star sensor output pulse and provides a gated star 2 output. A ground command which controls sensor slit is gated for attitude data measurements The star advance command causes the gated star pulse occurring in gate 2 to reset the phase of the PLL to zero, thus repositioning the star gate 1 to accept the star pulse previously occurring in star gate 2 as the new SIR; i.e., advancing the phase lock from star 1 to star 2.

Angle Delay Generator

The angle delay generator may be used to generate the star 2 gate start angle or the jet fire start angle or small probe release signal. The 10 bit delay word is stored in a delay register. At zero angle, the delay word is transferred to a ripple counter which counts 2^{10} pulse from PLL. A first pulse is produced at the commanded angle (θ) and a second pulse (θ + 180 deg) is produced 180 deg after the first pulse. The first pulse is used by the star 2 gate and sent to the small probe release logic. Both pulses are sent to the angle logic in the jet control electronics.

Attitude Sensor Processor

The attitude sensor processor (ASP) has two blocks:

1) The attitude measurement electronics

2) The ASP control

The attitude measurement electronics is basically a ripple counter which counts clock pulses between various sensor pulses inputs as controlled by the ASP control. The clock rate is 2 kHz and the measured pulse interval data is parallel transferred to a shift register and read serially onto the telemetry line. The ASP control is a two state counter which cycles through the following sun and star modes:

Counter State	Sun Mode Measurement	Star Mode Measurement
1	ψ - Select 1	ψ^* - Select 1
2	ψ - Select 2	ψ^* - Select 2

Select 1 and Select 2 are independently determined by a magnitude command word to be any of the following: ψ, ψ_2, ψ^*, ψ^*_2 or MIP. The control counter mode and selected star pulse are added as an address to the measured data.

Jet Control Electronics

The jet control electronics (JCE) has the following component blocks:

1) Jet select and firing

2) Enable logic

3) Angle logic

4) Countdown logic

Jet Selector and Firing and Enable Logic

The jet selector selects by ground command any or all of the three axial (two axial on the probe) and four radial jets. Ground command selects whether the jets are fired from pulses from the angle logic or continuously for a commanded time. The jets can be fired at the commanded delayed angle θ or (if two pulse mode is commanded) at θ and also at $\theta + 180$ deg. The enable logic stores the time/angle command and enables the appropriate firing bus line. The enable logic also switches power to the rest of the JCE. Power is turned on only by a "JCE ON" pulse command. Power is turned off by a "JCE OFF" pulse command, a PLL loss of lock signal or completion of the firing sequence. The enable logic is set to the disable state at power turn on and can only be enabled by a JCE start pulse command.

Angle Logic

The angle logic produces pulses 30 or 117 ms wide at the fire angle generated by the delay generator. The pulse width is commanded by ground command.

Countdown Logic

The countdown is a 12-bit counter which counts either 0.5 sec clock time pulses or the number of θ pulses fired. The counter is preset with a number representing the desired number of pulses fired or the desired length of time. The counter is started by a "start" pulse command and ends when the full count has been reached. An initialization signal or a loss of PLL lock will also stop the execution of a maneuver in progress.

Input – Output Electronics

This subunit contains the following blocks:

1) Command distribution

2) Telemetry processing

3) Power conditioning

4) Clock

Command Distribution

The command distribution (CD) receives the commands sent to the ADP from the command subsystem and generates the proper signals to enable the distribution of these commands to their destination. The magnitude commands are received serially and transmitted in parallel to subunits. Pulse commands are buffered by the CD.

Telemetry Processing

The telemetry processing collects the digital telemetry lines throughout the unit and sends out the data serial format compatible with the telemetry subsystem. Analog telemetry is sent directly to the data subsystem.

Power Conditioning

The power conditioning subunit performs the following functions:

1) Generates several regulated dc voltages

2) Protects the unit from bus variations and bus transients

3) Separates power and signal returns

4) Provides power on/off buffering and switching

5) Provides failure protection (overvoltage and undervoltage protection, current limiting and fusing)

The power is turned on and off by pulse commands.

Attitude Data Processor Tradeoff Summary

The basic tradeoffs in the electronics mechanization are summarized below. No tradeoffs were performed where the requirements lead to a single simple mechanization. Tradeoffs on the detailed circuit design are beyond the scope of this study. All factors are stated as a percentage of a single baseline ADP unit.

Phase Lock Loop

Factor	Analog (Baseline), percent	Digital (Alternate) percent
Weight	15	25
Failure rate	10	25
Risk	Low	Low
Cost	10	25
Performance	Meets specification	Better

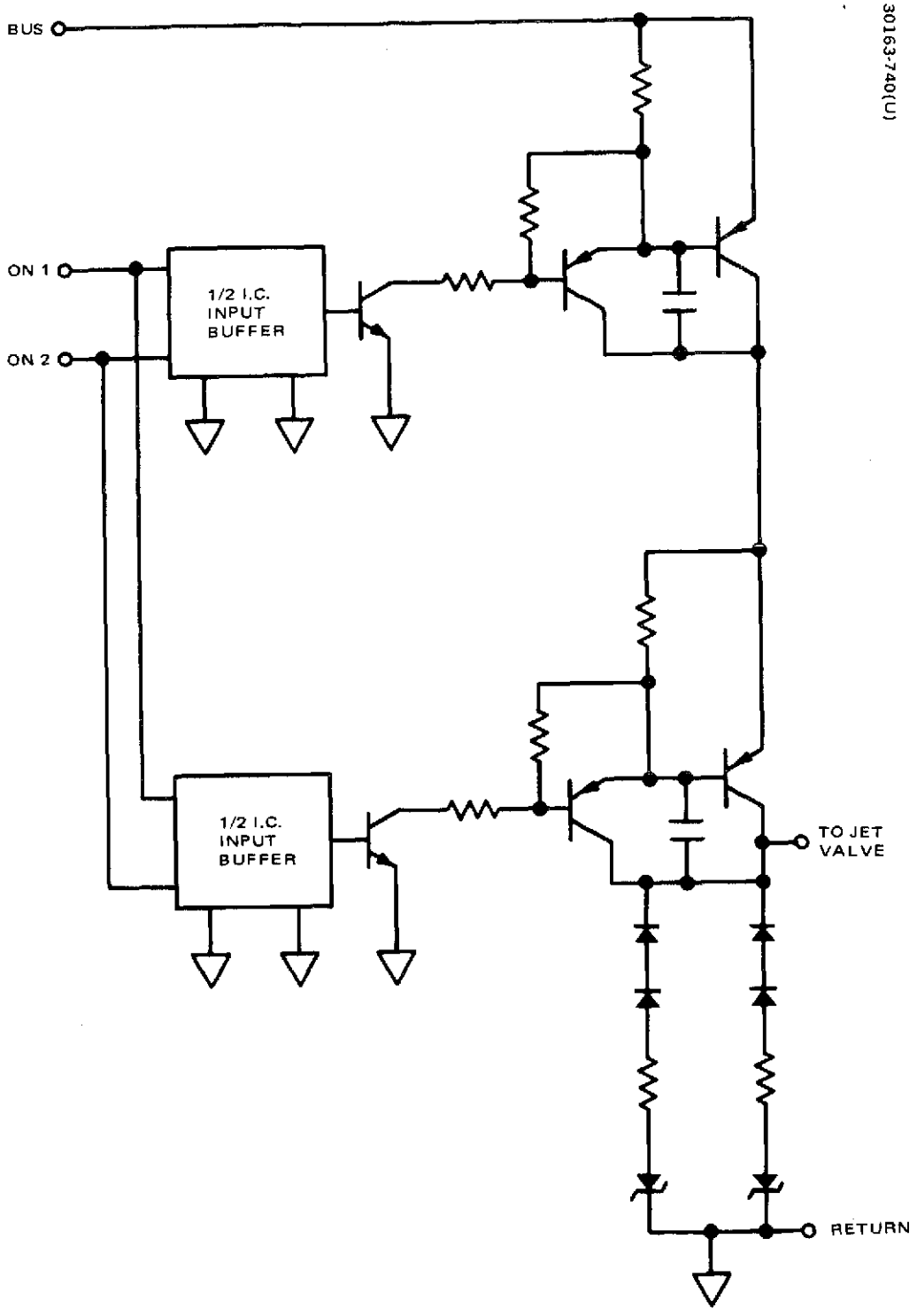

FIGURE C-11. TYPICAL SOLENOID DRIVER

Delay Gate for Star, JCE & Probe

Factor	Shared (Baseline), percent	Separate (Alternate), percent
Weight	4	10
Failure rate	6	15
Risk	Same	Same
Cost	5	12
Performance	Meets specification	More flexible

Logic Components Selection

Factor	(Baseline) Standard TTL, percent	(Alternate) Custom MOS LSI, percent
Weight	40	20
Failure rate	50	25
Risk	Low	High
Cost	40	High development
Performance	(LSI is difficult to change for requirement changes)	

SOLENOID DRIVER ELECTRONICS UNIT DESIGN

The solenoid unit (one per spacecraft) provides drive power for the reaction control jets and latching valves. Properly timed command signals are provided by either of two ADP (JCE) units. The latching valve commands are generated in the command decoders (command subsystem). Each latching valve driver consists of one ON and one OFF driver.

To preclude a single component failure from inadvertently firing a jet, series redundancy is incorporated in the solenoid drivers. Each driver consists of two power transistors in series, each with its own predriver circuitry. Surge suppression diodes are series-parallel redundant. Design simplification is achieved by making all drivers identical. A typical driver circuit is shown in Figure C-11. The solenoid driver design has been space flight proven on several Hughes built satellites, i.e., Intelsat IV, and Telesat.

The solenoid driver electronic unit design is a modification of the Intelsat IV satellite design. The modification will require minor logic changes and the addition of one driver circuit for the orbiter spacecraft. Table C-8 summarizes the characteristics of the solenoid driver unit.

Solenoid Driver Tradeoff Summary

Three basic configurations were considered for the solenoid driver mechanization (seven jet valve drivers and four latching valve drivers).

TABLE C-8. SOLENOID DRIVER UNIT CHARACTERISTICS SUMMARY

Physical Characteristics	
Parts count	ICs; discretes
Weight	1.0 kg (2.2 lb)
Size	25.4 x 15.2 x 3.8 cm (10 x 6 x 1.5 in)
Power	0.05 W (nominal) plus 3.0 W/active jet
Performance	
Number of drivers	Seven jet valve Two latching valve ON Two latching valve OFF
Electrical characteristics, each driver	
Output current	1.0 A maximum
Bus voltage drop	3.0 V maximum at 1.0 A
ON/OFF delay	150 μsec maximum
Rise/fall time	1.0 ms maximum

They are as follows:

1) Eleven identical two transistor (redundant drivers similar to Intelsat IV/OSO (22 power transistors).

   Weight 2.0 lb

   Standby power 33 mW

   Advantage. High reliability, lowest risk and development cost

   Disadvantage. Weight and power

2) Four redundant latching valve drivers, nonredundant jet valve drivers, with two line switches (17 power transistors).

Weight	1.89 lb
Standby power	18 mW

Advantage. Lower weight and power than (1)

Disadvantage. Additional commands for line switches, less redundancy

3) Eleven identical two-hybrid drivers mounted in ADP unit.

Weight (added to ADPs)	1.0 lb
Standby power	33 mW

Advantage. High reliability, lowest weight

Disadvantage. Requires development of hybrid and mounting technique, highest risk, long development time.

Configuration (1) was chosen as the baseline on the basis of greatest redundancy at the lowest risk and cost.

DESPIN CONTROL ELECTRONICS (DCE)

The despin control electronics (DCE) uses shaft angle encoder (SAE), master index pulse (MIP) and attitude data processor (ADP) pulse trains to provide motor drive signals which point the orbiter high gain antenna towards the earth. The DCE description has been partitioned into the following topics:

1) Position loop and sector signal processing

2) Rate loop signal processing

3) Ground command torque bias

4) Motor drive operation

5) Failure detection/correction logic

Position, rate, and command bias capability was covered in Subsection 5.4. To facilitate understanding of the despin control system. Items 4 and 5 are covered below.

Motor Drive Operation

The baseline motor is a dc brush motor with K_T = 0.9 ft-lb/A and motor resistance of 45 ohms. The motor driver will be a voltage controlled voltage source. The output bridge is able to apply voltage of either polarity to the motor. The motor driver will be current limited to protect the electronics and brushes from a shorted motor coil. Each unit will drive its own set of motor brushes.

Failure Detection/Correction Logic

A relative rate of the wrong polarity will be detected with a MIP 2 input a few deg from the MIP, and corrective torque applied through the rate loop. When too large a relative rate of either polarity is detected, the unit will be shut off.

Overvoltage and undervoltage detection in the power supply can turn the unit off and prevent possible spurious operation.

Despin Control Electronics Characteristics Summary

Physical Characteristics

1)	Parts count	≈125 integrated circuits ≈520 discretes
2)	Weight	3.7 lb
3)	Size	10.0 x 5.8 x 2.7 in.
4)	Average power dissipation	3.3 W with motor driver off 5 W with motor driver at 0.05 ft-lb friction torque
5)	Peak power dissipation	13 W peak

Electrical Characteristics

1)	Position loop gain	0.5 ft-lbs/rad
	a) Position loop quantization	0.176 deg

	b)	Position loop range	±11.25 deg (±0.098 ft-lb)
	c)	Position loop sample rate	16 x (spin speed)
	d)	Position integrator gain	0.05 ft-lb/rad/sec
	e)	Ground command pointing quantization	0.352 deg
2)	Sectors		16 sectors of 22.5 deg
3)	Rate loop gain		3 $\frac{\text{ft-lb*}}{\text{rad/sample}}$
	a)	Rate loop quantization	0.00153 rad/sample
	b)	Rate loop range	±0.046 rad*/sample (±0.147 ft-lb*)
	c)	Rate loop sample rate	128 x (relative rate)
4)	Ground command torque quantization		0.0094 ft-lb ±0.15 ft-lb
5)	Ground commands		3 magnitude 7 pulse or bit
6)	Telemetry outputs		2 analog 1 bilevel
7)	Reference inputs		Fs 2^{12}Fs MIP SAE MIP 2

Despin Control Electronics Tradeoff Summary

The basic tradeoffs in the electronics mechanization are summarized below. These tradeoffs only consider the electronics design and not the sensor or motor complexity. No tradeoffs were performed where the requirement led to a single simple mechanization. The factors below are stated as a percentage of a single baseline DCE.

*These may be doubled by ground command.

Electronics For Motor Types

Factor	(Baseline) Brush Motor, percent	(Alternate) Brushless Motor, percent
Weight	10	30
Failure rate	7	20
Risk	Low	Low
Cost	8	25
Performance	–	20 more power

Motor Crosstrapping

Factor	(Baseline) Redundant Brushes, percent	(Alternate) Relay Switching, percent
Weight	0	15
Failure rate	0	5
Risk	Low	Low
Cost	0	5
Performance	–	–

Encoder for MIP and SAE

Factor	(Baseline) Optical Encoder, percent	(Alternate) Magnetic Encoder, percent
Weight	4	13
Failure rate	4	15
Risk	Low	Low
Cost	5	15
Performance	–	Noise problems

Logic Component Selection

Factor	(Baseline) Standard TTL, percent	(Alternate) Custom MOS LSI, percent
Weight	25	10
Failure rate	60	15
Risk	Low	High
Cost	35	High development
Performance	LSI is difficult to modify for control parameters which typically change late in the program.	

Analog Versus Digital Processing

The most basic tradeoff in the design of the DCE electronics was whether the position and the rate loop processing shall be performed with analog or digital signal processing circuits. The accuracies and sample times are not as critical as they have been in previous Hughes DCE designs, thereby making the analog approach seemingly attractive. However, analog approach for the error processing was discarded because of the large spin speed range which yielded a loop gain which was inversely proportional to spin speed. Thus, in order to achieve the necessary stability margins over the entire spin speed range, numerous commandable gain changes would have to be incorporated into the analog error processing design. This, in turn, results in a higher parts count, higher cost and lower reliability. The digital approach chosen varies the error sample period with the spin synchronous clock from the phase lock loop, therefore, maintaining a constant gain with spin speed.

BEARING AND POWER TRANSFER ASSEMBLY

The BAPTA provides the mechanical and electrical interface between spinning and despun sections of the spacecraft; its role, therefore, is both structural and functional. The assembly, shown in cross sectional view (Figure C-12) consists of four major subassemblies.

1) Brush motor assembly (provides despin control torque)

2) Main bearing assembly (provides relative rotation)

3) Master index pulse generator (MIPG) and shaft angle encoder (SAE) (provides relative azimuth angle data)

4) Electrical contact ring assembly (ECRA), provides electrical power across the spinning/despun interface.

The BAPTA design is the result of extensive experience in the design, fabrication, test, and successful orbital operation of high reliability despin bearing assemblies for Hughes Tacsat, Intelsat IV, and Telesat Domestic and Military Satellites. Design characteristics of the BAPTA are summarized in Table C-9 for the one motor design criteria and Table C-10 for two motor design criteria.

The BAPTA design minimizes the use of screw-threads, screws, and lock wire within the spinning housing structure. Where their use is unavoidable, integrally machined bosses are employed to ensure entrapment of metallic chip debris in blind (nonthrough) threaded holes.

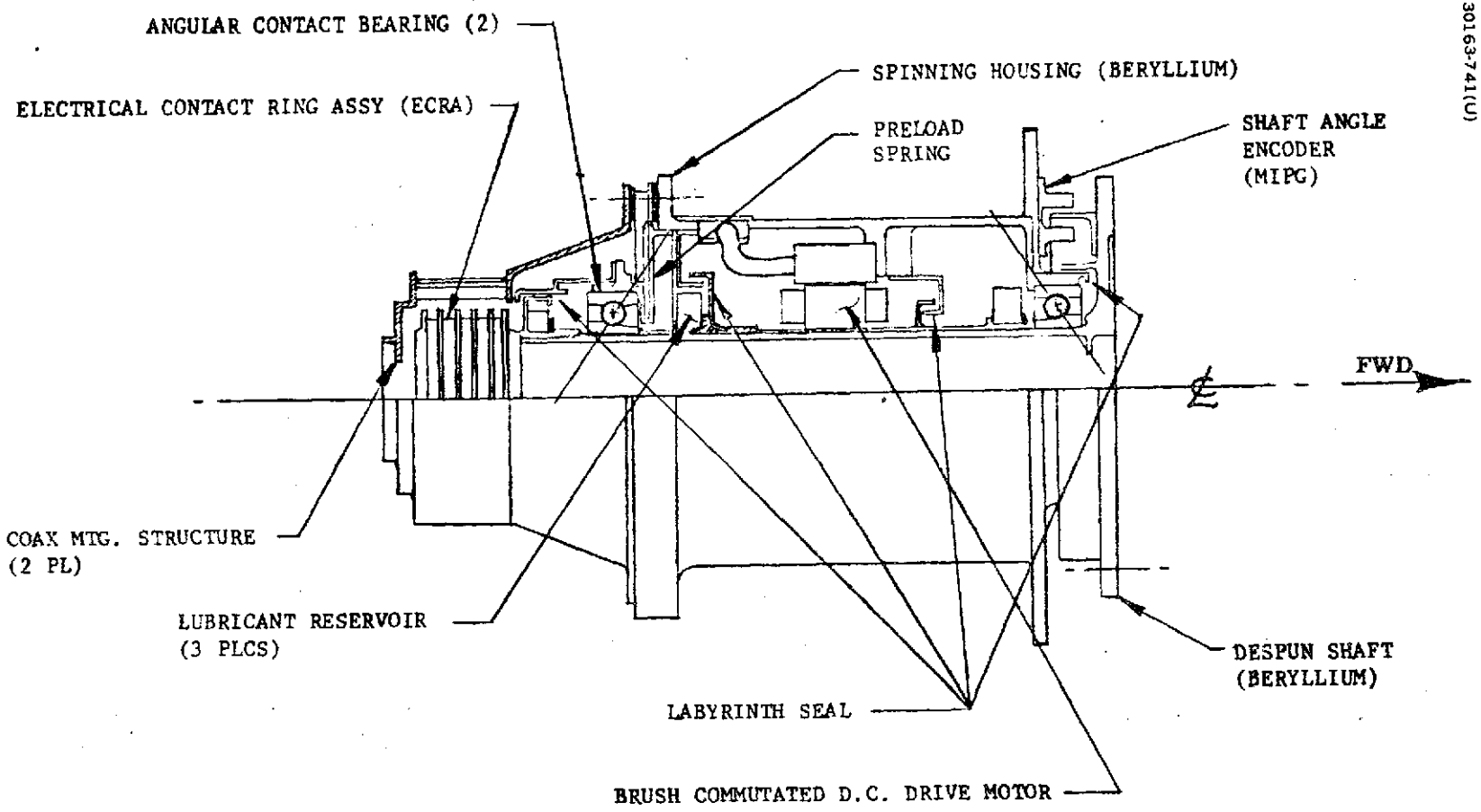

30163-741(U)

FIGURE C-12. BAPTA SINGLE MOTOR DESIGN

TABLE C-9. BAPTA DESIGN CHARACTERISTICS – SINGLE MOTOR DESIGN CRITERIA

Parameter	Capability
Bearings:	
Type	Angular contact, 40.0 mm bore, 16 balls 5/16 in. diameter, 440C CEVM material, Class ABEC 9, Grade 5 balls
Loads (static)	
Radial	2900 lb.
Axial	4120 lb.
Motor:	
Peak torque, 24V, 0 rpm	0.49 ft-lb
BAPTA friction torque, maximum	0.10 ft-lb (at 35 rpm and 30°F)
Torque margin	4 to 1 (minimum volts, maximum friction)
Torque sensitivity (K_T)	0.92 ft-lb/A ± 10 percent
Back EMF (K_B)	1.248 V/rad/sec ± 10 percent
Motor type	Brush commutated dc torquer, dry lubricated brushes (Boeing 046-45 compact matl)
Speed range (ω_s)	0 to 35 rpm
Pulse generators	
MIPG	Single pulse/rev
SAE	Shaft angle encoder (128 pulses/rev.)
Rotational sense	Direction readout capability
Pulse output	≈2V across 10 KΩ resistor
Type	Solid state, light emitting diode
ECRA	
Signal rings	Two circuits } 1A at 75 A/in^2 per brush
Power rings	Three circuits } 1A at 75 A/in^2 per brush
Physical Data	
Total weight	<11.2 lb. (incl 0.70 lb. coax-cable)
Size	≈9.3 length x 6.5 diameter

TABLE C-10. BAPTA DESIGN CHARACTERISTICS – REDUNDANT MOTOR DESIGN CRITERIA

Parameter	Capability
Bearings:	
Type	Angular contact, 40.0 mm bore, 16 balls, 5/16 in. diameter, 440C CEVM material, Class ABEC 9, Grade 5 balls
Loads (static)	
Radial	2405 lb.
Axial	4120 lb.
Motor:	
Peak torque, 24V, 0 rpm	0.30 ft-lb per motor
BAPTA friction torque, maximum	0.15 ft-lb (at 35 rpm and 30°F)
Torque margin	2 to 1 per motor (minimum volts, maximum friction)
Torque sensitivity (K_T)	1.16 ft-lb/A ± 10 percent
Back EMF (K_B)	1.57 V/rad/sec ± 10 percent
Motor type	Brush commutated dc torquer, dry lubricated brushes (Boeing 046-45 compact matl)
Speed range (ω_s)	0 to 35 rpm
Pulse generators	
MIPG	Single pulse/rev
SAE	Shaft angle encoder (128 pulses/rev.)
Rotational sense	Direction readout capability
Pulse output	≈2 V across 10 K resistor
Type	Solid state, light emitting diode
ECRA	
Signal rings	Two circuits } 1 A at 75 A/in^2 per brush
Power rings	Three circuits }
Physical data	
Total weight	<13.4 lb. (incl 0.70 lb. coax cable)
Size	≈9.3 length x 6.5 diameter

The bearings, preload spring and assembly housing/shaft are designed for adequate structural stiffness to attain acceptable dynamic response of the supported spacecraft sections during launch accelerations. Bearing suspension and preload design compensate for local thermal gradients over the mission operating temperature range, to minimize frictional torque variation.

The component tradeoffs performed involved a brush versus brushless motor study and several types of shaft angle encoders. The tradeoff study on both of these items is presented in Tables C-11 and C-12, respectively. The detail rationale for the selection of the brush mode and optical shaft angle encoder is given in the Tradeoff Section.

Brush Motor Assembly

The brush motor assembly employs a single brush commutated dc torque motor as the baseline design. As mentioned previously, a brush motor assembly employing two brush commutated dc torque motors was considered for reliability considerations. Both designs are presented herein with emphasis on the single motor design. These direct-drive torquers are particularly suited to high torque at low speed applications. They provide a large torque-to-inertia ratio at the load shaft, high acceleration capability, high coupling stiffness, and high mechanical resonant frequency.

The motor selected for the low inertia control system resulted from an optimization study/evaluation of available direct-drive dc torque motor candidates. The motor design criteria are as follows:

1) Minimum bus voltage = 26 Vdc

2) Bus to motor voltage drop = 2 Vdc, maximum

3) Maximum motor speed required = 35 rpm = 3.66 rads/sec

4) BAPTA system friction, maximum (magnetic + coulomb + viscous) at 35 rpm, and initial temperature = 30°F — 0.10 lb-ft (0.15 lb-ft for two motors)

5) At minimum bus voltage, the motor shall be capable of providing torque equal to 4 (2 for motor case) times the maximum system friction torque.

TABLE C-11. BAPTA MOTOR TRADEOFF SUMMARY

Characteristics	Brush-Type Torquer	Brushless-Type Torquer
Wear	Brush-wear small and predictable	None
Mechanical friction	Low-commutation brush friction	None
Torque ripple	≈5 percent operating torque	≈2 percent operating torque
Motor drive electronics	Relatively simple Mass ≈ 0.45 kg (1.0 lb)/ spacecraft Cost ≈ 20K/spacecraft	Complex Mass ≈ 0.91 kg (2.0 lb)/ spacecraft Cost ≈ 50K/spacecraft 20 percent higher power dissipation
Motor cost ratio	1	1
Motor availability	Available Off-shelf designs can be modified to suit	Available Telesat motor is capable of modification
Failure mode	Winding short/open brush/commutator failure	Winding short/open
Motor mass	0.98 kg (2.15 lb)	1.22 kg (2.70 lb)
Motor reliability	0.994 (600 failures/10^9 h)	0.9994 (74 failures/10^9 h)
Historical experience	Surveyor mechanicms TACSAT 3 year mission lasted 3.8 years HS-331 } 1 year mission (OSO) } 4 year design	Intelsat IV 7 yr mission (4 spacecraft in orbit) Telesat 10 yr design (2 spacecraft in orbit)

TABLE C-12. SHAFT ENCODER TRADEOFF SUMMARY

Characteristics	Optical Encoder, with Gallium Arsenide Emitter-Detector	Magnetic Encoder Employing Passive Pickup	Magnetic Encoder Employing Active Pickup	Mechanical Encoder
Wear	None	None	None	Yes
Failure mode	Power supply emitter or detector	Winding open or short	Winding open or short, power supply	Wear of contacts (good only to 10^7 revolutions)
Friction or drag	None	Not measurable	Not measurable	Small
HAC historical experience	None space qualified for NASA	HS312, 318, 333, 331	None – Extensive aircraft engine usage	None
Availability in this size	Yes	Yes	Yes	Yes
Power requirement	≈0.15 W for three light sources (0.05 W each)	None	0.012 W for three pickups	Friction torque dissipation, contact current
Detector weight, kg (lb)	Σ = 0.14 (0.30)	Σ = 0.51 (1.13)	Σ = 0.18 (0.37)	Σ = 0.06 (0.13)
Commutator weight, kg (lb)	Disc = 0.11 (0.25)	Serrated annulus: 0.45 (1.0) (ferromagnetic)	Serrated annulus: 0.36 (0.8) (ferromagnetic)	Commutator disc approximately 0.1 (0.6)
Installed total weight, kg (lb)	Generous separation between disc and detector: no bearing or coupling required. Weight = 0.27 (0.60)	Annulus plus three pickups = 1.02 (2.25)	Annulus plus three pickups = 0.57 (1.25)	Brush plus disc 0.15 (0.35)
Output	2 V pulse across a 10KΩ resistor	0.050 V at 4 rpm, 0.750 V at 60 rpm (peak-peak) at 0.008 in. gap	0.2 to 0.5 V (peak-peak) at 0.015 in. gap	Depends upon contact resistance
Special precautions	Focused (available) light source required to obtain clearances greater than 0.051 cm (0.020 in.) between disc and detector. Slotted metal disc to minimize capacity/reflection	Tooth spacing and thickness is critical to smoothness of wave shape. Two rings required to obtain directional information.	Same as passive pickup. Minimum tooth size for any speed must be ≥ 0.102 cm ≥0.040 in.)	Protect the contacts during vibration against wear
Size (detector), cm (in.)	2.54 L x 1.02 H x 0.76 wide (1.00 L x 0.40 H x 0.30 wide)	3.0 x 2.5 x 1.9 (1.2 x 1.0 x 0.75 in.) for each pickup	1.1 x 3.8 (7.16 dia x 1.5 long) for each pickup	Wiper configuration
Environment survivability	0° to 100°C space qualified by NASA	-40° to +90°C. No problem surviving aircraft engine or spaceborne dynamic environments	Same as passive pickup	No temperature problem. Some bounce may occur during vibration.

TABLE C-13. COMPARISON OF DC BRUSH TYPE MOTOR SPACE APPLICATIONS

		Ref	Number of Units	Vacuum Exposure Duration (Years) (1)	(2)	(3)	(4)
Wet lubricated Apiezon "C" plus lead napthanate	OSO I despin (space)	1	1				
	OSO II despin (space)	1	1				
	OSO III despin (space)	1	1				(20.2)
	OSO IV despin (space)	1	1				
	TACSAT I (space)	2	1				(105)
	TACSAT I life (lab)	3	1				(54)
	Hughes fixture drive (lab)	4	1				
Dry lubricated Boeing 046-45	OLSCA (test)		1				
	FRUSA (space)		2				
	ATM (test)		1				(26.2)
	BBRC (silver) (test)	(5-1)	6				
	BBRC (gold) (test)	(5-2)	6				
	BBRC (copper) (R&D) (test)	(5-3)	8				
	SPAR (R&D) (test)	(6-2)	1				
	Fairchild (test)	(6-4)	1				(24.0)
	NASA (development test)	(7-1)	Several				(114.0)
	NASA (for ATM) (test)	(7-2)					(26.0)
	Surveyor						
	Skylab						
	Navy (classified) (space)		Many				
				1 2 3 4	5 6 7 8	9 10 11	12 13 14

Component revolutions (x 10^6)

Motor Brushes

Features of the motor design include redundant cartridge held brushes employing constant force negator springs. Fully encapsulated motor windings and laminations ensure electrical and mechanical integrity, and preclude damage during handling. A high reliability of success can be predicted for the dry lubricated brush design employed by the spacecraft motor or motors. This material is relatively insensitive to speed and is not susceptible to time and temperature dependent effects such as oil migration and evaporation, and brush hydrodynamic planing, as are wet lubricated brushes. Table C-13 illustrates the dry lubricated compact space mission usage versus a wet brush design.

Brush/Commutator Materials

1) Brushes – dry lubricated compact (Pure Carbon Co. #PM105) molybdenum/tantalum/MoS_2 (same as Boeing #046-45).

2) Commutator –

   a) Material: pure copper (ETP/QQ-C-576)

   b) Finish: 16 μin.

Main Bearing Assembly

The main bearing assembly consists of a beryllium shaft and housing utilizing both integral and fitted labyrinth seals, a 15-5 PH CRES preload spring, and two 440 C CEVM angular contact ball bearings. This portion of the BAPTA provides the mechanical interface between spinning and despun sections of the spacecraft. The spacecraft despun platform and antenna support structure are mounted to the BAPTA shaft. The spacecraft rotor support structure mates directly with the BAPTA outer housing forward flange. The BAPTA is electrically isolated at both mounting interfaces (10 KΩ/min resistance) to preclude stray current passage through the bearings. Additional protection is provided by grounding the spinning and despun BAPTA structure via a slip ring such that a static charge cannot build up to cause trickle current discharge through the bearings.

Bearings

The bearings selected are stainless steel angular contact bearings, having a 40 mm bore. A nominal contact angle of 25 deg minimizes the Hertzian stresses due to combined axial and radial loads imposed during launch, apogee motor burn, and orbital operation. The ball and race material is 440C consumable electrode vacuum melt (CEVM) stainless steel. This material provides maximum corrosion stress resistance, and a minimum of foreign particle inclusion, to maximize bearing fatigue life. The race hardness is a minimum of 58 on the Rockwell C scale; the balls are 1 to 2 points harder. The bearings are manufactured to AFBMA ABEC-9 class

TABLE C-14. SIGNIFICANT TEST AND APPLICATION EXPERIENCE

Lubricant	Satellite or Vacuum Test	Pressure, Torr	Temperature, °F	Speed, rpm	Load, lb	Duration, h	Number of Bearings and Size	Remarks
*Vac-Kote	OSO 1 through V	10^{-8}	50 nominal	30	2 to 5	152,000 total (17,000 to 42,000 h)	3308 - R18	Duty cycle; on 40 min, off 20 min
*Vac-Kote	Various ground vacuum test	10^{-8} to 10^{-8}	50 to 70	30 to 60	0.5	28,600 total (4,800 to 13,200 h per test)	2 at 1 in. outside diameter 1 - 3308 1 - R18 6 -	OSO
*Vac-Kote	TACSAT	10^{-8}	75	60	150	25,000	2 each	In orbit since February 1969; still operating successfully after 3.5 years
*Vac-Kote	Intelsat IV F-2 through F-5	10^{-8}	Cycling 70 to 100	60	60	25,900 total (1,600 to 13,000 h)	2 per spacecraft 3,543 bore	All four spacecraft still operating successfully in orbit
*Vac-Kote	Intelsat IV BAPTA vacuum life test	10^{-8}	Cycled 0 to 100	60	60	8,600	2 each, 3,543 bore	Test concluded - successful (1 year operation)
Hughes Lube (HMS 20-1727)	Basic Bus Satellite BAPTA vacuum life test	10^{-8} to 10^{9}	Cycled 5 to 110	60	150	16,000	2 each of 2 sizes (BAPTA and ECRA). 5,905 and 1.5 bore	Test presently operating (started November 1970)
Hughes Lube (HMS 20-1727)	Telesat bearing vacuum life test	10^{-8}	70	100	45	6,500	2 each, 2,362 bore	Test concluded - successful
Hughes Lube (HMS 20-1727)	Various short vacuum tests	10^{-8}	70	60 to 100	60	6,500 in intervals of 100 to 1,000 each test	2 to 6 bearings per test 2,362 bore	All tests successful
Hughes Lube (HMS 20-1727)	Vacuum test	10^{-8}	130	60, 120 and 180	10, 20 and 40	5,270	1 each 1.5 bore	Test concluded - successful
Hughes Lube (HMS 20-1727)	OSO bearing life test	1×10^{-6}	76	6	60	1,500	2 each, 3,543 bore	Test presently operating successfully

*Vac-Kote is a lubricant that is in the same family as the Hughes HMS 20-1727 Aprezon C lead napthanate system. Analysis cannot distinguish between Vac-Kote and the Hughes material.

tolerances and utilized grade 5 balls. One shoulder of the inner race is machined away to allow disassembly without the use of force or differential heating and cooling techniques. The retainer design is outer race riding, and retains the balls with the outer race after removal of the inner race. These nonstandard features greatly simplify BAPTA assembly.

Preload Spring

An axial load must be applied to the angular contact bearings to maintain ball-to-race alignment, to prevent ball skid, and achieve the required bending stiffness during operation. Use of an axially soft preload spring in conjunction with the angular contact bearings enables the assembly to absorb large thermal gradients and temperature excursions without significant radial differential expansion (such as cold outer race, hot inner race) the races move axially, to change the contact angle and use up part of the bearing diametral clearance. Longitudinal (axial) differential expansion is absorbed directly by axial motion against the preload spring.

The axial load is provided in the BAPTA by a Hughes developed system utilizing a single flexural preload spring on the aft bearing. This preload system combines high radial stiffness with low axial stiffness, and avoids the difficulties inherent in conventional wavy washer or helical coil spring concepts installed against a slip fit sliding race. Radial looseness of the sliding race in the conventional preload system can cause nutational instability and contribute to spin axis wobble. The Hughes developed system also avoids the possibility of sliding race wear, cocking, or subsequent jamming in the slip fit diameter.

Lubrication

Selection of Lubricant

The oil selected for bearing lubrication is a mixture of 95 percent Apiezon C low vapor pressure hydrocarbon oil and 5 percent lead nepthanate extreme pressure additive. The oil is controlled by Hughes material specification HMS 20-1727. The special additive material contains approximately 31 percent lead. Consistent with Company policy for materials for spacecraft applications, the lubricant selection was made on the basis of significant successful spacecraft applications and extensive research and testing accomplished at Hughes as detailed in Table C-14. Considerable research has been conducted on the physical and chemical properties of the lubricant, and on oil transfer mechanics from the retainer to the bearing parts. The lead nepthanate surface film has been studied using the electron microscope and spectrographic analysis.

Test and Flight History

Results of continuous testing for 7 months at pressures of 10^{-8} to 10^{-9} Torr on nine different groups of bearings operating at three speeds and three preloads provided data indicating that HMS 20-1727 is an acceptable lubricant for the BAPTA application. During vacuum testing, bearing and lubricant

system performance was monitored with strain gage torque transducers, thermocouples, and lubricant film measurement. There was no indication of failure or impending failure during or after the test. At the conclusion of the test, all bearings appeared well wetted with lubricant and in excellent condition. Wear measurements by neutron activation analysis after the test indicated average wear over the ball and race contacting surfaces of 2 to 5 millionths of an inch. This is on the order of the surface roughness of the races.

In addition to the successful 7-month test at Hughes, a considerable history of successful life test and spacecraft flight experience has been accumulated on bearings lubricated with essentially the same material and process (see Table C-14). The selected lubricant is presently being used in the advanced satellite, Intelsat IV and Telesat spacecraft applications.

A vacuum life test of a complete flight quality BAPTA using HMS 20-1727 lubrication is still operating successfully after having run in the 10^{-9} to 10^{-10} Torr pressure range continuously for the past 28 months. Bearing torque in this life test is running steadily at 0.29 ft-lb with no indication of degradation or impending failure of the bearings or lubricant. A complete Intelsat IV BAPTA was also vacuum life tested for 1 year with no degradation of bearings or lubricant performance. Both life test BAPTAs were thermally cycled over the expected orbital temperature ranges.

Electrical Contact Ring Assembly (ECRA)

The purpose of the ECRA is to transfer electrical power and signals between the spinning and despun sections of the orbiter. The ECRA shaft is mounted on the BAPTA despun shaft, signal and power leads are embedded in the core of the shaft material, and each one is connected to a separate signal or power slip ring. Brushes, mounted on the BAPTA spinning housing, make contact with individual rings to complete the electrical circuits. The leads coming from each ECRA section terminate in connectors for attachment to the spinning and despun mating connectors.

Two separate power paths with a common return and two signal circuits are provided by the ECRA. An electrical ground of the BAPTA bearings is attained by means of a signal level slip ring transfer path to ensure that residual voltage potential between spinning and despun sections is minimized to preclude detrimental current flow through the bearings.

The ECRA is a dry lubricated system utilizing coin silver rings and composite brush material of 85 percent silver, 12 percent MoS_2 and 3 percent graphite. The dry lubricated slip ring technology employed in the BAPTA is the result of extensive long term ground vacuum testing conducted to support the development of power transfer assemblies for previous programs. Design details of the ECRA were borrowed directly from these programs as follows:

1) Brush/ring material: TACSAT, Intelsat IV, and advanced satellites

2) Signal brush design: Advanced satellites

The brushes have been designed for mechanical redundancy so that should one brush on any ring fail to make contact, the ECRA current, noise and voltage drop requirements are met. Shielding is provided on each signal channel, and each circuit is insulated from adjacent circuits.

A summary of the ECRA design characteristics is shown in Table C-15.

Summary of Dry Lubricated Tests

Extensive development testing of dry lubricated slip ring systems has been conducted during recent years at Hughes, as summarized in Table C-16. Over 25 different brush/ring material combinations have been evaluated in long term vacuum tests, with brush wear, brush wear rate, contact resistance, and electrical noise monitored during each test. The best material candidates were tested further to determine the effect on performance of the design variables of brush mount geometry, brush force (pressure), spring rate, contact area, number of brushes per wear track, contact angle, mold pressure orientation, current density, brush and ring surface preparation techniques, and run-in procedures. In addition, the effect on performance of ring surface speed variations was analyzed to determine the validity of accelerated speed testing. Of these parameters, the mechanical characteristic at the brush/ring interface, as provided by the brush support geometry, contact geometry, brush spring rate, and number of brushes per wear track have the strongest effect on performance.

Hughes has recently determined that the vacuum pressure level in the slip ring environment also has a strong effect on noise and wear performance.

Lubrication Process

The brush material proposed is a sintered composite of 85 percent Ag, 3 percent Gr, and 12 percent MoS_2 per Hughes Aircraft Company Specification HMS 20-1652 (Stackpole Carbon Company, Grade SM 476). The brushes are fabricated by mixing powders of the various materials, pressing the mixture into a mold, and maintaining pressure while sintering at a temperature near the melting point of silver. This fuses the silver particles together to provide mechanical strength of the brush, while maintaining a uniform distribution of the solid lubricant through the brush. Pore size in the brush is controlled by the applied pressure and sintering time. The resultant block of material is then cut and dry ground to the proper dimensions, with a minimum of at least 0.03 in. removed from any as-molded surface per Hughes requirements. The resultant brush has a

TABLE C-15. ECRA DESIGN CHARACTERISTICS

Brush material:	85% Ag, 3% Gr, 12% MoS_2 per HMS 20-1652 (Stackpole Grade SM 476)
Ring material:	Coin silver, full hard, temper 6, per MIL-S-13282, 12 μin. rms surface finish or better
Signal and power brushes:	
Tip size	0.060 x 0.245 in^2
Contact area	0.014 in^2/25
Brush pressure	3.9 psi
Spring rate	196 gm/in
Steady state rating	1 A at 75 A/in^2 (per brush)
Impulse rating	3 A (per brush)
Available wear length	0.125 in. to zero brush force 0.075 in. to 0.10 brush force
Mount type	Cantilever spring

grain pattern. With the direction of molding pressure oriented parallel to the ring motion, the lubricant feed process and area coverage of the wear track is optimized, because no straight-line wear path can be constructed across the wear face in the direction of ring motion that does not intersect several lubricant pockets.

As ring motion occurs, lubricant in the brush is fed directly to the brush/ring interface and smeared onto the ring, such that a film of lubricant is gradually burnished into the ring. Initially, when a clean metal ring condition exists, the brush wear rate is high. As the lubricant film develops the brush wear rate reduces, thereby reducing the rate of lubricant supply to the ring. The lubrication process is thus self-regulating, with the brush wear determined by the equilibrium between the rate of removal of lubricant from the ring and the rate of resupply as the brush wears. Wear performance of the proposed signal and power brush design has been determined in many long term vacuum tests, and is heavily dependent on the vacuum pressure environment near the brush/ring interface. Wear lifetime calculations are based on $>1 \times 10^{-6}$ Torr internal ECRA pressure, where the wear lifetime of the brushes is as follows:

TABLE C-16. SLIP RING TEST SUMMARY – DRY LUBRICATED TESTS

Test Ref. No.	Fixture	Ring Material and Number of Rings	Diameter, in.	Duration, h	Slip Ring Environment Pressure Range, Torr	Rotation Rate, rpm	Ring Travel (10^7 in.), in.	Revolutions (10^6)	Brush Material	Brush-Type Dimensions
1	Stepped fixture Test A	Coin silver (12 total), 3 each, 4 diameters, 0.25 A wide)	1 2 4.75 10	3,000	5×10^{-4} to 2×10^{-8}	200	1 - 10 2 - 20 4-3/4 - 47 10 -116	36	SM476 SM487 BAC4-53-3	Cartridge mount 0.187 x 0.187 tip area; 2 brushes/track, 2.6 A/brush
2	Stepped fixture Test B	Coin silver (12 total, 3 each, 4 diameters, 0.25 A wide)	1 2 4.75 10	2,426	9×10^{-7} to 5×10^{-7}	60	1 - 2.5 2 - 5.6 4-3/4 - 12.0 10 - 25.0	8.7	SM476	Same as Test A, 40, 60, and 80 gram brush forces
3	Stepped fixture Test C	Coin silver (12 total, 3 each, 4 diameters, 0.25 A wide)	1 2 4.75 10	1,056	2×10^{-9}	60	10 - 11.0	3.8	SM476	Same as Test B
4	Geometry fixture Phase I	Coin silver (20 total, 0.5 in.	1	2,160	8×10^{-6} to 1×10^{-6}	60	2.4	7.8	SM476	TDRSS design: cartridge mount 0.220 x 0.220, 1 and 2 per track, 3.6 A/brush, 40, 60, 80 gram force Cantilever spring mount - 0.050 x 0.145 up area, signal brush, 50 mA/brush Rocker arm mount - same tip as cantilever spring
5	Material fixture	• Coin silver • Electro-deposited silver (two types) • Copper • Rhodium plate (20 total, 0.5 in. wide)	1	2,060	8×10^{-6} to 1×10^{-6}	60	2.3	7.4	SM476 SM428 SM487 SM492	TDRSS design (cartridge mount 0.220 x 0.220) 2 brushes/track, 3.6 A/brush, 80 brushes total, 4 of each of 20 material combinations
6	OLSCA slip ring	Coin silver Pure silver	3	~500	10^{-6}	1	0.03	0.03	SM476 SM487 BAC-4-53-3 BAC 046-45	Cartridge, power 0.680 x 0.220, 8.2 A/brush, cantilever spring, signal
7	TACSAT life test (dry lube)	Coin silver (2 power 2 sec power, 20 signal)	1	~2,800	Unknown in ECRA, 10^{-8} to 10^{-9} in chamber	55 500 1,000	12.0	38	SM476	Cantilever spring: Two types Power: 0.145 x 0.220 Signal: 0.045 x 0.145 2 brushes/track Power: 2.5 A/brush Signal: 50 mA/brush
8	Modified TACSAT	Electrodeposited silver (same as above unit)	1	3,500	10^{-6} to 10^{-7}	55	3.6	11	SM476	Same as life test unit above
9	Geometry fixture Phase II	Coin silver (20 total 0.5 in. wide)	1	7,220	10^{-8} to 10^{-9}	60 90	12.1	38.7	SM476	Same as Phase I
10	Signal brush fixture	Coin silver (8 total, 0.5 in. wide)	1	7,220	10^{-8} to 10^{-9}	60	7.86	25.1	SM476	TDRSS design (cantilever spring 0.060 x 0.245) rocker arm 0.060 x 0.245; Signal, 2/track, 50 mA each
11	Accelerated life test fixture	Coin silver, electrodeposited silver, (20 total, 0.5 in. wide)	1	11,956	10^{-7} to 10^{-9}	60 180 300 600	91.1	289.9	SM476 SM428 SM487	TDRSS design (cartridge 0.220 x 0.220) 1 and 2 per track, 2.5 A/brush
12	Intelsat IV life test - BAPTA	Coin silver (4 total)	1	8,760	10^{-5} to 10^{-6} in ECRA, 10^{-7} to 10^{-9} in chamber	60	9.9	31.5	SM476	TDRSS design (cartridge, 0.220 x 0.220) 1 per track 2.5 A/brush
13	*HS-318 BAPTA life test	Coin silver (2 power 20 signal)	1-1/8	12,240	Unknown in ECRA 10^{-7} to 10^{-9} in chamber	60	15.5	44.0	SM476	TDRSS design (cartridge, 0.220 x 0.220) 1 per track, 3.6 A/brush (cantilever spring, 0.60 x 0.345) 2 per track, 50 mA/brush

Brush composition:

SM476	85 % Ag, 3 % Gr, 12 % MoS_2
SM487	83.5 % Ag, 2.5 % Cu, 15 % MoS_2
SM428	85 % Ag, 15 % MoS_2
SM492	85 % Ag, 15 % $NbSe_2$
BAC4-53-3	16.5 % Ag, 12.5 % Mo, 4 % Ta, 67 % MoS_2
BAC046-45	Same as 4-53-3 except without Ag

* Test still in operation.

	Conservative Worst Case (>1 x 10^{-6} Torr)	
	Wear in 7 years	Total lifetime*
Signal and power brushes	0.046 in.	20.67 yrs.

*Based on available wear length of 0.075 in. for signal brushes.

Several design features have been incorporated in the Pioneer Venus ECRA design to reduce internal pressure to a minimum, as follows:

1) All materials, coatings, insulation, etc., used in construction will be carefully screened for selection of lowest outgassing rate.

2) Elevated temperature vacuum curing will be applied to certain component parts prior to installation in the assembly and to the ECRA as a whole prior to final flight acceptance testing.

3) Venting paths are provided for each slip ring section (signal section, positive power bus, and return bus). Wear debris is prevented from leaving the ECRA by cavities along the vent path which trap particles through centrifugal force, while providing low resistance to gases in the molecular flow pressure range.

4) Protective covers over the vents and dry nitrogen purging during ground test and handling will prevent moisture, debris, or other contamination from entering the ECRA.

NUTATION DAMPER DESIGN

Nutation damping for both probe and orbiter is provided by a passive mercury tube nutation damper of the design type utilized on Syncom, ATS, and Telesat. The nutation damper consists of a fiberglass tube partially filled with mercury and mounted with its long axis parallel with the rotor spin axis. The end caps of the tube are plastic, and are bonded to the tube by an epoxy adhesive. The mercury to tube fraction-fill is determined by optimization of damping performance over the required mission profile. The damper design features are summarized in Table C-17 and illustrated in Figure C-13.

The extensive design, analysis, test, and flight data correlation completed to date on similar nutation damper designs for the Syncom,

TABLE C-17. NUTATION DAMPER CHARACTERISTICS

Size	
Tube inside diameter	1.91 Cm (0.75 in.)
Tube outside diameter	2.44 Cm (0.96 in.)
Tube length	71.12 Cm (28.00 in.)
Fraction-fill	0.2
Damper radial location	101.60 Cm (40.00 in.)
Mass	
Mercury weight	0.55 kg (1.22 lb)
Tube/cap, weight	0.31 kg (0.68 lb)
Total weight	0.86 kg (1.90 lb)
Performance	
Refer to Figure 5-20, Section 5	

Intelsat II, and ATS programs obviates the need for experimental verification of the damper time constant. Qualification and flight acceptance environmental testing is usually performed on the damper at unit level. The inflight experience of this damper design type affords a high reliability exceeding 0.9999 for a 7-year mission.

MECHANISMS

Design Considerations

Four mechanism designs were considered as part of this baseline configuration: 1) thermal louvers, 2) pyrotechnic devices for locking bicone antenna and magnetometer boom, 3) deployment mechanism for extending bicone antenna into the cruise mode configuration, and 4) magnetometer boom deployment mechanism. The detail rationale for the thermal louver design is given in detail as part of the thermal control subsystem report and it suffices to say that only the detail louver mechanism design will be discussed herein. Tradeoff studies on the remaining three mechanisms will be discussed to the extent that the overall spacecraft design

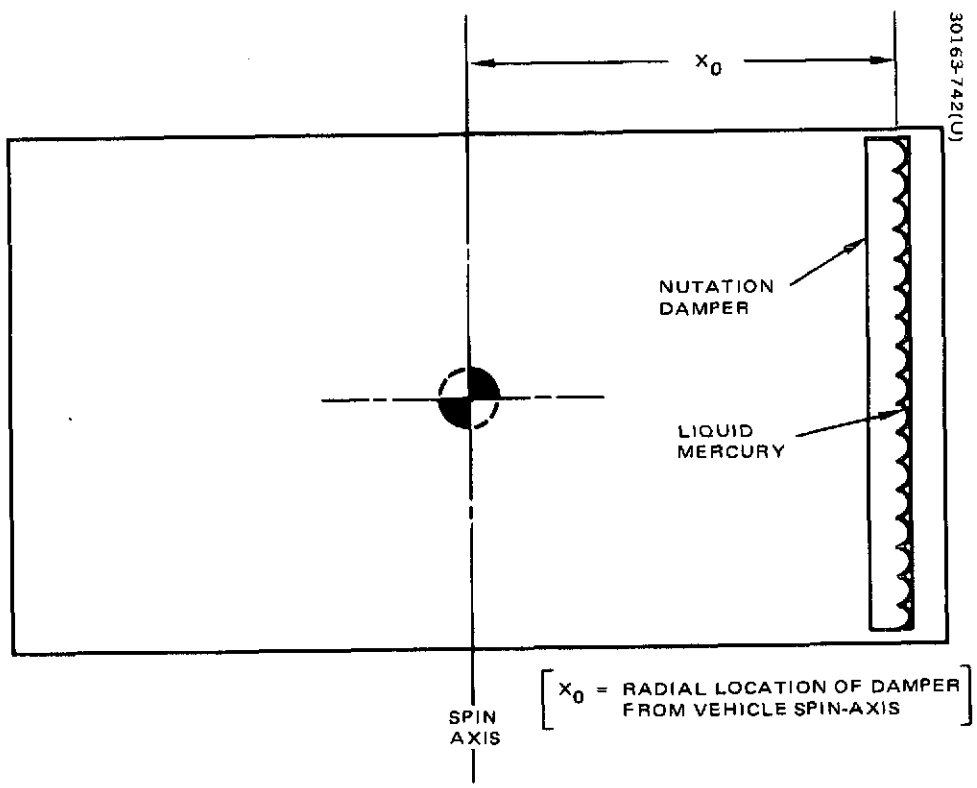

FIGURE C-13. DAMPER LOCATION RELATIVE TO SPACECRAFT

allowed the trades to be carried out; e. g., the bicone antenna deployment mechanism was constrained to extend along the spacecraft spin axis for a specified length and to be attached to the spacecraft main structural members.

Design Descriptions

Thermal Louvers

The louvers (Figure C-14) operate in an analogous fashion to venetian blinds. When the blades are closed, they act as a radiation shield between the heat source and the heat sink. When the blades are open, heat is directly radiated to space from the high emittance interior surface of the thermal controller. For blades with polished aluminum surfaces, the apparent infrared emittance of a system of blades covering a high emittance surface can be expected to be as low as 0.1 (closed position). When the blades are in the vertical position (open) with respect to the mounting surface, the apparent emittance is increased to 0.7 or greater. Each controller weighs a maximum of 0.65 lb and covers an area 8 by 16 in.

The controllers maintain temperature within the given range by effectively varying the emittance of the mounting surface with temperature. Figure C-15 shows the typical performance over a wide range of dissipation. Effective emittance of the controller is automatically regulated as a function of average surface temperature under the thermal controller. The louver blades begin to rotate as the mounting surface temperature increases to approximately 60°F. As the louver blades rotate, they expose the high emissivity surface of the equipment shelf to allow heat to dissipate from the spacecraft. In the open position, the louvers are positioned to allow approximately 128 in^2 of radiation surface areas to be exposed per controller. Effective emittance in the open position permits approximately 27 W to be radiated at 85°F from each controller. With the system closed, the highly polished blade surfaces are exposed to space, presenting a low emittance surface which allows approximately 4.2 W to be radiated at 60°F for each controller.

Rotation of the louver blades is performed by conversion of heat energy into mechanical motion by use of a bimetallic actuator. The bimetallic actuator is wound so that the strip of material with the greater coefficient of expansion forms the outer surface of the spring. This construction causes the actuator to contract or close when heated sufficiently and expand or open when sufficiently cooled. The actuators are keyed to their respective louver blade so that the louver rotates with the actuator movement. Each louver blade set (two blades) is individually actuated with a bimetal element. An adjustment on the controller assembly permits each actuator to be set so that the temperature at which the blade begins to open can be fixed. The blades in this case shall begin to open at 55 ± 2°F.

Heat is transferred to the actuators from the mounting surface by radiation. The actuators are conductively isolated from the controller structure so that louver blade position follows the mounting surface temperature (equipment shelf temperature) due to this heat transfer mechanism.

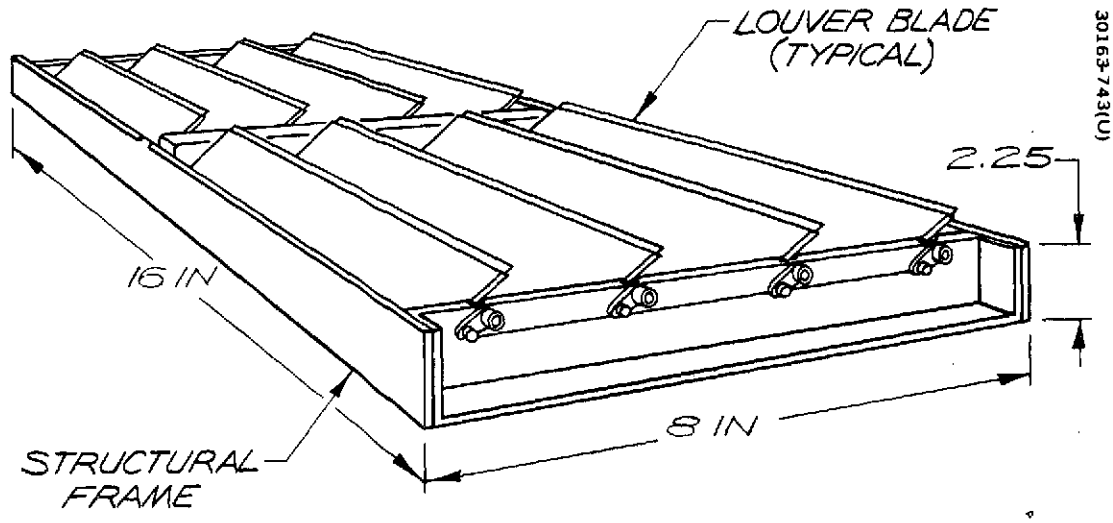

FIGURE C-14. THERMAL CONTROL LOUVER DESIGN

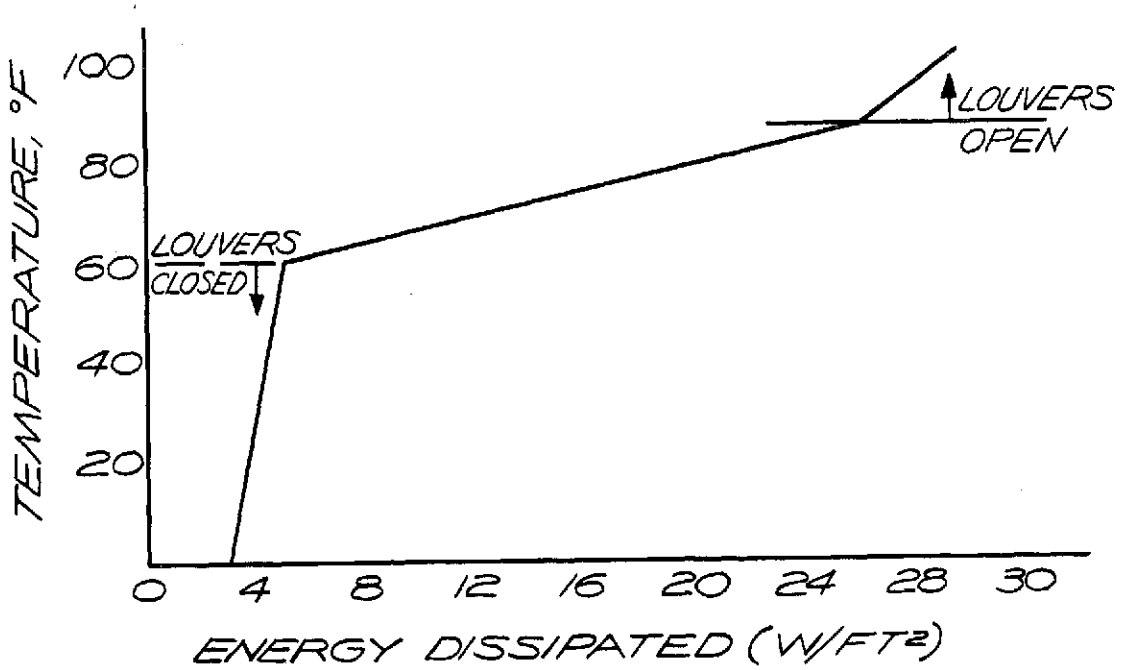

FIGURE C-15. LOUVER PERFORMANCE

The thermal louvers design has been space qualified and flown on Hughes built satellites.

Pin Pullers

The pin puller design selected has been used in many space applications at Hughes with no failures. The dual pressure cartridge feature has been added for the OSO-I program. All materials, with the exception of the A286 steel shaft, are aluminum. Both electrical and pyrotechnic redundancy is provided with the use of two pyrotechnic pressure cartridges.

The single bridgewire Apollo standard intiator has been selected as the pin puller pressure cartridge. This is a man-rated unit that was used extensively on the Apollo program, and is being utilized as the basic pyrotechnic unit on the Skylab program.

Characteristics:

Weight	0.14 lb
Power	5.0 to 12.0 A per initiator

Bicone Antenna Deployment Mechanism

The bicone antenna mast assembly is stored in a tucked and locked configuration during launch (Figure C-16 for two views). The deployment sequence is initiated by actuation of a pyrotechnic pin puller.

The deployment mechanism consists of two tubes, one mounted inside the other, two negator extension springs with drums and bearings, and a dual cartridge pyrotechnic pin puller for releasing the stowed antenna after launch.

The outer or support tube is flanged at one end. It carries the two constant force negator spring drums and bearing supports. The inner tube is flanged at one end and attaches to the bicone antenna at the flange. The extended ends of the negator springs are attached near the opposite end of this tube. At the spring attach end is also located the bracket for engaging the shaft of the explosive pin puller which is mounted to the other support tube flange.

The inner tube is provided with a grooved guide engaging a guide rod along the inside of the outer support tube. This guide rod prevents rotational displacement of the antenna combination during deployment. A tapered collar attached to the inner tube engages a tapered cylindrical insert near the deployed position end of the outer tube to provide positive stopping (energy dissipation) without rebound at deployment. A spring-loaded plunger provides a positive locking and retention mechanism. The relative position of the collar and insert are such as to maintain substantial overlap of the two tubes at the end of deployment.

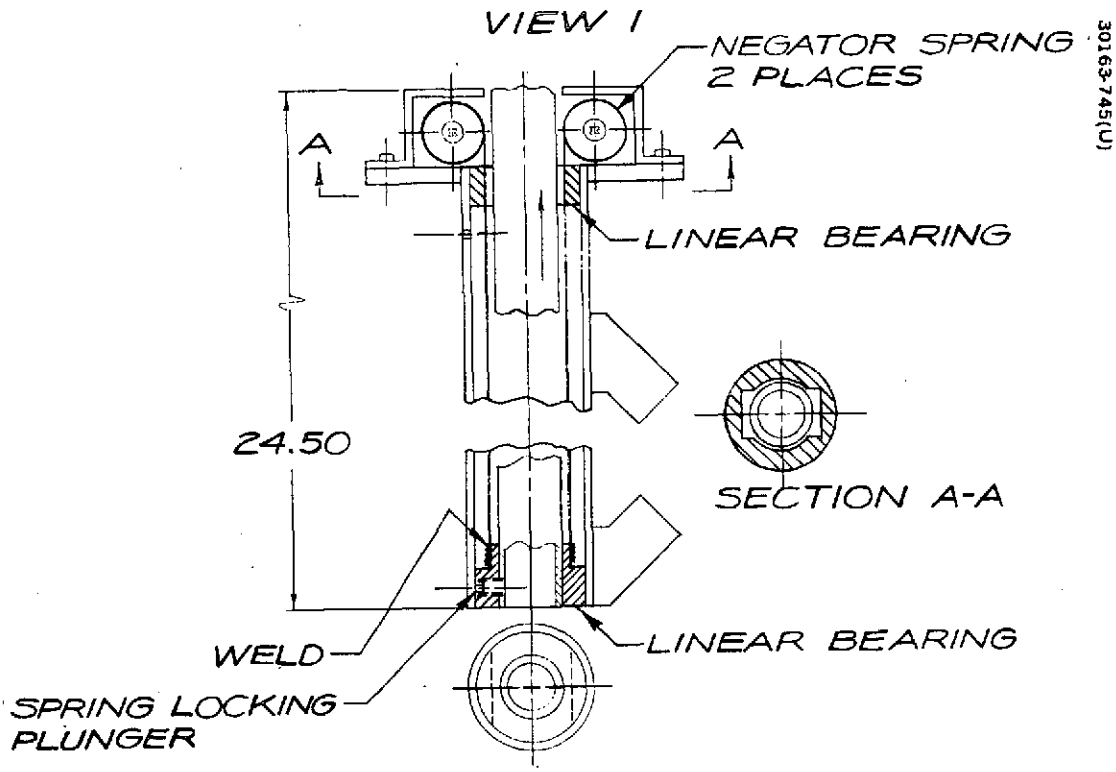

FIGURE C-16. BICONE ANTENNA DEPLOYMENT MECHANISM

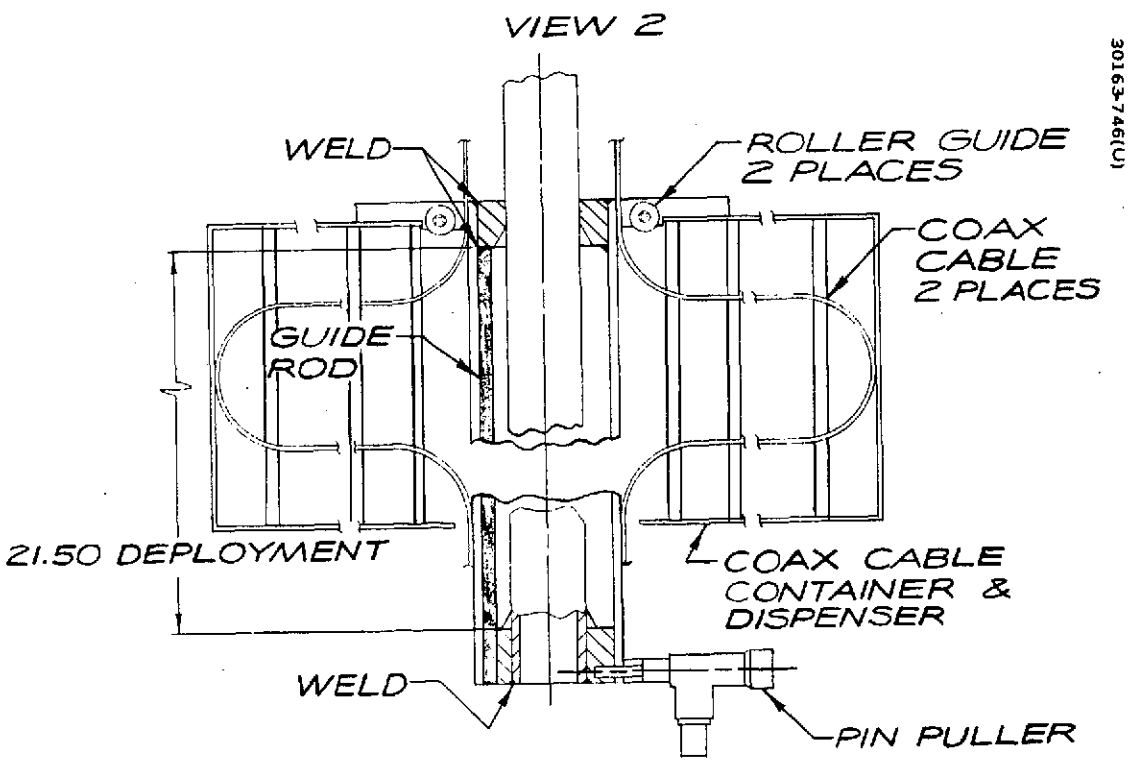

FIGURE C-16. (Continued) BICONE ANTENNA DEPLOYMENT MECHANISM

Two coax cable canisters mounted to the outside tube contain the cable in a large loop configuration during launch and provide a positive guide during deployment.

Weight Summary

Mechanism	1.0 lb
Mast	0.8 lb
Coax guide	0.15 lb
Total	1.95 lb

Magnetometer Boom

The selected design utilizes a one-piece, rigid, pivoting titanium tube of 1 in. outside diameter and approximately 0.25 in. wall thickness. The tube is cantilevered and rotates at two bearing pivot shaft mechanisms which contain a cam-riding lock pin engaging a tapered slot at the deployed position. The sensor end of the tube is restrained and supported by a pin puller latch and bracket during the launch environment. Following deployment, the 10-g retro firing force (orbiter) bending stress is safely limited to approximately 30,000 psi. (An aluminum tube of 1 in. outside diameter and approximately 0.062 in. wall thickness will also provide the necessary bending strength and torsional stiffness, but with a weight increase for the tube alone of approximately 0.25 lb.)

Since there is abundant centrifugal force developed for deployment, the principal problem with this design is the absorption of the kinetic energy generated as a result of the angular velocity obtained as the boom pivots through an angle of approximately 130 deg. The available system restraints, except for bearing friction torque, are the cam-riding lock pin, fritction torques, and the cable bending force as shown in Figure C-17. These forces are to some extent environment related and cannot be relied upon to provide predictable restraint. It is therefore proposed to incorporate two spiral clock or motor springs into the mechanism at the pivot joint to absorb most of the generated kinetic energy, which in unrestrained rotation will be approximately 50 ft-lb at 60 rpm. Because of variations in system friction, these restraining springs will be adjustable in position so that enough energy remains in the boom assembly to assure positive locking at the end of deployment. The nominal value of the restraining spring torque will be set, as shown in Figure C-18, for the desired spin speed (±1 rpm) to allow the unrestrained boom to overshoot a TBD number of degrees. This will insure that the boom deploys to its full extended position, as shown in Figure C-19. The remaining energy will then be absorbed by the tube and lock mechanism, capable of safely absorbing approximately 120 in-lb of energy, thus assuring positive locking.

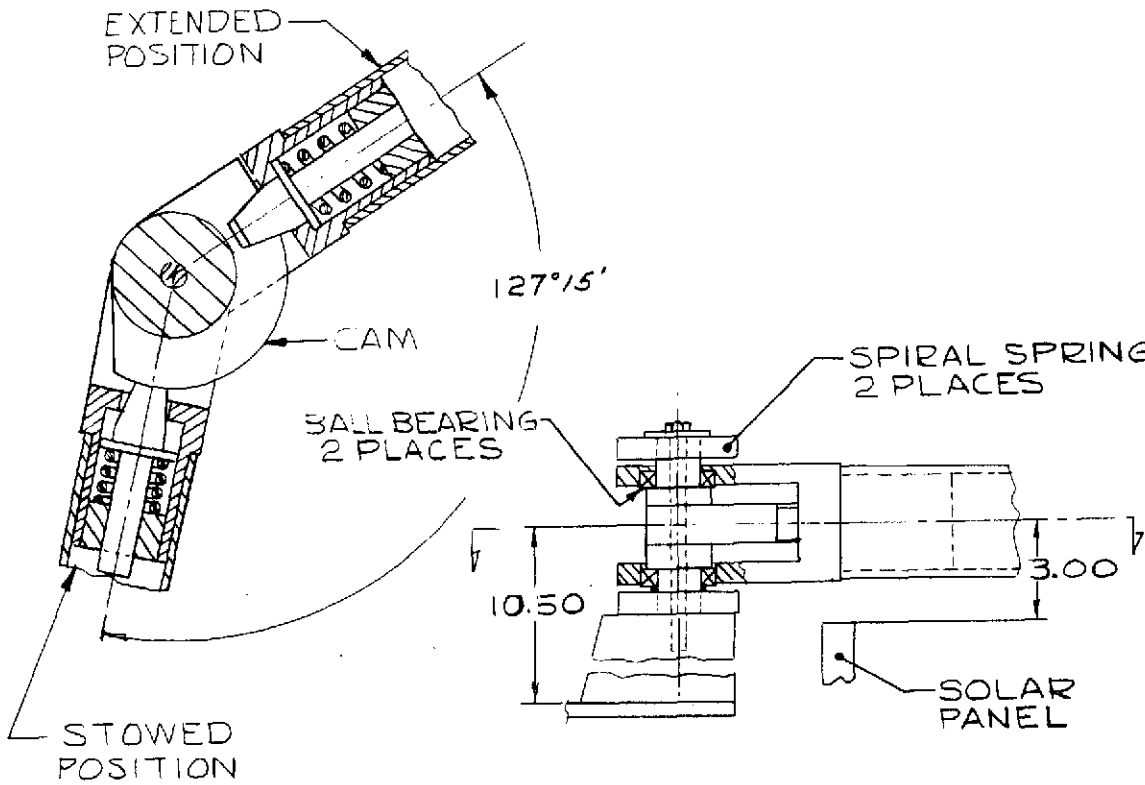

30163-747(U)

FIGURE C-17. MAGNETOMETER BOOM LOCKING MECHANISM, (42 INCH)

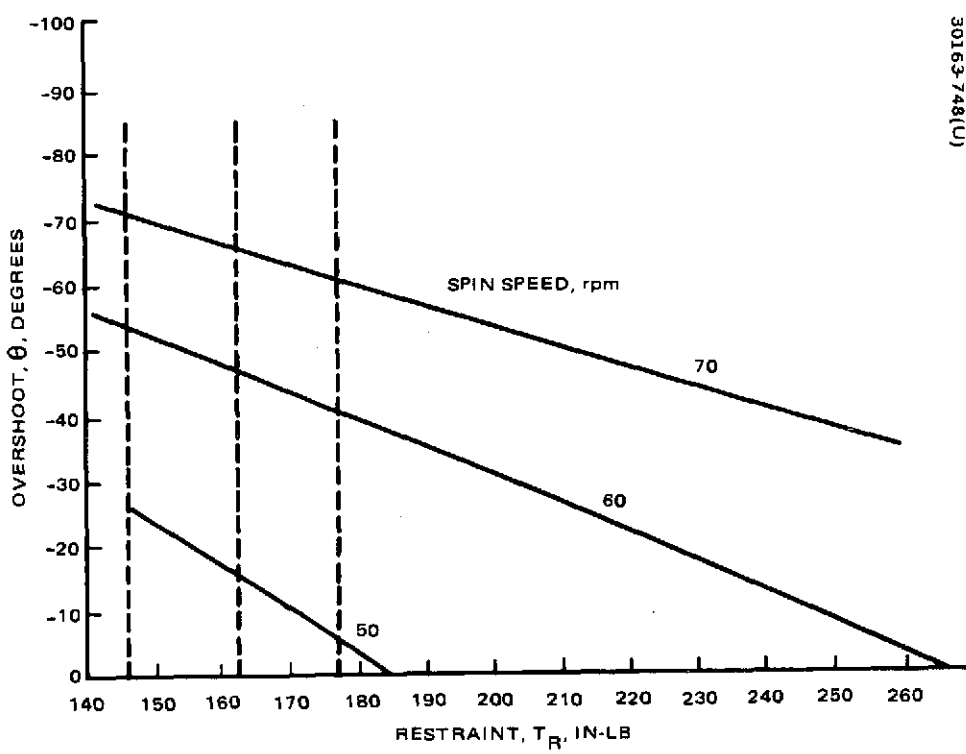

30163-748(U)

FIGURE C-18. VARIATION OF BOOM OVERSHOOT WITH SPIN SPEED AND RESTRAINT

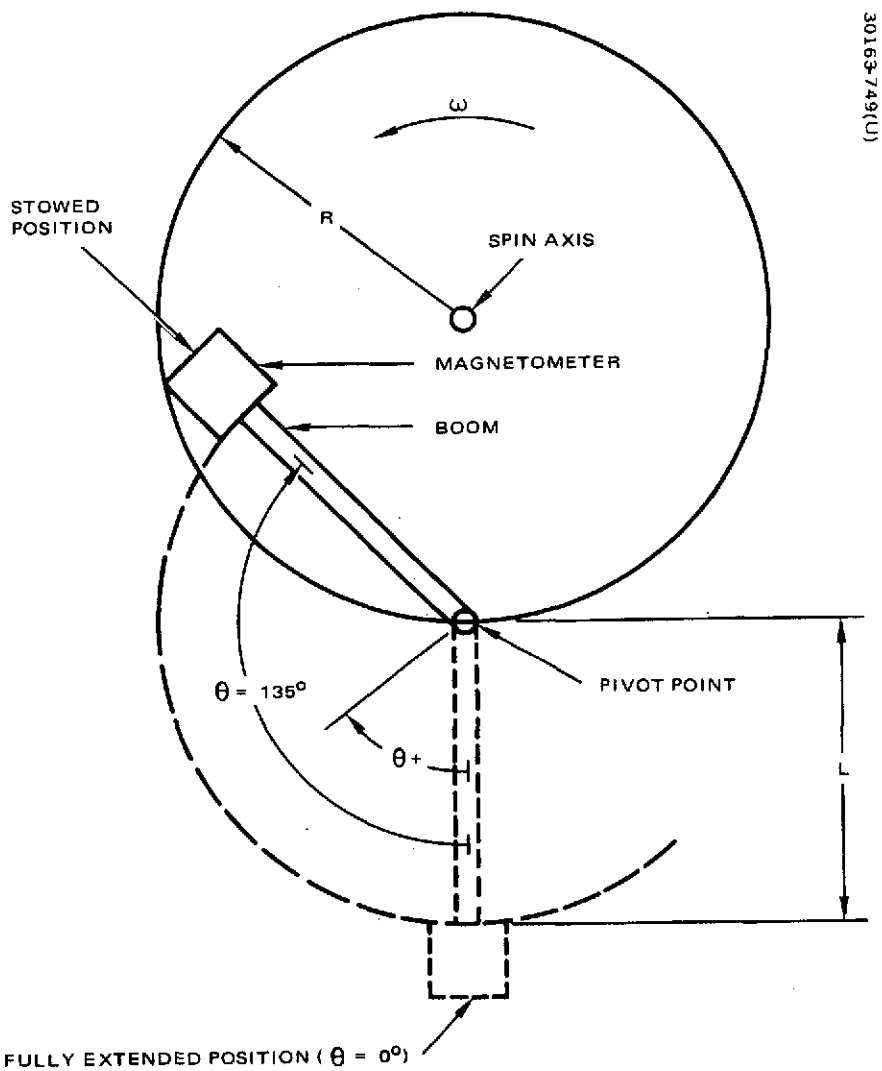

30163-749(U)

FIGURE C-19. BOOM GEOMETRY (RELATIVE TO SPACECRAFT)

Weight	
Sensor (tip mass)	1 lb
Boom	1.6 lb
Mechanism assembly	1.3 lb
Cable	0.25 lb

Design Tradeoffs

Pyrotechnics

The magnetometer boom assembly and the bicone antenna mast assembly will be stowed in a retracted and locked position during launch. Release of these mechanisms for deployment will be accomplished by the actuation of a pyrotechnic device. A number of pyrotechnic devices have been qualified to accommodate these functions; they are separation bolts, separation nuts, cable cutters and pin pullers.

The design of the mechanisms require that the pyrotechnic device be either a rotational or linear movement restraining device rather than a primary load-carrying member. Separation bolts and nuts are utilized in areas that require structural load-carrying characteristics as well as load release capability. Consequently, these devices are heavy and have more complex mounting provisions. Cable cutters are not as heavy but have the added problem of loose cables. Pin pullers provide simplicity of operation as well as minimum weight and, therefore, have been selected as the most suitable device for both deployment applications.

Magnetometer Deployment Mechanism (Thor/Delta Baseline)

The mission requires that a magnetometer sensor package weighing approximately 1.2 lb be placed outboard of the spinning spacecraft section after launch. The deployed position of the sensor is 42 in. outboard of the solar panel substrate with the sensor axis aligned relative to the spacecraft axis to within 1 deg.

The relatively short extension required and the availability of storage within the spacecraft contour obviate the necessity for telescoping, folding or extensible type booms. However, these designs have been considered to point up any obvious performance advantages peculiar to any of them.

Extensible type power-driven boom designs provide controlled deployment rates and preclude the need for snubbing or damping devices to limit extension forces. However, this type of device requires power and control elements for the motor. The inherent motor and control mechanism weight peanlties are not in this case offset by the boom length storage capability afforded by a rolled-up ribbon type configuration. Substitution of a centrifugal force actuated device still requires the mechanism (and weight) associated

with the ribbon storage cassette and looses the advantage of the controlled deployment rate. Either type of device requires a provision for cable stowage prior to extension and a cable unreeling mechanism for extension. Except for the bi-stem or zipper-type configuration, this type of device lacks torsional stiffness.

A telescopic tube design involves overlapping joint and joint locking design, will weigh more than a single tube, retains the cable stowage problem and in general offers no apparent performance advantages over the selected design.

Articulated, inged joint extension devices relieve the cable deployment difficulties and provide greater boom length capabilities, however, they do require pivot, energy dissipation and pivot locking designs at each joint. The baseline design selected consists of a single rigid tube which is rotated from the stowed and locked position inboard of the solar panel substrate by the centrifugal force component about a single pivot axis.